

**OPTIMAL PARAMETER SELECTION FOR BACKREAMING  
OPERATIONS WITH FLUID ASSISTED, MINI-  
HORIZONTAL DIRECTIONAL  
DRILLING MACHINES**

By

**FLOYD RAY GUNSAULIS**

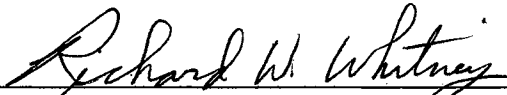
Bachelor of Science  
University of Arkansas  
Fayetteville, Arkansas  
1988

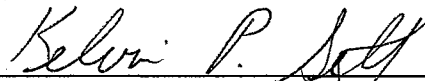
Master of Science in Agricultural Engineering  
University of Arkansas  
Fayetteville, Arkansas  
1990

Submitted to the Faculty of the  
Graduate College of the  
Oklahoma State University  
in partial fulfillment of  
the requirements for  
the Degree of  
**DOCTOR OF PHILOSOPHY**  
December, 1996

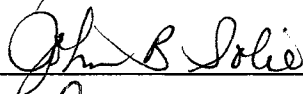
OPTIMAL PARAMETER SELECTION FOR BACKREAMING  
OPERATIONS WITH FLUID ASSISTED, MINI-  
HORIZONTAL DIRECTIONAL  
DRILLING MACHINES

Thesis Approved:


  
Thesis Adviser









  
Dean of the Graduate College

## ACKNOWLEDGEMENTS

I express my appreciation to Dr. Kelvin Self, Dr. Don Snethen, Dr. John Solie, and Dr. Marvin Stone for serving on my graduate committee. I express special thanks to Dr. Richard Whitney who served as my primary advisor during this study.

I wish to thank Mr. Rex Nelson and Mr. Mark Kern of the Charles Machine Works for their assistance and guidance. I thank Mr. Leonard Branen and the Charles Machine Works for committing to, and supporting this work.

I thank Mr. Damon Webb of the Charles Machine Works and the student workers from Oklahoma State University for sweating it out with me in the field.

I express my love and my deep appreciation for my wife, Cindy, who put up with me and encouraged me greatly during this project.

I give my highest appreciation and praise to my God and my Lord Jesus Christ for the ability and the opportunity.

*“And I gave my heart to seek and search out by wisdom concerning all things that are done under heaven: this sore travail hath God given to the sons of man to afflict them.”*

*Ecclesiastes 1:13*

## TABLE OF CONTENTS

<i>Chapter</i>	<i>Page</i>
I) Introduction/Review of Literature.....	1
The Mini-Directional Drilling Process.....	1
Challenges of Fluid Assisted, Mini-Directional Horizontal Boring.....	7
Factors Affecting Horizontal Boring Backreaming Operations.....	9
Basic Forces Involved in Soil Cutting.....	10
<i>Other Factors Involved in Cutting Force Requirements.....</i>	<i>14</i>
Product Installation Loading Concerns.....	17
Research on Influence of Parameters on Boring Unit Performance.....	20
Research Objectives.....	22
II) Experimental Parameters and Design.....	24
<i>Coyle Test Site.....</i>	<i>24</i>
<i>Stillwater Creek Test Site.....</i>	<i>26</i>
III) Test Locations and Equipment Used For Study.....	29
Test Locations.....	29
<i>Coyle Test Site.....</i>	<i>29</i>
<i>Stillwater Creek Test Site.....</i>	<i>29</i>
Boring Unit.....	30
The Hydraulic Power Supply.....	32
Electronics/Data Acquisition Systems on the Boring Unit.....	37
<i>Computer/Data Acquisition Interface.....</i>	<i>37</i>
<i>Pressure Transducers.....</i>	<i>37</i>
<i>Rotational Speed Sensor.....</i>	<i>40</i>
<i>Displacement/Velocity Transducer.....</i>	<i>44</i>
<i>Temperature Circuit.....</i>	<i>46</i>
<i>Flow Control Circuitry.....</i>	<i>48</i>
The Fluid System.....	50
The Trailer.....	52
Backreaming/Compacting Tools.....	52
Penetrometer/Soil Sampling Unit.....	55
Electronics/Data Acquisition Systems on Penetrometer Unit.....	60



Fluid Mixing/Supply Truck.....	61
Pipe Pull Load Measurement System.....	63
Computer Program for Boring Unit Performance Data Acquisition.....	66
 IV) Procedure.....	 73
Calibration.....	73
<i>Pressure Transducers</i> .....	73
<i>Displacement Transducers</i> .....	75
<i>Velocity Transducer</i> .....	75
<i>Temperature Sensor</i> .....	76
<i>Rotational Speed Calibration</i> .....	77
Coyle Test Site: Test Bore.....	78
Coyle Test Site: Bores 1 to 4, The Abandoned Data.....	79
Deviation from Original Pull Rate Settings.....	80
Procedure for Conduction of Bores.....	81
Penetrometer Soundings/Soil Samples.....	85
The Reaming/Pullback Process.....	88
Soil Tests.....	97
<i>Particle Size Analysis</i> .....	97
<i>Atterberg Limit Testing</i> .....	99
<i>Soil Classification</i> .....	100
<i>Direct Shear Testing</i> .....	100
<i>Standard Penetration Tests</i> .....	104
<i>Moisture Content of Coyle Soil Samples</i> .....	110
Drilling Fluid Analysis.....	110
 V) Data Reduction and Analysis.....	 115
Reduction of Bore Data.....	115
Reduction of Penetrometer Data.....	118
Reduction of Polyethylene Pipe Pull Data.....	120
Statistical Analysis of Boring Data.....	122
 VI) Results and Discussion.....	 124
Reaming/Pullback Process Conceptualization.....	124
Coyle Test Site.....	125
<i>Rotational Torque</i> .....	127
<i>Pulling Force at the Boring Unit</i> .....	138
<i>Pulling Force at the HDPE Pipe</i> .....	144
Stillwater Creek Test Site.....	149
<i>Rotational Torque</i> .....	149
<i>Pulling Force at the Boring Unit</i> .....	161
<i>Pulling Force at the HDPE Pipe</i> .....	168

VII) Summary and Conclusions.....	175
Boring Unit/Data Collection System.....	175
Tests in Non-cohesive Soil at the Coyle Test Site.....	177
<i>Coyle Test Site: Spindle Torque.....</i>	177
<i>Coyle Test Site: Boring Unit Pull Force.....</i>	178
<i>Coyle Test Site: Polyethylene Pipe Pull Force.....</i>	178
<i>Coyle Test Site: Total Power Usage.....</i>	179
Tests in Cohesive Soil at the Stillwater Creek Test Site.....	180
<i>Stillwater Creek Test Site: Spindle Torque.....</i>	180
<i>Stillwater Creek Test Site: Boring Unit Pull Force.....</i>	181
<i>Stillwater Creek Test Site: Polyethylene Pipe Pull Force.....</i>	183
<i>Stillwater Creek Test Site: Total Power Usage.....</i>	183
General Comparisons Between Soil Types.....	184
Limitations of Test Method.....	184
Recommendations for Future Research.....	185
References.....	186
Appendix.....	189
Section A: Glossary of Terms.....	190
Section B: Omnidata Polycorder Program.....	193
Section C: Boring Unit Data Acquisition and Control Program.....	195
Section D: Bore Profiles.....	210
Section E: Soil Particle Size Analysis.....	220
Section F: Penetrometer Readings .....	225
Section G: Pull Force Readings on HDPE Pipe.....	231
Section H: Data from Boring Tests.....	237

## LIST OF TABLES

<i>Table</i>	<i>Page</i>
1. Pull Rate Summary.....	81
2. Classification of Test Soils.....	101
3. Properties of Soil Samples from Stillwater Creek Test Site.....	105
4. Bore Log: Standard Penetration Tests at Coyle Test Site.....	108
5. Relative Density and Angle of Internal Friction for Soils at Coyle Test Site Based on Standard Penetration Test orrelations.....	109
6. Soil Sample Moisture Contents - Coyle Test Site.....	111
7. Drilling Fluid Viscometric Properties.....	114
8. ANOVA Table for Torque Model at Coyle Test Site.....	127
9. ANOVA Table for Boring Unit Pulling Force at Coyle Test Site.....	138
10. ANOVA Table for Polyethylene Pipe Pulling Force Model at Coyle Test Site.....	144
11. ANOVA Table for Torque Model at Stillwater Creek Test Site.....	149
12. Stillwater Creek Torque Means for Fluted and Winged Reamers.....	151
13. ANOVA Table for Boring Unit Pulling Force at Stillwater Creek Test Site.....	161
14. Stillwater Creek Boring Unit Pulling Force Means for Fluted and Winged Reamers.....	163
15. ANOVA Table for Polyethylene Pipe Pulling Force at Stillwater Creek Test Site.....	168
16. Stillwater Creek HDPE Pipe Pull Means for Fluted and Winged Reamers.....	173

## LIST OF FIGURES

<i>Figure</i>	<i>Page</i>
1. Typical Slanted-faced Cutter Head for a Mini-HDD System.....	3
2. Illustration of Typical Backreaming Process.....	6
3. Loaded Soil Element and Resulting Mohr's Circle.....	11
4. Soil Cutting With a Rough Raked Blade.....	13
5. Relationship Between Soil Moisture Content and Soil-to-Tool Adhesion.....	16
6. Picture of Jet Trac 4/40A Boring Unit Ready to Begin Backreaming Procedure.....	31
7. Hydraulic Schematic for Modified Jet Trac 4/40A Boring Unit.....	33
8. Original Jet Trac 4/40A Hydraulic Schematic.....	35
9. Daqbook 100 Pin Connection Diagrams.....	38
10. Boring Unit Pressure Transducer Electrical Connections.....	41
11. Boring Unit Rotational Speed Measurement Circuit.....	43
12. Position/Velocity Transducer Mounted at Back of Boring Unit.....	45
13. Position/Velocity Transducer and Oil Temperature Sensor Electrical Connections.....	47
14. Fluid Control Electrical Connections.....	49
15. Drilling Fluid Hydraulic Schematic.....	51
16. Fluted Reamer Used at Coyle and Stillwater Creek Test Sites.....	53
17. Two-staged Reamer/Compactor Used at Stillwater Creek Test Site.....	54
18. Penetrometer Rig in Use at Coyle Test Site.....	57

19. Penetrometer Cone and Push Rods.....	58
20. Penetrometer Unit Hydraulics.....	59
21. Penetrometer Instrumentation Connections.....	62
22. Polyethylene Pipe Pull-load Measurement Apparatus.....	65
23. Pull Force Electrical Connections.....	67
24. Flow Chart for Boring Unit Data Acquisition/Control Program.....	68
25. Typical Bore Geometry Used During Testing.....	84
26. Computer and Signal Conditioning Box Mounted at the Operator's Station on the Boring Unit.....	90
27. Polycorder, GPIE Interface, and Battery Pack Mounted in Trailer Behind Polyethylene Pipe.....	90
28. Approximate Location of Standard Penetration Test Borings Relative to Bore Paths at Coyle Test Site.....	106
29. Illustration of Typical No-load Torque Correction Plot.....	117
30. Illustration of Typical No-load Pull Force Correction Plot.....	117
31. Illustration of Forces Acting on Reamer/Compactor During Backreaming Operation.....	126
32. Measured vs. Predicted Rotational Torque from Coyle Test Site Based on Best Regression Model with Controlled Test Variables.....	129
33. Mean Torque vs. Drilling Fluid Flow Rate at a Given Rotational Speed at the Coyle Test Site.....	130
34. Mean Torque vs. Rotational Speed at a Given Drilling Fluid Flow Rate at the Coyle Test Site.....	130
35. Mean Torque vs. Drilling Fluid Flow Rate at a Given Reamer Pull Rate at the Coyle Test Site.....	132
36. Mean Torque vs. Reamer Pull Rate at a Given Drilling Fluid Flow Rate at the Coyle Test Site.....	132

37. Mean Torque vs. Drilling Fluid/Soil Volumetric Ratio at Coyle Test Site.....	134
38. Measured vs. Predicted Torque at the Coyle Test Site Based on the Pulling Force at the Boring Unit and Distance Pulled.....	135
39. Measured vs. Predicted Torque at the Coyle Test Site Based on the Depth of Cut (Pull Rate ÷ Rotation Rate) and the Penetrometer Index, $q_u$ .....	135
40. Mean Power Usage at Boring Unit as a Function of Rotation Speed at the Coyle Test Site.....	137
41. Measured vs. Predicted Boring Unit Pulling Force at the Coyle Test Site as a Function of the Controlled and Covariate Variables.....	140
42. Mean Boring Unit Pull Force vs. Drilling Fluid Flow Rate at a Given Rotation Speed at the Coyle Test Site.....	141
43. Mean Boring Unit Pull Force vs. Rotational Speed at a Given Drilling Fluid Flow at the Coyle Test Site.....	141
44. Mean Boring Unit Pull Force vs. Reamer Pull Rate at a Given Drilling Fluid Flow at the Coyle Test Site.....	143
45. Mean Boring Unit Pull Force vs. Length of Pull at a Given Flow Rate at the Coyle Test Site.....	143
46. Measured vs. Predicted Pull Force at the Polyethylene Pipe as a Function of Distance and Drilling Fluid Flow Rate at the Coyle Test Site.....	146
47. Mean Polyethylene Pipe Pull Force vs. Drilling Fluid Flow Rate at a Given Rotation Speed at the Coyle Test Site.....	146
48. Mean Pull Force vs. Drilling Fluid Flow Rate as Measured at the Boring Unit and at the Polyethylene Pipe at the Coyle Test Site.....	147
49. Measured vs. Predicted Torque for the Fluted Reamer at the Stillwater Creek Test Site as a Function of Controlled and Covariate Variables.....	152
50. Measured vs. Predicted Torque for the Winged Reamer at the Stillwater Creek Test Site as a Function of Controlled and Covariate Variables.....	152
51. Mean Torque vs. Reamer Rotation Speed for the Winged and Fluted Reamers at the Stillwater Creek Test Site.....	154

52. Mean Torque vs. Reamer Pull Rate for the Winged and Fluted Reamers at the Stillwater Creek Test Site.....	157
53. Measured vs. Predicted Torque for the Fluted Reamer as a Function of the Force Differential Between the Boring Unit and Polyethylene Pipe.....	158
54. Measured vs. Predicted Torque for the Winged Reamer as a Function of the Force Differential Between the Boring Unit and Polyethylene Pipe.....	158
55. Mean Power Usage at Boring Unit as a Function of Rotation Speed at the Stillwater Creek Test Site for Both Winged and Fluted Reamers.....	160
56. Measured vs. Predicted Boring Unit Pull Force for the Fluted Reamer as a Function of Controlled and Covariate Variables.....	164
57. Measured vs. Predicted Boring Unit Pull Force for the Winged Reamer as a Function of Controlled and Covariate Variables.....	164
58. Mean Boring Unit Pull Force vs. Reamer Rotation Speed at the Stillwater Creek Test Site.....	165
59. Mean Boring Unit Pull Force vs. Reamer Pull Rate at the Stillwater Creek Test Site.....	165
60. Measured vs. Predicted Boring Unit Pull Force as a Function of the Pull Force at the Polyethylene Pipe for the Fluted Reamer.....	167
61. Measured vs. Predicted Boring Unit Pull Force as a Function of the Pull Force at the Polyethylene Pipe for the Winged Reamer.....	167
62. Measured vs. Predicted Polyethylene Pipe Pull Force for the Fluted Reamer as a Function of Controlled and Covariate Variables.....	170
63. Measured vs. Predicted Polyethylene Pipe Pull Force for the Winged Reamer as a Function of Controlled and Covariate Variables.....	170
64. Measured vs. Predicted Polyethylene Pipe Pull Force for the Fluted Reamer as a Function of Controlled, Covariate, and Soil Sample Moisture Content Variables.....	172

## Chapter 1

### Introduction/Review of Literature

The use of fluid assisted, mini-horizontal directional drilling (mini-HDD) machines is rapidly becoming the method of choice for the installation of utility services in locations where open-cut trenching is undesirable. Common areas of use include river crossings, trafficway crossings, and utility installation in regions of well established landscaping. The use of directional boring systems can yield significant savings of time, decrease overall project costs, and reduce inconvenience to the public near project sites.

Mini-horizontal directional drilling equipment typically refers to machinery which has an effective range for boring and utility installation of up to 600 feet (180 m), at depths of 15 ft (4.6 m) or less (Khan, et. al., 1994). The preliminary, or pilot, bores for these units are typically less than 5 inches (127 mm) and the installed utility services are 8 inches (203 mm) or less in diameter (Stangl, 1991). Fluid assisted equipment refers to drilling units whose primary cutting action in soil is mechanical, yet also provide a pressurized fluid jet to assist with the soil cutting (Cary, 1993).

#### ***The Mini-Directional Drilling Process***

Fluid assisted, mini-horizontal directional drilling is generally composed of two phases: the pilot bore, and the backream/pullback. {Note: A glossary of terms associated with the mini-HDD process (Khan et al., 1994) is provided in Section A of the Appendix.} During the pilot bore, a rotating cutter head is launched into the ground at a shallow angle (normally 5 to 20 degrees) on the end of a string of drill pipe. The cutter head rotates as it



is slowly pushed into the ground. At the same time, drilling fluid is pumped through the drilling pipe and out an orifice located on the cutting head. For most soils, operating pressures from 300 to 1400 psi (2.1 to 9.7 MPa) are sufficient to maintain proper fluid flow. For harder soil formations, pressures from 1400 to 4000 psi (9.7 to 27.6 MPa) may work best. The fluid serves not only as an aid in soil cutting, but also lubricates the cutting head and drill stem to make rotation and advancement easier, provides cooling for the cutting head to prevent overheating damage to the locational transmitter normally located inside, and helps to stabilize the walls of the bore hole to prevent cave-in (Bennett, et al., 1995).

The drilling fluid used in mini-HDD applications is normally composed of water or water mixed with bentonite and/or a commercial drilling polymer. Water alone may be satisfactory in some clay and silt soils. If highly plastic or expansive clay soils are encountered, polymer mixed with water will improve the hole lubrication and reduce the swelling tendency of the clay. In non-cohesive formations, a mixture of bentonite and water is recommended (Bennett, et. al.). Bentonite is a commercially available grade of montmorillonite clay  $[(OH)_4Al_4Si_8O_{20} \cdot nH_2O]$  with high swelling potential (Chilingarian and Vorabutr, 1981).

The usual method of steering of the drill pipe with the fluid assisted, mini-directional horizontal boring units is through the use of a slanted faced cutter head (See Figure 1, Page 3). When drilling in a straight path, the cutter head is continually rotated as it is advanced into the ground. When the head is advanced into the soil without rotation, the normal force acting on the face of the head causes the pipe to deflect away from the

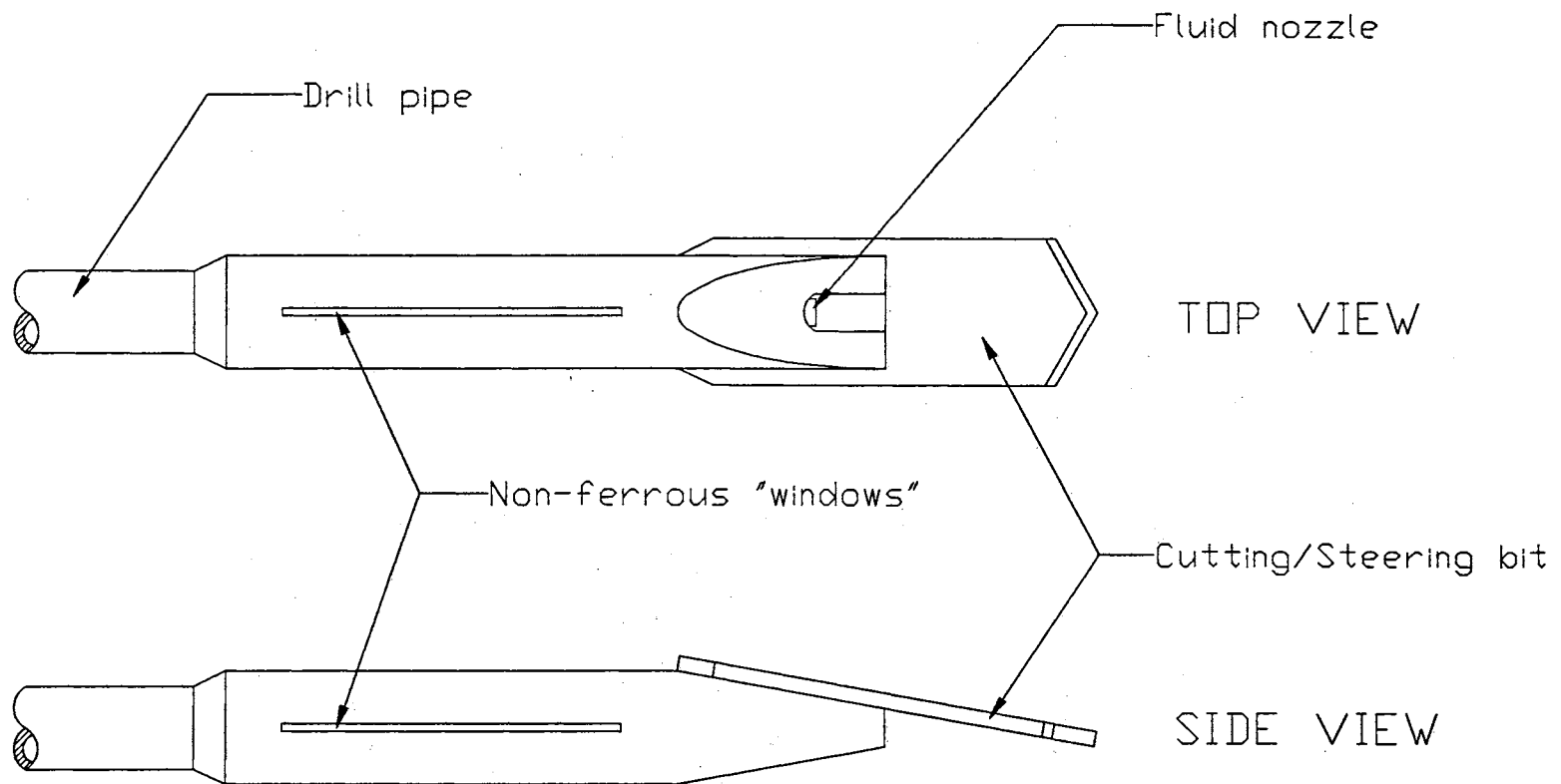


**Figure 1:** Typical slanted-faced cutter head for a mini-HDD system.

slanted face. By properly orienting the head and pushing without rotating, the drilling pipe may be gradually steered in the desired direction.

The orientation and depth of the cutter head may be determined by the use of a radio transmitter located in the head of the drilling device. Non-ferrous slots or "windows" in the drilling head allow the radio signal to pass through the housing walls. These slots are typically filled with a hardening epoxy or similar material. The transmitter will normally provide information on the location and depth of the head, the orientation of the head with respect to the rotation of the drill pipe, the pitch (upward or downward slope) of the drilling head, and in some cases, the temperature of the drilling head. Accuracy of the drilling head depth reading is given by most manufacturer's in the range of 3 to 5% of the drilling head depth (Khan, et. al., 1994). Information from the drilling head may be read by a drilling crew member with a hand held receiver who locates the position of the head and relays the pertinent information to the boring operator. Some advanced locating systems may use other methods of cutting head position determination and transmission. Among these are the use of micro-gyroscopes whose signals are transmitted along the drill string to the operator (Tanwani and Iseley, 1994).

The pilot bore progresses in a repetitive pattern of adding another joint of drilling pipe, orienting the cutting head to make any necessary course corrections, advancing the pipe into the hole using combinations of straight pushes and rotating pushes to direct the pipe, and then reevaluating the location and orientation of the drilling head. Accuracy of these systems can be very good with an experienced drilling crew. Often target locations can be reached within a 12 inch (300 mm) circle (Stangl, 1991).

Once the path of the drilling string has advanced to the desired location, the installation of the utility service may begin. Frequently, this will require that the pilot hole be reamed out to a larger diameter to allow room for the utility service to be pulled into the hole. The Institute of Electrical and Electronics Engineers (IEEE, 1994) recommends that the reamed diameter of the bore hole be at least 1.5 times the diameter of the product line being installed.

The process of enlarging, or reaming, the pilot hole consists of four main components: the cutting of the soil material; the mixing of the severed soil material with drilling fluid; the stabilization of the hole walls in non-cohesive materials; and the removal of the soil/drilling fluid slurry from the hole itself, either by compaction into the hole walls or slurried conveyance out of the hole. A typical downhole tool configuration for performing a backreaming operation is illustrated in Figure 2, Page 6.

As the drilling pipe is rotated and drawn into the ground, the cutter will gouge loose the soil at the leading edge of the reamed hole. Drilling fluid is pumped out at the front of the cutter to reduce soil/cutter adhesion and begin to put the soil into a slurry. Additional fluid may be added behind the cutter to help mix the soil material into a slurry. In highly compressible soils, the majority of the slurry material may be compacted into the side of the hole, providing the bore is of sufficient depth to prevent surface heave and damage to neighboring pipelines is not a concern. In soils with low compactability and in bores where soil surface damage or neighboring pipe damage is a concern, the slurry must be allowed to pass by the reamer/compactor and be conveyed out of the hole along the annulus between the pipe and the hole.

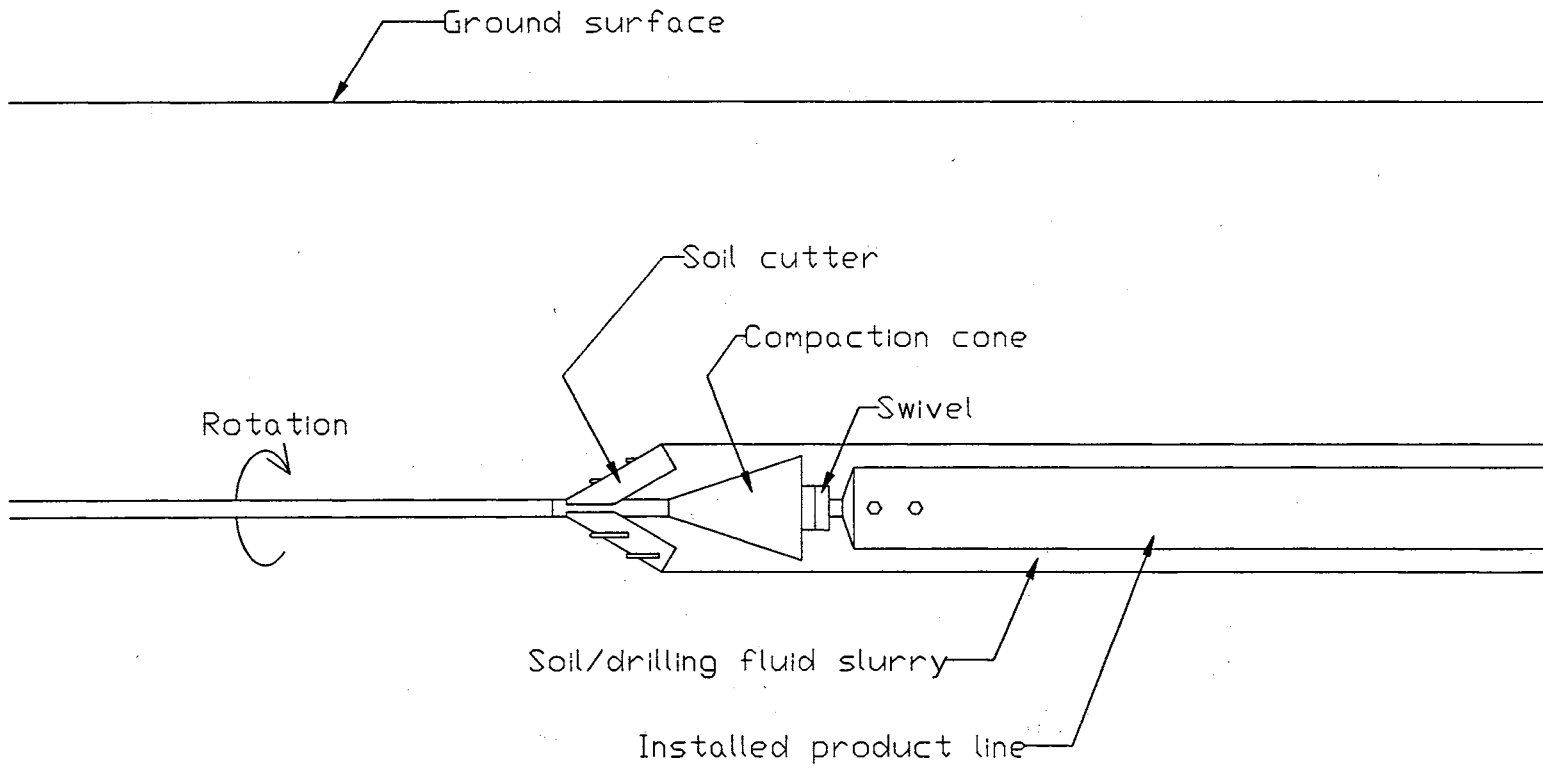


**Figure 2:** Illustration of typical backreaming process.

A swivel is placed between the installed service line and cutter/compaction cone assembly to prevent the installed pipeline from rotating as it is pulled into the ground. Rotation of the installed utility service could lead to damage during installation and would greatly increase the torque requirements of the boring unit.

### ***Challenges of Fluid Assisted, Mini-Directional, Horizontal Boring***

While the advantages of utility installation using horizontal drilling techniques are many, failures during boring, particularly during the process of bore-hole reaming and the actual pulling in of the utility service, can be costly, time-consuming, and create the need for major open excavations to retrieve boring components lost downhole. Thus, any information that may be applied to the boring system to reduce the possibility of a boring failure is of great interest.

In addition to the need to make the boring process as reliable as possible, there is also a need to make efficient use of available power at the boring unit. This is important both to those who develop the boring equipment and to those who use the equipment in the field. The developers of boring equipment seek to provide a product that is capable of installing many types of utility services (gas lines, water lines, electric lines, etc.) in a wide variety of soil conditions. Overdesign of equipment due to an incomplete understanding of how to make it perform efficiently can lead to unnecessarily high product costs, reducing a manufacturer's competitive edge.

During the process of bore hole reaming, referred to as backreaming, and the pulling in of the utility service, referred to as pullback, there exists a tradeoff in how the available hydraulic pressure and power will be utilized. Each boring machine has a limit to the amount of torque it can apply to a drill pipe, the speed with which it can rotate a drill pipe,

the thrust load it can apply to the pipe (whether pushing or pulling), and the available power to accomplish each of these tasks. The power consumed in drill pipe rotation is dictated by the equation:

$$P_R = \frac{2\pi \times T \times \omega}{33,000} \quad \text{Eq. (1)}$$

Where:  $P_R$  = the power used in rotation (hp)

$T$  = the torque on the pipe (ft-lb)

$\omega$  = the rotational speed of the pipe (rev/min)

The power consumed by pushing or pulling the pipe is dictated by the equation:

$$P_P = \frac{F \times V}{33,000} \quad \text{Eq. (2)}$$

Where:  $P_P$  = the power used in pulling the pipe (hp)

$F$  = the pushing or pulling force on the pipe (lb)

$V$  = the rate of travel of the pipe into or out of the ground (ft/min)

Using a high rotation rate during a backream operation may limit the amount of torque available for cutting the soil. On the other hand, a slower rotation rate may fail to adequately mix a sandy soil into a flowable slurry resulting in high stresses on the installed utility service. A rapid pullback rate may cause excessively high torque values. A very slow pullback rate may result in low productivity and unnecessary expenditure of drilling fluid.

### ***Factors Affecting Horizontal Boring Backreaming Operations***

To help manage the challenges associated with backreaming operations of fluid assisted, mini-directional, horizontal boring systems, it is necessary to understand the factors which influence the performance of the drilling system. The rotational torque requirement and the pulling force requirement for the boring unit during backreaming may be influenced by any or all of these factors:

- a) Soil type and condition
- b) Rotational rate of the drill pipe and cutter
- c) Advance rate of the cutter into the soil profile
- d) Cutter and compaction cone design
- e) Drilling fluid flow rate and physical properties
- f) Turns or deviations in the bore path
- g) Size of the bore hole
- h) Length of the bore

These factors do not all function independently of each other, but are involved in a complex system of interactions. During the boring process, the values of almost all of these parameters can be determined to some extent by the drilling crew, with the possible exception of the soil type and the condition of the soil (moisture content, in situ soil stresses, compaction under traffic ways, etc.). However, once a backreaming process is under way the only parameters which may be altered are the rotation rate of the drill pipe, the advance rate of the cutter into the soil, and the flow rate and physical properties of the drilling fluid used during the bore.



### ***Basic Forces Involved in Soil Cutting***

To understand how rotational torque may be influenced by the listed parameters, a basic understanding of the soil cutting process is helpful. Soil cutting, like that performed during the backreaming process, typically involves a passive failure of a soil surface. By passive, it is implied that the soil fails under stresses induced when an object is forced into a soil profile near the surface. As the object moves forward the soil stresses build up until the soil fails in front of the moving object along a plane dictated by the soil structure.

Before discussion of the actual soil cutting process, a discussion of the principles behind passive failure and soil cutting will be given. The shearing strength of a soil is a function of two mechanical processes within the soil; friction and cohesion (McKyes, 1985). The total mechanical shear strength of a soil may be described by the equation:

$$s = c + \sigma_n \tan\phi \quad \text{Eq. (3)}$$

where:  $s$  = the soil shear strength (shear force per unit area)

$c$  = soil cohesion (force per unit area)

$\sigma_n$  = the normal pressure acting along the failure plane

$\phi$  = the angle of internal friction

To understand the components of the shear strength equation and how they apply to the failure of a soil it is necessary to look at an element of soil under loading and the resultant Mohr's circle from the applied stress condition (See Figure 3, page 11). Here an element of soil is shown loaded along its principal axes. The external shearing components are equal to zero. The stress  $\sigma_1$  represents the major principal stress and  $\sigma_3$  the minor principal stress value. The illustration shows the  $\sigma_1$  stress in the vertical direction and  $\sigma_3$  in the horizontal. While it is common in soil mechanics to find the major

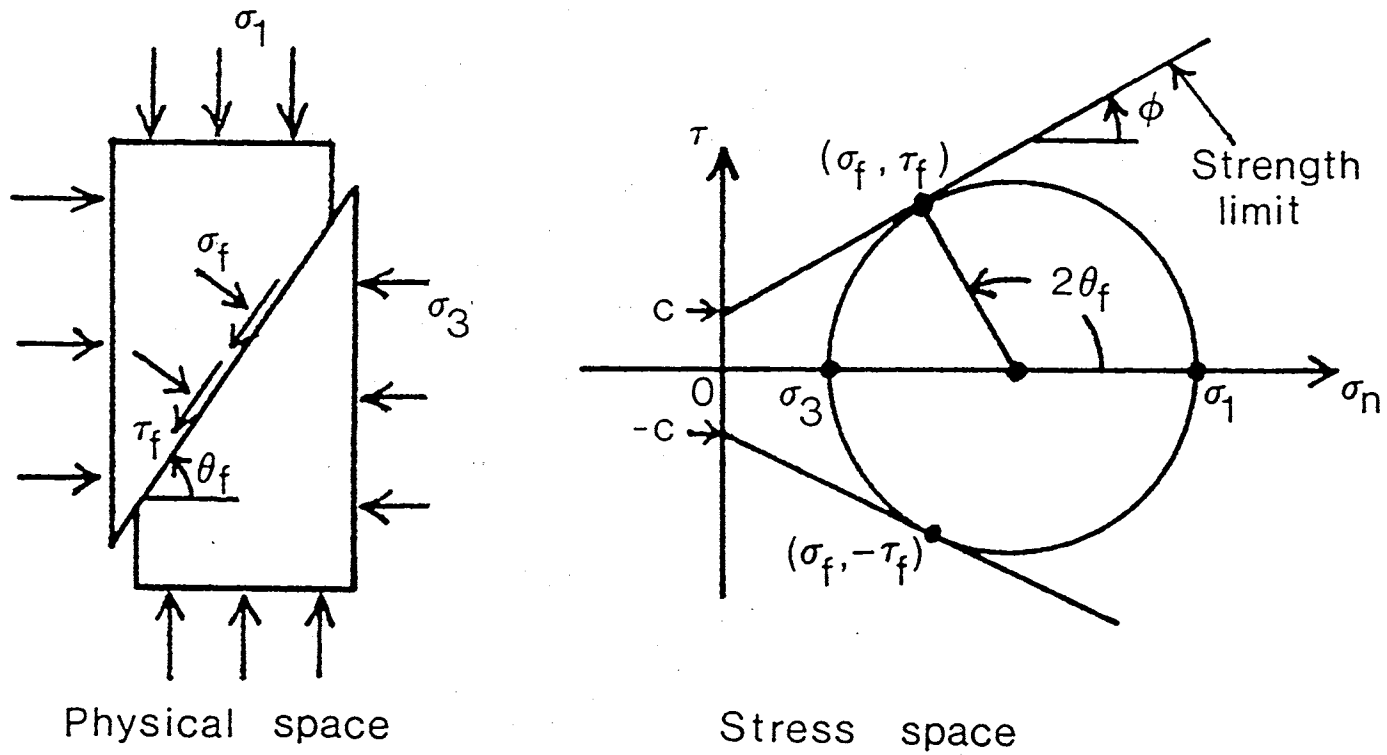


**Figure 3:** Loaded soil element and resulting Mohr's circle.  
(McKyes, 1985)

principal stress in the vertical direction due to the overburden pressure of the soil, it may lie in other planes depending on how the soil is loaded.

The Mohr's circle diagram depicts the stresses shown on the element of soil as  $\sigma_1$  and  $\sigma_3$ . The diagram also depicts the strength limit lines for the soil. The radial line from the center of the circle to the point of tangency of the strength limit line to the circle is used to define the angle  $2\theta_f$ , where  $\theta_f$  is the angle of the soil failure line relative to the plane of  $\sigma_1$  (McKyes, 1985). The angle  $\theta_f$  is related to the angle of internal friction,  $\phi$ , by the equation:

$$\theta_f = \pm (45 + \phi/2) \text{ in degrees} \quad \text{Eq. (4)}$$

From Mohr's circle, other parameters may also be determined. The soil cohesion coefficient,  $c$ , is found from the intersection of the soil strength line with the  $\tau$  axis. The average normal stress is represented by the center of the Mohr's circle. The angle between the line of action of  $\sigma_1$  and the failure surface may also be found. This angle is normally denoted as  $\mu$ . It is easily shown that  $\mu + \theta = 90^\circ$ .

Reece (1965) developed an equation for describing the force necessary to cut soil with a tool. His derivation was based on Terzaghi's work on bearing capacity for shallow foundations (Terzaghi, 1943). The equation, given below, is known as the universal earth moving equation.

$$P = (\gamma g d^2 N_\gamma + c d N_c + q d N_q) \cdot w \quad \text{Eq. (5)}$$

Where:  $P$  = the lateral force needed for cutting

$\gamma$  = the soil density

$g$  = the acceleration due to gravity



that the strength between the soil and the tool is taken to be equal to the soil's internal strength. The magnitude of  $\tau_b$  is equal to  $c + \sigma_b \tan \phi$ . The value  $\sigma_b$  is the soil to blade normal pressure. The resultant force,  $P$ , acting on the blade is then (McKyes, 1985):

$$P = \frac{\sigma_b \times L}{\cos \phi} \quad \text{Eq. (6)}$$

where:  $L$  = the length along the cutting face of the blade

This is further broken down into components of stress due to soil cohesive forces and surcharge on the soil. McKyes' final form of the equation is:

$$P = cdN_c + qdN_q \quad \text{Eq. (7)}$$

where  $N_c$  and  $N_q$  are functions of  $\phi$ ,  $\alpha$ , and  $\mu$

#### Other Factors involved in Cutting Force Requirements

One key factor in the determination of the forces required to cut and move a quantity of soil from its place is the rate at which the cutting occurs. When soil particles are sheared and accelerated rapidly, inertia forces come into play as an important contribution to the overall force required to cut the soil. Another factor to consider is the change in shear strength with change in shear rate. Non-cohesive soils do not display marked changes in shear strength with shear rate. However, tests with clay soils at different shearing rates revealed that as the shear rate increased, the force required to cut the soils increased faster than could be explained by inertial forces alone. Wismer and Luth (1972), when studying cutting of a clay soil using blades, found that the relationship between the draft force required to pull a blade or penetration cone through a clay soil was directly proportional to the log of the rate at which it was pulled. The ASAE

Standards (1993) list draft requirements for unit cross sections of furrow slice of various tillage implements. For tillage implements, ASAE lists draft to be a function of the square of the speed at which the implement is pulled.

The amount of frictional resistance between the cutting surface and the soil is important in determining the total force required to cut the soil. In the derivation leading to Equation (5), the soil-to-tool friction was assumed to be zero. In the derivation for Equation (7), soil-to-tool friction was assumed equal to the internal strength of the soil. In actuality, the soil-to-tool friction will almost always lie between these two extremes. Frictional forces of soils acting on cutting tools are the result of two factors, soil-to-tool adhesion and soil-to-tool friction. The shear strength along the soil/tool interface may be found by (McKyes, 1985):

$$s = c_a + \sigma_n \tan \delta \quad \text{Eq. (8)}$$

Where:  $s$  = shear strength at interface

$c_a$  = soil-to-tool adhesion

$\sigma_n$  = force normal to face of the tool

$\delta$  = tool-to-soil friction angle

The tool-to-soil friction angle,  $\delta$ , is primarily a function of the roughness of the tool surface. Adhesive forces are primarily due to moisture films, and their magnitude is dependent upon moisture content of the soil. As it is impossible to separate the soil-to-soil friction component and the adhesion friction component when discussing the soil-to-tool friction, these may be combined into one term,  $\mu'$ , known as the apparent coefficient of friction, where  $s = \sigma_n \mu'$ . Figure 5 shows the general relationship between soil-metal friction and moisture content originally described by Nichols (1931). In the friction phase,

adhesive forces are small and the coefficient of friction is essentially independent of moisture content. In the adhesion phase, moisture films develop between the soil particles and the metal, thus creating adhesive forces that cause the apparent coefficient of friction to increase. In the lubrication phase, the soil has enough moisture to act as a lubricant and the apparent coefficient of friction decreases (Kepner, et al., 1982).

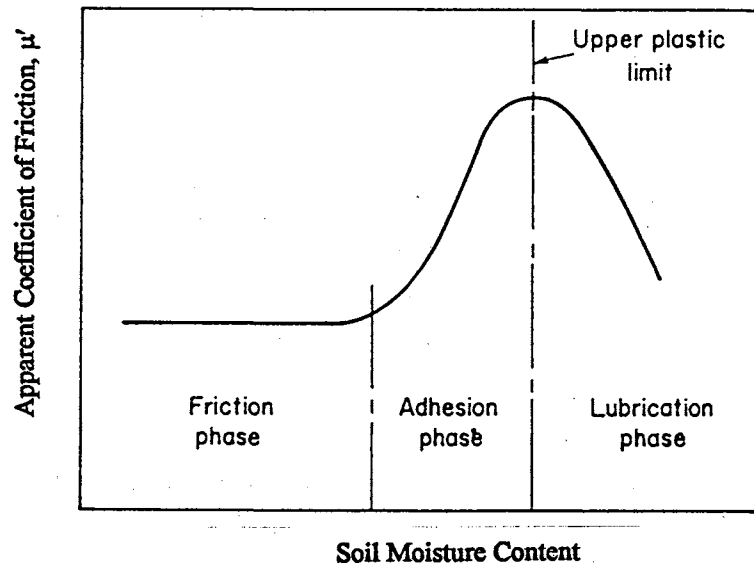


**Figure 5:** Relationship between soil moisture content and soil-to-tool adhesion. (Kepner, et al., 1982)

The transition moisture content between phases increases with clay content of the soil. Apparent coefficients of friction are higher for clays than for sandy soils. Typical ranges of  $\mu'$  for soil on smooth steel are 0.2 to 0.5 for sands, and 0.35 to 0.8 for clay soils (Kepner, et al., 1982).

To reduce the rotational torque required for horizontal directional drilling applications, Wilcox (1990) advocated the need to calculate the ratio of volumetric flow of drilling fluid to the volumetric amount of soil excavated during the reaming process.

Wilcox gave the following formula:

$$\frac{V_f}{V_s} = \frac{Q_f}{\frac{D^2}{24.5} \times R_b} \quad \text{Eq. (9)}$$

Where:  $V_f/V_s$  = the volumetric ratio between drilling fluid and soil excavated during the backreaming process

$Q_f$  = the flow rate of drilling fluid in gallons/minute

$D$  = the reamed hole diameter in inches

$R_b$  = the cutter advance rate in ft/minute

Wilcox indicated that the volumetric ratio between drilling fluid and excavated soil required for minimizing torque could be as high as 2 depending on the soil type, boring equipment, and cutter configuration.

### ***Product Installation Loading Concerns***

The concerns of boring parameter selection are not limited to the efficient use of power to the boring unit alone. It is also vital, and perhaps more important, to select the parameters which will produce the least stress on the installed service lines and yield the highest probability of a completed bore. If the drilling unit is operating at maximum efficiency yet the utility service is pulled apart, the bore is still a failure.

The pulling force applied to the installed service line could be affected by, but is not limited to, any of the following:

- a) The size of the utility line compared to the size of the hole
- b) Bore path geometry, including: length of bore, number of turns or deviations in the hole, and radius of turns in hole



- c) The viscometric properties of the soil/drilling fluid slurry in the annulus of the hole around the line
- d) The stability of the hole walls (whether cave-in is a problem)
- e) Settling out of slurry suspension and deposition of soil material along the installed line
- f) Gravitational forces as the product line makes elevational changes

A horizontal boring operator must make decisions during the boring process that will affect each of these parameters associated with the pulling forces on the product line.

Huey et al. (1996) and Kirby et al. (1996) demonstrate that the total stress on the installed pipelines line is composed of more than just the stress due to pulling force tension. Bending stresses due to curved bore paths and hoop stresses caused by external pressure on the pipe line must ultimately be considered in determining whether a product line may be safely installed by horizontal directional drilling.

For straight pull sections where cave in of the borehole walls is not a problem, Huey et al. (1996) give the following model for change in tension along a length of pipe:

$$T_2 = T_1 + F_f + F_v \pm W_s \times L \times \sin \theta \quad \text{Eq. (10)}$$

Where:  $T_2$  = the tensile force in the pipe at an arbitrary point, 2

$T_1$  = the tensile force in the pipe at a separate location, 1

$F_f$  = the frictional force between the pipe and the surrounding soil

$F_v$  = the viscous drag of the drilling fluid acting on the moving pipe

$W_s$  = the effective (submerged) weight/length of pipeline

$L$  = the distance between points 1 and 2

$\theta$  = the angle of the axis of the straight section of the hole relative to  
horizontal

The frictional drag force was given as:

$$F_f = W_s \times L \times \cos\theta \times \mu_{soil} \quad \text{Eq. (11)}$$

Where:  $\mu_{soil}$  = average coefficient of friction between pipe and soil,  
recommended values referenced by Huey et al. (1996) of  
between 0.21-0.30

The viscous drag force due to the drilling fluid was given as:

$$F_v = \pi \times D \times L \times \mu_{mud} \quad \text{Eq. (12)}$$

Where:  $D$  = the outer pipe diameter

$\mu_{mud}$  = the fluid drag coefficient, for steel tube pulled through mud a  
recommended value is referenced as 0.05 psi (0.34 kPa)

In sandy soils, Jonnes (1995) demonstrated that, in a laboratory setting, frictional forces acting along a pipeline are greatly diminished if the sand particles mixed with the drilling fluid can be kept suspended in the drilling fluid. Jonnes demonstrated the ability of commercially available drilling fluid additives to greatly reduce fluid percolation rates into a sandy material when mixed with a bentonite and water drilling fluid. By reducing fluid loss out of the walls of the bore hole, the soil cut loose during the backreaming process will tend to remain in a more fluidized state, thus reducing frictional drag along the installed pipeline.

### ***Research on Influence of Parameters on Boring Unit Performance***

Bennett, Khan, and Iseley (1994) conducted a test using horizontal boring machines from two different manufacturers in silt, sand, clay, and clay gravel soil conditions. The purpose of the testing was to evaluate the influence of soil on drilling unit performance. Measured parameters were thrust/pullback force, torque, drilling fluid pressure, and drilling fluid flow. Testing was conducted at the Waterways Experiment Station (WES) in Vicksburg, MS.

Horizontal bores ranging in lengths from 120 to 150 ft (37 to 46 m) were made through a pit of selected backfill materials. The backfilled pit was 25 ft (7.6 m) wide. On either side of the pit was an in-situ silt soil. Bore depths ranged from 3 to 6 ft (1 to 2 m). A 4.5 in (11.4 cm) o.d. high density polyethylene (HDPE) pipe was pulled in after each of the pilot bores were completed. Thrust/pulling force, spindle torque, and drilling fluid pressure were all monitored via the pressure gauges on the boring units. Average drilling fluid flow rate was measured based on volumetric changes in the fluid mixing tanks during the length of the bore.

For pilot bore operations, Bennett, et al. found that rotational torque was directly proportional to the thrust required when boring through clay or sand backfill material. When boring through backfilled silt or in situ silt material, an inversely proportional relationship between thrust and rotational torque was noted.

When conducting backreaming operations, thrust and torque requirements were directly proportional in sand and silt, both backfilled and in-situ. No clear relationship between thrust and torque was noted in the backfilled clay material. A clay-gravel

material showed no clear relationships between thrust and torque in either pilot boring or backreaming operations.

No substantial variation in required pulling force for the backreaming operation was noted as compared to pullback distance. Sharp peak values in torque and thrust were noted in areas of large steering corrections within the bores.

In general, the reaming/pullback operation required lower thrust than the pilot bore operation, but required more torque than the pilot bore. The sand backfill required the lowest torque for the pullback operation and the highest torque for the pilot boring operation of the four soil materials tested.

Khan (1995) reported on additional testing conducted during a horizontal boring demonstration at Orlando, Florida subsequent to the WES tests. The soil at the test site was a silty sand. Boring units from three different manufacturers were used to a variety of sizes of HDPE pipes. Each of the bores at the Orlando demonstration featured a gradual horizontal curve near the middle of the bore as a demonstration of the steering capability of the units. Thrust, pulling force, and rotational torque data were collected in the same manner as at the test conducted at the Waterways Experiment Station. No mention was made as to the design of the reamer/compactors used during the test.

Khan (1995) reported that the thrust requirement for the pilot boring operations for the machines tested was found to gradually increase as the length of the bore increased. A correlation coefficient,  $R$ , of 0.73 was found in relating the thrust required to the bore distance at the Orlando test site. Relationship between pullback force and bore distance was very weak with an  $R$  value of 0.09. Pullback force was found to be strongly influenced by sharp deviations in the borepath.

For one of the boring units at the Orlando test, rotational torque during the pilot hole drilling process was found to exhibit a slight increase as bore length increased. Torque during the backreaming/pullback process was found to be higher and more uniform than that required for the pilot bore. No strong trend with bore distance was noted. Sharp deviations in bore path were found to increase torque in both the pilot boring and backreaming/pullback operations.

### ***Research Objectives***

Currently, there are few published studies dealing with the effects of boring parameters used during backreaming (e.g. rotational speed of pipe and cutter, rate of pull back, drilling fluid flow rate, cutting tool geometry, etc.) on the performance of the drilling unit and the forces on the installed utility lines. Drilling unit "performance", as used here, specifically refers to rotational torque level, pulling force level, and overall power usage. The interactions between these parameters, and between these parameters and soil type, are not well understood.

This project; funded in part by Charles Machine Works, Inc., a major manufacturer of horizontal boring equipment sought to:

- a) develop a methodology for repeatably and quantitatively testing the effect of changes in drilling parameters on the boring unit performance and the tensile force applied to the installed utility service line.
- b) determine relationships and interactions of selected parameters involved in boring to each other and to the drilling system.

- c) determine effects of parameter modifications in both cohesive and non-cohesive soil types and make qualitative assessments of any noted differences between the soil types.

By accomplishing these objectives, it was desired to give a more fundamental understanding of the backreaming/pull back process of horizontal boring. This should serve to improve boring success rates and provide more efficient utilization of available power for fluid assisted, mini-horizontal directional drilling systems.

## Chapter 2

### Experimental Parameters and Design

The boring parameters used in this study and their associated values were developed in consultation with Mr. Rex Nelson, Mr. Mark Kern, and Mr. Brent Stephenson of the Charles Machine Works in Perry, Oklahoma. The parameters used represent the areas of knowledge deemed most needed by the horizontal boring industry and the Charles Machine Works in particular. Procedures for the testing were developed by Mr. Floyd Gunsaulis, primary researcher for the project and author of this report.

At each site it was desired to test the effects of spindle rotation rate and pullback rate on spindle torque, pulling force (both at the boring unit and at the pipe), and, by extension, power usage. A factorial experiment was developed with four predetermined rotation speeds and three pullback rates, for a total of twelve combinations. The experimental design for both of the test sites was generated in consultation with Dr. Mark Payton (1996) of the Oklahoma State University Statistics Department. A description of each of the test sites is given in Chapter 3 of this report.

#### Coyle Test Site

The experimental design used at the Coyle test site was a split plot model with fluid flow rate serving as the whole plot factor. Under the flow rate randomization restriction was a 4 X 3 factorial comprised of rotational speed and pullback rate. Predetermined, randomized order for the rotational speed/pull rate combinations within each bore were selected before the start of the test. The fluid flow rates tested were 7.4,

10.6, and 15.5 gal/min ( 28.0, 40.1, and 58.7 l/min). The rotational speed rates used were 96, 128, 160, and 192 rpm. Pull rates used were 1.8, 2.7, and 3.6 ft/min (0.55, 0.82, and 1.10 m/min). Four replications were made with each drilling fluid flow rate for a total of 12 bores at the Coyle test site.

The experimental model may be appropriately expressed as:

$$M_{ijkl} = \mu + P_{ijkl} + D_{ijkl} + F_i + B_{j(i)} + R_k + V_l + RV_{kl} + FR_{ik} + FV_{il} + FRV_{ikl} + \delta_{ijkl}$$

Where:

$M_{ijkl}$  = the measured reading (whether Torque, Pulling force at the boring unit, or Pulling force at the HDPE pipe) of a sample using the  $i^{\text{th}}$  fluid flow rate, during the  $j^{\text{th}}$  bore within that flow rate, at the  $k^{\text{th}}$  rotational speed, being pulled at the  $l^{\text{th}}$  pull rate.

$\mu$  = the overall mean of the torque, boring unit pull force, or pipe pull force readings

$P_{ijkl}$  = the soil strength effect as determined by the penetrometer reading corresponding to the  $M_{ijkl}$  reading

$D_{ijkl}$  = the effect of distance along the borepath corresponding to the  $M_{ijkl}$  reading, included only in models involving pull force and not in torque model

$F_i$  = the effect of the  $i^{\text{th}}$  drilling fluid flow rate

$B_{j(i)}$  = the effect of the  $j^{\text{th}}$  bore nested within the  $i^{\text{th}}$  flow rate (Used as the error term for analysis of Flow rate)

$R_k$  = the effect of the  $k^{\text{th}}$  rotational speed

$V_l$  = the effect of the  $l^{\text{th}}$  pull rate

$RV_{kl}$  = the two way interaction effect between rotation speed  $k$  and pull rate  $l$



$FR_{ik}$  = the two way interaction effect between flow rate  $i$  and rotation speed  $k$

$FV_{il}$  = the two way interaction effect between flow rate  $i$  and pull rate  $l$

$FRV_{ikl}$  = the three way interaction effect between flow rate  $i$ , rotation speed  $k$ , and pull rate  $l$

$\delta_{ijkl}$  = the random error term for an individual observation

$F$ ,  $R$ ,  $V$ ,  $FR$ ,  $FV$ ,  $RV$ , and  $FRV$  are all fixed effects.

$P$ ,  $D$ , and  $B$  are all random effects.

One key assumption was made for the purpose of simplification of the analysis. A completely randomized design would have chosen flow rates for each bore at random. Flow rates between bores 5-12 were chosen randomly between the 7.4 and 10.6 gpm (28.0 and 40.1 lpm) flow rates. Because of the need for special setup and equipment to conduct the 15.5 gpm (58.7 lpm) bores, as discussed further in Chapters 3 and 4, these were conducted in bores 13-16. An assumption is made that no substantial change of ground conditions occurred during these bores such that any change in the performance of the boring unit due to inability to fully randomize the order of the bores, is negligible.

#### Stillwater Creek Test Site

The experimental design used at the Stillwater Creek test site was a split plot model with reamer/compactor design serving as the whole plot factor. Under the reamer/compactor design randomization restriction was a 4 X 3 factorial comprised of rotational speed and pullback rate. Predetermined, randomized order for the rotational speed/pull rate combinations within each bore were selected before the start of the test. Two different reamer/compactor designs were used. These are described further in Chapter 4, Procedures. Illustrations of the reamers are given in Figures 16 and 17 on

Pages 53 and 54. The rotational speed rates used were 96, 128, 160, and 192 rpm. Pull rates used were 1.8, 2.7, and 3.6 ft/min (0.55, 0.82, and 1.10 m/min). Four replications were made using each reamer/compactor design for a total of 8 bores at the Stillwater Creek location.

The experimental model may be appropriately expressed as:

$$M_{ijkl} = \mu + P_{ijkl} + D_{ijkl} + C_i + B_{j(i)} + R_k + V_l + RV_{kl} + CR_{ik} + CV_{il} + CRV_{ikl} + \delta_{ijkl}$$

Where:

$M_{ijkl}$  = the measured reading (whether Torque, Pulling force at the boring unit, or Pulling force at the HDPE pipe) of a sample using the  $i^{\text{th}}$  reamer design, during the  $j^{\text{th}}$  bore utilizing that reamer, at the  $k^{\text{th}}$  rotational speed, being pulled at the  $l^{\text{th}}$  pull rate.

$\mu$  = the overall mean of the torque, boring unit pull force, or pipe pull force readings

$P_{ijkl}$  = the soil strength effect as determined by the penetrometer reading corresponding to the  $M_{ijkl}$  reading

$D_{ijkl}$  = the effect of distance along the borepath corresponding to the  $M_{ijkl}$  reading, included only in models involving pull force and not in torque model

$F_i$  = the effect of the  $i^{\text{th}}$  reamer/compactor design

$B_{j(i)}$  = the effect of the  $j^{\text{th}}$  bore nested within the  $i^{\text{th}}$  reamer design (Used as the error term for analysis of Reamer)

$R_k$  = the effect of the  $k^{\text{th}}$  rotational speed

$V_l$  = the effect of the  $l^{\text{th}}$  pull rate

$RV_{kl}$  = the two way interaction effect between rotation speed  $k$  and pull rate  $l$

$CR_{ik}$  = the two way interaction effect between reamer design  $i$  and rotation speed  $k$

$CV_{il}$  = the two way interaction effect between reamer design  $i$  and pull rate  $l$

$CRV_{ikl}$  = the three way interaction effect between reamer design  $i$ , rotation speed  $k$ , and  
pull rate  $l$

$\delta_{ijkl}$  = the random error term for an individual observation

$C$ ,  $R$ ,  $V$ ,  $CR$ ,  $CV$ ,  $RV$ , and  $CRV$  are all fixed effects.

$P$ ,  $D$ , and  $B$  are all random effects.

## Chapter 3

### Test Locations and Equipment Used For Study

#### *Test Locations*

##### Coyle Test Site

The first set of test bores was conducted in a wheat field located along the Cimarron River between Stillwater and Coyle in Payne County, Oklahoma. Legal description of the site is the SE  $\frac{1}{4}$  of the NE  $\frac{1}{4}$  of Section 14, Township 17N, Range 1E, of the Indian Meridian. The USDA Soil Conservation Service (1987) soil survey map lists the soil as belonging to the Hawley series. These soils are made up of alluvial sand/loam deposits. Typical soil textures are a fine sandy loam from 0-10 inches (0-25 cm) in depth, fine sandy loam to loam from 10-32 inches (25-81 cm), and a stratified loamy fine sand to a silty clay loam from 32 to 60 inches (81-152 cm). The soils are typically non-plastic or have low plasticity with Plasticity Indexes less than 10%.

##### Stillwater Creek Test Site

The second set of tests were conducted on land belonging to Oklahoma State University along the west side of Oklahoma Highway 86 running between Highway 51 and Perry, Oklahoma. The land was situated just north of Stillwater Creek at the upper end of Lake Carl Blackwell in Payne County. Legal description of the location is the N  $\frac{1}{2}$  of the N  $\frac{1}{2}$  of the NE  $\frac{1}{4}$  of Section 10 of Township 19N, Range 1W of the Indian Meridian. This area is described by the USDA Soil Conservation Service (1987) as belonging to the Pulaski series as a fine sandy loam. The soil is more correctly described by Gray and Nance (1978) as being a Port loam. Port soils are described as a dark,

reddish brown loam from 0-25 in (0-63 cm) and a reddish brown clay loam from 25-65 in (63-165 cm).

### ***Boring Unit***

The boring unit used for the study was a modified version of the Jet Trac® 4/40 A directional drilling unit manufactured by the Charles Machine Works (CMW) in Perry, OK. The serial number of the unit was 2K0871. A picture of the unit is given in Figure 6 on Page 31. The boring unit, as produced by CMW, has a theoretical rotational torque capability of \*1125 ft-lb (1530 N-m) and thrust and pullback capabilities of \*7700 lb (34.2 kN) and \*9600 lb (42.7 kN), respectively. The unit has a theoretical maximum spindle rotation speed of \*162 rpm. (\* Note: The values listed here are theoretical. These are based on calculation given the components and relief settings on the 4/40 A boring unit, and do not represent the manufacturer's published values.)

The modifications made for testing purposes included a change of the sprocket on the hydraulic motor driving the spindle. The unit was originally equipped with a 14 tooth double No. 60 sprocket on the hydraulic motor driving a 25 tooth sprocket on the spindle. The sprocket on the hydraulic motor was replaced with a 15 tooth sprocket to yield a higher rotational speed. To ensure that torque capability was not diminished, the relief setting on the high side of the loop driving the rotational motor was increased from 2500 psi (17.2 MPa) to 2750 psi (19.0 MPa). Thus, theoretical torque for the unit was increased to 1155 ft-lb (1570 N-m).

The directional control valve bank was also altered. The boring unit, as produced, utilizes a Gresen V-20 valve stack. The manual actuation valve sections responsible for control of thrust and rotational speed were replaced with Gresen V20-EPC-IH electronic

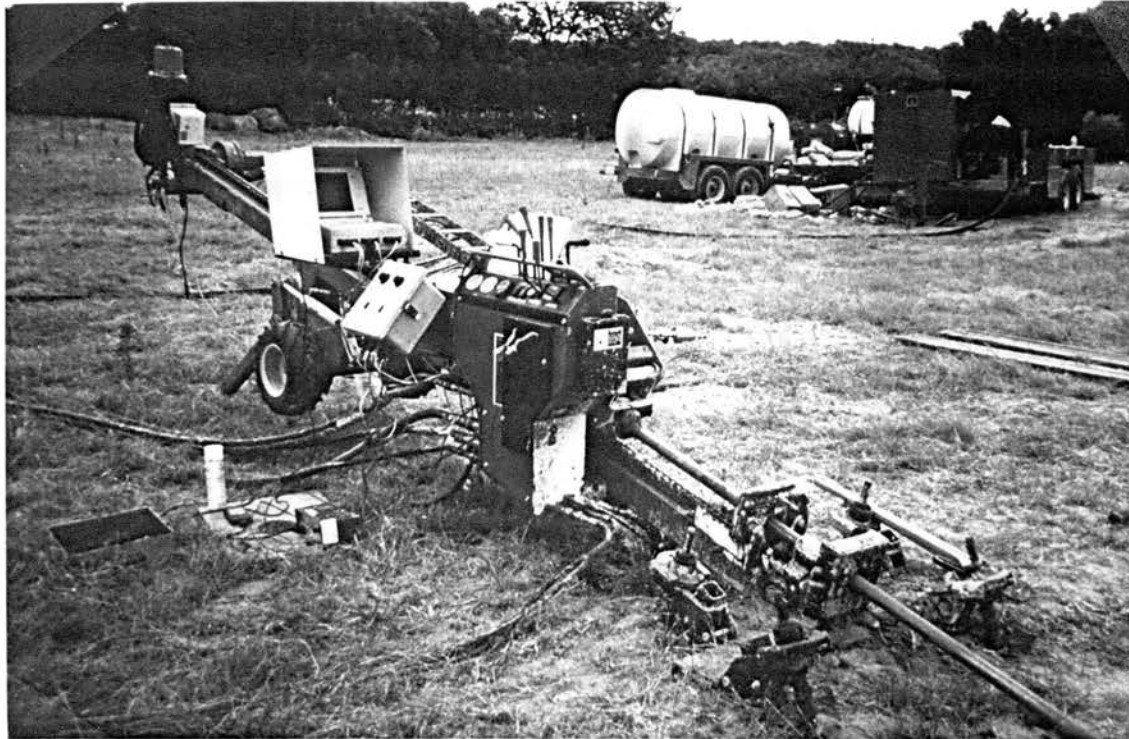


**Figure 6:** Picture of Jet Trac 4/40A boring unit ready to begin backreaming procedure.  
Note equipment trailer with hydraulic power supply in background.

proportional control valve sections. The valve sections utilize a pulse-width modulated signal to control a solenoid which regulates hydraulic oil flow. The Gresen V20-EPC-IH sections are unique in that they also have a manually actuated handle so that the valve sections may be operated either manually or by electronic proportional control. These sections were used so as to allow the pilot bore to be controlled manually and the backream/pull back of the installed service line to be accomplished with computer control.

The V20-EPC-IH valve sections require a pilot pressure signal to be able to operate under pulse-width-modulated control. This pilot pressure was provided by a Gresen 20-SOL-I-UT-12 utility section placed just before the outlet cover on the Gresen V-20 valve stack (See Figure 7 on Page 33). When actuated by a 12 volt signal, this valve section provides a 250 psi (1724 kPa) pilot pressure to the EPC valve sections via internal pilot ports within the valve stack. Since the EPC sections were not immediately adjacent to the utility section in the V-20 valve stack, the pilot ports had to be specially drilled in each directional control section between the 20-SOL-I-UT-12 section and the EPC sections. This was accomplished according to drawings provided by Gresen indicating the size and locations of the pilot ports.

### ***The Hydraulic Power Supply***

The Jet Trac® 4/40 A comes from the factory with a Ditch Witch® PP50 hydraulic power supply. This unit utilizes a 50.4 hp (37.6 kW) Deutz diesel engine to drive the hydraulic pumps for the unit. It was recognized that since rotational speed and pull rate regulation during the backreaming sections of a bore control were going to be accomplished using electronic proportional control, a substantial amount of power would be wasted during the low-speed runs of the boring unit. This was due to the fact that full

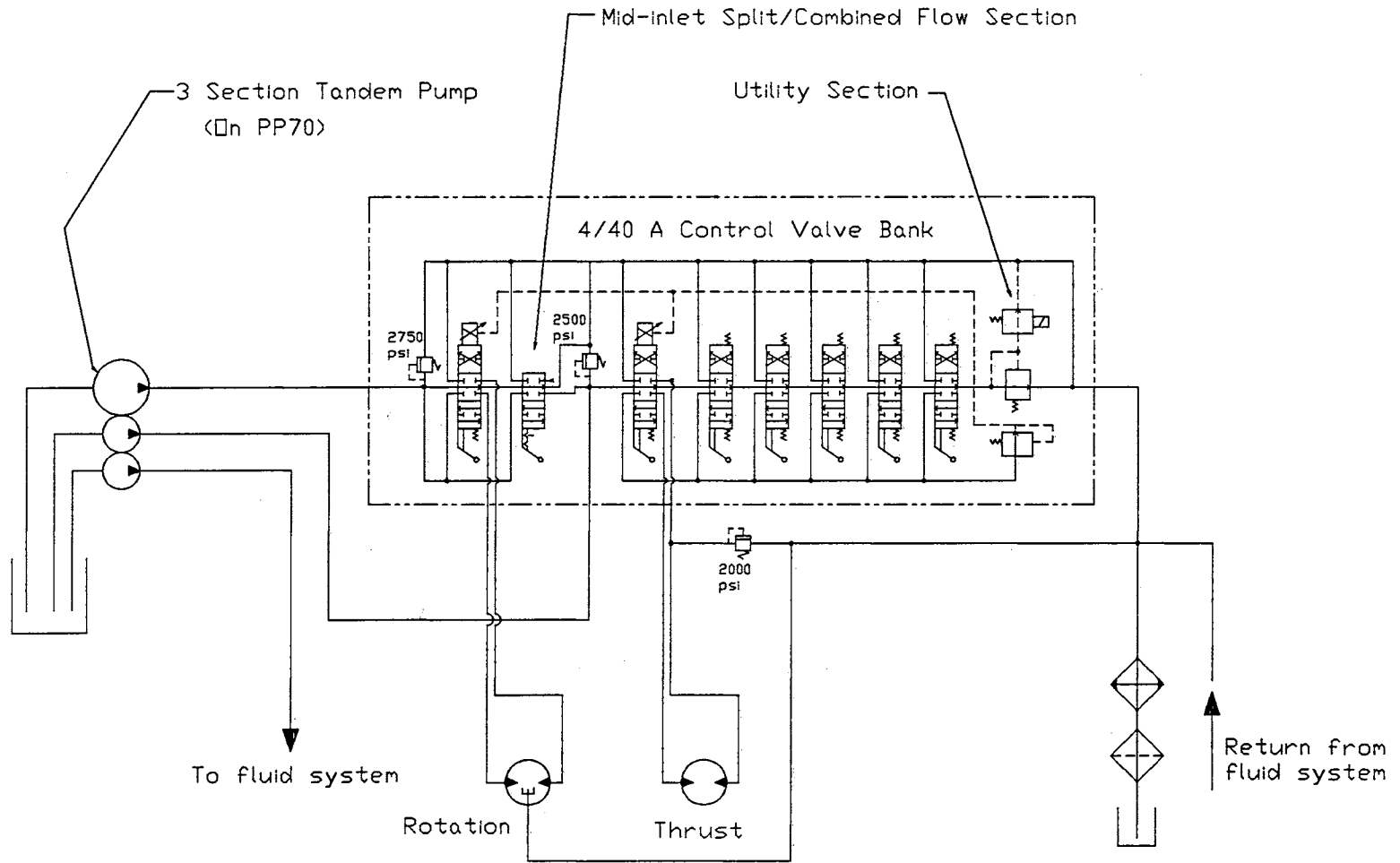


**Figure 7:** Hydraulic schematic for modified Jet Trac 4/40 A boring unit.



hydraulic oil flow came into the EPC valve sections, but only a small portion of that would be metered out to the designated hydraulic motor. The rest of the flow, at an elevated pressure, would be dumped back to the return line. This dumping of pressurized flow is the cause of the hydraulic inefficiency. To compensate for this inefficiency, the PP50 power supply was replaced with a Ditch Witch PP 70 power supply, serial number 6K0221. This power supply features a 68 hp (50.7 kW) turbocharged version of the Deutz diesel engine found on the PP50.

It was desired for the purposes of the field testing to have independence of the thrust/pullback and rotational functions at the boring unit. As manufactured, the 4/40 A boring unit has a tandem hydraulic gear pump with two pump sections. The smaller pump provides hydraulic oil for driving the fluid mixing and pumping system on the equipment trailer. The second, larger displacement hydraulic pump supplies oil for all functions on the boring unit (See Figure 8, Page 35). The displacements of the pump sections for the boring unit functions and the fluid system functions were 2.24 in<sup>3</sup>/rev (36.7 ml/rev) and 1.17 in<sup>3</sup>/rev (19.2 ml/rev), respectively. Rated operating speed for the power supply engine was 2500 rpm. This resulted in theoretical flow capacities of 24.2 gal/min (91.8 l/min) and 12.7 gal/min (48.1 l/min) for the boring unit and fluid system functions, respectively.

A diverter valve in the Gresen V-20 valve stack on the boring unit is used to allocate oil flow between the hydraulic motors used for thrust and rotation when conducting a bore. Typical operation involves placing the directional control valve section for spindle rotation in the fully open mode and then utilizing the diverter to shunt enough oil flow to the thrust motor to handle the pulling rate requirements. This hydraulic

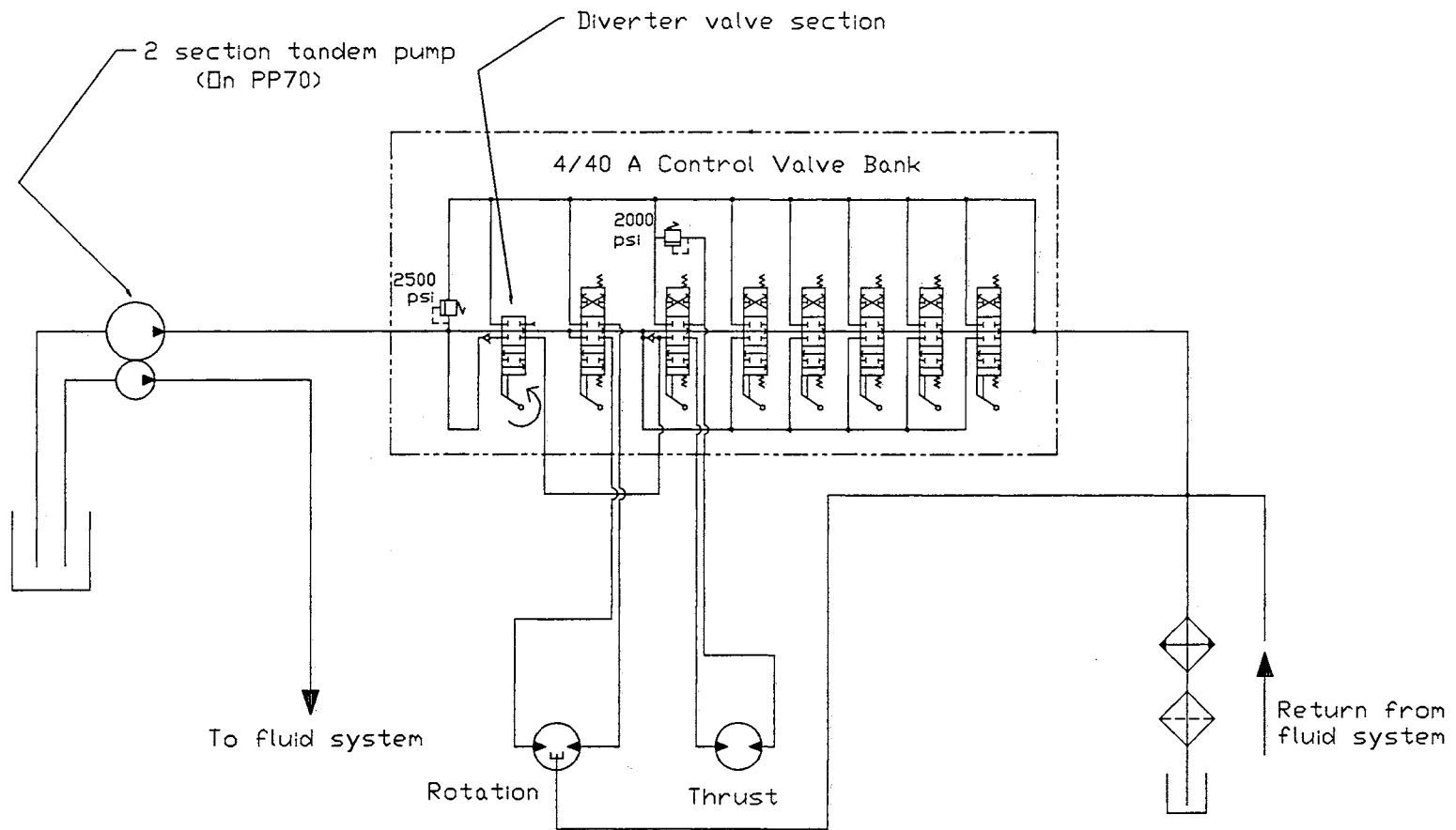


**Figure 8:** Original Jet Trac 4/40 A hydraulic schematic.

arrangement works acceptably for most purposes, but changes in the rate of pull affect the rotation speed of the unit (Gunsaulis, 1996).

To eliminate this problem, a three-section tandem pump was attached to the engine of the hydraulic power supply (See Figure 7, Page 33), allowing one pump to provide oil for thrust and auxiliary functions, a second pump to be used for the rotation function of the boring unit, and the third pump to supply oil to the drilling fluid system. By running a second set of hoses to the boring unit and eliminating the diverter section from the V-20 valve stack on the boring unit, independence of function was gained for thrust and rotation. A special mid-inlet section on the valve stack on the boring unit allowed the combining of thrust and rotation flows at the boring unit for the purpose of obtaining rapid movement of the boring unit carriage during the addition or removal of joints of drilling pipe (See Figure 7 Page 33). The flow could be easily combined when rapid carriage travel was desired, and then separated again before beginning another pullback of a drilling pipe.

Displacements on the three-section tandem pump were 2.92 in<sup>3</sup>/rev (47.9 ml/rev), 1.20 in<sup>3</sup>/rev (19.7 ml/rev), and 0.66 in<sup>3</sup>/rev (10.8 ml/rev) for the rotation function, drilling fluid system, and thrust and auxiliary functions, respectively. Operating speed of the power pack was reduced to 2350 rpm. The resulting theoretical maximum flow for the rotation function was 29.7 gal/min (112.4 l/min). The increase in flow coupled with the 15 tooth sprocket replacement on the boring unit yielded a theoretical maximum rotational speed of 217 rpm. Resulting theoretical maximum flows for the fluid system and thrust functions were 12.2 gal/min (46.2 l/min) and 6.7 gal/min (25.4 l/min), respectively.

## *Electronics/Data Acquisition Systems on the Boring Unit*

### Computer/Data Acquisition Interface

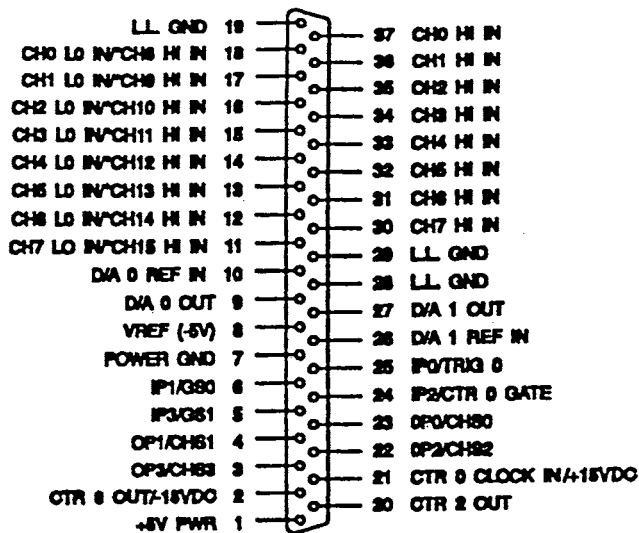
Boring unit performance data was collected and stored on a Toshiba T2200SX laptop computer, serial number 09116276. The computer had a 386 microprocessor with a clock speed of 20 MHz. The data acquisition interface for the computer was an IOTech Daqbook 100 data acquisition system, serial number 070030.

The Daqbook 100 data acquisition system features three input/output ports. Port P1 is the analog input/output port. Port P1 has 8 differential or 16 single ended analog/digital input channels and 2 digital/analog output channels. Each of the analog input channels utilizes a 12 bit A/D converter. Port P2 is the digital input/output port. Port P2 has 24 digital/input output channels. Port P3 is the pulse/frequency/high speed digital input port and is responsible for pulse counting functions. Figure 9 on Page 38 shows the pin connections for each of the three ports on the Daqbook 100 as listed by IOTech (1993).

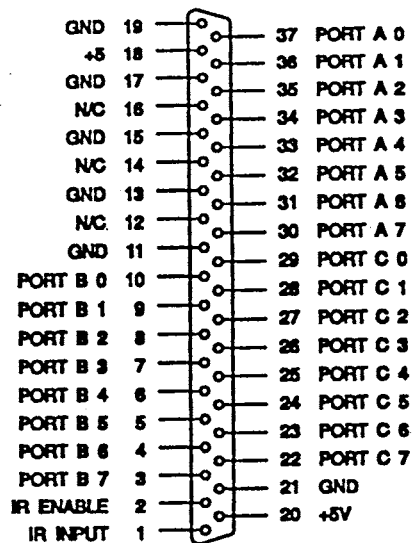
For the test, the Daqbook 100 was configured internally to accept single ended analog inputs. Analog channels may be set for 1, 2, 4, or 8X gain. Gains were set for each of the analog channels via software commands from the Toshiba laptop computer. Analog input ranges at a 1X gain for the Daqbook 100 are  $\pm 5$  V dc in the differential mode and 0-10 V dc in single ended mode.

### Pressure Transducers

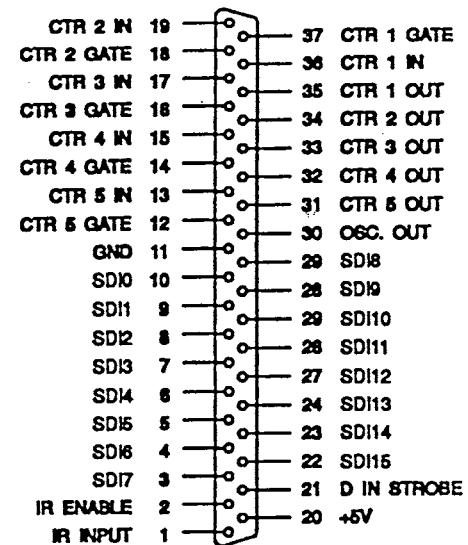
Four strain-gauge type pressure transducers were used on the boring unit. A transducer was mounted on each of the high and low pressure sides of the thrust and rotation loops at the boring unit. The transducers were mounted at the inlet and outlet



Port P1 Analog I/O



Port P2 Digital I/O



Port P3 Pulse/Frequency/  
High Speed Digital Inputs

Figure 9: Daqbook 100 pin connection diagrams. (IOtech, 1993)

ports of the hydraulic motors driving the thrust and rotation functions. Quick-connect hydraulic fittings were installed at each of the mounting locations so the transducers could be quickly removed on a nightly basis to protect them from the weather and vandalism.

The pressure transducers used on the high pressure side of the thrust and rotation loops were Viatran Model 118 0-5000 psig (0-34.5 MPag) transducers with a nominal output of 3 mV/V of excitation at maximum rated pressure. The transducers are rated by the manufacturer to have a static error band within  $\pm 0.4\%$  of the calibrated span. Serial numbers for the original transducers used for the thrust and rotation functions were 1498300 and 14981400, respectively. Difficulty in obtaining consistent readings was experienced with transducer 1498300 during the first part of Bore 13 at the Coyle test site. It was replaced with a similar Viatran Model 118 0-5000 psig (0-34.5 MPag) pressure transducer, serial number 193295.

As the high-side transducer had a nominal output of only 3 mV/V at 5000 psi (34.5 MPa), this resulted in an output of approximately 30 mV at full pressure. The analog input channels on the Daqbook 100 have a maximum resolution of 0.305 mV (12 bit conversion of 1.25 V) when the unit is in single ended operation mode with the internal gain for a given channel set at 8X. This results in a maximum pressure resolution of approximately 51 psi (352 kPa). Since a resolution of this magnitude was entirely unacceptable for the experiment, separate signal conditioning modules had to be implemented for the high-side transducers.

Two Omega OM-5 strain gauge signal conditioning modules were used to amplify the pressure transducer output signal to an acceptable magnitude. The modules provided a linear amplification of a 0-30 mV input signal to a 0-5V output. An Omega OM-5-BP-

2-C two-channel back plane was ordered for mounting of the OM-5 modules, and to provide for physical connection of wiring to the OM-5 conditioning modules.

Omega PX603-3KG5V amplified pressure transducers were used for the pressure transducers placed on the low pressure side of the thrust and rotation loops. The serial numbers for the thrust and rotation transducers were 50709592 and 50608058, respectively. The transducers had a rated pressure range from 0-3000 psig (0-20.7 MPa) and were rated by the manufacturer to have an accuracy of  $\pm 0.4\%$  full scale from the best fit straight line (BFSL). The transducers have an internal amplification circuit and produce an output signal from 1 to 5 V dc which is directly proportional to the pressure across the full scale range. The transducers had to be selected with pressure ratings capable of full system pressure. The statement that these transducers were on the "low pressure" side of the thrust and rotation loops only pertains during the actual process of backreaming/pullback. During the process of creating a pilot bore, and as drilling rods are connected and disconnected from the boring unit, the pressures on the side of the loop where the Omega PX603 transducers were mounted can reach full system pressure. A wiring diagram of the drilling unit pressure transducers and their electrical connections is given in Figure 10 on Page 41.

#### Rotational Speed Sensor

Rotational speed was measured using a Shimpo Model MP-10 magnetic proximity pickup. As ferrous materials pass in close proximity to the magnetized sensor pole, a voltage spike is produced proportional to the change in magnetic flux intensity over the change in time. The face of the speed pickup was mounted so that it was in close proximity ( $\approx 0.05$  in, 0.13 cm) to a 120 tooth gear mounted on the output shaft of the

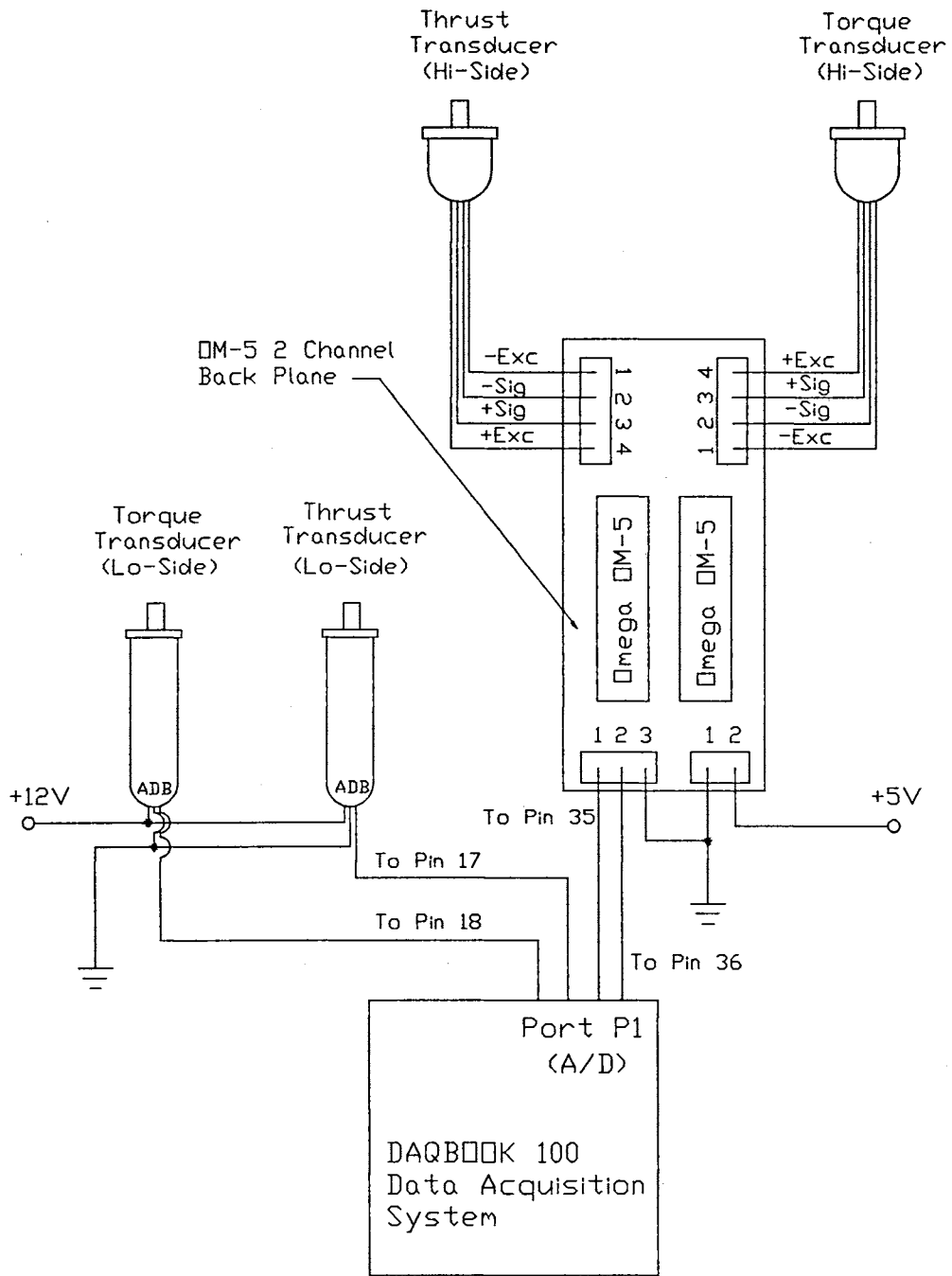


**Figure 10:** Boring unit pressure transducer electrical connections.



hydraulic motor which drove the spindle rotation. As the motor shaft rotated, the gear tooth passage in front of the magnetic pickup generated a sinusoidal output signal with frequency equal to that of the passing gear teeth. By measuring the number of teeth passing over a known time period, it was possible to measure the rotational speed of the hydraulic motor shaft, and by extension, the rotational speed of the spindle.

One problem which was faced was that the speed needed to be measured quickly. The control loop for the boring machine, which is further discussed in the Computer Program section of this chapter, was desired to execute at a rate of approximately 10 Hz. This meant that all measurements had to be taken in 100 ms or less. If tooth passage of a 120 tooth gear is counted over a 0.10 sec time interval, each tooth counted represents 5 rev/min of the hydraulic motor shaft.

A resolution of  $\pm 2$  rpm of the spindle was desired. To enhance the resolution of the speed measurement, the sinusoidal signal from the magnetic pickup was rectified and amplified using an absolute value circuit given by Frederiksen (1984). The rectified sine wave gives two pulses per gear tooth passage, in essence, doubling the resolution of the reading. Figure 11 on Page 43 gives an electrical connection schematic for the rotational speed measurement circuit. The amplification value of the absolute-value circuit is the ratio of the large to small resistance values plus 1. Thus, the circuit shown in Figure 11 has an amplification value of 11X.

To give a pure pulse for the counter on Port P3 of the Daqbook 100 to read, the rectified sinusoidal signal was passed through two inverting Schmitt triggers. The inverting Schmitt trigger produces a logical value of 0 when the incoming signal exceeds the threshold voltage level. When the incoming voltage signal to the inverting Schmitt

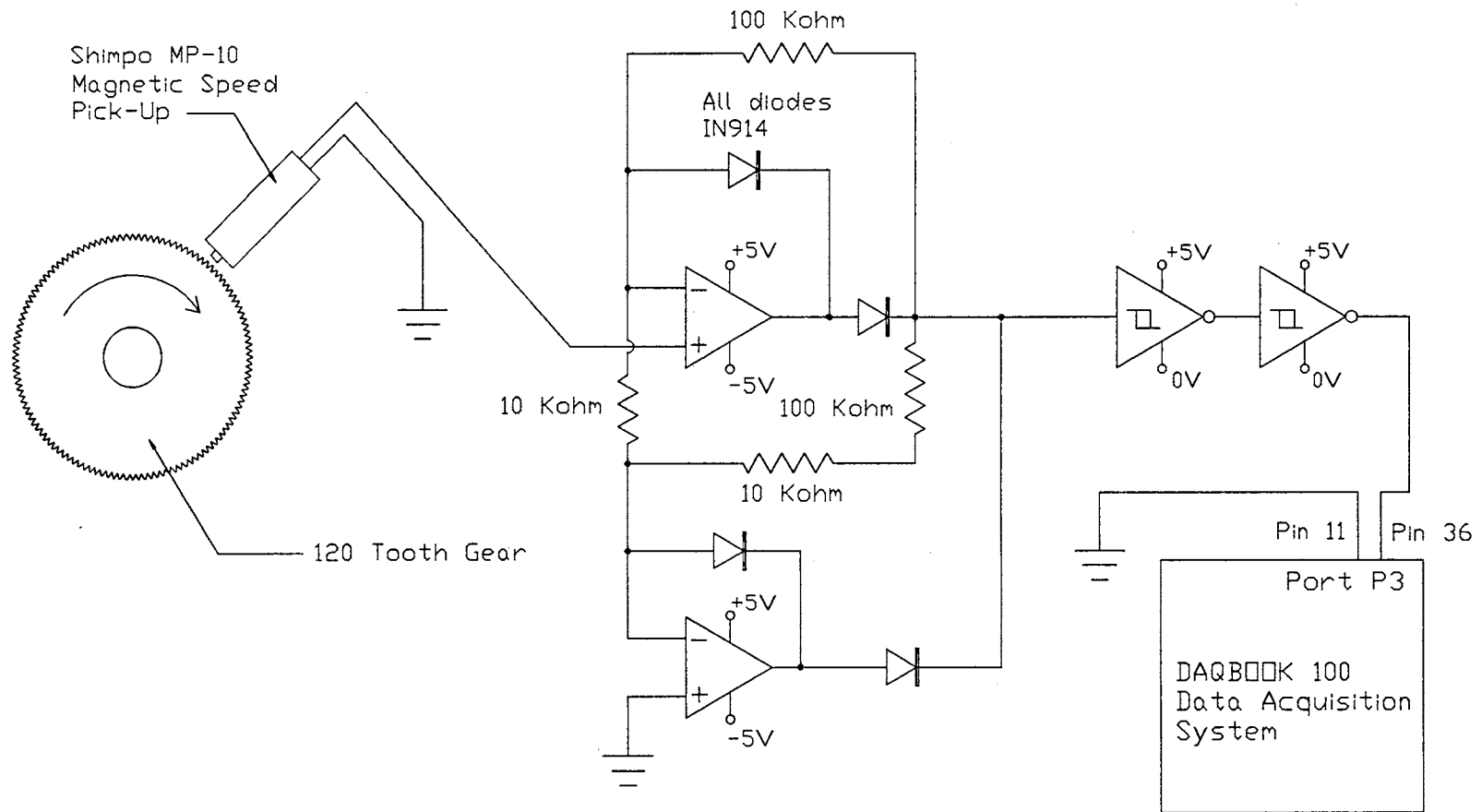


**Figure 11: Boring unit rotational speed measurement circuit.**

trigger drops below the threshold voltage level, a logical value of 1 is produced, equivalent to the supply voltage to the chip. By utilizing dual inverting Schmitt triggers, a stationary voltage pulse of  $\approx 5$  V was produced each time the rectified voltage reading surpassed the threshold voltage level of the Schmitt trigger chip.

To allow time for execution of other functions in the data acquisition control program, the rotational speed was sampled over a 90 ms time interval. By obtaining two pulses per every tooth pass on a 120 tooth gear, each additional tooth counted over the 90 ms time interval accounts for 2.78 rev/min. The ratio of the rotational speed of the hydraulic motor to that of the spindle is 5:3. Thus, the resolution of rotational speed obtained at the spindle was  $3/5$  of 2.78 rev/min, or 1.67 rev/min. This was within the desired 2 rev/min range.

#### Displacement/Velocity Transducer

A UniMeasure VP-150A position/velocity transducer, serial number 25013603, was used to measure the position and rate of travel of the carriage on the boring unit. A retractable cable in the transducer extended from the transducer housing to a hook on the drilling carriage (See Figure 12 on Page 45). As the drilling carriage traversed along the boring unit, the moving cable caused a multi-turn potentiometer in the transducer to adjust. The change in resistance in the potentiometer was calibrated to match the extension distance of the cable. At the same time, the movement of the cable drove a rotary tachometer which produced a voltage output proportional to the rate of travel of the cable, thus giving a measurement of the speed of the carriage.

A diagram of the electrical connections of the transducer is given in Figure 13 on Page 47. A unity gain voltage follower circuit was used to echo the voltage output from



**Figure 12:** Position/velocity transducer mounted at back of boring unit. Note the pressure transducers at the inlet and outlet of the hydraulic thrust motor.

the rotary tachometer to the data acquisition unit. This was done as the driving current output of the transducer by itself was low and caused problems with channel “cross-talk” on the Daqbook 100 data acquisition system. Measurement of the carriage position using the potentiometer circuit required the excitation voltage for the sensor to be known since the output of the potentiometer circuit was in  $mV/V_{\text{excitation}}/\text{distance}$ . The transducer required a 12 V excitation voltage, but the Daqbook 100 would only measure up to a +10 V signal. To measure the excitation voltage, a simple voltage divider circuit was used. The midpoint voltage was used as an input to the data acquisition system representing half of the excitation voltage.

### Temperature Circuit

Hydraulic oil temperature at the boring unit was monitored using a National LM-34DZ integrated-circuit temperature sensor. The LM-34DZ produces an output voltage which is linearly proportional to the Fahrenheit temperature of its case. The sensor was embedded in a 1/4” NPT pipe plug threaded into a fitting located within the console of the boring unit on the return side of the hydraulic oil loop. A small hole was drilled into the pipe fitting and the sensor was mounted into it using epoxy. Thus, the temperature sensor did not make direct contact with the hydraulic oil, but the brass fitting was in contact with the oil returning to the power pack. The return side of the hydraulic oil loop contained the hottest oil in the hydraulic system. The circuit for temperature sensing is also given in Figure 13 on Page 47. The output from the temperature sensor was also echoed to the data acquisition unit via a unity gain voltage follower.

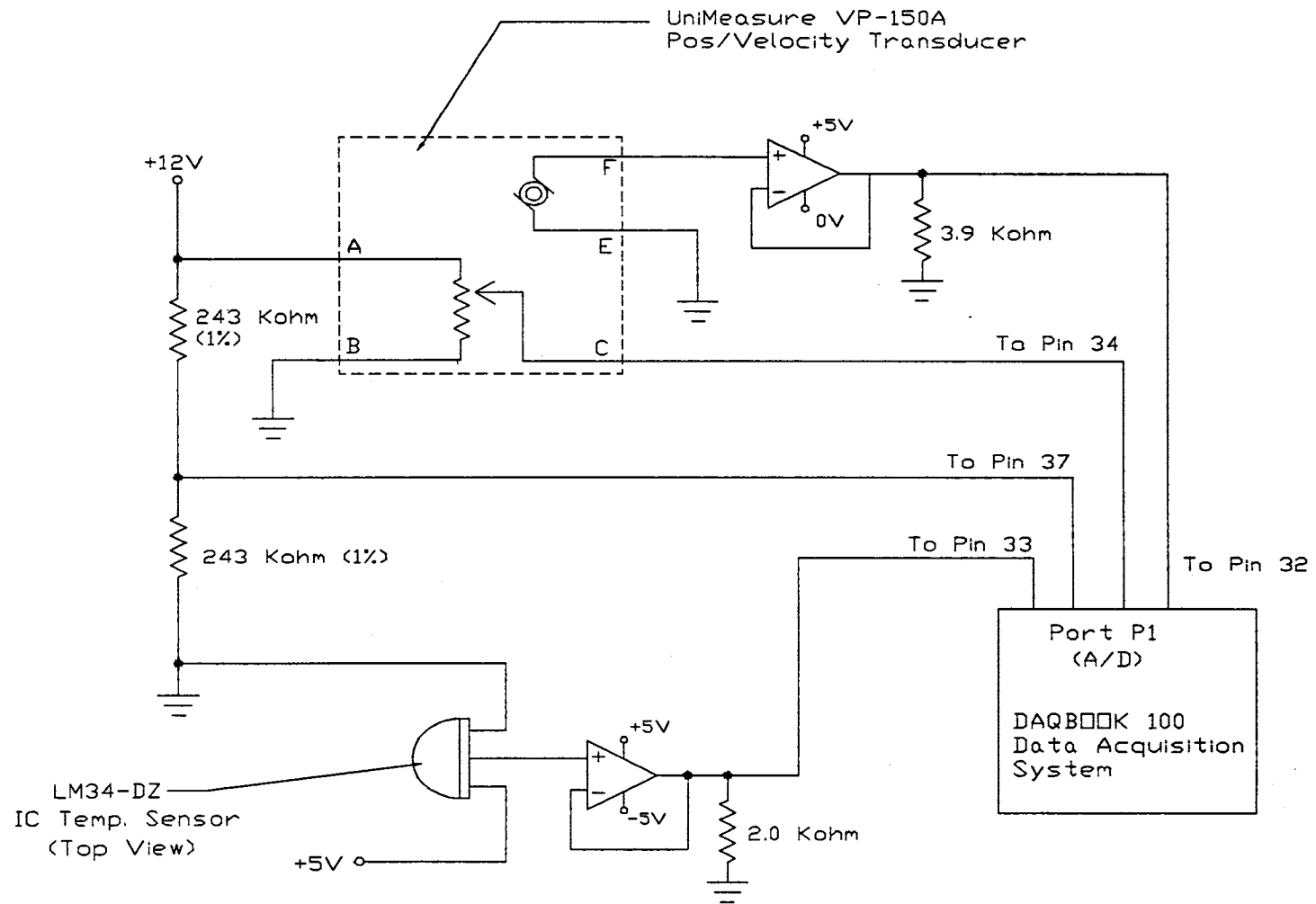


**Figure 13:** Position/velocity transducer and oil temperature sensor electrical connections.

### Flow Control Circuitry

A diagram of the circuitry involved in driving the hydraulic fluid control solenoids on the Gresen V20-EPC-IH directional control valve sections on the boring unit is given in Figure 14 on Page 49. Before the solenoid control sections can operate correctly, the Gresen 20-SOL-UT-12 must be actuated. A simple rocker switch connected to a 12 V power source was used to accomplish this task. A second rocker switch was used to dictate whether the directional control solenoids would operate under “manual” or “automatic” control.

When the switch was in the “manual” operation mode position and the data acquisition control program was executing, the laptop computer was programmed to measure the voltage at the wiper on the rotation and thrust potentiometers. The Daqbook 100 would then echo that same voltage back out of the two D/A output pins on Port P1. This signal went to the Gresen ABD-12 driver board where it was converted into a corresponding pulse-width-modulated signal to the directional control solenoids.

When the switch was in the “automatic” mode position, the computer would echo the voltage measured at the wipers of the potentiometers back out the D/A output pins on Port P1 until both the rotational speed and pull rate were within 10% of the set point values entered by the operator at the start of the execution of the control program. Once both the rotational speed and pull rate set points were reached, the control loop within the computer program would begin to execute and the voltages sent through the D/A outputs were dictated by the control algorithm and not by the potentiometers.

The Gresen ABD-12 driver board had adjustable mini-potentiometers for setting the offset and gain values for the output signals to the directional control solenoids. The

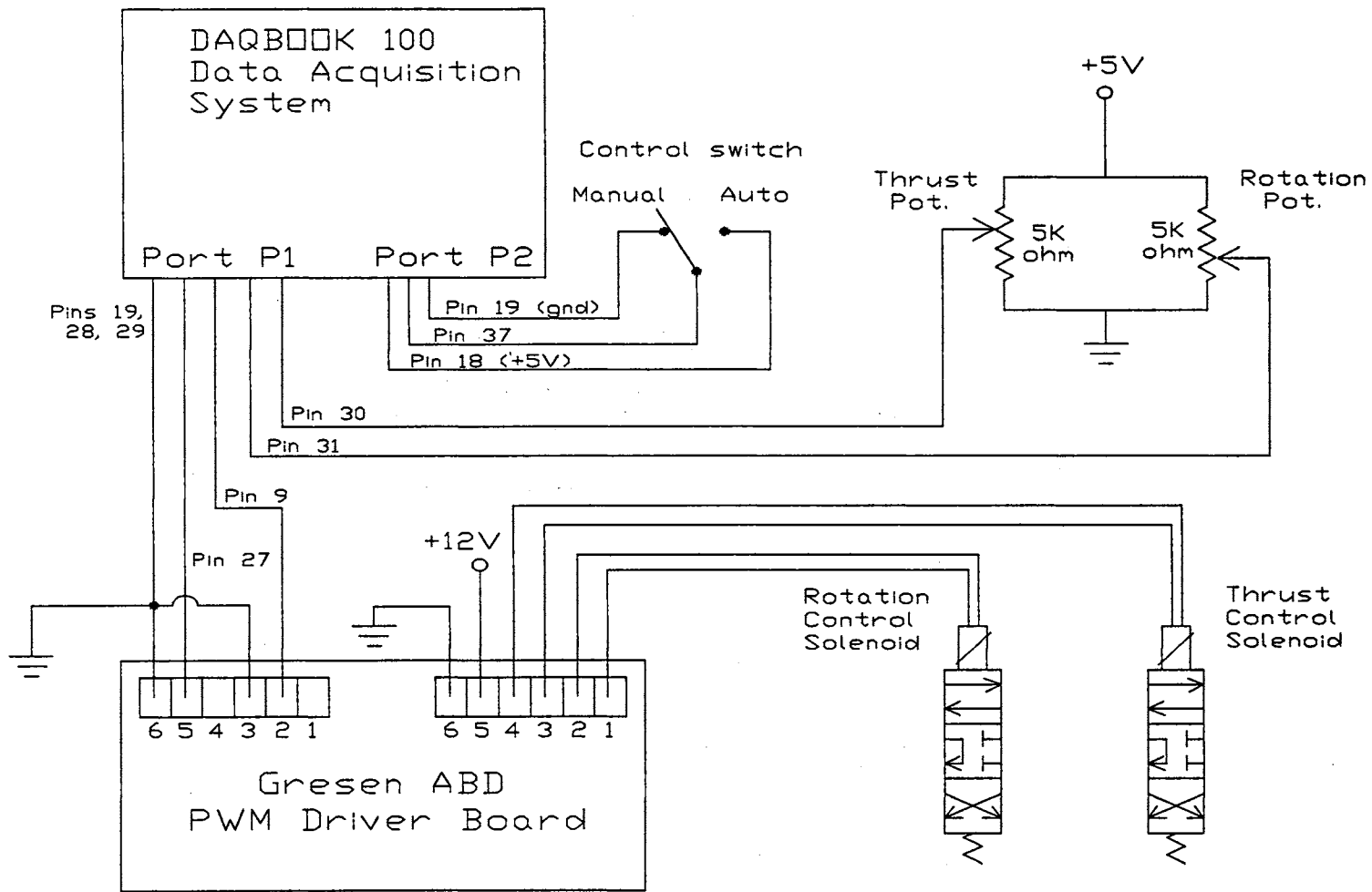


**Figure 14: Fluid control electrical connections.**



offset and gain potentiometers were adjusted until an input voltage signal of 0 V produced no flow through the control valve sections (0% “on” PWM signal), and an input voltage signal of 5 V produced full flow through the valve sections (100% “on” PWM signal).

### *The Fluid System*

The system for provision of drilling fluid to the boring unit is comprised of three main parts: the holding and mixing tank for the drilling fluid, the fluid pump, and the hydraulic system which powers both the fluid mixer and the fluid pump. The major change made in this system was to the hydraulic motor which drove the drilling fluid pump. The system was originally equipped with a 6.2 in<sup>3</sup>/rev (101.6 ml/rev) 2000 Series Char-lynn hydraulic motor. This motor was reworked and a two speed end section was added to it. This section allowed the motor to operate just as before when the motor was in the low speed setting. Addition of a 100 psi (690 kPa) pilot pressure source to the two speed end of the motor caused the motor to shift to a high speed mode in which the displacement of the motor was cut in half to 3.1 in<sup>3</sup>/rev (50.8 ml/rev). This action both doubled the speed of the motor and caused the maximum theoretical torque to be cut in half. The two speed set-up was to allow the fluid pump to provide up to 15 gpm (56.8 lpm) of drilling fluid flow. The fluid flow system was adjustable from the boring unit. A schematic of the hydraulic circuit for the drilling fluid system is given in Figure 15 on Page 51.

A potentiometer located at the drilling unit was used to adjust an Apitech flow control valve which metered flow to the hydraulic motor driving the fluid pump. Thus, in high speed mode, the fluid pump should have been capable of infinitely variable flow rates between 0 and 15 gpm (0 and 56.8 lpm). To help compensate for the loss of torque at the

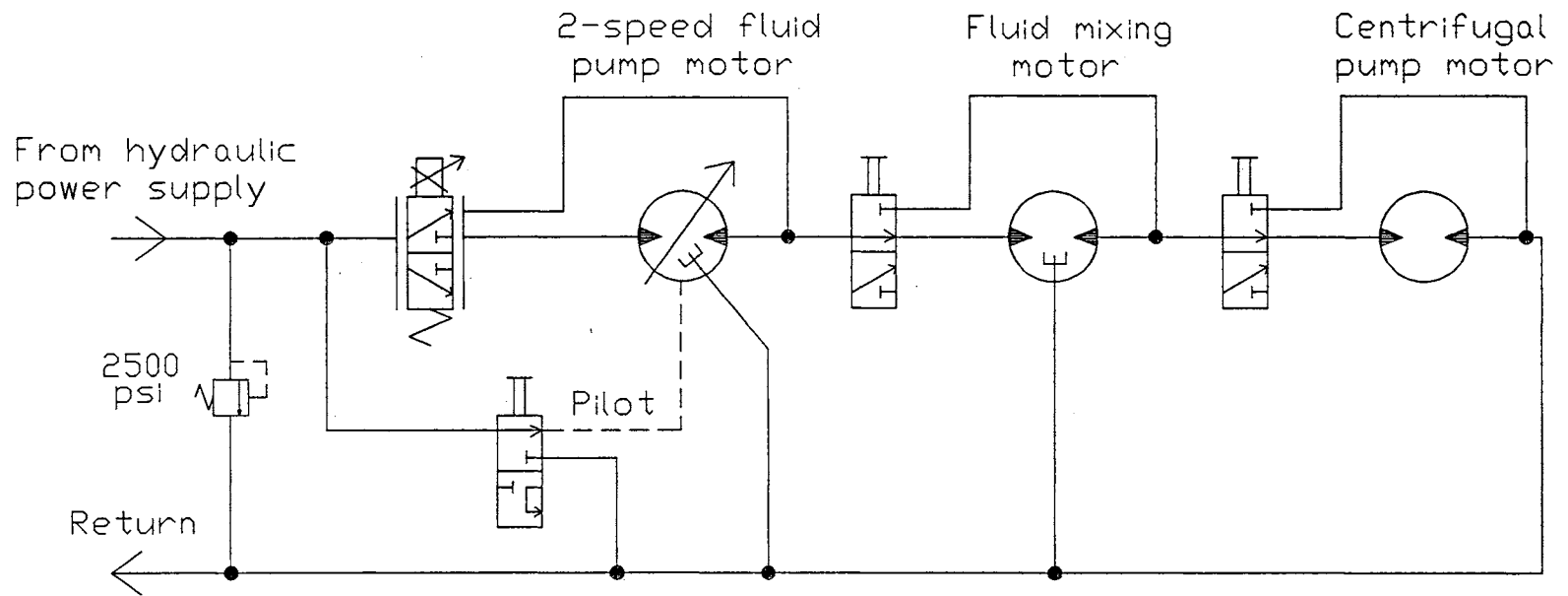


**Figure 15:** Drilling fluid hydraulic system schematic.

high speed setting, the hydraulic system relief on the fluid pump motor was increased from 2000 psi (13.8 MPa) to 2500 psi (17.2 MPa).

### ***The Trailer***

A Ditch Witch® TP 18 trailer was used for hauling the boring unit, hydraulic power pack, and drilling fluid mixing and pumping system. Two primary changes had to be made to the trailer. First, a hole had to be cut into the floor of the trailer underneath the PP70 hydraulic power supply. The hole was approximately 16 in X 36 in (41 cm X 91 cm). The purpose of the hole was to allow hot air within the power pack to escape through the floor of the trailer to aid the power pack in its ability to cool the hydraulic oil.

The second major change to the trailer was the addition of a second hose reel on the front of the trailer. The second hose reel was for the purpose of conveying oil from the pump on the engine responsible for flow for the thrust/pullback functions on the boring unit. To allow the power pack engine to be started when the boring unit was disconnected, or when the ambient temperature was cold, a bypass loop was plumbed for both hose reels to allow the hydraulic oil to circulate directly back to the reservoir instead of flowing through the umbilical hoses when the appropriate selector valves were shifted.

### ***Backreaming/Compacting Tools***

The backreamer used for all bores at the Coyle test site was a Charles Machine Works compact fluted reamer, CMW part number 359-333 (See Figure 16 on Page 53). The reamer had three "flutes" or spiral passageways along its length to allow the soil/fluid slurry to pass by. Along each of the flutes were two fluid orifices, for a total of six orifices on the reamer. At the Coyle test location, six orifices with 0.130 in (0.33 cm) opening diameters were used. At the Stillwater Creek location, the orifices were changed to 0.090

FRONT VIEW

SIDE VIEW

Outer Cutting Diameter

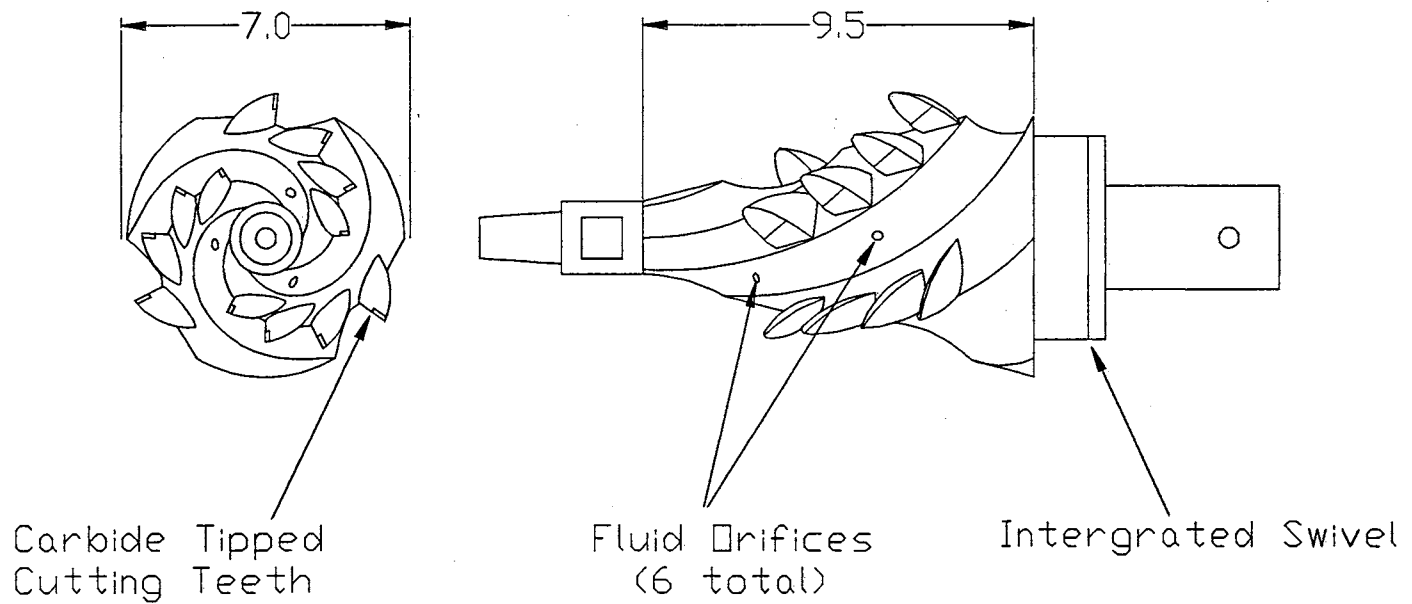


**Figure 16:** Fluted reamer used at Coyle and Stillwater Creek test sites.  
(Dimensions given in inches)

FRONT VIEW

SIDE VIEW

Outer Cutting Diameter

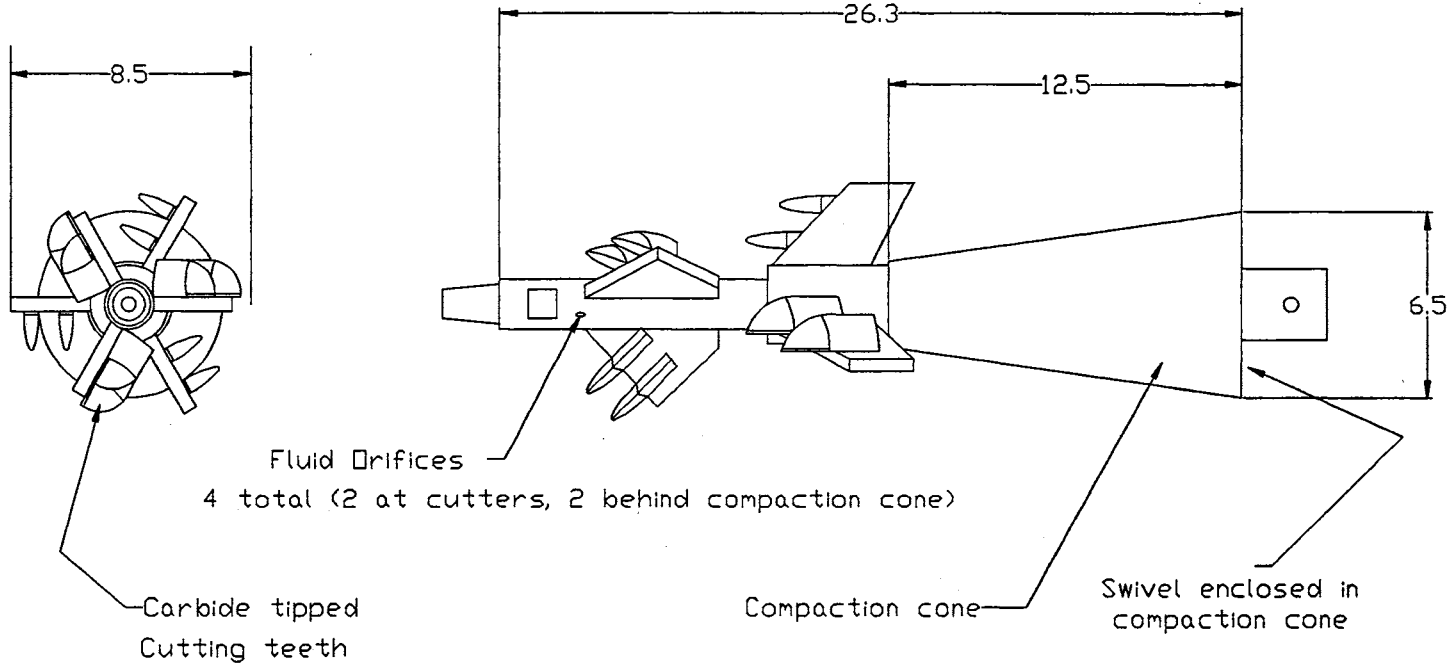


**Figure 17:** Winged reamer/compactor used at Stillwater Creek test site.  
(Dimensions given in inches)

in (0.23 cm) diameter openings. Carbide tipped cutting teeth along the ridges between the flutes provided the bulk of the soil cutting performed by the reamer. Outer cutting diameter for the reamer was 7.0 inches (17.8 cm). The swivel was integrated into the fluted cone, giving a compact design.

At the Stillwater Creek test site, the compact fluted reamer was used for half of the eight test bores, and the reamer/compactor shown in Figure 17 on Page 54 was used for the other half of the bores. The second, larger diameter wing cutter and the compaction cone both slid onto a swivel assembly with a hexagonal outer profile for transmitting torque to the cutter and compactor. The CMW part numbers for the swivel assembly and compaction cone were 355-364 and 355-635, respectively. The front cutter assembly and the second wing cutter were prototypes which were slight modifications of CMW part numbers 355-352 and 355-354, respectively. The outer cutting diameter of the front cutter was 7.25 in (18.4 cm), and the outer cutting diameter of the second cutter was 8.5 in (21.6 cm). Each cutter had three "wings" and each wing had 2 carbide tipped cutting teeth attached to it. There were two fluid orifices located near the first wing cutter, and two more orifices located within the hollow compaction cone. Diameter of the four orifices was 0.090 in (0.23 cm).

### ***Penetrometer/Soil Sampling Unit***

For this study, it was desired to have an index of the soil strength at various locations along the bore path to allow effects of changes in soil strength to be separated from the other variables measured in the test. A penetrometer/soil sampling unit was designed and constructed for this purpose as an attachment to a Ditch Witch® 6510 tractor owned by the Oklahoma State University Department of Biosystems and

Agricultural Engineering (See Figure 18, Page 57). The penetrometer cone was constructed and operated in accordance with specifications given in ASTM D 3441-86 (1994). Cone tip resistance alone was measured and no side friction readings were taken. An illustration of the penetrometer cone and push rods is given in Figure 19, Page 58. The penetrometer push rods were 28.4 in (72.1 cm) in length. Three of the rods were used for the test. Typical maximum measurement depth was  $\approx$  85 in (216 cm).

The penetrometer/soil sampling attachment consisted of an instrumented, flow controlled hydraulic cylinder for pushing the penetrometer rods into the ground, and a hole drilling apparatus. The hole drilling apparatus was composed of a hydraulic motor which was able to drive auger sections attached sequentially, end-to-end. A separate hydraulic cylinder was used to advance and retract the auger sections during the soil sampling operations.

Hydraulic power for the penetrometer/soil sampling unit was provided by the hydraulic ground drive circuit of the 6510 tractor. A schematic of the hydraulic circuit for the unit is given in Figure 20 on Page 59. A Brand Hydraulics model FCR 51 hydraulic flow control valve was used to maintain the 2 - 4 ft/min (1-2 cm/sec) penetrometer advance rate specified in ASTM D 3441-86 (1994).

The penetrometer cylinder and the soil sample apparatus were mounted on rollers on a frame built behind the tractor. Either attachment could be slid from the side to the centerline position on the attachment. In the cohesive soil locations, this gave the ability to auger a hole in the centerline location down to the depth of the bore. The auger attachment could then be pushed back to the side, and the penetrometer cylinder moved to the centerline position. By using an adapter, a 3 inch (7.6 cm) sampling tube could be



**Figure 18:** Penetrometer rig in use at Coyle test site. Auger sampling device is to the right of the penetrometer push cylinder.



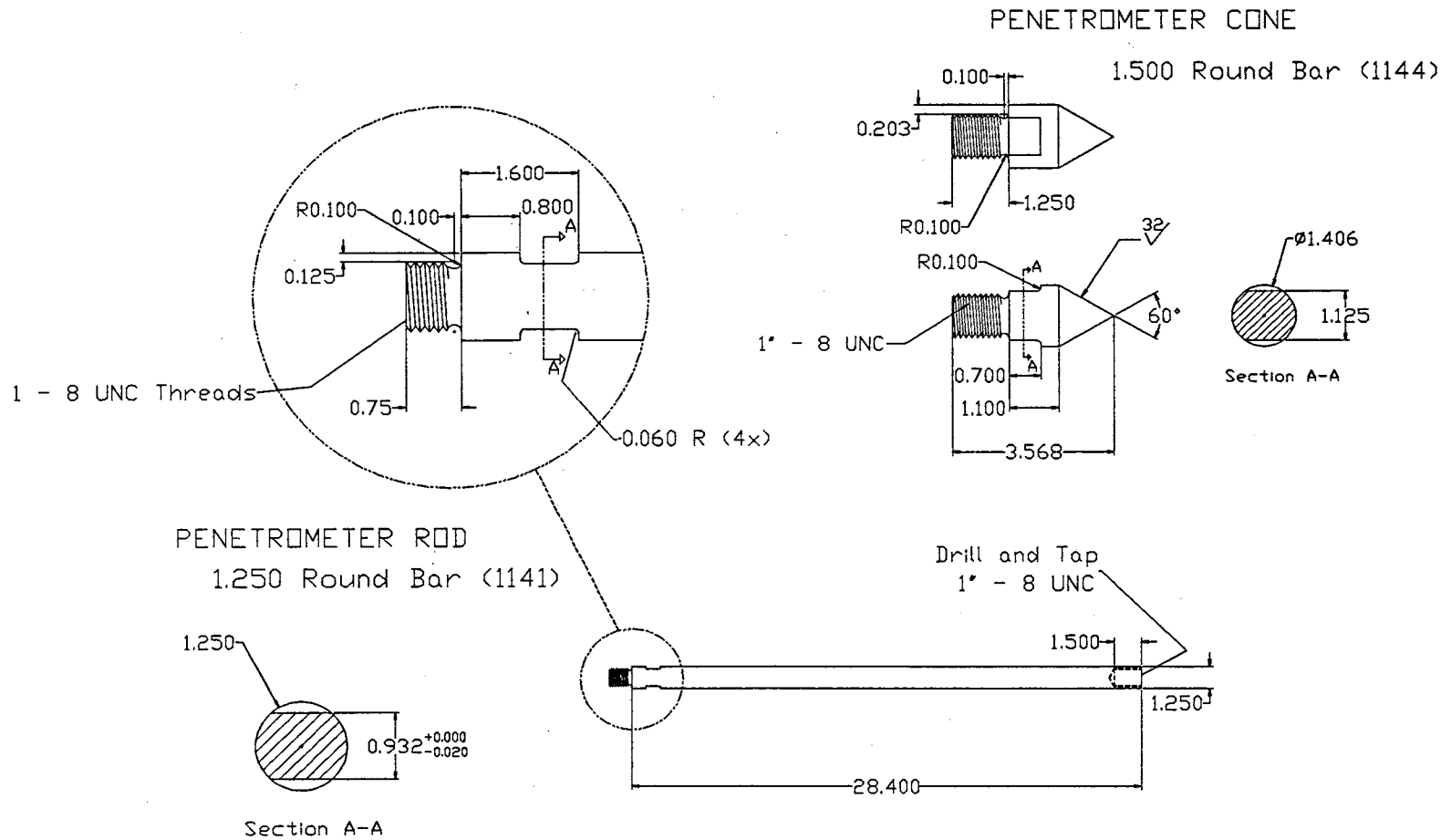


**Figure 19: Penetrometer cone and push rods.**  
(Dimensions in inches.)

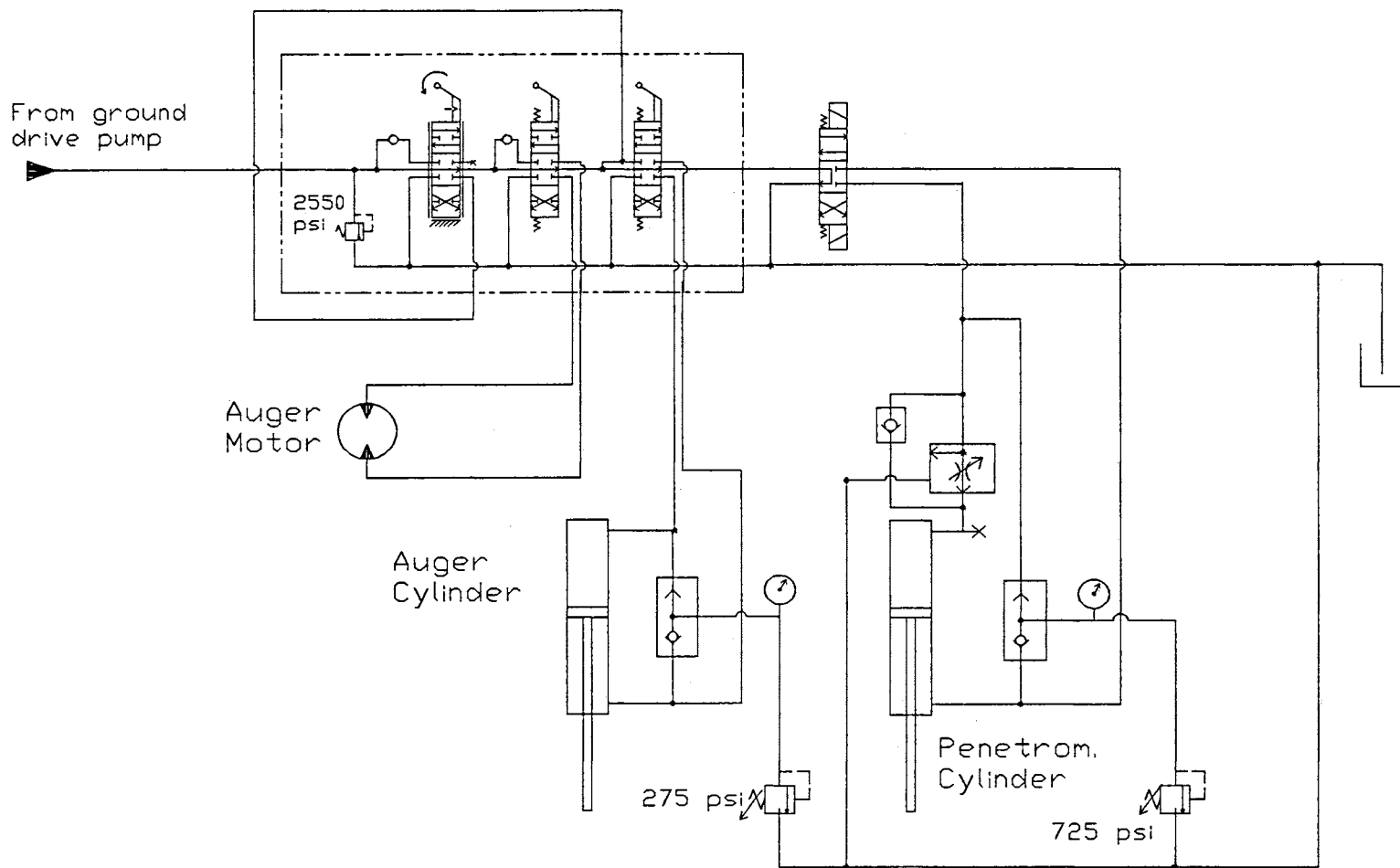


**Figure 20:** Penetrometer unit hydraulics.

attached to the penetrometer rods and an undisturbed soil core taken at the depth of the bore.

### ***Electronics/Data Acquisition Systems on Penetrometer Unit***

The same Toshiba T2200SX laptop computer and IOtech Daqbook 100 data acquisition interface that was used on the boring unit was used for collection of the penetrometer data. The data acquisition program was constructed in Snap-Master, a commercial data acquisition and manipulation package. The program read the sensor excitation voltage, and the signal voltages from the pressure and displacement transducers. It converted the penetrometer cylinder pressure readings into force values, provided an on-screen display of force vs. depth, and stored all data for later retrieval and analysis. Start and stop of the program were triggered manually. Readings were taken at a rate of 4 Hz.

The pressure transducer used for the penetrometer readings was a Setra Model 206, 0-1000 psig (0-6.9 MPa) capacitance type transducer, serial number 496417. The pressure transducer was rated by the manufacturer to have an accuracy of within 0.13% of the full scale reading from a best fit straight line calibration. The transducer was mounted at the outlet of the flow control valve which supplied oil to the barrel end of the penetrometer cylinder. Excitation voltage was provided using a regulated 12-V source mounted on the 6510 tractor.

The displacement transducer used for the penetrometer readings was a UniMeasure Model P-40A, serial number 24093100. The transducer used a retractable cable to measure the movement of the cylinder rod which pushed the penetrometer rods into the ground. The transducer was mounted on the side of the hydraulic cylinder body

and the retractable cable was attached to the connector between the end of the cylinder rod and the threaded connections on the penetrometer rods. Excitation voltage was provided using a 9.6 V regulated supply on the 6510 tractor. A diagram of electrical connections between the transducers and the data acquisition system is given in Figure 21 on Page 62.

### ***Fluid Mixing/Supply Truck***

As explained further in the Procedures section of this report, as each of the bores requiring 10.6 gal/min (40 l/min) or less was conducted, drilling fluid was mixed on a separate truck and pumped across to the holding tank on the boring unit equipment trailer. The pumping/mixing system on the supply truck was a Ditch Witch Fluid Pac 35. The unit is powered by a 34 hp (25 kW) Lister-Petter LPWS4 diesel engine.

The use of the separate system for drilling fluid mixing assured that during a backreaming/pullback procedure, no time was lost in having to stop the backreaming process to mix fluid on the boring unit trailer. It also allowed drilling fluid mixtures to be held consistent, as a full batch of drilling fluid could be mixed each time in the ratios prescribed for each soil type.

As described in the Procedures section of this report, the drilling fluid system on the equipment trailer proved unable to provide consistent flows at 15 gal/min (56.8 l/min). To enable bores to be successfully conducted at these higher flow rates, the Fluid Pack 35 was used as the pumping system during the high flow rate bores. The Fluid Pack 35 used was configured to allow pumping of drilling fluid at infinitely variable rates from 0 to 25 gal/min (95 l/min) at pressures up to 1500 psi. To allow the Fluid Pack 35 to be used for

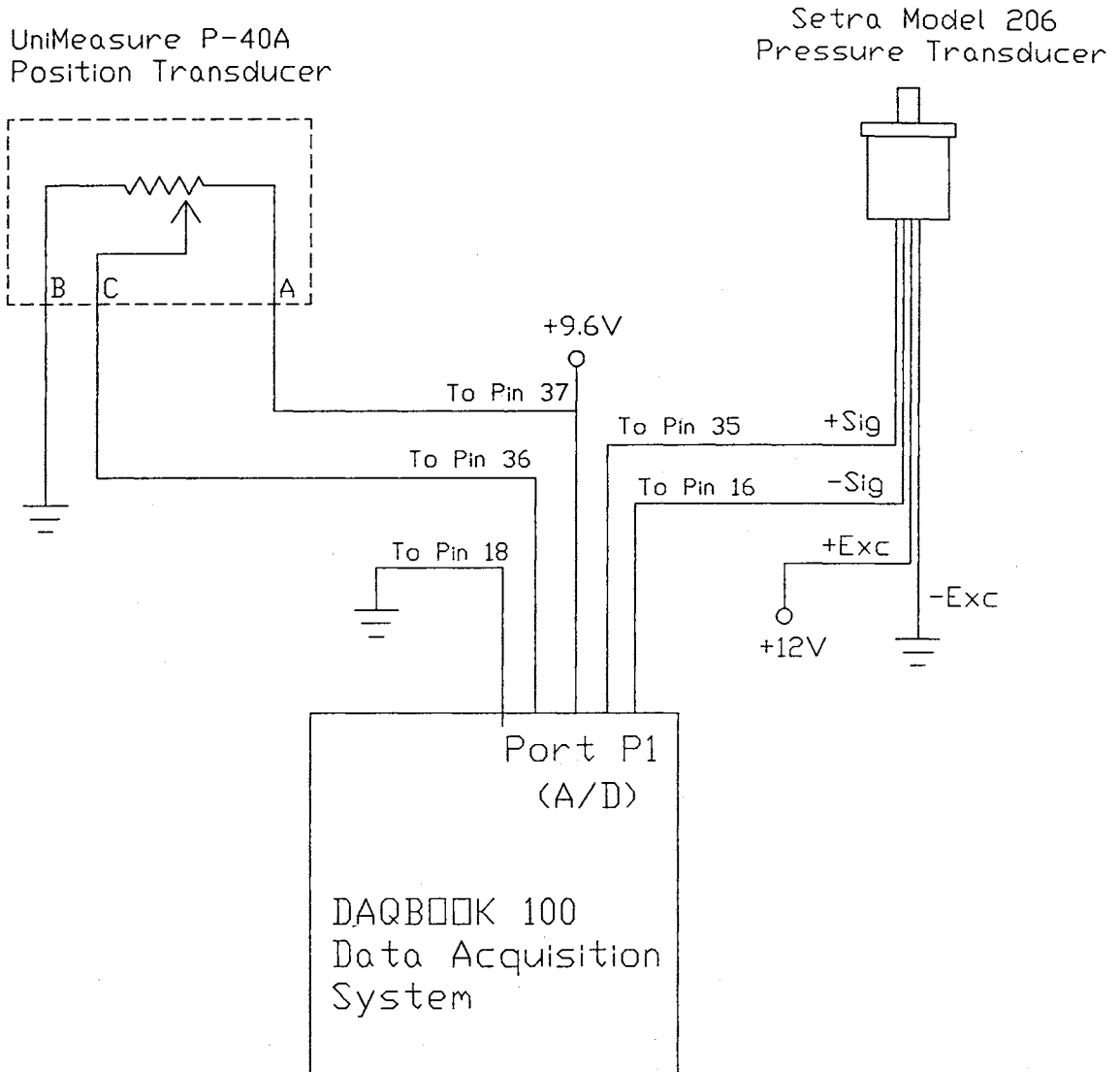


**Figure 21:** Penetrometer instrumentation connections.

pumping of drilling fluid through the 4/40 A boring unit, two equipment modifications were necessary.

The Fluid Pack 35 (FP 35) was designed for use as the primary pumping/mixing system on boring units produced by the Charles Machine Works of later model than the 4/40 A. The hydraulic motor which drives the F.E. Myers CP15-15 drilling fluid pump on the FP 35 has an intrinsic hall effects magnetic speed pick up which produces 30 pulses per revolution. The boring units designed to utilize the FP 35 system have a digital flow readout at the operator station of the boring unit which is based on a conversion of this electric pulse signal. The 4/40 A drilling unit has no readout for flow at the operator station. A digital tachometer was installed on the side of the FP 35 enclosure where it was visible from the operator's position of the boring unit. The tachometer was adjusted to read the rotational speed of the fluid pump. Calibration was performed using an oscilloscope to measure the time period between pulses from the intrinsic speed pick up on the hydraulic motor.

The second change made was to the potentiometer on the 4/40 A which is used to adjust the flow rate of the fluid supply system. The FP 35 requires a Ditch Witch part number 217-781 potentiometer for correct operation. The 4/40 A uses a Ditch Witch part number 215-915 potentiometer. The 217-781 potentiometer was installed on the 4/40 A prior to the 15.5 gal/min (59 l/min) tests at the Coyle test location.

### ***Pipe Pull Load Measurement System***

To measure the tensile force placed on the polyethylene pipe, a specially modified hydraulic cylinder was placed in front of the polyethylene pipe being drawn into the ground. The cylinder was connected to the polyethylene pipe through bolts which passed

through the wall of the pipe into a customized gland at the end of the hydraulic cylinder. The rod of the hydraulic cylinder was connected to the swivel located behind the reamer/compactor used for each bore. An illustration of the connection is given in Figure 22 on Page 65. The section of pipe containing the hydraulic cylinder had to have a larger inner diameter than the rest of the pipe being pulled into the hole in order to accommodate the hydraulic cylinder.

A Sensotec Model 440/7230, 0 - 3000 psig (0-20.7 MPag) pressure transducer was used to measure the pressure trapped in the rod end of the hydraulic load cylinder and converted the pressure reading to a 4-20 ma output signal. The serial number for the transducer was 437508. The cylinder had a 2.00 in (5.08 cm) bore diameter, and the cylinder rod had a 1.25 in (3.18 cm) diameter. Thus, the piston face area on the rod end of the cylinder was 1.914 in<sup>2</sup> (12.35 cm<sup>2</sup>). The pulling force on the cylinder was calculated directly as pressure times area.

The transducer was mounted just behind the hydraulic cylinder inside the polyethylene pipe as shown in Figure 22. The milliamp signal produced by the transducer was transmitted via shielded cable through the length of the polyethylene pipe and out the end to a small trailer which housed the data acquisition system used for reading the signal. The relatively long distance between the transducer and the data acquisition unit was the reason for selecting a milliamp output transducer. This prevented signal degradation from traveling through the cable. At the trailer, the milliamp signal was converted to a voltage value by running it across a shunt resistor. Excitation for the pressure transducer was provided by 3 rechargeable 6-V batteries wired in series. The rechargeable battery pack was also placed in the trailer along with the data acquisition unit.

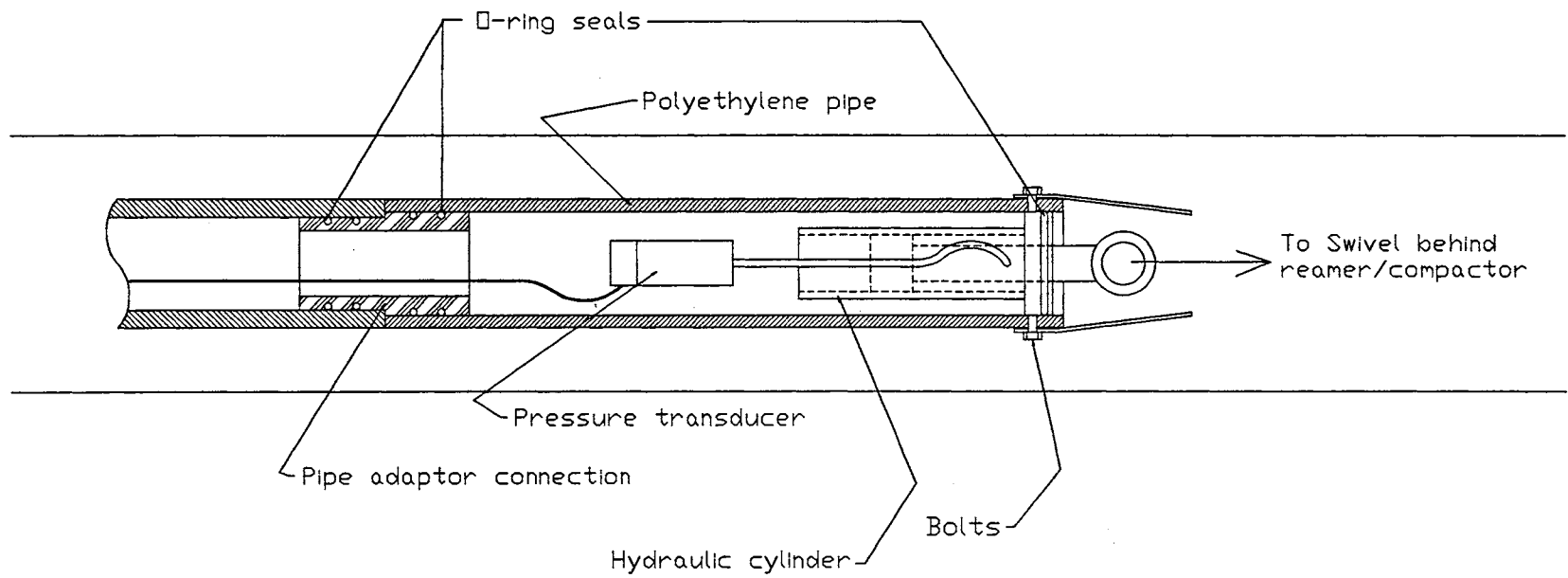


**Figure 22:** Polyethylene pipe pull-load measurement apparatus.



The data acquisition unit used to measure the pull force on the polyethylene pipe was an Omnidata Polycorder Model PC-706 stand-alone data recorder, serial number 925-203. Physical interface for the Polycorder and the voltage signal was provided using an Omnidata General Purpose Interface Enclosure (GPIE) box, model PA-710. A diagram of the wiring connections for the Polycorder box is given in Figure 23 on Page 67.

A copy of the "Polycode" program for the Polycorder data logger is included in Section B of the Appendix of this report. The original Polycode program was written by Mr. Mark Kendle, an electronics technician at Charles Machine Works.

### ***Computer Program for Boring Unit Performance Data Acquisition***

Control of the data acquisition process, and electronic feedback control of the boring unit during the backreaming operation was accomplished using a computer program written in C++. A full listing of the program is given in Section C of the Appendix. A flowchart for the program is given in Figure 24 on Page 68. The program was written by this author, with the exception of the millisecond timer routine provided by Mr. Gordon Couger, Senior Software Specialist with the Department of Biosystems and Agricultural Engineering at Oklahoma State University. Several function calls used for the program are unique to the use of the Daqbook 100 and are provided in function library files provided by the manufacturer.

The basic flow of the program was as follows. When executed, the program first initialized all internal constants. The operator was then polled for the name of the data file, the rotational speed set point, and the pull rate set point to be used for the test. After allowing the operator to verify the input information, the program initialized the Daqbook data acquisition system and configured the Digital I/O port (P2) on the unit. The program

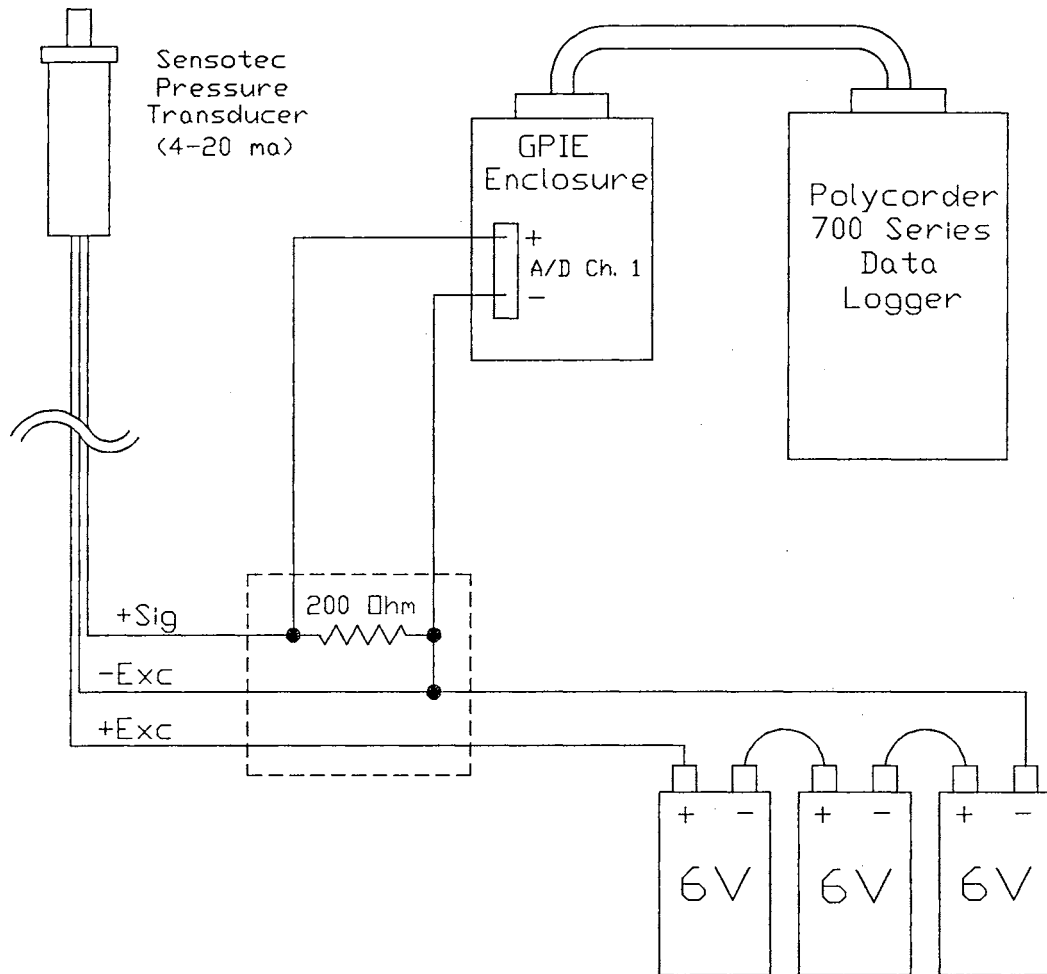


**Figure 23:** Pull force electrical connections.

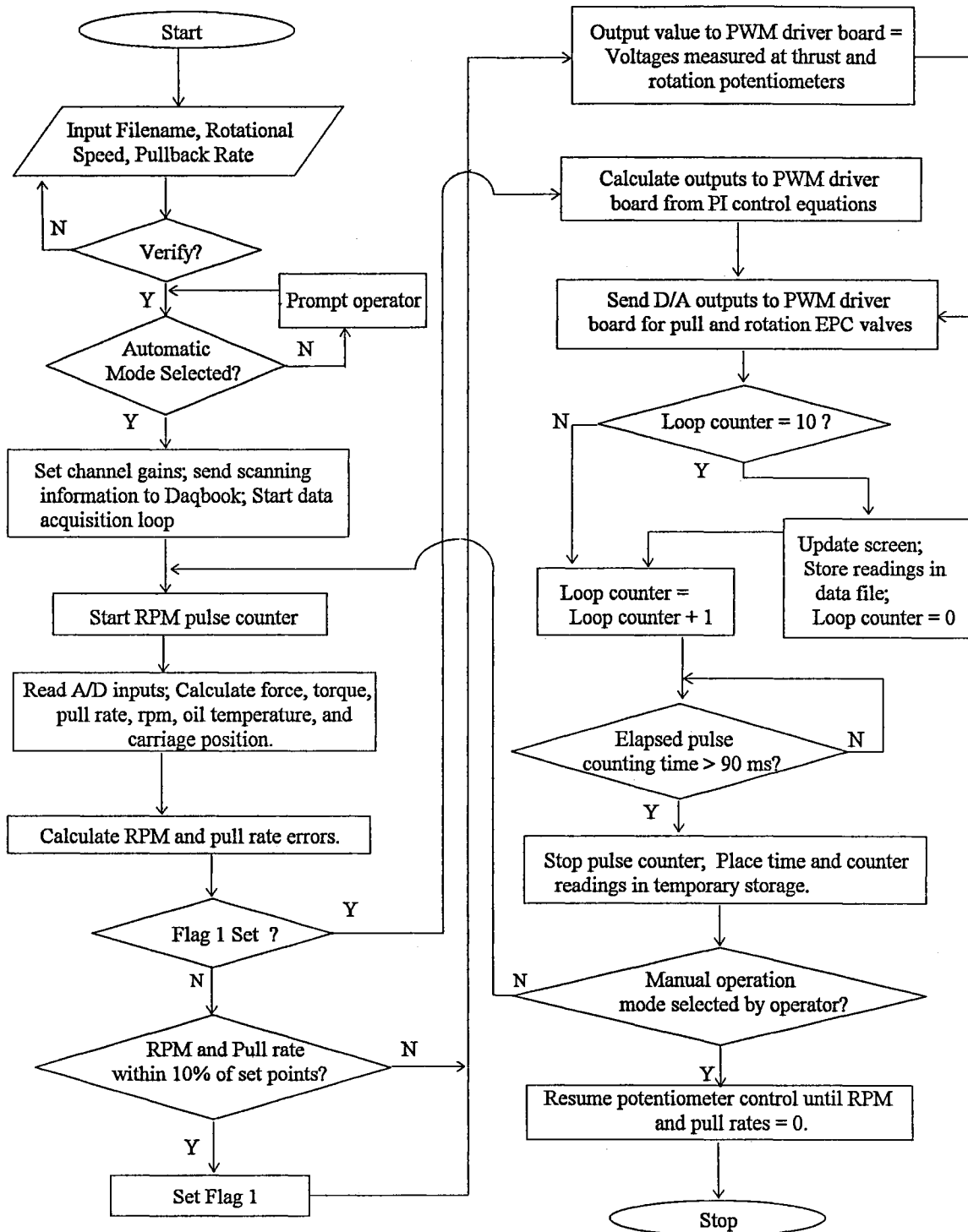


**Figure 24:** Flow chart for boring unit data acquisition/control program.

next verified that the boring unit control system was set in "automatic" operation mode. If it was not, the operator was prompted to do so. The internal gains for the A/D channels were set, and the data scanning information needed by the Daqbook 100 was sent. The viewing screen for the operator was initialized and the header information was sent to the data file.

The primary data acquisition loop then began to execute. The counter port (P3) was triggered to begin counting pulses coming in from the magnetic speed pickup. Next, the inputs from each of the 10 A/D channels were read. To reduce random "noise" from the readings, each channel was sampled 10 times and the values from the 10 readings were averaged. Readings were taken at a rate of 5000 Hz. Thus, taking 10 samples from 10 A/D channels accounted for a time span of 20 ms. Rotational torque, pulling force, pulling rate, carriage position, and hydraulic oil temperature were all calculated from the averages of the A/D inputs from the sensors. Rotational speed was calculated from the previous execution of the main control loop based on the number of pulses counted over the pulse measurement time.

Error terms for rotational speed and pull rate were calculated as the difference between the measured values and the set points given by the operator. The program then checked to see if the condition had been met for the computer to begin the feedback control loop. This condition occurred when both rotational speed and pull rate were within 10% of their set points. If the feedback control condition had not been met, the voltages measured from the thrust and rotation potentiometers were echoed back to the PWM driver board for the EPC hydraulic valve sections through the A/D output pins on Port 1 of the Daqbook 100.

If the start condition for the control section had been met, then the thrust and rotational speed error terms were sent to the subroutine which calculated the output voltage required. Proportional/Integral (PI) control loops were used to dictate the output voltage signals to the PWM driver board for maintaining the thrust and rotation speeds at their desired levels. The control functions in the program were generated with the assistance of Dr. Marvin Stone (1995) of the Biosystems and Agricultural Engineering Department of Oklahoma State University.

A PI control loop provides an output signal to a controlled function which is composed of a constant times the current perceived error in the function, plus a second constant times the integral of the error from the beginning of the control cycle. A mathematical representation of a PI control output calculation is given by:

$$O = (K_c \times e) + \frac{K_c}{\tau_i} \int_0^t e \cdot dt \quad \text{Eq. (13)}$$

Where:  $O$  = the driving signal sent to a controlled process

$e$  = the error between the measured value in a process and the desired value

$K_c$  = the proportional gain constant

$\tau_i$  = the integral reset time constant

$t$  = the elapsed time from the start of the control process

Since continuous sampling of the status of a controlled variable is not possible, the equation is typically rearranged into a finite difference form to take advantage of the actual discrete time increment ( $\Delta t$ ) between measurements of the controlled variable. Taking the

first derivative of Equation 13, placing it into a finite difference form, and manipulating algebraically, the equation becomes:

$$O_n = O_{n-1} + e_n \cdot \left( K_c + \frac{K_c \cdot \Delta t}{\tau_i} \right) - K_c \cdot e_{n-1} \quad \text{Eq. (14)}$$

Where values denoted with subscript  $n$  are the current output or error terms, and values denoted with subscript  $n-1$  are from the previous time increment ( $t - \Delta t$ ).

The format used for Equation 14 is the format in which the PI control equations occur within the computer program. The  $K_c$  and  $\tau_i$  control constants were generated by trial and error as those values which would produce a rapid response to changes in rotational speed or pullback rates, minimize steady state error, and yet not result in instability in either of the functions.

Once the output values from the control loop were calculated, program control was again reverted to the main loop of the program. The calculated output values were then sent to the PWM driver board for the EPC hydraulic valve sections via the D/A output pins on Port P1 of the Daqbook 100. The measured error values and output values were stored in memory for use as the  $n-1$  time step values in the next pass through the control loop.

The program then checked the elapsed time since the beginning of the pulse counting process. The program was put into a waiting loop until the elapsed time surpassed 90 ms. The elapsed time and the number of pulses counted were then read and the information stored for use in the next pass through the loop. Every tenth pass through the main loop of the program, the computer would update the screen with the information

from that pass, and store the information from that pass in the output data file. Updates occurred at roughly one second intervals.

The pull rate and rotation speed of the unit remained under the control of the electronic feedback control loop until the manual/automatic control switch was switched to "manual". Thrust and rotation rates were then dictated by the signal voltage from their respective potentiometers until both pull rate and rotation were set to zero, at which point program execution terminated.

## Chapter 4

### Procedure

#### *Calibration*

##### Pressure Transducers

It was necessary to calibrate all measurement systems used during the testing procedures. All pressure transducers were calibrated using a Mansfield and Green static hydraulic pressure tester, type MP-1A, serial number 435. The tester was comprised of a manual piston-type hydraulic pump attached to a small oil reservoir. A release valve on the tester allowed the hydraulic oil to be pumped to a desired pressure and the pressure held constant while calibration readings were taken. By opening the valve the pressure was easily released. The pressure developed by the tester was read using an Ashcroft 0-3000 psi temperature compensated test gauge, Type 1082 SS. The gauge was a Bourdon tube type with a needle readout. The gauge was certified by the supplier to within 0.25% F.S. accuracy. Serial number for the gauge was Q-4901. All pressure transducers used in the study were easily snapped in place on the pressure tester using quick connect fittings.

The procedure for the calibration of all pressure transducers, including the four transducers used on the boring unit, the pressure transducer used on the penetrometer unit, and the pressure transducer used to measure the pressure trapped in the hydraulic cylinder located in the polyethylene pipe was as follows. The transducer was snapped in place on the pressure tester at a pressure of 0 psig (0 MPag) and the reading from the transducer measured using the same data recording device as used for the data collection. The pressure was then incrementally increased up to the maximum pressure the transducer



was expected to measure during the testing process. For the pressure transducers used on the boring unit this value was 3000 psig (20.7 MPag) for the high side transducers and 1500 psig (10.3 MPag) for the low-side transducers. For the transducer used on the penetrometer unit a value of 1000 psig (6.9 MPag) was used. And for the downhole transducer, a value of 2500 psig (17.2 MPag) was used. Measurement increments for the transducers were 500 psi (3.4 MPa) for the high-side transducers on the boring unit and the downhole transducer, 300 psi (2.1 MPa) for the low-side transducers on the boring unit, and 200 psi (1.4 MPa) for the penetrometer transducer. Pressure was remeasured at one value near mid-scale and again at 0 psig (0 MPag) as the pressure was released from the transducer to test for hysteresis effects.

Once the full sequence of readings was taken for each transducer, the values measured by the data recording devices were compared with those measured by the test gauge. The range and offset constants (m and b from the expression:  $\text{Pressure} = mx + b$ ) for the transducers were recalculated to match the test-gauge values. The test was then reconducted for each transducer. This process was repeated until the measured values from the transducers matched those from the test gauge as closely as possible.

All pressure transducers were recalibrated before the start of testing at each test site and at other times during when it was deemed necessary. Such a case would have existed if a pressure reading taken before start up of the boring unit was found to deviate significantly from zero.

### Displacement Transducers

The displacement values from both the UniMeasure P-40 displacement transducer on the penetrometer unit and the UniMeasure VP-150 displacement/velocity transducer on the boring unit were calibrated using a Stanley 25 ft (7.6 m) Power-lock II tape measure, Model 33-425. With the data acquisition system running, the cable on each of the transducers was pulled out in distance increments and measured using the Stanley tape measure. The incremental measurements continued until the cables were extended to the full length required for the given application. The maximum pulled distance for the P-40 transducer on the penetrometer unit was 32 in (81 cm). The maximum distance for the VP-150 transducer on the boring unit was 10.6 ft (3.2 m). The values measured by the data acquisition systems were compared to those measured by the Stanley tape. The offset and range constants were adjusted in the data acquisition system until the recorded distances closely matched those read from by the Stanley tape.

### Velocity Transducer

The velocity-signal output from the UniMeasure VP-150 transducer was not a "pure", linear signal. Instead, if any vibration was introduced into the transducer during the measurement process, the output signal was sinusoidal with a frequency which appeared to be related to the rate of cable travel. The frequency of the sinusoidal signal was well above the sampling frequency of the data acquisition program. The mean of the sinusoidal signal was proportional to the rate of cable travel, but a reading taken at any instant could have errors as large as  $\pm 60\%$  or more. To compensate, the gain settings on the control loop were set lower than they would have been otherwise. This slowed the

response of the control system and allowed the system to maintain the pull rate based on the mean of the incoming velocity signal.

Because of the non-linear signal, calibration of the velocity reading from the UniMeasure VP-150 position/velocity transducer on the boring unit was accomplished indirectly. Calibration was based on the measured time of travel of the drilling carriage over a set distance when the boring unit was operating under feedback control. Following calibration of the position signal of the VP-150 transducer, the boring unit was set to operate at carriage speeds of 2.0, 3.0, 4.0, 5.0, and 6.0 ft/min (0.61, 0.91, 1.22, 1.52, and 1.83 m/min). The time required for the drilling carriage to travel 5.0 ft (1.52 m) was measured using a stopwatch. The resulting average pulling speeds over the 5.0 ft (1.52 m) pulling distance were then compared to the set points. The offset and range constants for the pull rate transducer were adjusted and the calibration tests re-run until the average speed over the 5.0 ft (1.52 m) travel distance closely matched the set points.

#### Temperature Sensor

The LM-34DZ temperature sensor was calibrated in a can of water. The brass plug containing the sensor was lowered into a can of water heated with a small electrical resistance heating coil. A Sargent-Welch Scientific 0-230 F (0-110 C) mercury thermometer, serial number S-80015-B, was used to monitor the temperature of the water in the can. Because of the mass of the brass pipe plug, the temperature sensor was found to have a fairly slow response time ( $\tau \approx 24$  seconds). During the calibration process the water was allowed to heat for a time and then the heating coil was disconnected. After a two minute wait ( $5\tau$ ), the thermometer temperature reading and the temperature reading given by the data acquisition system were recorded. This process was repeated numerous

times as the water temperature was increased from 80 to 200 F (27 to 93 C). After the water reached a temperature of 200 F, the heating coil was removed and the water was allowed to cool. Readings were taken with the thermometer and the LM-34DZ sensor every 2 minutes initially, and then every 3 minutes as the water became cooler. The offset and range constants for the temperature sensor were adjusted to closely match the temperature values given by the thermometer.

### Rotational Speed Calibration

No traditional "calibration" was necessary for rotational speed measurement of the boring unit since the process involved only a simple counting of tooth passage over a set length of time. What was required was a verification that the data acquisition program could accurately count and convert the tooth passage frequency to a rotational speed reading. To verify that the computer could correctly measure the rotational speed, the 120-tooth gear was mounted on a variable-speed electric motor. The Shimpo MP-10 magnetic pickup was mounted such that the face of the speed pickup was located 0.05 in (0.13 cm) from the tips of the gear teeth. An oscilloscope was connected to the output of the magnetic pickup. As the motor speed was varied, the period of the produced sine wave was measured on the oscilloscope. This time period was taken to represent the passage time for an individual gear tooth. Concurrently, the rotational speed was measured using the Toshiba laptop computer and the Daqbook 100 data acquisition system, and was displayed on the computer screen. The data acquisition program was set to display the actual rotation speed and not the 3:5 scaled rate at which the spindle rotated in comparison to the hydraulic motor. This value was recorded by hand. If the rotational speed value was vacillating between two values, the value displayed the most frequently

was recorded. The variable-speed electric motor was adjusted over a speed range from 140 rpm to above 400 rpm, which corresponded with spindle rotation rates between 84 and 240 rpm.

### ***Coyle Test Site: Test Bore***

One bore was conducted at the Coyle, OK test site for the purpose of final verification of test parameters and to find any potential problems associated with the unit before beginning formal tests. The boring unit was staked down and the bore was made according to the procedure described later in this chapter. The penetrometer soundings were taken in accordance with the procedures used in the formal testing. During the backreaming process, special attention was given as to whether the drilling unit was capable of running all possible combinations of rotational speed rate (96, 128, 160, 192 rpm) at the desired pull rates. A decision was made that pull rates of 2, 3, and 4 fpm (0.61, 0.91, and 1.22 m/min) would be acceptable for the tests at this location. The boring unit proved capable of maintaining rotational speed at all given combinations of pull rate and rotational speed rate. The actual pull rates used in the test were slightly (10%) lower than the original 2, 3, and 4 fpm values. This is discussed later in this section of the report.

Initially, a decision was made to do a similar test bore at the Stillwater Creek location as well. However, the bore that was to have been the “test bore” was made to the same dimensions as the bores of record at the Coyle location. After pulling the first two drilling rods during the backream/pullback of the test bore at the Stillwater Creek location, it was clear that the same pull rate/rotation rates that were used at the Coyle

location would be adequate. Thus, what was to have been the “test bore” was counted and the data was used as Bore 0 of the Stillwater Creek location data set.

Pull-load data was measured and recorded from the Sensotec pressure transducer located inside the polyethylene pipe pulled into the ground. The data appeared reasonable and no problems were noted.

### ***Coyle Test Site: Bores 1 to 4, The Abandoned Data***

During the first four bores at the Coyle test site, a single pressure transducer was utilized on the high-pressure side of the oil loop for the thrust and rotation functions. It was assumed that a pressure reading could be taken at a “no-load” condition and that reading subtracted from each of the loaded readings to obtain the actual value. This assumption proved to be substantially flawed.

When the boring unit was running under a “no-load” condition, the engine on the power pack driving the hydraulics would run at, or very near, the set high-idle speed, in this case about 2450 rpm. This meant that the oil flow rate through the system was at a maximum, and thus, pressure drop due to viscous resistance in the hoses was at a maximum. It was at this condition that the no-load readings were taken. However, when the boring unit was running under a loaded condition, the engine speed would droop, perhaps as much as 8-10% in speed. Engine droop at the power pack would mean that the oil flow would also slow down, and thus the pressure drop due to viscous resistance in the hoses would also drop. Bernoulli’s principle makes it clear that pressure drop is proportional to the square of fluid velocity. Thus, an 8% drop in engine speed should change the observed pressure drop in the lines by more than 15%. This meant that the no-

load readings were higher than they should have been. The end result was that the high side pressure readings wound up lower than they should have been.

To correct this problem, pressure transducers were installed at both the high and low pressure sides of the hydraulic motors as discussed in the Instrumentation section of the procedure. The use of dual pressure transducers on the hydraulic motors solved the problem, since a true pressure drop was measured in every case regardless of flow rate.

Four bores, numbered 1 to 4 had been completed at the Coyle test site before this problem was found. It was decided to exclude the data from those bores from the analysis and essentially start over beginning with Bore 5 and continue through Bore 16.

### ***Deviation from Original Pull Rate Settings***

When the boring unit was brought in from the field after Bore 4 (Coyle test site) and the pressure transducers were added to the "low-pressure" side of the thrust and rotation loops, the calibration for pull rate was thrown off slightly. The reason for the change could not be discerned, but pull rates were consistently reduced by almost exactly 10% from their previous calibrated values.

The actual pull rates for the field tests were calculated based on the data files acquired during the boring tests. The change in position of the drilling carriage occurring over a two minute period was used to calculate the rate of pull. The data acquisition program was found to acquire 123 readings over a two minute period. Thus, position readings in the data file located 123 readings apart were subtracted and divided by 2 minutes to estimate the actual pull rates. The actual pull rates calculated from the field test data are summarized in Table 1.

Table 1

## Pull Rate Summary

Pull Rate	Low (ft/min)	Mid (ft/min)	High (ft/min)
Average	1.794	2.695	3.594
Std. Deviation	0.041	0.050	0.045

The pull rates were from the data files were tightly grouped about the mean values as evidenced by the small standard deviation values in Table 1. The low, mid, and high pull rate values were rounded off to the nominal values of 1.8, 2.7, and 3.6 fpm (0.55, 0.82, and 1.10 m/min). These nominal values were used in the analysis of the data.

***Procedure for Conduction of Bores***

The boring unit, trailer with fluid system, and hydraulic power supply were moved to the test location. Test locations were selected as being relatively flat, having a reasonable consistency of the desired soil type (whether cohesive or non-cohesive), being free from cobbles or major underground obstacles, and being available for use.

In each field a site was selected as having only slight surface undulations for a distance of the approximate bore length of 250 ft (76 m). The selected test areas were wide enough to allow all necessary bores at the location to be made parallel to each other with approximately 15 ft (4.6 m) between each bore.

Once a location was picked within a field, the boring unit was moved to the desired site for the beginning of the bore and staked down using the auger stakes provided with the 4/40 A. The necessary hydraulic and water hoses for the boring unit were unrolled from the hose reels on the trailer and connected to the boring unit. A batch of



drilling fluid appropriate to the soil type was mixed in the fluid tank on the trailer. The first rod of drill pipe was placed in the boring unit and snugged.

The Subsite® Model 84 BRP radio transmission beacon was checked to ensure adequate battery strength and verify that it was functioning correctly. This check was conducted by laying the beacon on the ground and measuring the response with the Subsite® Model 80RP (Serial Number 29026) walk-over locator. Once it was determined that both the transmitter beacon and locator were working properly, the transmitter beacon was installed in the boring unit cutter head. The cutter head was then attached to the first joint of drill pipe and tightened. The pitch (up or down slope) signal from the beacon was then used to set the entrance angle of the drilling unit. A pitch of 24% down (13.5° down) was used as the entry angle for each of the bores. The entry angle was set by adjusting the leveling feet on the 4/40 A boring unit via the hydraulic cylinders attached to the feet.

Once the entry angle was set with both the transmitter beacon and walkover locator working, the pilot bore was set to proceed. The boring crew consisted of three crew members. One crew member was in charge of operation of the boring unit, including all steering done during a bore. For this group of tests, Mr. Damon Webb, a test technician for the Charles Machine Works experienced with directional boring, was in charge of running the boring unit and making necessary steering corrections. A second member of the test crew was in charge of operating the walkover location equipment, record keeping of the bore path, and “flagging” the bore path. Flagging is a process whereby a small plastic flag on a wire stem, similar to those used by the highway department, is inserted into the ground at the exact location of the strongest signal picked

up by the locator at the end of each joint of pipe. The location of the strongest signal was assumed to lie directly above the location of the transmitter housing under ground. By flagging the location of the housing every 10 ft (3.0 m), the boring unit operator has a visual picture of the progress of the bore and can make left and right path adjustments as necessary. For each of the test bores, the task of location and data collection was performed by this author.

The third member of the boring crew was in charge of loading drill pipes into the boring unit as they were required. This task was performed by student workers from Oklahoma State University.

Each of the bores for the test followed a bore path geometry similar to that shown in Figure 25, Page 84. Each of the bores proceeded down to a depth of 6 ft (1.8 m), then ran at a comparatively uniform depth of typically  $6 \text{ ft} \pm 6 \text{ in}$  ( $1.8 \text{ m} \pm 0.2 \text{ m}$ ). Depth readings for all bores is given in Section D of the Appendix. The bores progressed at the 6 ft (1.8 m) depth for a distance of 150 ft (46 m), and then were brought to the surface.

Every 10 ft (3.0 m) along the bore path, a record was made of the depth of the boring head and the pitch of the boring head in the ground from the information provided by the 80 RP walk over locator. Every 10 ft (3.0 m), and occasionally at 5 ft (1.5 m) intervals, information regarding the depth, pitch, and roll angle of the boring head were relayed back to the operator of the boring unit. This information allowed the operator to make necessary bore path corrections. Information was relayed between the location crew member and the drilling crew member by means of a Subsite® 80 DT transmitter, worn by the locator, to a Subsite® 80 D receiver located near the operator. The 80 DT transmitter encoded the 80 RP location unit information into a radio signal picked up by the 80 D

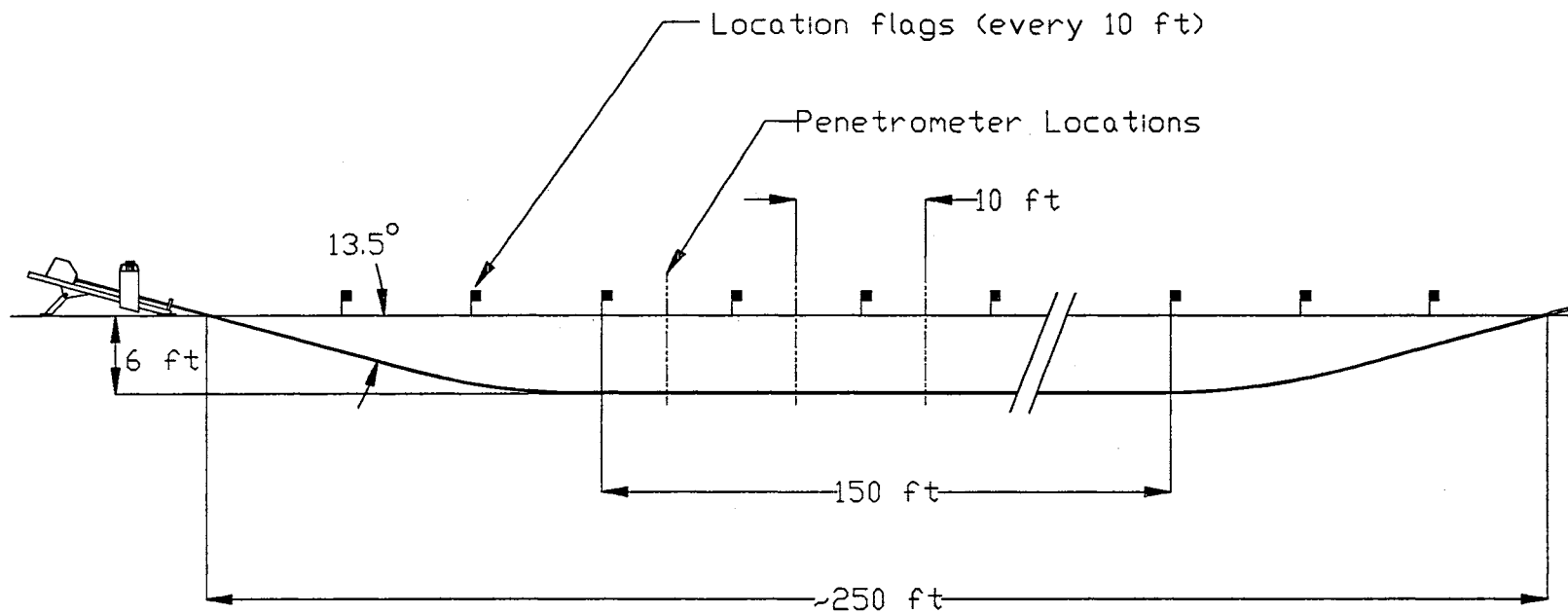


**Figure 25:** Typical bore geometry used during testing.

receiver. Additional information was relayed between the boring unit operator and the locator by means of hand held “walkie-talkie” radios.

### *Penetrometer Soundings/Soil Samples*

Once the pilot bore was completed, a series of penetrometer readings were taken along the bore path. The flags left in the ground during the pilot bore served as an indicator of the location of the endpoints of each 10 ft (3.0 m) steel drill pipe used during the conduction of the bore. Penetrometer readings were taken at the midpoint of each joint of drill pipe (midway between two flags) along the first 140 ft (43 m) of the uniform depth section of the bore, starting from the first horizontal joint of pipe closest to the boring unit. Thus, a total of 14 penetrometer soundings were taken for each bore.

The penetrometer soundings were made approximately 3 ft (1 m) to the side of the path of the pilot bore as viewed from above. The penetrometer probes extended down below the depth of the drilling pipe. A typical penetrometer probing extended to a depth of approximately 85 in (2.2 m). Taking the soundings 3 ft (1 m) from the actual bore path was a necessary compromise. Possibly, a more accurate reading could have been obtained closer to the drilling pipe, however a penetrometer hole directly adjacent to the drill string would have served as a “vent” hole for drilling fluid during the backream/pullback section of the bore. Such a venting action would have been a possible source of alteration in the otherwise imposed on the pipe. Taking the penetrometer sounding very near the bore path would have also given some opportunity to have hit the drilling pipe with the penetrometer probe, a possible source of damage to one or both.

The penetrometer soundings were taken using the attachment constructed on the Ditch Witch 6510 tractor described in the Equipment section of the report. Before

readings were taken, the Toshiba laptop computer was mounted on the fender of the 6510 tractor. All electrical connections between the Daqbook 100 data acquisition unit mounted below the computer, the power supply, and the signal wires to and from the transducers were connected. The Setra Model 106 pressure transducer was snapped in place onto its quick-connect port, and the UniMeasure P-40 position transducer was mounted onto the hydraulic cylinder responsible for pushing the penetrometer probes into the ground. A 12-V DC to 110 V AC power converted was connected to the battery of the 6510 tractor to provide supplemental power for the laptop computer during the test.

Once all connections were made and the computer and the data acquisition software were found to be working, the tractor was driven into position for the first penetrometer sounding. The backfill blade on the front of the 6510 tractor was lowered to the ground to provide greater weight transfer to the penetrometer attachment during the soundings. The data acquisition system was then started. Readings of excitation voltage, penetrometer push cylinder extension, and pressure on the barrel side of the push cylinder were taken at a rate of 4 Hz. At each location, before a rod was pushed into the ground, a short extension was made with the hydraulic cylinder of 6-10 inches (15-25 cm) to measure the pressure due to friction within the hydraulic cylinder and any back pressure in the lines. This value was later subtracted from the measured values to correct for the no-load pressure.

The first penetrometer rod and cone tip were screwed into the adapter on the hydraulic cylinder. The rod was then advanced to the point where the tip of the cone was just seated into the surface of the ground. At this point, a pause of approximately 5 seconds was made to establish the location of the ground surface on the data set recorded

on the computer. The rod was then advanced into the ground until the connection for the first rod was just above the ground surface. Subsequently, the second and third penetrometer rods were added in series and also pushed into the ground. Once all three rods were fully into the ground, the computer program acquiring the data was stopped. The three rods were then pulled back out of the ground, the tractor driven to the next penetrometer location, and the process repeated until all 14 penetrometer soundings were complete for each bore.

When the penetrometer readings were finished, the 6510 tractor was driven to the approximate midpoint of the bore, typically near drill pipe 12 or 13. A soil sample was then taken roughly 3 ft (1 m) to the side of the bore path at the depth of the drilling pipe.

At the Coyle location, since the soil was a non-cohesive silt, the soil sample collected was a disturbed auger cutting sample. The auger sampler on the 6510 attachment was used to bore a 4 in (10 cm) vertical hole down to the depth of the drill pipe at the desired location. The last material to come up from the auger, once a sufficient depth was reached, was collected in a resealable plastic storage bag, labeled, and placed in an ice chest until it could be transferred to a cool storage room for storage before use.

At the Stillwater Creek location, the soil was a cohesive clay. The auger cutter was used to bore a 4 in (10 cm) vertical hole down to a depth of approximately 68 in (1.73 m). The auger was allowed to rotate in the hole without advancing until virtually all of the material had been removed to that depth. The auger was then removed from the hole. A hollow sample tube 3 in. (7.6 cm) in diameter was attached to the end two penetrometer push rods screwed together. The sample tube was gently lowered into the hole until it rested on the bottom. The penetrometer push cylinder was then moved in place over the

hole and connected to the push rods holding the sample tube. The penetrometer push cylinder was then used to push the sampler into the soil at the bottom of the hole. A tape measure was used to measure the length of each push to make certain that it did not go too far and unnecessarily compact the soil in the sample tube. Tubes with 12 to 14 in (30 to 36 cm) sample capacity were used. The tube was then extracted from the hole, wrapped tightly in plastic wrap, and placed in the shade until it could be transferred to a cool room for storage until it was extracted from the sample tube.

### ***The Reaming/Pullback Process***

While the penetrometer soundings were being conducted, one crew member would remove the cutting head, protruding from the ground at the end of the bore, from the string of steel drilling pipe. In its place the reamer/compactor to be used for the given bore was attached. At the Coyle test site, the 7 in (18 cm) fluted cone reamer with cutting teeth was used for all bores (See Figure 16, Page 53). At the Stillwater Creek location, the fluted cutter was used for 4 bores and the staged wing cutter with compaction cone (See Figure 17, Page 54) was used for the other 4 bores. Located behind each of the cutters was a swivel to prevent rotational motion from being transferred to the attached polyethylene pipe.

Once the reamer/compactor was attached to the drilling pipe, the 4.5 in (11.5 cm) o.d. polyethylene pipe was connected behind the swivel of the cutter. Connection to the polyethylene pipe was made through the rod of the hydraulic load cylinder described in the Equipment section of the report (See Figure 22, Page 65).

The Toshiba laptop computer and Daqbook 100 data acquisition box were moved from the penetrometer tractor and mounted on the boring unit, along with the

interface/signal conditioning box (See Figure 26, Page 90). The pressure transducers for the thrust and rotation functions were plugged onto the hydraulic quick-connects at the inlet and outlet ports of their respective hydraulic motors. The electrical connectors for the pressure transducers were plugged into their respective slots.

The cable for the UniMeasure position/velocity transducer was hooked to the back of the traversing carriage of the boring unit. All electrical connections to and from sensors were plugged into the interface/signal conditioning box. The leads from the box were then plugged into the appropriate ports on the Daqbook 100 data acquisition box.

The 12-V dc to 110 V ac power inverter was connected to the battery of the PP70 hydraulic power pack. Supplemental power to the computer was provided from the inverter box to the external plug for the computer via an extension cord. Electrical power connection was also made between the 12-V power available at the console of the boring unit and the interface/signal conditioning box. This power connection was used to provide excitation voltage for the pressure transducers, position/velocity transducer, and integrated chip temperature sensor. The 12-V supply also supplied the required power for the pulse width modulated (PWM) driver board for the Gresen electronic proportional control valves.

Once the computer was in place and all electrical connections were made, the computer was turned on and the data acquisition program was loaded into RAM. The program was started with all hydraulic power to the boring unit shut off to check all transducers before commencing backreaming. Any readings which appeared questionable triggered a check of corresponding electrical connections and, if needed, recalibration of one or more pressure transducers before beginning the bore.



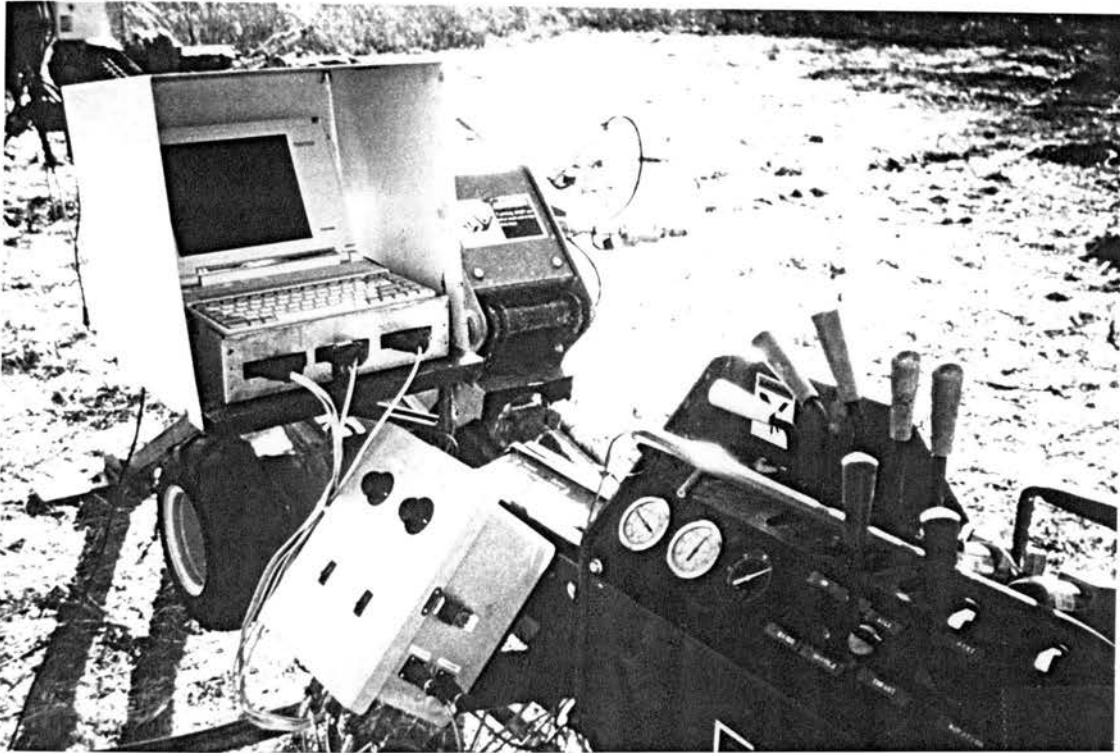


**Figure 26:** Computer and signal conditioning box mounted at operator's station on boring unit.

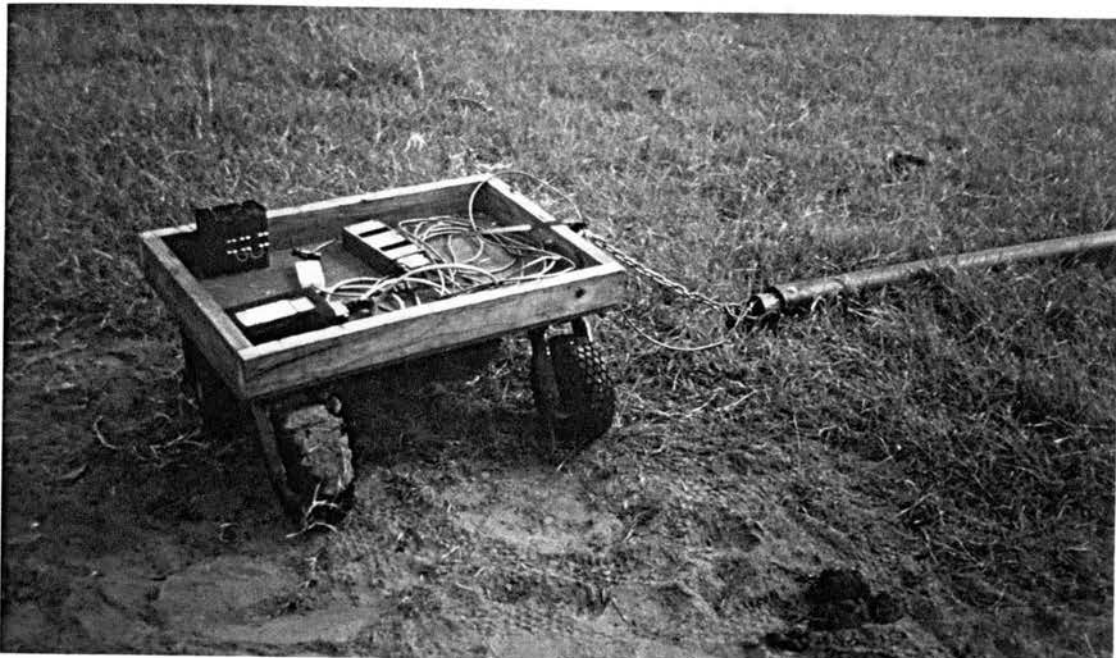


**Figure 27:** Polycorder, GPIE interface, and battery pack mounted in trailer towed by polyethylene pipe.

Next, the Omnidata Polycorder stand-alone data acquisition unit was placed in a small trailer connected behind the polyethylene pipe (See Figure 27, Page 90). With all necessary electrical connections made, the Polycorder was turned on and programmed to begin reading the signal from the pressure transducer. The Polycorder was set to read and record the pressure value once every 10 seconds, and was allowed to continue until the bore was completed.

While the data recording equipment was being readied, the designated fluid mixer for the boring tests, Mr. Damon Webb, began mixing drilling fluid for the backreaming operations. Fluid mixing was done on the back of a 2½ ton truck which held two 300 gallon (1.14 kl) water tanks and a Ditch Witch® Fluid Pack 35 drilling fluid mixing/pumping system.

The same drilling fluid mixture was used for every bore at a test location. At the Coyle location, the drilling fluid mixture included two 50 lb (22.7 kg) sacks of Baroid Quick-Gel® in 300 gallons (1.14 kl) of water. Quik-Gel is a finely ground, premium-grade sodium bentonite designed for applications where high-yield and fast-yielding drilling mud is required (Baroid, 1992). The fluid was mixed uniformly by means of hydraulically operated stirrers located in the fluid tank and circulation through a centrifugal fluid pump.

The drilling fluid at the Stillwater Creek test site was a consistent mixture of 1 quart ( 0.95 l) of Baroid EZ-Mud® anionic polymer and 300 gallons of water. EZ-Mud is a sodium polyacrylide polyacrylamide in a latex solution used as a viscosifier in drilling fluids (Baroid, 1992). The fluid was mixed in a similar manner to that used at the Coyle

test site. A drilling fluid flow rate of 7.4 gpm (28.0 lpm) was used for all bores at the Stillwater Creek test site.

When bores requiring 7.4 or 10.6 gpm (28.0 or 40.1 lpm) of drilling fluid were conducted, the drilling fluids were pumped into the fluid tank on the TP18 transport trailer. The F.E. Myers CXPM8-15 fluid pump on the trailer was used to pump the fluid from the tank and down the bore hole through the drilling pipe. While in the fluid tank on the TP18 trailer, the boring fluids were kept stirred by a hydraulically driven tank stirrer. For the 15.5 gpm (58.7 lpm) bores at the Coyle location, the F.E. Myers CP15-15 fluid pump included with the Ditch Witch® FP35 fluid system on the fluid truck was used to provide the necessary flow. The fluid pump on the truck was used since the system on the TP18 trailer proved unreliable in providing drilling fluid flow rates above 10.6 gpm (40.1 lpm).

For the pullback operation, the test crew responsibilities changed from those during the bore. One person was in charge of mixing all drilling fluids and pumping them to the boring unit trailer. One member operated the boring unit and data acquisition equipment. They also monitored the flow rate of the drilling fluid and kept track of the progress of the bore. The third crew member was responsible for the unloading of drill pipe from the drilling unit, and stacking the drill pipe on the ground.

Before and after each run was made, a set of “no-load” data was taken with the boring unit disconnected from the drill pipe. The data set was used to obtain the parasitic loads associated with just moving the parts on the boring unit with no loading present. These data were used to correct the loaded readings obtained with the boring unit. The

purpose of taking no-load readings at the beginning and end of the bore was to have two markedly different hydraulic oil temperatures represented.

Each no-load run was comprised of essentially two phases. The data acquisition system was in operation during both phases of a no-load run to capture all data as recorded in an actual working run. In the first phase, the boring unit was operated in increments across the full span of spindle rotation speeds used in the test (96, 128, 160, and 192 rpm) while the pull rate was held at zero. The rotation speed was held at each of the set levels for approximately 5 seconds before proceeding to the next level. In the second phase of the test, the rotation speed was left at the final level used in phase one. The pull rate was then varied to a number of different levels from less than 1 ft/min (0.3 m/min) to more than 10 ft/min (3.0 m/min). The pull rates were selected randomly and each rate was held for approximately 5 seconds before proceeding to another. This was continued until the carriage on the boring unit had traversed most of its span of travel.

All drill pipes pulled from the hole during the backreaming process were under the control of the electronic feedback control system, with the exception of the last two or three pipes in some of the bores after the data collection runs had been completed. The pipes pulled as the cutter was progressing into the ground and leveling off, typically the first 5-6 pipes during any given bore, were run at an intermediate rotation speed and flow rate. The normal rates used were 160 rpm and 2.7 ft/min (0.82 m/min). The first few drill pipes pulled in each bore served as a form of daily "shake down" of the boring unit, data acquisition system, and electronic controls. The data collected at the boring unit from the first few and last few rods from each bore was not saved. The only data of interest was that along the uniform depth section where the penetrometer soundings were made. This

was done to prevent the bore path curvature at the beginning an end of the bore from unnecessarily influencing the data set.

The drill pipes pulled in which were located along the uniform depth were pulled in at predetermined levels of rotation speed and pull rate. All possible combinations of the 96, 128, 160, and 192 rpm rotation rates with the 1.8, 2.7, and 3.6 ft/min (0.55, 0.82, 1.10 m/min) pull rates were used. The order of the combinations used for each bore was randomized using a random number table. Four rotation rates and three pulling speeds gave a total of 12 possible combinations. Data was collected on 14 rods during each bore. The last two rods pulled through the uniform depth section of the bore served as “spares” in the event any problems occurred with the first 12 rods. The data from these spare rods were excluded from the final data set unless readings from one or two of the original rods were questionable.

The process of backreaming the hole for a distance of one drill pipe was conducted in the following manner. The computer program written for the data acquisition and control was started. A description of this program is given in the Computer Program segment of the Equipment section of this report. The program prompted the operator for the desired rotation speed, the desired pull rate, and the name of the data file for the collected information. Once the information was input and verified, the computer program prompted the operator to place the manual/automatic control rocker switch to the “automatic” position, if it was not already. Control of the thrust and rotation functions of the boring unit were, at that point, under the control of the 3/4 turn potentiometers on the interface/signal conditioning box. The utility section of the Gresen V-20 valve stack was switched to the “on” position to provide the pilot pressure necessary for the electronic

proportional control valve sections to operate correctly. The rocker switch for the drilling fluid pump was activated to begin pumping drilling fluid to the cutter.

After a delay of 3-5 seconds to allow steady state of drilling fluid to the cutter, the potentiometer in charge of the rotation function was slowly turned until the spindle was rotating near the desired set point. At that point, the potentiometer in charge of the pull function was slowly turned until the pull rate was near the desired set point. When both the pull and rotation rates were within 10% of the desired set points, the computer program assumed control of both functions. The computer program took readings of high and low rotation pressures, high and low pull pressures, pull rate, carriage position, rotation rate, pressure transducer excitation voltage, spindle rotation rate, and hydraulic oil temperature at a rate of 10 Hz. The measured pull rates and measured rotation rates were compared with the set points, and adjustments were made to the given rates using the PI control loop at a 10 Hz rate, as well. Once every 10 runs (approximately once per second), the readings of pull rate, rotation rate, calculated rotational torque, high-side pressure for the torque loop, calculated pulling force, high-side pressure for the pull loop, carriage position, and hydraulic oil temperature were written to the specified data file.

While the drilling rod was being pulled, the boring unit operator would check on the rotation rate of the drilling fluid pump. This was the only control used on the rate of flow of the drilling fluid. For the 7.4, and 10.6 gpm (28.0 and 40.1 lpm) flow rates, this was done using a H.H. Sticht Model 2301 direct contact rotational tachometer to measure the speed of the shaft on the fluid pump. A rotational speed of 395 rpm corresponded to a flow rate of 7.4 gpm (28.0 lpm). A rotational shaft speed of 590 rpm corresponded to a flow rate of 10.6 gpm (40.1 lpm). For the 15.5 gpm (58.7 lpm) fluid flow rate, a digital

tachometer was used to monitor the rotation rate of the fluid pump. The tachometer, mounted on the FP35 unit in clear sight of the boring unit operator, was wired to read the 30 pulse/revolution signal generated by the hydraulic motor turning the fluid pump on the FP35 fluid system. A rotation rate of 330 rpm was needed to provide the desired flow rate. Rotational speed was kept within  $\pm 10$  rpm from these target speeds. Any fluid pump speed adjustment made was done using the potentiometer at the drilling unit for pump speed control. It is important to note that the fluid flow calibrations made were made with water at whatever pressure was necessary to pump the fluid through the drilling fluid hose and out an open end. The viscometric properties of the drilling fluid and the changes in drilling fluid pressure experienced during boring could have changed the actual values of these flows slightly due to changes in volumetric efficiency of the positive displacement pumps. Thus, the 7.4, 10.6, and 15.5 gpm (28.0, 40.1, and 58.7 lpm) flow rates should be considered "nominal", or "best estimate" flow rates.

When a drill pipe was within 3-6 in (8-15 cm) of the point needed to disconnect the pipe, the manual/automatic control rocker switch on the interface/signal conditioning box was switched to the "manual" position. Once switched, control of the pull rate and rotation rate reverted to the potentiometers on the interface/signal condition box. When the drilling pipe reached the point necessary for disconnection the thrust and rotation potentiometers were turned back to the point that these functions stopped. Once the thrust and rotation rates dropped to zero, the execution of the computer data acquisition program automatically terminated.

Upon completion of a bore, the polyethylene pipe was disconnected from the swivel behind the cutter/reamer. The Polycorder data logger collecting data from the

pressure transducer inside the pipe was disabled. A crawler tractor was then hooked to the tail end of the HDPE pipe and the pipe was pulled back out of the bore hole for re-use during the next bore.

The stakes holding the boring unit were removed from the ground. and the boring unit was then moved over a distance of approximately 15 ft (4.6 m). The 15 ft (4.6 m) distance was selected as being a reasonable distance to prevent any significant interaction between the bores. The next bore was started from this point and run more or less parallel to the previous bore.

### *Soil Test*

#### Particle Size Analysis

The procedures for soil particle size analysis were based upon ASTM standards D421-85 (Standard Practice for Dry Preparation of Soil Samples for Particle-Size Analysis and Determination of Soil Constants) (1994) and D422-63 (Standard Test Method for Particle-Size Analysis of Soils) (1994). Also consulted were the procedures given in Measuring Engineering Properties of Soil by W.K. Wray (1986).

A combined mechanical and hydrometer soil particle size analysis was conducted. A mechanical analysis using the U.S. No.'s 6 (3.35 mm) and 10 (2.00 mm) sieves was first used to determine the coarse material fractions of the soil samples. Hydrometer analysis was used on material passing through the No. 10 sieve as directed in ASTM D422-63. One, 2, 5, 15, 30, 60, 240, and 1440 minute readings were taken during the hydrometer analysis. After a hydrometer analysis was completed on a soil sample, the material in the hydrometer was washed across a U.S. No. 200 (75  $\mu\text{m}$ ) sieve and rinsed with purified water. The material retained on the No. 200 sieve was oven dried, and subsequently sifted



through a stack of sieves composed of U.S. No.'s 30 (600  $\mu\text{m}$ ), 50 (300  $\mu\text{m}$ ), 100 (150  $\mu\text{m}$ ), and 200 (75  $\mu\text{m}$ ).

A two-point temperature correction curve for the 152-H hydrometer was generated according to the procedure given in Sections 7.2 and 7.3 of ASTM D422-63. The straight line plot was used to correct the hydrometer readings for errors due to water temperature fluctuation and reading from the top of the meniscus. Correction values were subtracted from the measured readings to yield the values used for analysis.

The particle diameter relating to the elapsed time during the hydrometer analysis was calculated using the equations and methodology provided by Wray (1986). The particle diameter relating to a given time reading is given by:

$$d = \sqrt{\frac{30 \times N \times L}{980 \times (G_s - G_w) \times t}} \quad \text{Eq. (15)}$$

Where:  $d$  = the particle diameter in mm

$N$  = coefficient of viscosity of water, poise

$L$  = distance from suspension surface to the depth at which the suspension is being measured, cm

$G_s$  = the specific gravity of the soil solids, assumed value of 2.70

$G_w$  = the specific gravity of water at the test temperature

$t$  = the elapsed time from the start of test, minutes

The percent finer than the diameter determined by Eq. (15) is given by:

$$P_f = \frac{a \times R}{W_s} \times (100 - P_c) \quad \text{Eq. (16)}$$

Where:  $P_f$  = the percentage of material finer than the diameter,  $d$

$a$  = the ratio of the specific gravity of the soil solids to 2.65

$R$  = the temperature-corrected hydrometer reading

$W_s$  = the corrected weight of the soil solids used in the hydrometer analysis, g

$P_c$  = the percent coarse material (equivalent to the corrected original sample weight divided by the oven dry weight of material retained on the No. 10 sieve)

Plots of the particle size analyses for the soil samples from all 20 bores are given in Section E of the Appendix.

#### Atterberg Limit Testing

Liquid and plastic limit tests were conducted on each of the soils from the Stillwater Creek test location. This testing was done according the procedure given by Wray (1986) in Chapter 4, Atterberg Limits. Air dried samples of soil material having passed a U.S. No. 40 (425  $\mu\text{m}$ ) sieve. The air dried soil material was moistened with purified water and allowed to cure for a minimum of 24 hours before conduction of the tests as directed by Wray. Four point liquid limit tests were conducted using the Casagrande liquid limit device. A fifth point was added if needed to ensure a minimum of two points on either side of the 25 blow line.

Plastic limit values were based on the moisture contents from two repetitions of the plastic limit test. A plastic limit test was attempted on the sample from Bore 16 at the Coyle test site. This soil was the finest grained of all samples collected from the Coyle site. The sample proved to be non-plastic. As the finest of these soils proved to be non-

plastic, no further plastic or liquid limit tests were conducted on the samples from the Coyle site. All of the Coyle samples were accepted to be non-plastic.

### Soil Classification

Soils were classified according to the Unified Soil Classification System (USCS) and the USDA soil classification system. The USCS system is based on both the particle size distribution and the Atterberg limits of the soil. Procedure for classification of the test soils according to the USCS system was given by Wray (1986) in Chapter 6, *Soil Classification*. The USDA soil classification is based solely on particle size. The relative percentages of sand, silt, and clay size particles determine the classification. Each of the disturbed, auger-cutting samples from the Coyle test site and the core samples obtained from each bore at the Stillwater Creek location were classified. The classifications of the soil samples are given in Table 2 on Page 101.

### Direct Shear Testing

To obtain a standardized, quantitative index of the shear strength of the soils at the Stillwater Creek test location, direct shear testing was performed on each of the core samples obtained at the location. Procedure for the shear testing was given by Wray (1986) in Chapter 11, *Direct Shear Testing*. Additional guidance for performing shear testing on the cohesive soil material was provided by Dr. Don Snethen (1996) of the Oklahoma State University Department of Civil Engineering.

On each of the cylindrical core samples, approximately 1 in (2.5 cm) of material was cut off and discarded from the end which had been at the top of the sample. The purpose of the removal of the topmost material from the sample was to discard loose cuttings which might have fallen back into the sample hole during the extraction of the

**Table 2****CLASSIFICATION OF TEST SOILS****Coyle Test Site**

Bore	USCS Classification	USDA Classification
5	ML Silt with sand	Silt loam
6	ML Sandy silt	Loam
7	ML Silt with sand	Silt loam
8	ML Sandy silt	Silt loam
9	ML Sandy silt	Sandy loam
10	ML Sandy silt	Loam
11	ML Silt with sand	Silt loam
12	ML Silt with sand	Silt with sand
13	ML Silt with sand	Silt loam
14	ML Sandy silt	Silt loam
15	ML Sandy silt	Silt loam
16	ML Silt	Silt loam

**Stillwater Creek Test Site**

Bore	USCS Classification	USDA Classification
0	CL Lean clay	Silty clay loam
1	CL Lean clay	Silty clay loam
2	CL Lean clay	Silty clay loam
3	CL Lean clay	Silty clay loam
4	CL Lean clay	Silty clay loam
5	CL Lean clay	Silty clay loam
6	CL Lean clay	Silty clay loam
7	CL Lean clay	Silty clay

auger. Any cuttings which fell back into the hole would have ended up at the top of the sample.

The remainder of the cylindrical core samples was cut transversely into four cylindrical sections of approximately equal length. A 2.00 x 2.00 in (5.08 x 5.08 cm) square, steel, trimming mold was used to obtain an appropriately sized sample for the square shear box used in the test. The trimming mold was 1.00 in (2.54 cm) in height. The soil in the short cylindrical sample sections was carefully worked into the trimming mold by alternately pressing the mold onto the sample sections a short distance, and then trimming the soil material from around the base of the mold with a knife. Once the soil sample completely filled the trimming mold, a knife was used to strike off the soil material on the top and bottom of the mold such that all that was left was the square trimming mold with a 4.00 in<sup>3</sup> (65.5 cm<sup>3</sup>) soil sample inside.

The trimming mold, of known weight, with the soil sample inside was then weighed. Having the weight of the known volume of soil in the trimming mold allowed a direct calculation of the wet density of the soil material.

The 4.00 in<sup>3</sup> (65.5 cm<sup>3</sup>) soil sample was pushed out of the trimming mold and into the shear box using a 2 x 2 in (5 x 5 cm) wood block to shove the sample out of the mold. The shear box was placed into the direct shear test machine and the test conducted.

The device used for the tests was a Geotest Instrument Corporation Model S2215 digital direct shear test machine, Serial Number 882-4. Horizontal and vertical displacement values during the shear testing were measured with linear variable displacement transducers (LVDT's) with sensitivities of 0.001 and 0.0001 in (3.9 and 0.39

$\mu\text{m}$ ), respectively. Shearing force was measured with a strain gauge type force transducer integral to the Model S2215.

Shear tests on each core sample were conducted at three different normal force values. The vertical loadings used during the test were 0.5, 1.0, and 2.0 ton/ft<sup>2</sup> (47.6, 95.2, and 190.3 kPa). Each test was conducted at a shear rate of 0.02 in/min (0.51 mm/min), the equivalent of 1% axial strain/min. Tests were allowed to continue until a maximum shearing force was achieved or until the total axial strain exceeded 10%. The maximum shearing force for this case was taken to be the shearing force at the 10% strain condition.

After each test was completed, the soil sample was removed from the shear box and placed in a pre-weighed drying tin. The sample was weighed to the nearest 0.1 g and placed in a drying oven at 110 C. The samples were dried for a minimum of 16 hours and then reweighed. The difference in wet and dry weights of the soil samples were used to calculate the moisture content of the sample at the time of test. Since the core samples were sealed with plastic wrap and kept in cold storage until testing, the moisture content at the time of test is assumed equal to the in-situ moisture content of the bore at the time of test.

The peak shear stress values for each of the samples was plotted versus the normal stress applied to the sample during the test. Vertical (normal) stress was plotted on the X axis, horizontal (shear) stress was plotted on the Y axis. Thus, for each core sample three points were plotted on the graph. The best fit line for these three points then represents the shear strength envelope for the soil. The equation for the shear strength envelope of a soil may be described by:

$$s = c + \sigma_n \cdot \tan \Phi \quad \text{Eq. (17)}$$

Where:  $s$  = the shear strength of the soil (force/area)

$c$  = the soil cohesive strength (force/area)

$\sigma_n$  = the vertical (normal) stress applied to the shear plane (force/area)

$\Phi$  = the angle of internal friction of the soil sample (degrees)

The soil cohesive strength,  $c$ , was taken to be the stress magnitude indicated where the best fit line through the three plotted points for each soil sample intersected the Y axis. The angle of internal friction,  $\Phi$ , was the angle, in degrees, made by the best fit line in relation to the X axis. Given these two parameters, the magnitude of the shear strength of the soil was determined given the pressure acting normal to the plane of shear. Table 3 on Page 105 gives the values of mean density, mean soil water moisture, cohesive strength ( $c$ ), and internal friction angle for the 8 soil cores taken from the Stillwater Creek test area.

#### Standard Penetration Tests

It was desired to have an equivalent index of soil shear strength and density for characterization of the soil at the Coyle testing site. The non-cohesive nature of the soil prevented sample collection by simple core sampling. It was impossible to determine density or undisturbed shear strength from the disturbed auger samples collected at the site. To obtain a standardized index of the density and shear strength at the Coyle site, a series of four Standard Penetration Test (SPT) soundings were conducted at the Coyle test site. Figure 28 on Page 106 gives an indication of the relative position of the SPT soundings in relation to the bore locations. The exact location of the soundings relative to the bore paths could not be determined as the field in which the bores were conducted was

Table 3

PROPERTIES OF SOIL SAMPLES FROM STILLWATER CREEK TEST SITE

Bore	$\phi$ (Degrees)	c (psi)	w <sub>c.b.</sub> (%)	Density (lb/ft <sup>3</sup> ) - w.b.	e <sub>0</sub>	w <sub>L</sub> (%)	w <sub>P</sub> (%)	I <sub>P</sub> (%)	I <sub>F</sub> (%)	I <sub>L</sub> (%)	Degree of Saturation
0	27	3.9	21.4	117.6	0.82	41.7	18.4	23.3	13.0	0.133	0.72
1	23	4.8	21.4	121.1	0.77	38.7	14.9	23.8	13.3	0.273	0.79
2	27	4.8	19.8	121.3	0.73	40.5	16.4	24.1	6.3	0.141	0.76
3	29	6.3	18.1	123.6	0.66	39.3	15.3	24.0	19.3	0.177	0.76
4	32	2.6	19.5	122.1	0.71	37.8	14.6	23.2	8.3	0.216	0.77
5	24.5	3.5	26.6	114.1	1.02	40.6	17.5	23.1	3.0	0.394	0.72
6	29.5	1.0	26.9	108.0	1.13	38.4	16.2	22.2	4.5	0.482	0.67
7	25	3.2	27.8	113.6	1.06	40.6	17.8	22.8	6.6	0.408	0.73

$\phi$  = angle of internal soil friction

c = cohesive strength of soil

w = dry basis moisture content of soil sample (Eq. 11)

Density = wet basis bulk density of soil sample

e<sub>0</sub> = void ratio of soil sample [= volume<sub>voids</sub>/volume<sub>solids</sub>]

w<sub>L</sub> = liquid limit

w<sub>P</sub> = plastic limit

I<sub>P</sub> = plasticity index [= w<sub>L</sub>-w<sub>P</sub>]

I<sub>F</sub> = flow index [= slope of Atter. Lim. flow curve ]

I<sub>L</sub> = liquidity index [= (w-w<sub>P</sub>)/I<sub>P</sub> ]



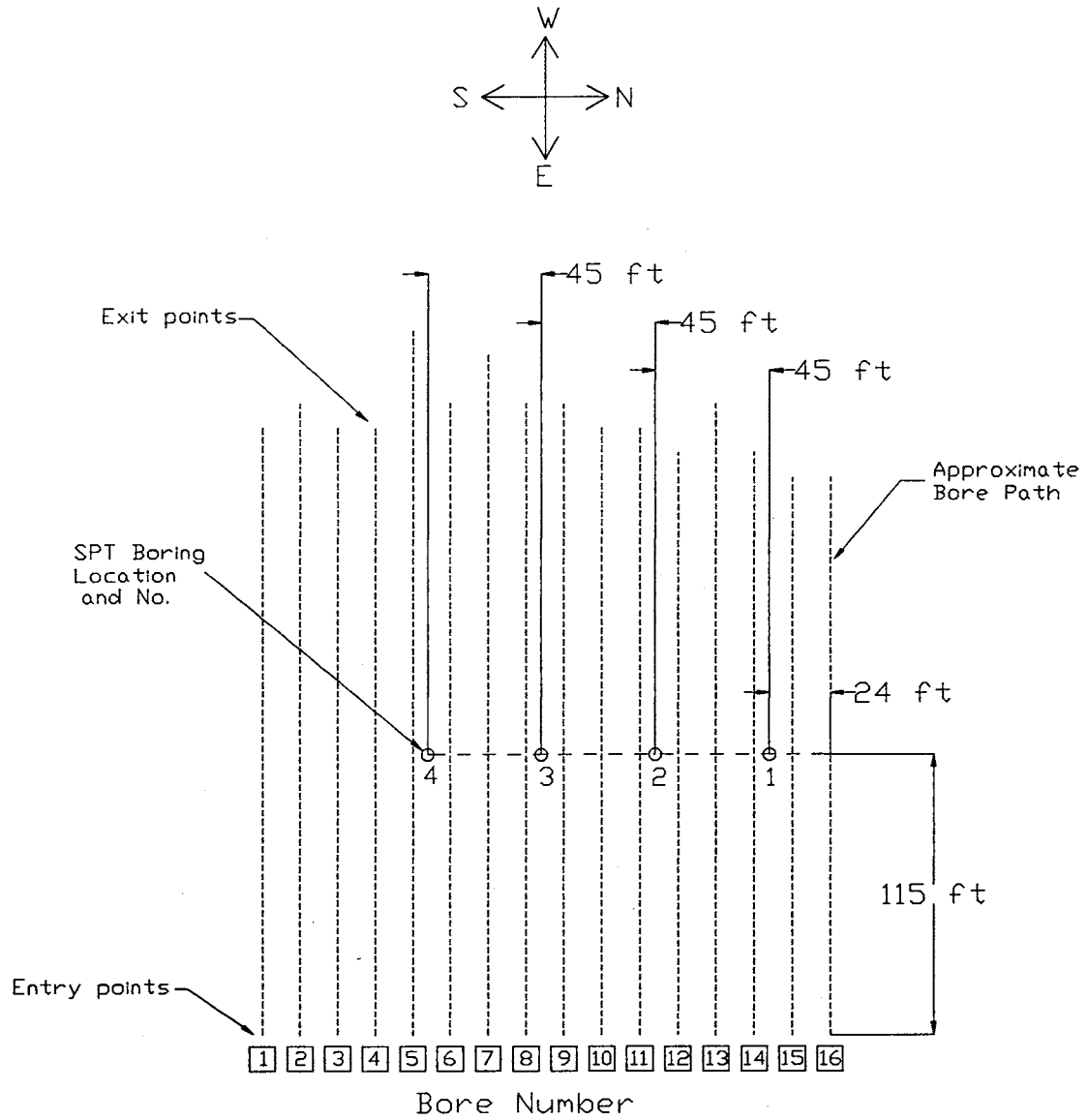


**Figure 28:** Approximate location of Standard Penetration Test borings relative to bore paths at Coyle test site.

tilled before the SPT testing was performed. The tilling of the field removed and buried the flags which marked the path of each of the bores. The entry and exit locations of Bore 16 were still apparent, however. Thus, Figure 28 is laid out relative to the average spacing of the bores and the spacing of the SPT soundings.

The SPT testing was conducted by the Alliance Drilling Company of Tulsa, Oklahoma. The basic procedure used in the test is outlined in ASTM D 1586-84 (1994), Standard Test Method for Penetration Test and Split-Barrel Sampling of Soils. A 2.00 in (5.1 cm) outer diameter split barrel sample tube was used during the tests. The sample tube was driven and removed in 2.0 ft (0.61 m) increments by a 140 lb (63.5 kg) hammer with a free fall of 30 in (0.76 m). The number of blows required to drive the sampler over each 6 in (0.15 m) increment was recorded. The soil collected in the split-barrel sample tube was visually inspected after each drive and the length and description of the sample was recorded. One deviation was made from the ASTM D1586-84 procedure. Each “drive” was 2 ft (61 cm) in length, consisting of four 6 in. (15 cm) segments, instead of 18 in (46 cm) as outlined in D 1586-84. The blowcount numbers and descriptions of the soil samples obtained are given in Table 4 on Page 108.

The blowcount readings from the site were used to generate an estimate of the soil internal friction angle and the material density based on the empirical correlations of Peck, Hanson, and Thornburn (1974). The blowcount totals from the third and fourth 6-inch drive segment were added to give the N value for the correlations. The values of internal friction angle and soil density are given in Table 5 on Page 109.

**Table 4****BORE LOG: STANDARD PENETRATION TESTS AT COYLE TEST SITE*****Boring 1***

Drive #	Blowcounts N/(6" intervals)	Cumulative Depth (ft)	Sample Description
1	1-2-4-3	2	0-8" Light brown, poorly graded, fine sand 8-17" Brown, fine sand/silt
2	1-2-2-4	4	0-4.5" Moist, dark brown sand/silt 4.5-19" Moist, reddish brown fine sand/silt
3	3-3-2-1	6	0-3" Brown sand/silt (fall back into hole) 3-21" Moist reddish brown fine sand/silt
4	2-3-3-3	8	0-18" Wet, reddish brown fine sand

***Boring 2***

Drive #	Blowcounts N/(6" intervals)	Cumulative Depth (ft)	Sample Description
1	2-2-3-3	2	0-8.5" Light brown, poorly graded, fine sand 8.5-22.5" Brown, fine sand/silt
2	1-1-2-3	4	0-21" Moist, reddish brown, fine sand
3	4-3-2-2	6	0-21" Reddish brown, fine sand. More red toward bottom of sample. Moist last 6".
4	5-7-9-10	8	0-9" Very wet, red fine sand/silt 9-20.5" Moist, fine, brown sand (a little coarser than above)

***Boring 3***

Drive #	Blowcounts N/(6" intervals)	Cumulative Depth (ft)	Sample Description
1	1-2-3-2	2	0-12" Moist, light brown, poorly graded, fine sand 12-21" Moist, brown, fine sand/silt
2	1-2-3-2	4	0-7" Moist, brown, clayey sand 7-19" Moist, fine, red sand
3	5-4-5-6	6	0-21.5" Moist, brown to reddish brown, fine sand. Darker at top of sample.
4	4-7-8-8	8	0-4" Very moist, brown/reddish brown, fine sand 4-19" Wet, brownish red, fine sand

***Boring 4***

Drive #	Blowcounts N/(6" intervals)	Cumulative Depth (ft)	Sample Description
1	1-3-2-2	2	0-9" Light brown, poorly graded, fine sand 9-20.5" Brown, fine sand/silt
2	1-1-2-2	4	0-15" Brownish red, very fine sand/silt 15-20" Moist, reddish brown, fine sand
3	2-4-6-4	6	0-21" Moist, brownish red, fine sand.
4	2-3-3-4	8	0-21" Wet, brown fine sand

Table 5

RELATIVE DENSITY AND ANGLE OF INTERNAL FRICTION FOR  
SOILS AT COYLE TEST SITE BASED ON STANDARD PENETRATION  
TEST CORRELATIONS

Boring No.	Drive No.	N*	Depth at N* (ft)	Relative Density	$\phi$
1	1	7	1-2	Loose	29
	2	6	3-4	Loose	29
	3	3	5-6	Very Loose	28
	4	6	7-8	Loose	29
2	1	6	1-2	Loose	29
	2	5	3-4	Very Loose	28
	3	4	5-6	Very Loose	28
	4	19	7-8	Medium	33
3	1	5	1-2	Very Loose	28
	2	5	3-4	Very Loose	28
	3	11	5-6	Medium	30
	4	16	7-8	Medium	32
4	1	4	1-2	Very Loose	28
	2	4	3-4	Very Loose	28
	3	10	5-6	Loose	30
	4	7	7-8	Loose	29

N\* = sum of last two 6 in. segments of each 2 foot drive.

$$= n_3 + n_4$$

Relative density and  $\phi$  (angle of internal friction) determined by empirical correlations of Peck, Hanson, and Thornburn (1974).

### Moisture Content of Coyle Soil Samples

Before the disturbed auger samples taken from the Coyle test location were dried for the particle size analysis testing, a moisture content measurement was taken from each sample. Two sub-samples of approximately 70 g each were collected from the resealable plastic bags containing the soil from the Coyle location. The sub-samples were placed in preweighed drying tins and weighed to the nearest 0.01 g. The samples were then dried for 24 hours at 110 C. Once dried, the sub-samples were weighed again. The moisture loss was used to calculate the moisture content of the samples by the equation:

$$w_{db} (\%) = \frac{m_w - m_d}{m_d} \times 100 \quad \text{Eq. (18)}$$

Where:  $w_{db}$  = the dry basis soil moisture content (%)

$m_w$  = the mass of the wet soil sample, grams

$m_d$  = the mass of the dry soil sample, grams

The moisture content of each sample was taken to be the average of the moisture content readings from the two sub-samples. These values are recorded in Table 6 on Page 111.

### ***Drilling Fluid Analysis***

Fluid property analysis was conducted on samples of drilling fluid used during bores at both the Coyle and Stillwater Creek test locations. Samples were taken from 5 bores at the Coyle location and from 4 bores at the Stillwater Creek location. Testing conducted included measurement of mud weight, and viscometric testing with both Marsh funnel and rotary viscometer methods. These tests were conducted for the purpose of characterization of the properties of the drilling fluids used during the testing.

Table 6

## SOIL SAMPLE MOISTURE CONTENTS - COYLE TEST SITE

Bore	Dry basis moisture content (%)
5	24.0
6	21.9
7	27.2
8	26.1
9	25.7
10	23.9
11	24.2
12	24.7
13	23.9
14	20.7
15	23.4
16	23.0

A Baroid mud balance was used to measure density of the drilling fluid. Procedure for mud balance tests was given by Chilingarian and Vorabutr (1981). The principle of the mud balance is simple. A known-volume cup mounted along a rigid bar a fixed distance from a fulcrum point is filled with the drilling fluid. On the other side of the fulcrum, a sliding weight is moved along the bar until the bar is level. Calibration marks along the bar indicate mud weight in pounds per gallon.

The rotary viscometer used was a Fann Model 35-A, 6-speed model, serial number 2438. Measurements were taken of 600 rpm, 300 rpm, 6 rpm, and 3 rpm dial readings. Drilling fluids are often assumed to behave as a Bingham plastic, having a yield point, or minimum shear stress required before shear will begin, and a linear relationship between shear rate and shear stress thereafter. Using this assumption the plastic viscosity of the drilling fluid was calculated using the following formula provided by Chilingarian and Vorabutr:

$$V_P = D_{600} - D_{300} \quad \text{Eq. (19)}$$

Where:  $V_P$  = the apparent viscosity in centipoise

$D_{600}$  = the 600 rpm dial reading

$D_{300}$  = the 300 rpm dial reading

The yield point of the drilling fluid was found using the following equation provided by Chilingarian and Vorabutr (1981):

$$Y = D_{300} - V_P \quad \text{Eq. (20)}$$

Where:  $Y$  = the yield point in lb/100 ft<sup>2</sup>

$D_{300}$  = the 300 rpm dial reading

$V_p$  = the plastic viscosity in centipoise

Marsh funnel viscosity readings were taken because of the widespread use of this viscosity index when dealing with drilling fluids. The Marsh funnel test measures the time, in seconds, required for 1 quart (0.95 l) of drilling fluid to flow out of a standardized funnel when the funnel is initially filled to a reference line. The Marsh funnel readings are influenced by drilling fluid temperature, density, rate of gelation, etc. The Marsh funnel readings cannot be converted to any standardized unit of viscosity and are only a pseudo-quantitative assessment of viscosity (Chilingarian and Vorabutr, 1981). Marsh funnel readings, in seconds, along with mud weight and the viscometric properties obtained from the rotary viscometer are given in Table 7 on Page 114.

Temperature of the drilling fluid at the time of testing was recorded and is also given in Table 7. Please note that while drilling fluid samples were taken during Bores 4, 8, 14, 15, and 16 at the Coyle test site, only the data from Bores 14-16 is given. Delays between time of sampling and time of testing for the samples taken during Bores 4 and 8 caused the viscosity readings to be artificially high. This was due to the nature of Bentonite mixes to continue to “yield” or thicken with time. Samples taken during Bores 14, 15, and 16 were all tested within 20 hours of the collection time.



Table 7

**DRILLING FLUID VISCOMETRIC PROPERTIES**

Test Location	Bore	*Mud Components	Density (lb/gal)	Temp. at test time (°F)	**600 rpm dial rdg.	**300 rpm dial rdg.	**3 rpm dial rdg.	10 sec. gel strength (cp)	Marsh funnel secs.	PV (c.poise)	YP (c.poise)
Coyle	14	Quik-Gel® + water	8.55	61	40.0	29.5	10.0	10.0	46	10.5	19
Coyle	15	Quik-Gel® + water	8.55	68	51.0	39.5	19.0	13.0	53	11.5	28
Coyle	16	Quik-Gel® + water	8.50	78	36.5	27.0	8.0	9.0	43	9.5	17.5
Stillwater Creek	1	E-Z Mud® + water	8.32	67	6.5	4.0	0	1.5	31	2.5	1.5
Stillwater Creek	2	E-Z Mud® + water	8.35	59	6.0	4.0	0.25	0.5	30	2.0	2.0
Stillwater Creek	6	E-Z Mud® + water	8.32	71	5.5	3.5	0.25	1.0	28	2.0	1.5
Stillwater Creek	7	E-Z Mud® + water	8.32	67	5.5	3.5	0.25	0.5	30	2.0	1.5

\* Quik-Gel® and E-Z Mud® are products of Baroid drilling fluids. Descriptions and mixing ratios included in "Procedures" section.

\*\* Fann 35-A viscometer dial readings are calibrated in centipoise.

PV = Plastic viscosity in centipoise (600 rpm reading - 300 rpm reading)

YP = Yield point in lb/100 ft<sup>2</sup> (300 rpm reading - PV)

## Chapter 5

### Data Reduction and Analysis

#### *Reduction of Bore Data*

For each bore conducted during the test, the data from the “no-load” runs at the start and end of the bore were pulled into a Microsoft® Excel spreadsheet program. The average of all hydraulic oil temperature readings taken during each no-load run of the boring unit was recorded as the reference temperature for that run.

Each no-load run was comprised of essentially two phases as discussed in the Procedure section of this report. The rotational torque values from the first phase, the parasitic torque readings, of each no-load run were then plotted against their corresponding rotational speed values. Using the linear regression analysis feature in Excel, a best fit straight line was fit through the plot of the torque values. The equation for the line was recorded.

Next, the pull force values from the second phase, the parasitic pulling force readings, of the no-load run were plotted against their corresponding pull rate readings from the pull rate transducer. A best-fit straight line was fit through the plot of the pull force values. The equation for the line was recorded.

Once the data from both no-load runs for each bore were reduced to individual temperature values and equations for the best fit lines of torque vs. spindle rotation rate and pull force vs. carriage pull rate, temperature-compensated torque and pull force correction curves were created. The torque correction curves consisted of plots of rotational torque versus temperature. Four lines representing the four rotational rates

used during the test were constructed on the graph between the two temperatures (See Figure 29 on Page 117). In a similar manner, the pull force correction curves consisted of plots of no-load pulling force versus temperature for each of the three pull rates used during the test (See Figure 30 on Page 117).

The data files from the 14 drilling pipes for which data was kept pulled in through the uniform depth section of each bore were individually loaded into Excel spreadsheets. Starting at the point where the position of the carriage was recorded as 10 ft (3.0 m) from its furthest rearward point, the difference in position after the next 123 readings (refer to pull rate calibration discussion in Procedures section of the report) represented the distance traveled in two minutes. This distance was used to calculate the actual carriage pull rate for the run in ft/min as discussed in the Procedures section of this report.

The rotational torque, pulling force, and hydraulic oil temperature readings used in the statistical analysis of the data came from the middle section of each drilling pipe pulled. The position transducer reading for the drilling carriage at the start of each run was 10.7 ft (3.26 m). The drilling rods were 10 ft (3.05 m) in length, thus the midpoint of each drilling rod occurred at a measured carriage position of 5.7 ft (1.74 m). The rotational torque, pulling force, and hydraulic oil temperature used in the statistical analysis of the data were the average of all values occurring between an indicated carriage position of 7.7 ft (2.35 m) and 3.7 ft (1.13 m), or  $\pm 2.0$  ft ( $\pm 0.61$  m) from the midpoint of the each drilling pipe. This was the section most closely corresponding to the penetrometer readings, which were taken at the approximate midpoint of each drilling pipe in the ground.

This procedure was repeated for the data from each of the 20 bores included in this study. While data was collected on 14 joints of drilling pipe from each bore, only the data

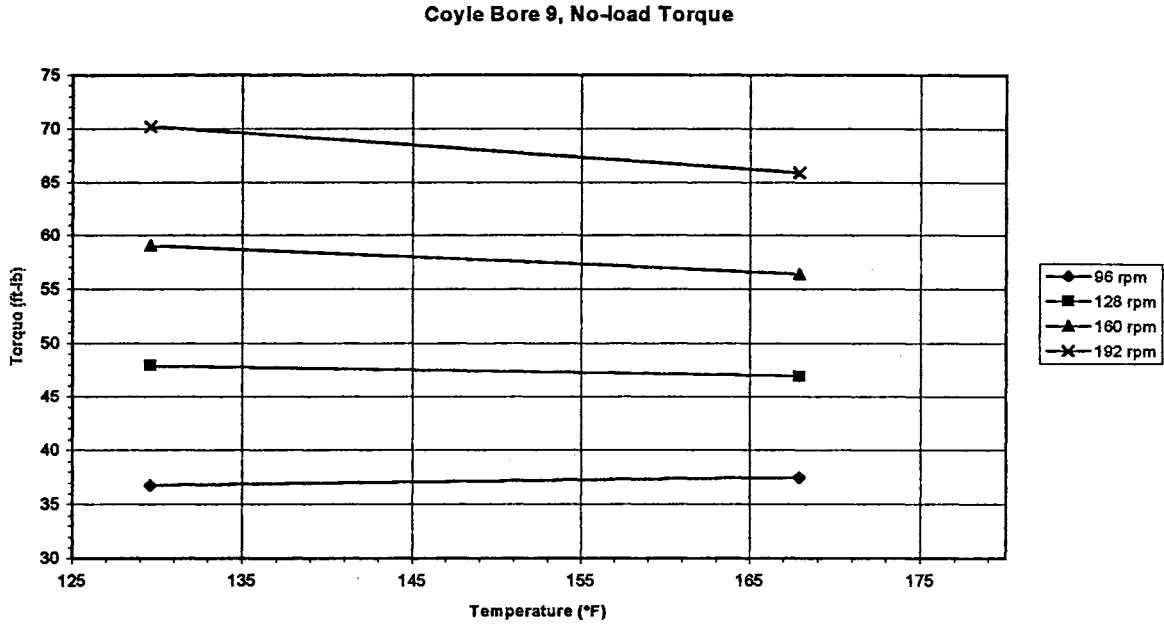


Figure 29: Illustration of typical no-load torque correction plot.

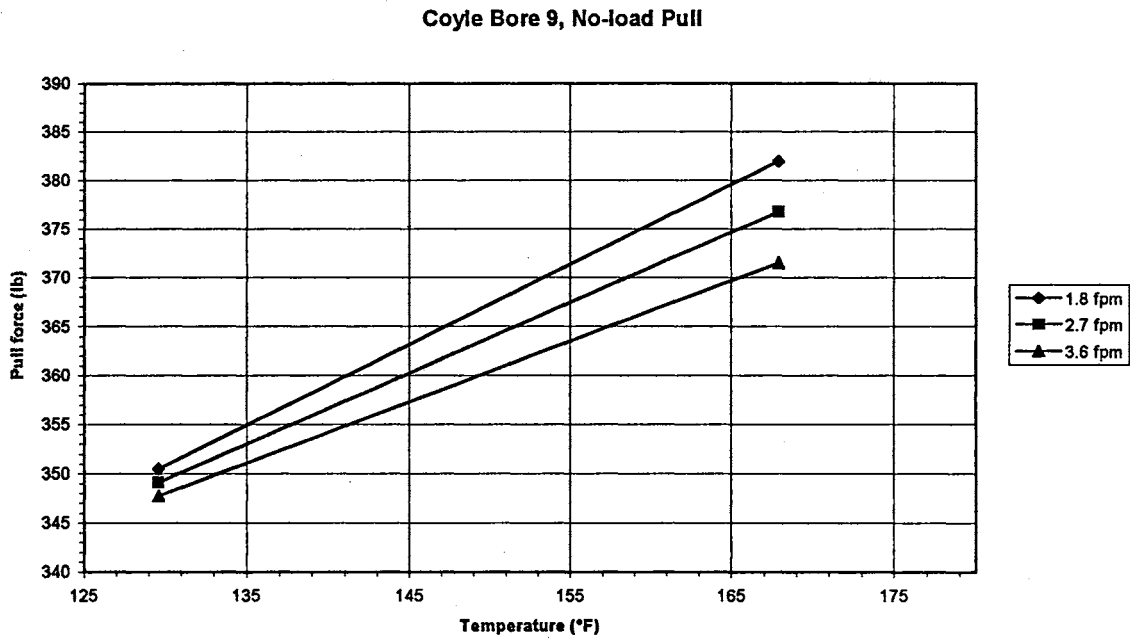


Figure 30: Illustration of typical no-load pull force correction plot.

from 12 of these was included in the statistical analysis. The data from the “spares”, drilling pipes 13 and 14, were not included unless a problem (electronic, hydraulic, procedural, etc.) occurred on one of drilling pipes 1 to 12 which would render its data readings suspect.

### ***Reduction of Penetrometer Data***

Fourteen penetrometer readings were taken along each bore corresponding to the 14 drilling pipes whose boring unit performance data was recorded. Once the data acquisition system was started during any penetrometer sounding, it continued to collect data at a rate of 4 Hz until the last penetrometer rod was completely in the ground. Consequently, each data file from the penetrometer readings consisted of: a) a short section of data where the penetrometer cylinder was advanced with no penetrometer rod attached to give an index of the frictional forces associated with cycling the cylinder, b) a section of unnecessary data where the cylinder was retracted and the first penetrometer rod was screwed on, c) a section of data where the first penetrometer rod was advanced to the point where the cone was just seated in the ground surface followed by a pause of approximately 5 seconds, d) the data as the first penetrometer rod was shoved into the ground, e) unnecessary data as the hydraulic cylinder was retracted and the second penetrometer rod was screwed on, f) sections (d) and (e) repeated for the second and third penetrometer rods were pushed into the ground.

Each data file was imported into a word processor program and the unnecessary data from the retracting of the cylinder and attachment of penetrometer rods (sections {b} and {e}) was deleted. The paired down data file was then resaved.

Each data file was then imported into an Excel spreadsheet. The no-load readings from section (a) were averaged to give a single value of parasitic force associated with the cylinder. The position readings taken with the penetrometer cone just seated into the ground surface (section {c}) were averaged to give the position readout associated with a depth of 0. Electronic noise associated with the data acquisition system caused these readings to fluctuate approximately  $\pm 0.1$  in ( $\pm 2.5$  mm) while the penetrometer was not in motion. The zero depth reading was then subtracted from all subsequent depth readings of the first penetrometer rod so that they represented the actual depth of the penetrometer cone.

For the second and third penetrometer rods, the position reading where the force reading again resumed at approximately the same level as at the end of the previous rod was taken as the zero point for that rod. The subsequent readings for the second or third rods were corrected for their respective zero points and their resultant depth readings were added to those of the rods preceding them. The result was a continuous, cumulative depth reading for all three penetrometer rods and their associated uncorrected force readings.

The frictional force value related to the movement of the hydraulic cylinder was then subtracted from each of the force readings for the sounding. This yielded a depth value from the ground surface and its corresponding corrected force reading for the entire length of the penetrometer sounding.

Before plotting, the force values were converted to a cone-tip pressure reading by dividing the force reading by the  $1.55 \text{ in}^2$  ( $10.0 \text{ cm}^2$ ) area of the cone tip. In geotechnical analysis, penetrometer cone tip pressures are typically designated as  $q_u$ . Plots of the full

depth penetrometer soundings for one bore at each of the test locations is given in Section F of the Appendix.

To arrive at a value to place into the data set for statistical analysis, it was necessary to determine the depth of the drilling pipe in the ground at the point where the penetrometer reading was taken. The depth value used was the average of the depth readings taken at the start and end of the drilling pipe in question. The fluted reamer used for all of the bores conducted at the Coyle test site and for half of the bores conducted at the Stillwater Creek test site cut a hole of 7.0 in (18 cm) in diameter. The penetrometer value entered into the data set for analysis was the arithmetic mean of all  $q_u$  values  $\pm 3.5$  in (8.9 cm) from the depth of the drilling pipe at the penetrometer location. This 7.0 in (17.8 cm) section was chosen as that corresponding to the material cut by the fluted reamer.

### ***Reduction of Polyethylene Pipe Pull Data***

The data from the Sensotec pressure transducer used to measure the pressure trapped in the rod end of the hydraulic cylinder located within the polyethylene pipe was pulled into a spreadsheet. The pressure data was converted to a force reading by multiplying by the area of the piston on the rod end of the cylinder. The force readings were plotted versus elapsed time from the start of the data acquisition system.

The plots consisted of a series of “hills and valleys”. While the pipe was moving as it was being pulled into the ground, the force reading increased to a certain magnitude associated with the conditions going on in the bore, and then leveled off. Once the drill pipe which was being pulled reached the disconnection point and was removed, the movement of the polyethylene pipe would stop. The stop in motion was accompanied by a sharp reduction in the measured force. Once the pipe started moving again the force

went back up. The starting and stopping of the pipe's progress accounted for the alternating high and low readings from the transducer. Plots of the force versus time for the bores are given in Section G of the Appendix.

The length of the "hills", or the elevated force readings, was determined by the rate of pull of the drilling pipes into the ground. The faster pulls resulted in narrower "hills", the slower pulls in wider plateaus. Each of the pulling force plots was compared to the schedule of pull rates for the test runs. By counting peaks and by comparing the pattern of long, medium, and narrow "hills", it was possible to establish which values corresponded to the force values measured at the boring unit.

Once the data associated with the period of data collection at the boring unit was located, the values of the force readings during the entire time the polyethylene pipe was in motion were averaged for each drilling pipe pulled in. The arithmetic average of these "hilltop" readings was the value entered into the data set for statistical analysis.

At the Coyle test location, much difficulty was experienced in keeping water from getting inside the polyethylene pipe. Efforts to seal the pipe and seal the pressure transducer from water insurgence were only partially successful. Once water would get into the transducer, the readings would become unpredictable and unreliable. The data from Coyle bores 6, 7, 8, 11, 12, 14, 15, and 16 have been excluded from analysis and presentation because of erroneous readings. Improved sealing of the transducer and the pipe before beginning the work at the Stillwater Creek location prevented the loss of any data from that location.



### *Statistical Analysis of Boring Data*

The analyses of variance from the statistical models given in Chapter 2 of this report were conducted using the General Linear Models (GLM) procedure in the Statistical Analysis System (SAS) software package. For each test site, three GLM procedures were conducted, one for each dependent variable evaluated in the test (rotational torque, pull force at the boring unit, and pull force at the HDPE pipe).

Statistical significance for each of the factors or interactions was defined at the 95% confidence level ( $\alpha=0.05$ ) unless otherwise noted in the discussion of the results. Factors involved in statistically significant two-way interactions received no evaluation of their one way effect terms as designated in the experimental models in Chapter 2. In cases where statistical comparisons between treatment means were warranted (such as in comparing the effect of reamer design at the Stillwater Creek test site), the comparisons were accomplished using simple one way contrasts in the GLM procedure within SAS.

Once the analysis of variance (ANOVA) testing was completed, regression analyses were performed to relate the controlled and covariate variables in the model statements to the dependent variable. The formation of the regression equations started with graphing of single variable effects and multi-variable interactions shown to be statistically significant in the ANOVA procedures. Once the general trends seen in the data were identified, regression equations were constructed and adjusted using the Regression procedure (PROC REG) in SAS. Various combinations of variables were tried until the potential was shown for achieving the highest coefficient of determination ( $r^2$ ) for the model. The SAS regression procedure was run using the STEPWISE selection criteria to ensure that all variables placed in the equation were significant. After the

general form of the regression equations were obtained, the coefficients in the equations were “tweaked” by utilizing the Non-linear regression procedure (PROC NLIN) in SAS.

Some additional regression analyses involving variables not listed in the model statements have been conducted as well. These were done to help demonstrate important observations made about the data or the processes involved with the backreaming operation. The results of the regressions are presented in graphical form in Chapter 6 with their corresponding discussion.

## Chapter 6

### Results and Discussion

#### *Reaming/Pullback Process Conceptualization*

The data from the boring tests are best interpreted in light of a conceptualization of the forces acting on the reamer/compactor and along the polyethylene pipe installed during the test. These forces are illustrated in Figure 31 on Page 126 and are described below.

$P$  = the pulling force transmitted through the pilot pipe string which pulls the reamer and installed utility into the ground.

$T$  = the rotational torque required by the boring unit to rotate the pilot pipe string, reamer, and compaction cone (if present) during the reaming operation.

$F_{PA}$  = the axial, frictional force acting along the pilot pipe.

$F_{RA}$  = the axial force acting on the reamer due to reaction from the soil profile as the reamer is drawn into it.

$F_{RR}$  = the radial force acting on the reamer from the surrounding soil profile as the hole is reamed. This force is caused by the expansion of the soil comprising the hole walls when the in-situ stress state of the soil is altered by the creation of the hole.

$F_{CA}$  = the axial force acting on the front face of the compaction cone (if present).

$F_{UA}$  = the axial force acting along the installed product line. This force is discussed by Huey et. al (1996). Refer to Product Installation Loading discussion in Chapter 1 of this report.

$F_P$  = the force generated on any surface due to pressure in the drilling fluid/soil slurry.

$M_{PF}$  = the moment caused by frictional resistance to turning of the pilot pipe string.

$M_{RS}$  = the moment created from the shearing of the soil at the front of the hole by the rotating reamer.

$M_{RFA}$  = the moment caused by soil-to-reamer adhesive and frictional forces as the reamer is rotated. This moment should be directly proportional to  $F_{RA}$ .  $M_{RFA}$  and  $M_{RS}$  are both generated from the soil cutting forces discussed in Chapter 1 of this report as they act on the face of the reamer.

$M_{RFR}$  = the moment caused by the frictional and soil-to-reamer adhesive forces resulting from  $F_{RR}$ , the radial soil pressure, acting on the reamer as it rotates.

$M_{RV}$  = the moment caused by viscous shearing stresses in the soil/fluid slurry as the reamer rotates.

$M_{CF}$  = the moment caused by the frictional and viscous forces on the face of the compaction cone as it rotates.

The pulling force,  $P$ , seen at the boring unit will be the sum of the axial forces acting on the pilot pipe ( $F_{PA}$ ), the reamer ( $F_{RA}$ ), the compaction cone ( $F_{CA}$ ), and the installed utility ( $F_{UA}$ ). The rotational torque,  $T$ , seen at the boring unit will be the sum of the moments acting along the pilot pipe ( $M_{PF}$ ), the reamer ( $M_{RS}$ ,  $M_{RFA}$ ,  $M_{RFR}$ , and  $M_{RV}$ ), and the compaction cone ( $M_{CF}$ ).

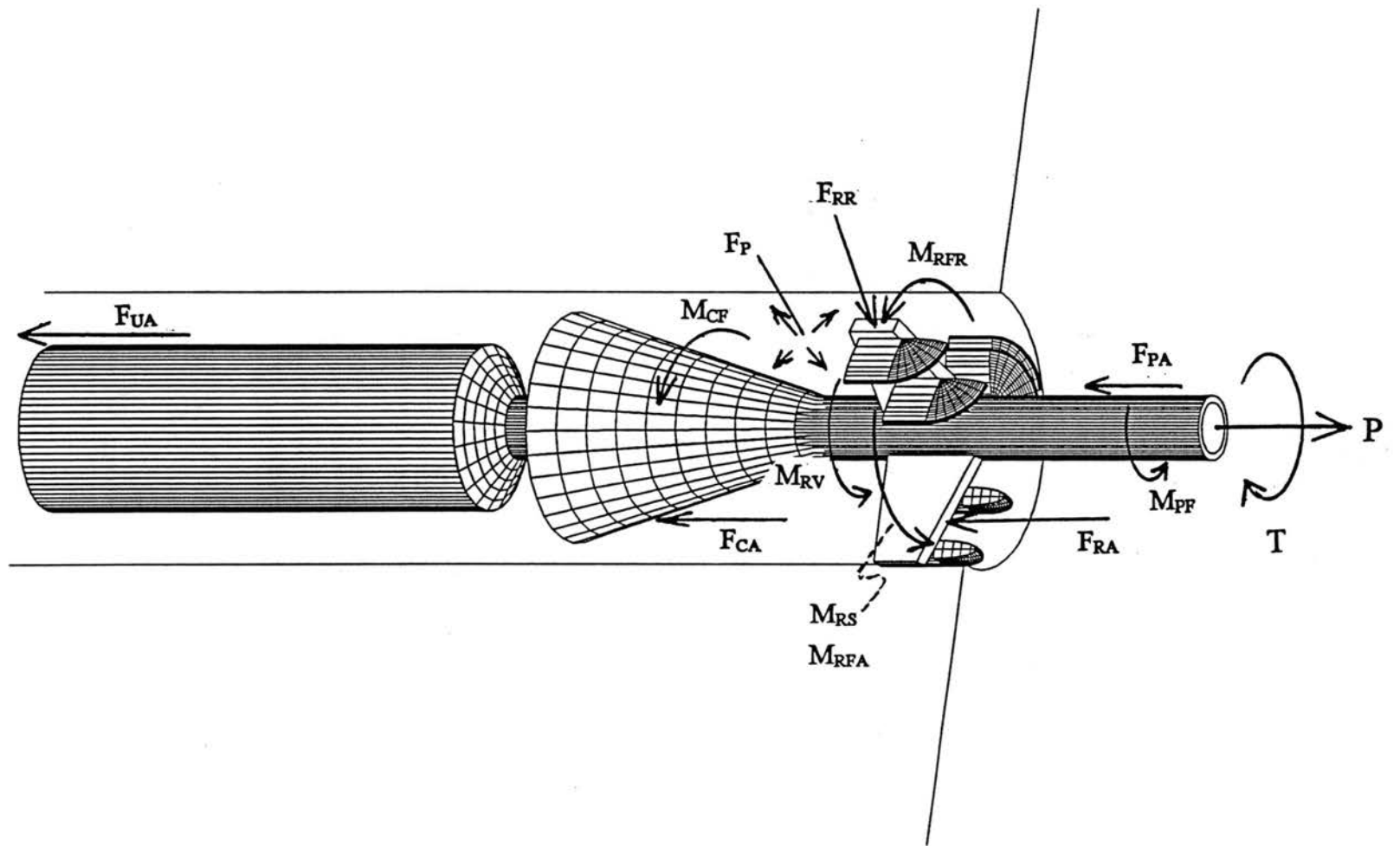


**Figure 31:** Illustration of forces acting on reamer/compactor during backreaming operation.

## Coyle Test Site

### Rotational Torque

The analysis of variance (ANOVA) table for the rotational torque data at the Coyle test site is presented in Table 8.

Table 8

ANOVA Table for Torque Model at Coyle Test Site

Source	Degrees of Freedom	Type I Sum of Squares	F Value	P
Penetrometer	1	151754	77.33	0.0001
Fluid Flow Rate	2	896305	228.37	
Bore(Flow Rate)	9	71082		
Rotat. Speed [RPM]	3	80303	13.64	
Pull Rate [FPM]	2	149051	37.98	
RPM x FPM	6	9508	0.81	0.5665
Flow Rate x RPM	6	60265	5.12	0.0001
Flow Rate x FPM	4	35451	4.52	0.0022
Flow Rate x RPM x FPM	12	21768	0.92	0.5260
Error ( $\delta$ )	98	192316		
<b>Total</b>	<b>143</b>	<b>1667803</b>		

As seen in Table 8, strong interactions exist between drilling fluid flow rate and rotation speed, and between drilling fluid flow rate and pull rate. Both interactions were significant well above the 99% confidence level.

Regression analysis was used to provide a best-fit equation to the data. The regression model found to most closely match the data was:

$$Torque = 2028 \cdot \left[ (fpm^{0.9}) \cdot \exp\left(\frac{-rpm}{160}\right) \cdot \exp\left(\frac{-flow}{33}\right) \right] + 0.040 \cdot q_u + 99 \quad \text{Eq.(21)}$$

Where: Torque = the rotational torque measured at the boring unit

corrected for “no load” readings. (ft-lb)

fpm = the pull rate of the reamer into the soil profile (ft/min)

rpm = the rotation rate of the reamer (rev/min)

flow = the drilling fluid flow rate (gal/min)

$q_u$  = the average penetrometer cone pressure at the given

location (lb/in<sup>2</sup>)

The model containing the product of the pull rate (fpm), the rotation rate (rpm), and the drilling fluid flow rate functions was found to give a better fit to the data than any models involving sums of functions involving the rpm, fpm, and flow terms. A plot of the measured torque versus the torque predicted in the regression model is given in Figure 32 on Page 129. The coefficient of determination ( $r^2$ ) for the model was 0.81.

Models may be fit to the data with the rpm and flow terms raised to negative exponents which fit equally well to the model presented in Equation 21. The decaying exponential form for the terms was chosen as it yields finite, positive values for torque regardless of the rotation rate or flow rate chosen. However, the stability of the model should not be viewed as a license to extrapolate the model to extreme values of pull rate, rotation rate, or drilling fluid flow rate and still expect to obtain accurate predicted values of torque.

The drilling fluid flow rate and rotation rate interactions are evident in Figures 33 and 34 on Page 130. In Figure 33, the mean value of torque from a given combination of drilling fluid flow rate and rotation speed are plotted versus the flow rate. In Figure 34, the torque values are plotted against the rotation speed. The regression lines in both

Coyle Test Site  
Measured vs. Predicted Torque

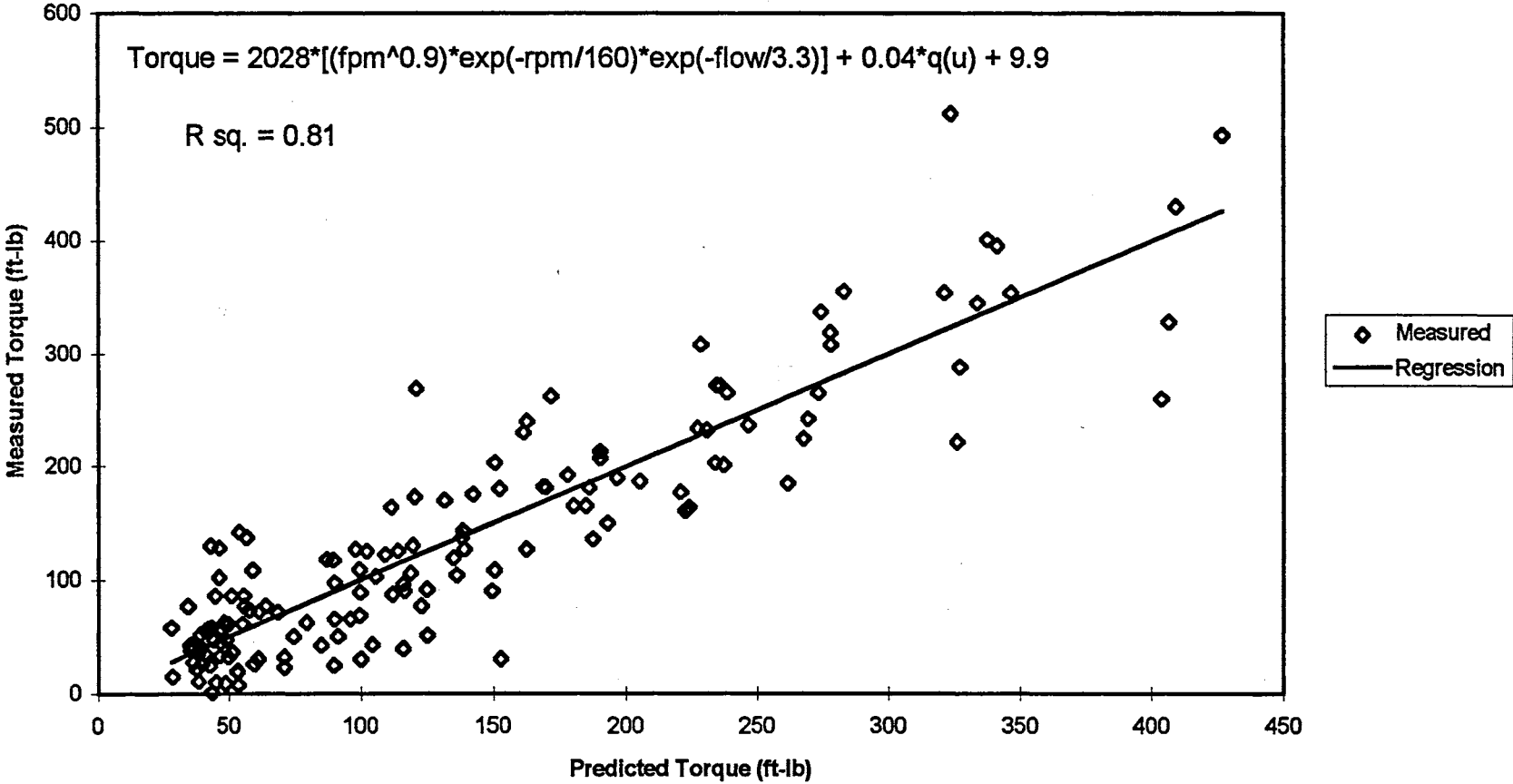
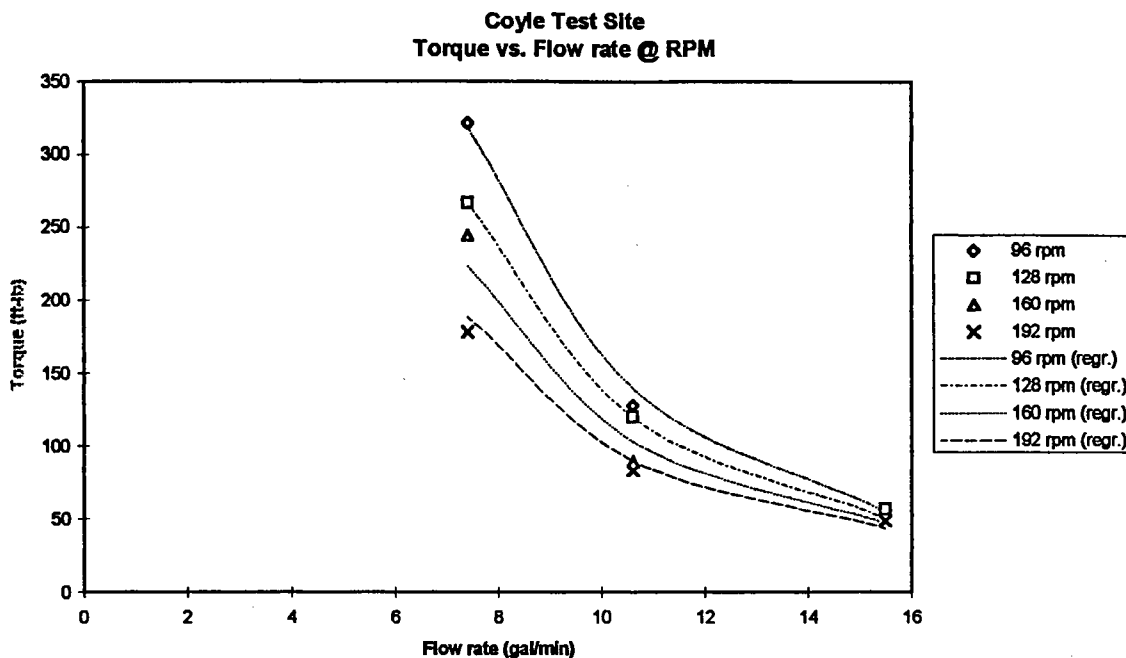
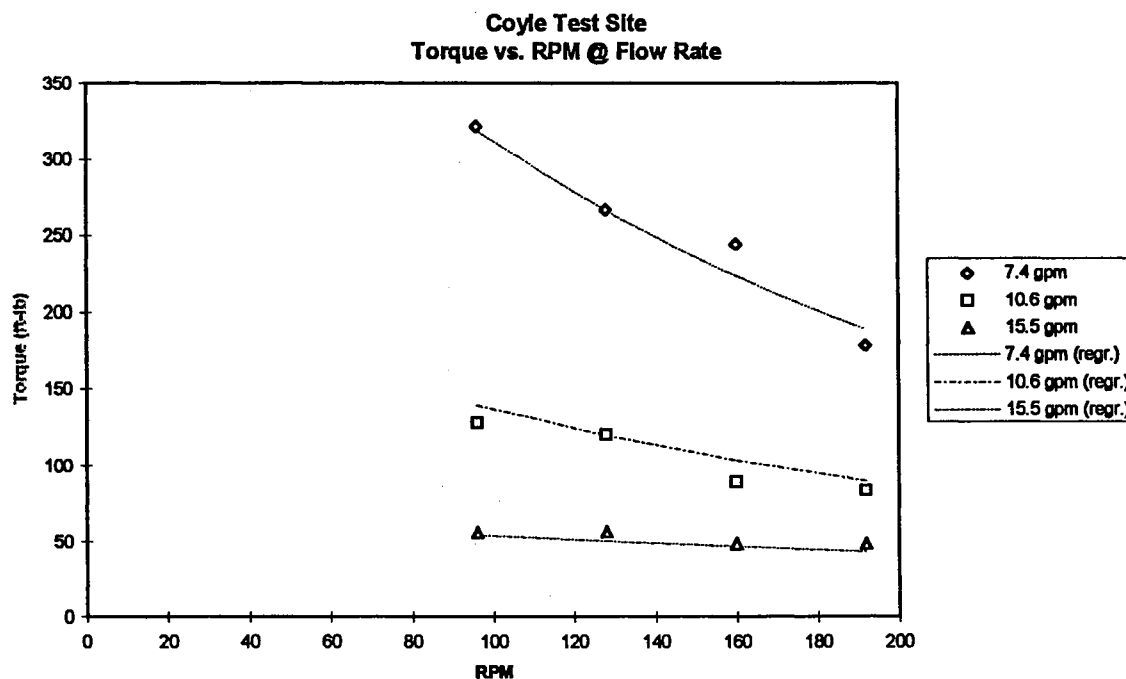


Figure 32: Measured vs. predicted rotational torque from Coyle test site based on best regression model with controlled test variables.





**Figure 33:** Mean torque vs. drilling fluid flow rate at a given rotational speed at the Coyle test site.



**Figure 34:** Mean torque vs. rotational speed at a given drilling fluid flow rate at the Coyle test site.

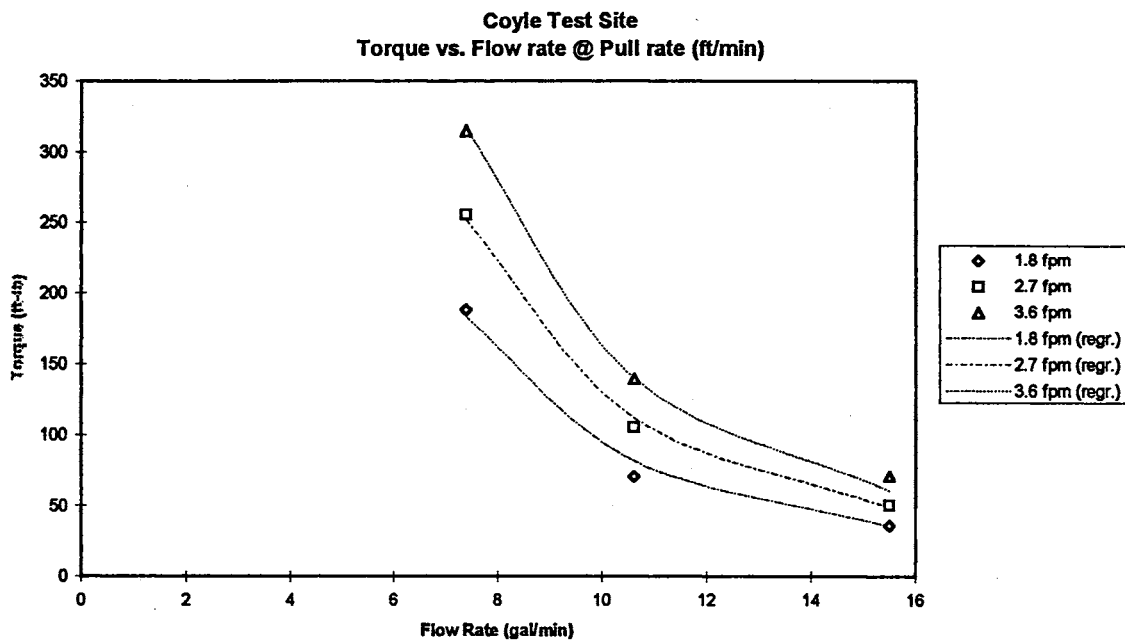
graphs were generated using Equation 21 with the mean values for the pull rate (2.7 ft/min) and the mean value for the penetrometer reading (500 psi).

Figure 34 clearly demonstrates that increases in the rotational speed of the reamer reduce the torque more rapidly at lower fluid flow rates than at the higher flow rates. At the 7.4 gal/min fluid flow rate, increasing the rotational speed from 96 to 192 rpm resulted in the rotational torque dropping from an average of 321.5 ft-lb to 178.3 ft-lb, a reduction of 143.2 ft-lb (44.5%). At the 15.5 gpm flow rate, a similar increase in rotational speed reduced the torque from an average of 56.0 ft-lb to 48.3 ft-lb, a reduction of 7.7 ft-lb (13.8%).

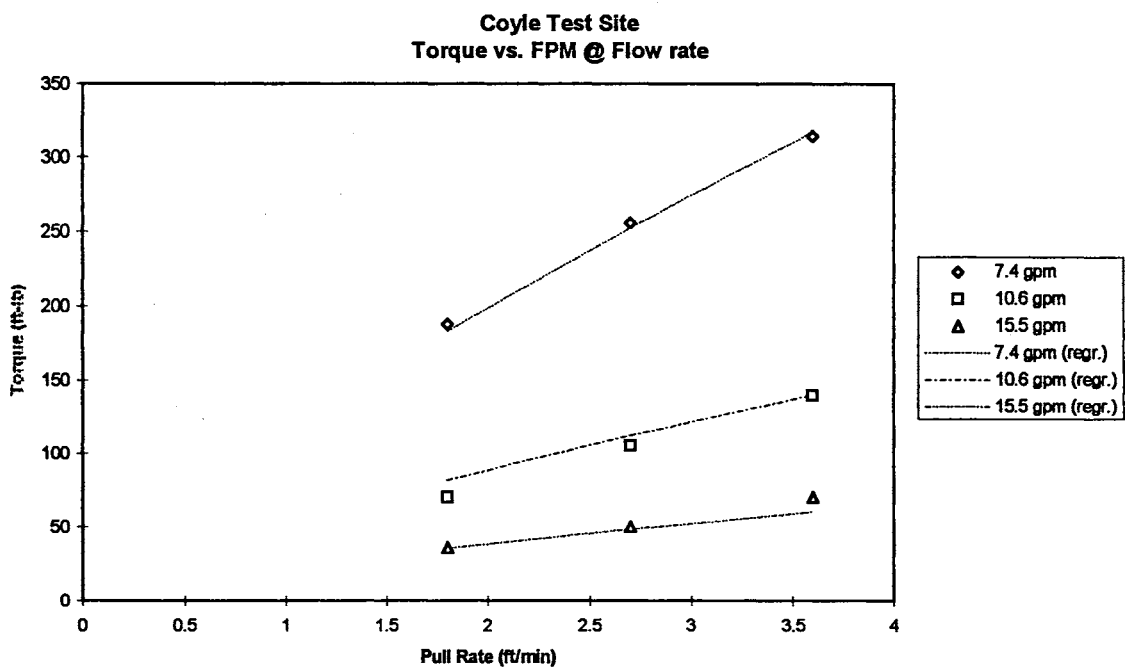
Figures 35 and 36 on Page 132 demonstrate the interaction between carriage pull rate and drilling fluid flow rate. In Figure 35, the mean values of torque at a given drilling fluid flow rate and carriage pull rate are plotted against the drilling fluid flow rate. In Figure 36, the mean torque values are plotted against the pull rate of the reamer. The plotted regression lines were generated using Equation 21 with the mean rotation rate (144 rpm) and the mean penetrometer reading for the Coyle test site (500 psi).

Figure 36 demonstrates that torque increases more rapidly with increasing pull rates as the flow rate is decreased. For the 7.4 gpm flow rate, the average torque reading increased from 188.1 ft-lb to 314.6 ft-lb, an increase of 126.5 ft-lb (67.3%), as the pulling rate increased from 1.8 to 3.6 ft/min. At the 15.5 gpm flow rate, the average torque reading changed from 36.2 ft-lb to 70.7 ft-lb, an increase of 34.5 ft-lb (95.3%).

Figures 33 and 35 both show a much sharper decrease in torque as the drilling fluid flow rate went from 7.4 to 10.6 gal/min than from 10.6 gal/min to 15.5 gal/min. The diminished effect on torque reduction as flow rate continues to increase matches the



**Figure 35:** Mean torque vs. drilling fluid flow rate at a given reamer pull rate at the Coyle test site.



**Figure 36:** Mean torque vs. reamer pull rate at a given drilling fluid flow rate at the Coyle test site.

intuitive appraisal. Clearly, as flow continues to increase, the rotational torque will never go negative. Hence, torque is expected to become asymptotic to a positive value slightly above the X-axis in both Figures 33 and 35 if flow were allowed to continually increase.

Figure 37 on Page 134 gives a plot of mean torque values versus the drilling fluid/soil volumetric flow ratio advocated by Wilcox (1990) [refer to soil cutting discussion in Chapter 1]. For the non-cohesive soil tested at the Coyle test site, Wilcox's ratio does have some merit, although in every case of similar volumetric ratios, the torque values obtained using the higher flow rates are substantially lower than the lower flow readings. Sizable reductions in torque are seen for fluid/soil volumetric ratios approaching values of 3. While Wilcox's ratio may provide an easy (and worthwhile) rule of thumb for an operator in the field, it should be noted that, at least for the soil tested in this study, increases in flow rate are shown to reduce torque more rapidly than decreases in the rate of pull for volumetric ratios below 3 for this non-cohesive soil.

A glimpse at the mechanisms most significant in the creation of rotational torque may be seen in Figures 38 and 39 on Page 135. Figure 38 is a plot of a regression analysis using only the pulling force at the boring unit and the length of polyethylene pipe (distance) pulled into the hole to predict the rotational torque. The coefficient of determination ( $r^2$ ) is 0.79, approaching that of the best fit model in Figure 32. Figure 39 is a plot of a regression analysis using only the depth of cut (pull rate/rotation speed) and the penetrometer cone tip pressure,  $q_u$ . The coefficient of determination ( $r^2$ ) is 0.23.

The terms used in the regression of Figure 38 should relate to the axial forces acting against the reamer ( $F_{RA}$  and  $F_{CA}$  in Figure 31). The distance value in the expression should act to correct the pulling force at the boring unit for changes in the axial force

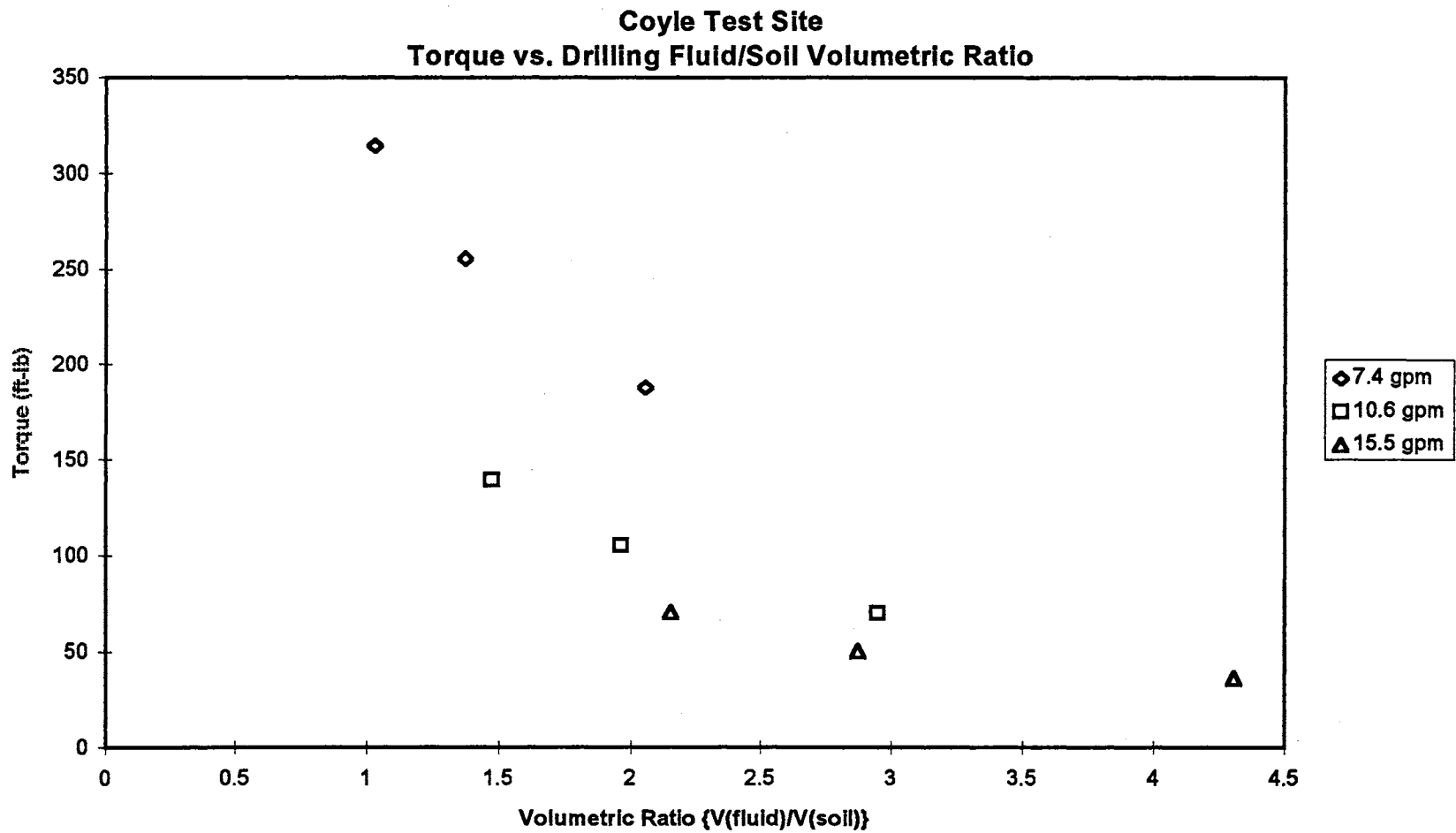


**Figure 37:** Mean torque vs. drilling fluid/soil volumetric ratio at Coyle test site.

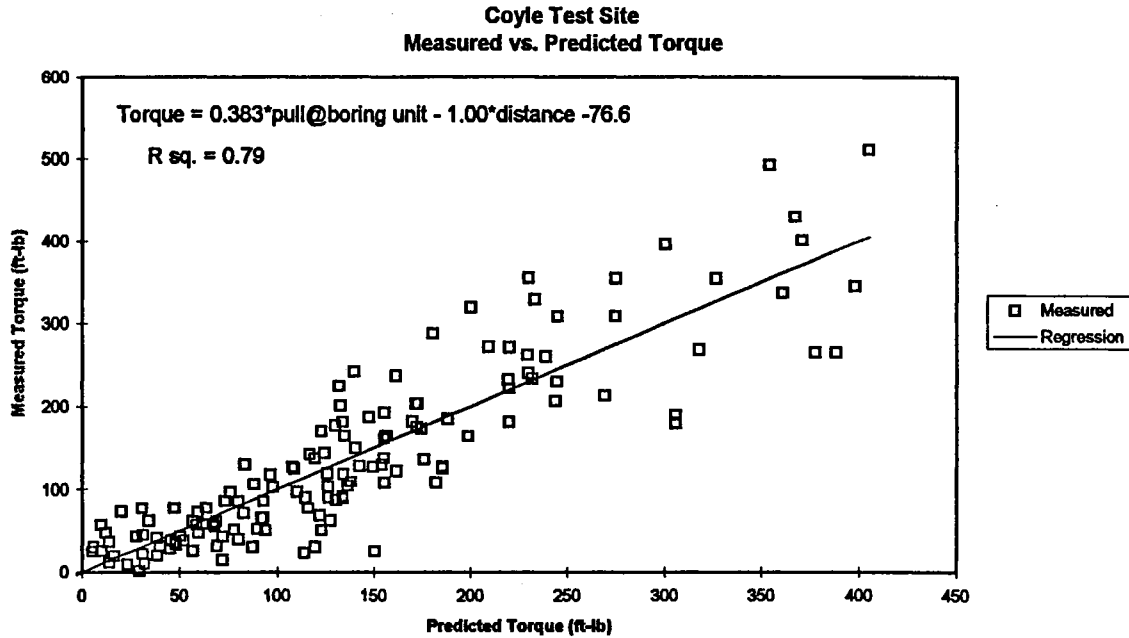


**Figure 38:** Measured vs. predicted torque at the Coyle test site based on the pulling force at the boring unit and distance pulled.

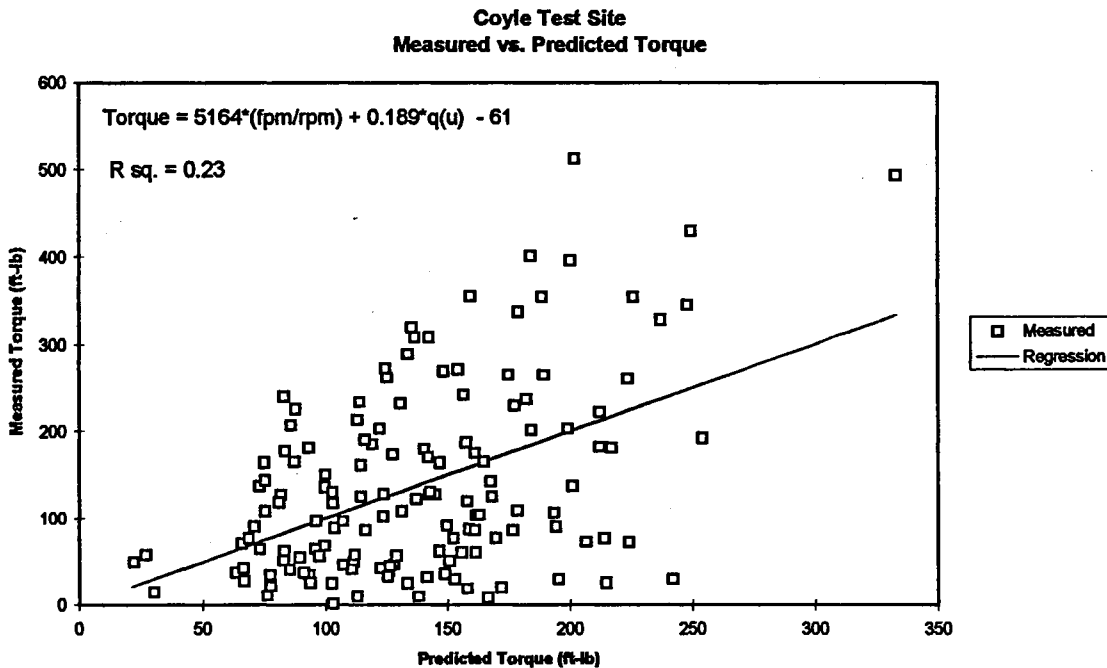


**Figure 39:** Measured vs. predicted torque at the Coyle test site based on the depth of cut (pull rate/rot. rate) and the penetrometer index,  $q_u$ .

acting along the polyethylene pipe ( $F_{UA}$ ) due to the length of pipe pulled into the ground. The axial forces acting on the reamer (and compactor in the case of the reamer used at the Coyle test site; refer to Figure 16) relate directly to the moment generated by the frictional and soil-to-tool adhesive forces ( $M_{RFA}$  and  $M_{CF}$ ) as the reamer is rotated. The depth of cut and penetrometer soil strength index should relate to the moment due to the shearing of the soil at the face of the reamer ( $M_{RS}$ ). Thus, from Figures 38 and 39 it is demonstrated that rotational torque at the boring unit is dominated by moments generated by frictional forces acting upon the reamer rather than forces related to the shearing stresses in the soil as it is cut for the non-cohesive soil at the Coyle test site.

Figure 40 plots the mean power output at the boring unit versus the rotational speed for the Coyle test site. The values plotted include both the power used in spindle rotation as well as pulling of the carriage (refer to Equations 1 and 2 in Chapter 1). The “Measured” values are the averages of all readings taken at the given flow rate and rotational speed. The regression lines were generated using the torque calculated from Equation 21 in Equation 1, along with the boring unit pull force calculated from Equation 22 in Equation 2. The mean pull rate value of 2.7 ft/min was used in Equations 21 and 22. Figure 40 indicates a decreasing rate of power usage as the rotational speed continues to increase. The “Measured” values for the 7.4 gal/min flow rate actually show a drop in power used as rotation speed goes from 160 to 192 rpm. The figure indicates that for the non-cohesive soil tested in this study, reductions in torque with increasing rotation speed are substantial enough to induce only slight increases in power usage (and possible decreases at low flow rates) as the rotational speed is increased from 96 to 192 rpm.

**Coyle Test Site  
Mean Power Curves (7 inch diameter cut)**

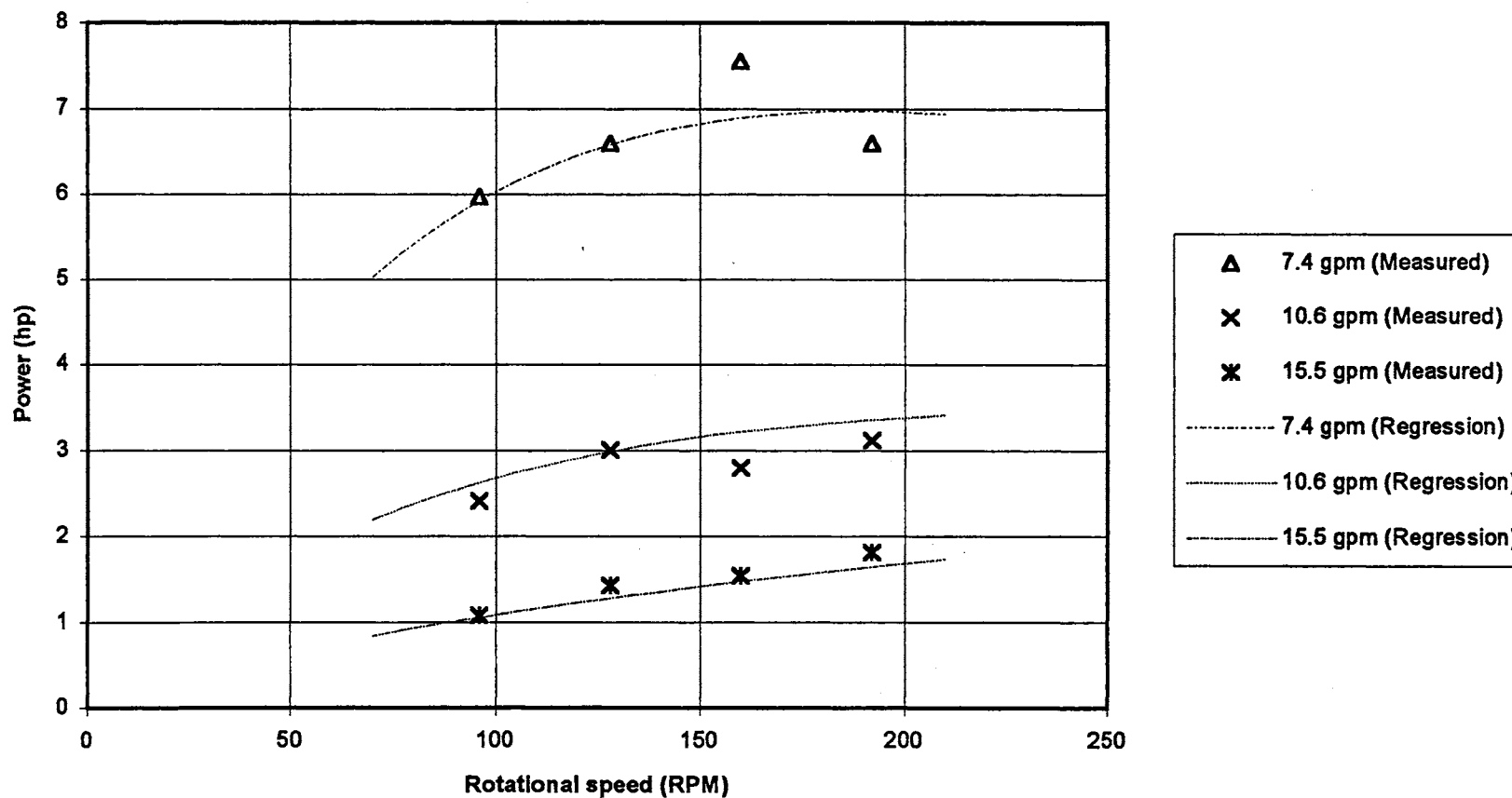


**Figure 40:** Mean power usage at boring unit as a function of rotation speed at the Coyle test site. Fluted reamer with 7.0 in (17.8 cm) outer cutting diameter in use.



### Pulling Force at the Boring Unit

The analysis of variance (ANOVA) table for the boring unit pulling force data from the Coyle test site is given in Table 9.

Table 9

ANOVA Table for Boring Unit Pulling Force Model at Coyle Test Site

Source	Degrees of Freedom	Type I Sum of Squares	F Value	P
Penetrometer	1	1919671	123.45	0.0001
Distance Pulled	1	326371	20.99	0.0001
Fluid Flow Rate	2	4260856	137.01	0.0003
Bore(Flow Rate)	9	871734		
Rotat. Speed [RPM]	3	227742	4.88	0.0033
Pull Rate [FPM]	2	275511	8.28	0.0005
RPM x FPM	6	123458	1.32	0.2542
Flow Rate x RPM	6	184081	1.97	0.0769
Flow Rate x FPM	4	74678	1.20	0.3156
Flow Rate x RPM x FPM	12	119733	0.64	0.8017
Error ( $\delta$ )	97	1508336		
<b>Total</b>	<b>143</b>	<b>9874173</b>		

Table 9 shows no significant interaction between drilling fluid flow rate and the rate of pull in terms of the effect on the pull observed at the boring unit. The interaction between drilling fluid flow rate and the rotational speed is significant at the 90% level of confidence, but not at the 95% confidence level. Since pull rate is not involved in any significant interaction, the effects of this term by itself may be analyzed. Table 9 shows pull rate to be significant at the 99% confidence level in determining pull at the boring unit. If the flow rate/rotation speed interaction is deemed non-significant, then the individual effect of drilling fluid flow rate and rotation speed are both shown to be

significant at the 99% confidence level. The best regression model obtained for the pulling force at the boring unit (given in Equation 22) contained a product term of rotation speed and flow rate values. Thus, for the remainder of the discussion, the fluid flow rate/rotation speed interaction will be treated as significant.

The best regression model for measured vs. predicted boring unit pulling force had a coefficient of determination ( $r^2$ ) of 0.77. The regression equation obtained is:

$$\begin{aligned} Pull_{unit} = & 0.0174 \times [(dist.)^{2.4} \cdot \exp(\frac{-flow}{3.6})] + 2797 \times [\exp(\frac{-rpm}{160}) \cdot \exp(\frac{-flow}{6})] \\ & - 63.1 \times fpm + 0.156 \times q_u + 283 \end{aligned} \quad \text{Eq. (22)}$$

Where:  $Pull_{unit}$  = the pulling force measured at the boring unit corrected for the  
“no-load” readings (lb)

dist. = the length of HDPE pipe pulled into the hole at the end of a given  
10 ft test section (ft)

rpm = the rotation rate of the reamer (rev/min)

flow = the drilling fluid flow rate (gal/min)

fpm = the pull rate of the reamer into the soil profile (ft/min)

$q_u$  = the average penetrometer cone pressure at the given  
location (lb/in<sup>2</sup>)

Figure 41 on Page 140 shows the measured pulling force values at the boring unit plotted against the values predicted from Equation 22.

Figures 42 and 43 on Page 141 give plots of the mean boring unit pulling forces for each drilling fluid flow rate/rotational speed combination. From Figure 42, the relationship between fluid flow rate and boring unit pull force is much closer to a linear relationship than that of flow rate versus torque (See Figures 33 and 35). Pulling force is

Coyle Test Site  
Measured vs. Predicted Pull at Boring Unit

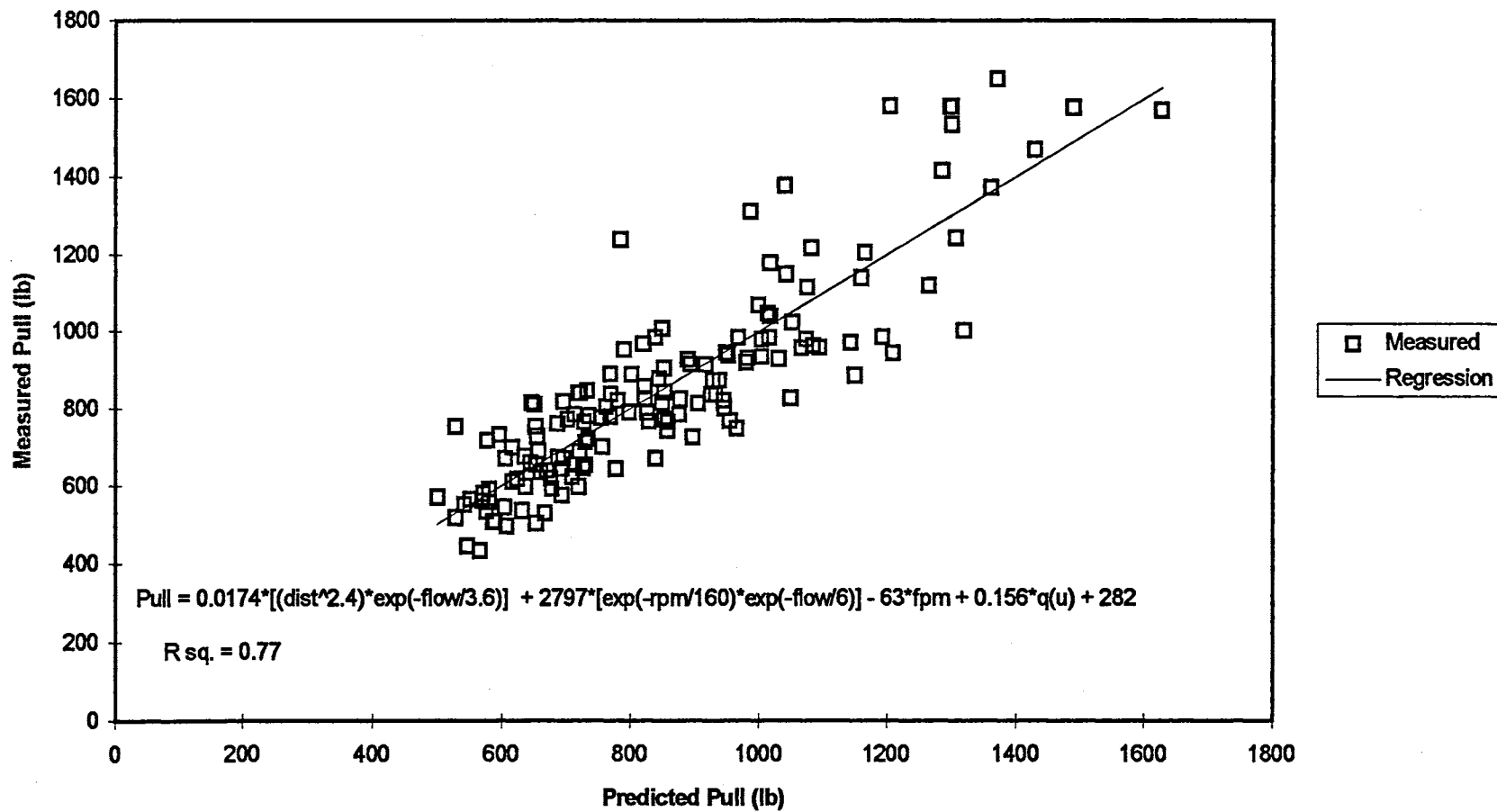
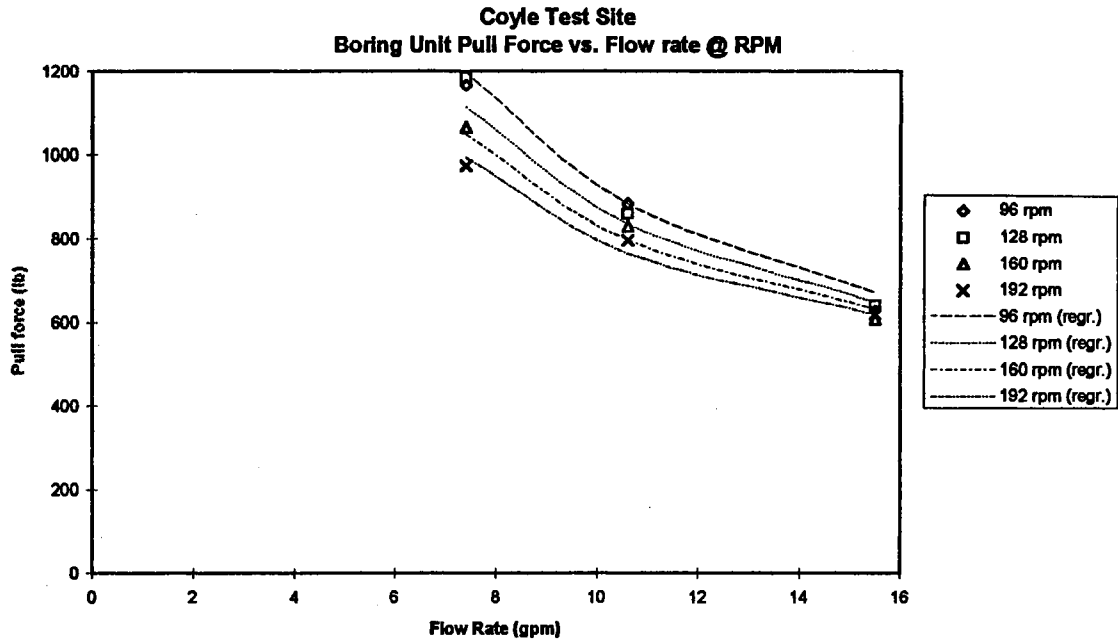
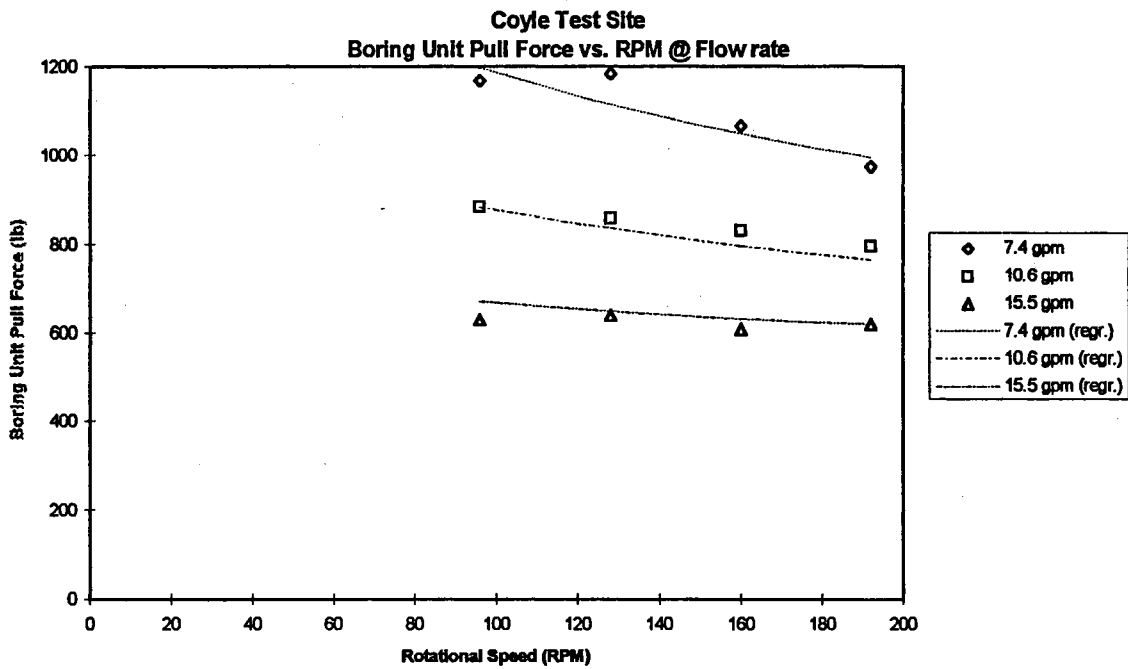


Figure 41: Measured vs. predicted boring unit pulling force at the Coyle test site as a function of the controlled and covariate variables.



**Figure 42:** Mean boring unit pull force vs. drilling fluid flow rate at a given rotation speed at the Coyle test site.



**Figure 43:** Mean boring unit pull force vs. rotational speed at a given drilling fluid flow at the Coyle test site.

also expected to become asymptotic to some positive value as fluid flow rate increases. From Figure 43, the interaction between fluid flow rate and rotational speed is not as pronounced for boring unit pulling force as it was for rotational torque, but the interaction is still evident. Pulling force increases more rapidly with decreasing rotational speed as drilling fluid flow rate decreases. The regression lines in Figures 42 and 43 were plotted using Equation 22 along with the mean values for pull rate (2.7 ft/min) and penetrometer reading (500 psi) from the Coyle test site.

The mean values for boring unit pull force versus pull rate at the three fluid flow rates is shown in Figure 44 on Page 143. Table 9 indicated no significant interaction between drilling fluid flow rate and pull rate as they relate to the pulling force at the boring unit. The relationship which best seems to satisfy the trend for each of the flow rates is a linear increase in pulling force versus pull rate. The regression lines plotted in Figure 44 were generated using Equation 22 with the mean rotational speed (144 rpm) and the mean penetrometer value for the Coyle test site (500 psi).

Figure 45 on Page 143 shows a plot of the mean pulling force at the boring unit versus the distance pulled for each of the three flow rates tested. The regression lines plotted on the graph were generated using Equation 22 with the mean values for pull rate (2.7 ft/min), rotation rate (144 rpm), and penetrometer reading (500 psi). Though not solidly defined, there does appear to be a trend toward more rapid increases in pulling force with distance as the drilling fluid flow rate decreases. This pulling force increase with distance should be attributed to increases in the axial pulling force along the polyethylene pipe ( $F_{UA}$ ). This implies that for this non-cohesive soil, the longer the bore is, the more critical it becomes to use a higher drilling fluid flow rate to <sup>prevent</sup> maintain tensile

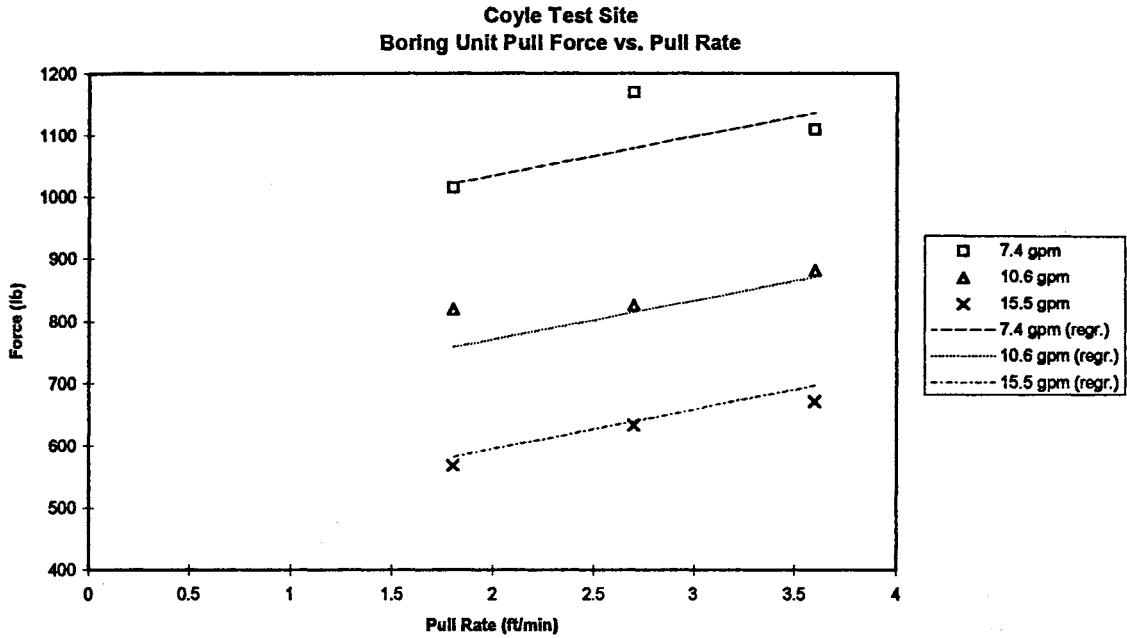


Figure 44: Mean boring unit pull force vs. reamer pull rate at a given drilling fluid flow at the Coyle test site.

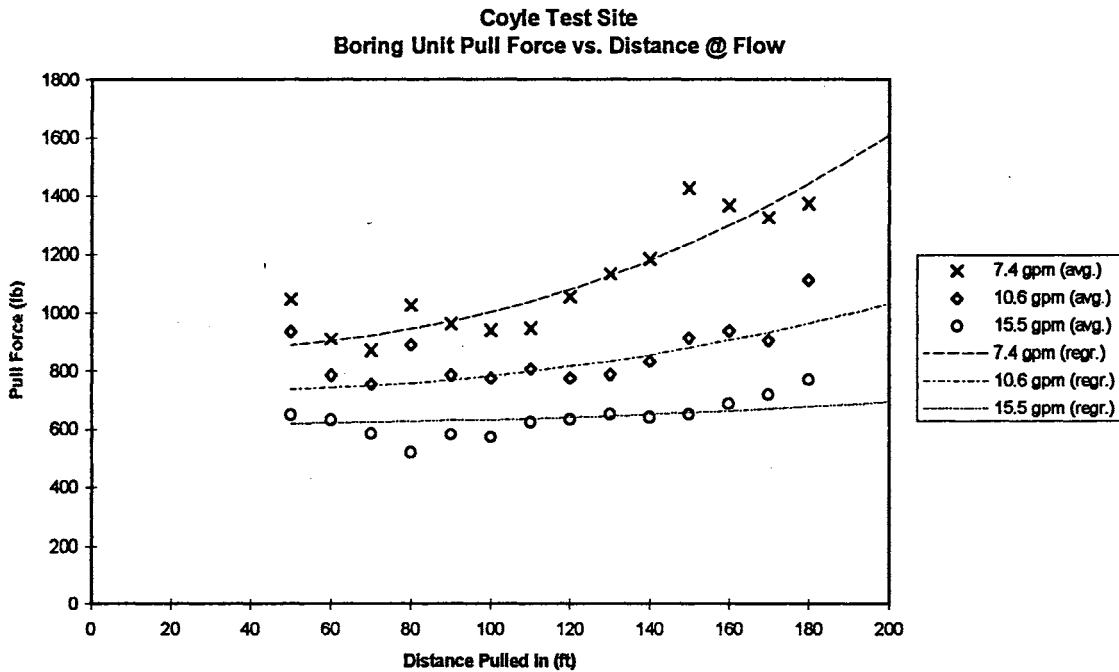


Figure 45: Mean boring unit pull force vs. length of pull at a given flow rate at the Coyle test site.

stresses in the installed utility from exceeding their critical values. This finding is in general agreement with Jonnes (1995) laboratory study which emphasized the importance of maintaining a non-cohesive soil in a fluidized state to reduce frictional drag along an installed pipeline.

Pulling Force at the HDPE Pipe

As indicated in Chapter 5, only the HDPE pipe pulling force data from Bores 5, 9, 10, and 13 have been retained. The analysis of variance (ANOVA) table for the polyethylene (HDPE) pipe pulling force is given in Table 10.

Table 10

ANOVA Table for Polyethylene Pipe Pulling Force Model at Coyle Test Site

Source	Degrees of Freedom	Type I Sum of Squares	F Value	P
Penetrometer	1	254336	58.69	0.0001
Distance Pulled	1	499758	115.33	0.0001
Fluid Flow Rate	2	453927	52.37	0.0209
Bore(Flow Rate)	1	199		
Rotat. Speed [RPM]	3	50982	3.92	0.0482
Pull Rate [FPM]	2	1399	0.16	0.8533
RPM x FPM	6	17871	0.69	0.6659
Flow Rate x RPM	6	101653	3.91	0.0334
Flow Rate x FPM	4	46856	2.70	0.0992
Flow Rate x RPM x FPM	12	146432	2.82	0.0640
Error ( $\delta$ )	9	39001		
<b>Total</b>	<b>47</b>	<b>1612413</b>		

Table 10 should be analyzed very conservatively given the very limited number of bores included in the data set. The data set includes only one bore from the 7.4 gpm and 15.5 gpm drilling fluid flow rates, and only two bores with the 10.6 gpm flow rate. Table

10 indicates an interaction between fluid flow rate and rpm which is statistically significant at the 95% confidence level. It will be shown later that this perceived interaction is probably due to the limited number of bores and not of true significance. The analysis will focus primarily on the drilling fluid flow rate and the distance pulled. The two terms account for almost 60% of the total sums of squares from the statistical model.

A regression equation was fit to the data using the flow rate and distance terms.

The equation is as follows:

$$Pull_{HDPE\ Pipe} = 0.636 \times [(dist.)^{1.6} \cdot \exp(\frac{-flow}{6.2})] + 475 \quad Eq. (23)$$

Where:  $Pull_{HDPE\ Pipe}$  = the pulling force measured at the connection to the polyethylene pipe (lb)

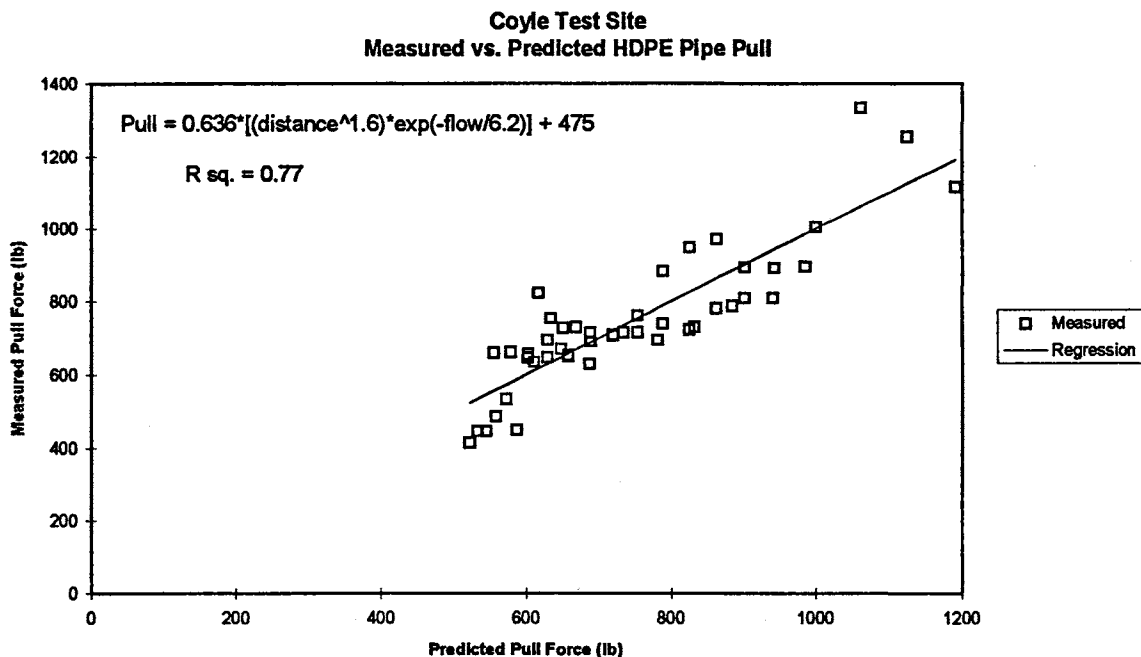
dist. = the length of HDPE pipe pulled into the hole at the end of a given 10 ft test section (ft)

flow = the drilling fluid flow rate (gal/min)

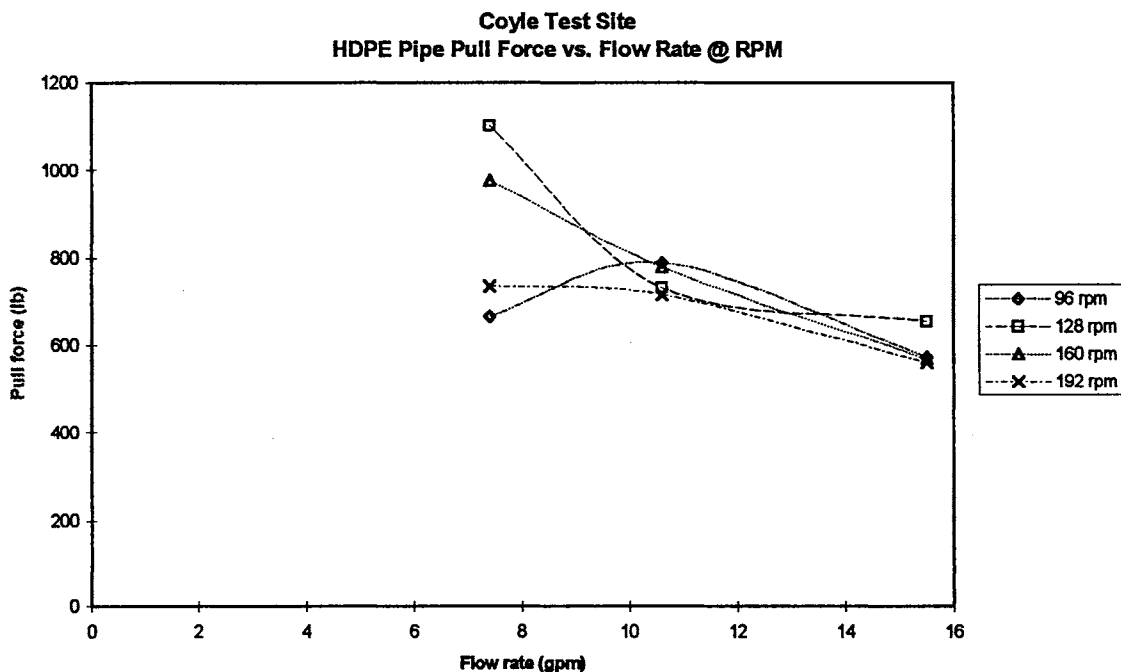
The coefficient of determination ( $r^2$ ) for the equation is 0.77. Figure 46 on Page 146 shows a plot of the measured pulling force values versus those predicted by Equation 23.

Figure 47 on Page 146 shows a plot of pulling force at the polyethylene pipe versus fluid flow rate at each rotational speed setting. The complex interaction shown is undoubtedly due to inadequate data to develop whatever relationship might truly exist. Figure 47 does seem to show a general decrease in pulling force with increases in flow rate.





**Figure 46:** Measured vs. predicted pull force at the polyethylene pipe as a function of distance and drilling fluid flow rate at the Coyle test site.



**Figure 47:** Mean polyethylene pipe pull force vs. drilling fluid flow rate at a given rotation speed at the Coyle test site.

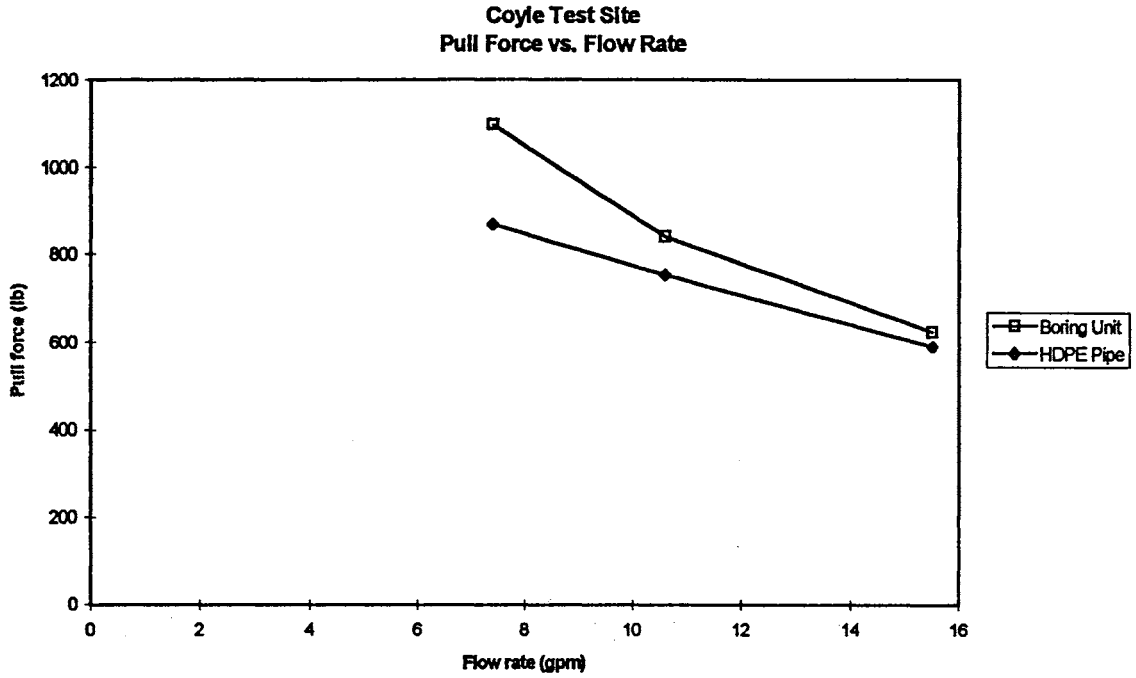


**Figure 48:** Mean pull force vs. drilling fluid flow rate as measured at the boring unit and at the polyethylene pipe at the Coyle test site.

Figure 48 on Page 147 shows a plot of average pulling force versus drilling fluid flow rate at both the HDPE pipe and at the boring unit for bores 5, 9, 10, and 13 at the Coyle test site. Both plots show decreasing pulling force as fluid flow increases. It is also shown that for the reamer used, and the soil type at the Coyle test site (See Figure 16 on Page 53), the pulling force along the polyethylene product pipe accounts for the majority of the pulling force at the boring unit. As drilling fluid flow rate increases, the pull at the product pipe accounts for a larger percentage of the pull at the boring unit.

## *Stillwater Creek Test Site*

### Rotational Torque

The analysis of variance (ANOVA) table for the rotational torque data from the Stillwater Creek test site is presented in Table 11.

Table 11

ANOVA Table for Torque Model at Stillwater Creek Test Site

Source	Degrees of Freedom	Type I Sum of Squares	F Value	P
Penetrometer	1	2242	1.21	0.2759
Reamer	1	215037	115.79	0.0005
Bore(Reamer)	6	28099		
Rotat. Speed [RPM]	3	28295	5.08	0.0032
Pull Rate [FPM]	2	85794	23.10	0.0001
RPM x FPM	6	4547	0.41	0.8711
Reamer x RPM	3	9615	1.73	0.1704
Reamer x FPM	2	2090	0.56	0.5724
Reamer x RPM x FPM	6	9508	0.85	0.5340
Error ( $\delta$ )	65	120714		
Total	95	505942		

Table 11 reveals no significant two-way or three way interactions between model terms contributing to torque. Reamer design, reamer rotational speed, and pull rate are all shown to be statistically significant at the 99% confidence level.

Regression equations were developed for the rotational torque measured using both the fluted and winged reamers (See Figures 16 and 17). Since the analysis of variance found no statistically significant interactions between pull rate and reamer, or between rotation rate and reamer, the equations were derived using the same terms and

same general format. The regression equation for the fluted reamer was found to have a coefficient of determination ( $r^2$ ) of 0.64. The regression equation is:

$$\begin{aligned} Torque_{fluted} = & 852 \times \exp\left(\frac{-rpm}{80}\right) + 862 \times \log\left(1 + \frac{rpm}{80}\right) + 34.3 \times fpm \\ & + 0.072 \times q(u) + 510 \end{aligned} \quad \text{Eq. (24)}$$

Where:  $Torque_{fluted}$  = the rotational torque measured at the boring unit when using the fluted reamer. The values are corrected for the “no-load” torque readings.

$rpm$  = the spindle rotational speed in revolutions per minute

$fpm$  = the carriage pull rate in ft/min

$q(u)$  = the penetrometer cone tip pressure corresponding to the location of interest ( $lb/in^2$ )

The best fit regression equation for the winged reamer had an  $r^2$  value of 0.38.

The equation is:

$$\begin{aligned} Torque_{winged} = & 1328 \times \exp\left(\frac{-rpm}{80}\right) + 1148 \times \log\left(1 + \frac{rpm}{80}\right) + 46.3 \times rpm \\ & + 0.049 \times q(u) - 648 \end{aligned} \quad \text{Eq. (25)}$$

Where:  $Torque_{winged}$  = the rotational torque measured at the boring unit when using the winged reamer. The values are corrected for the “no-load” torque readings.

$rpm$  = the spindle rotational speed in revolutions per minute

$fpm$  = the carriage pull rate in ft/min

$q(u)$  = the penetrometer cone tip pressure corresponding to the location of interest ( $lb/in^2$ )

Plots of measured torque versus torque predicted by the regression equations are given in Figures 49 and 50 on Page 152. The  $r^2$  value relating the measured versus predicted torque values for the winged reamer is low, but there is one apparent outlier reading approaching 500 ft-lb.

Table 12 presents the mean torque values measured with the two reamers.

Table 12

Stillwater Creek Torque Means for Fluted and Winged Reamers

Reamer	Corrected Mean Torque Reading (ft-lb)
Fluted	160
Winged	253

The winged reamer was found to require an average of 58% more torque than the fluted reamer during the test. The difference in torque for the reamers was found to be statistically significant at the 95% confidence level. {A note to the reader who has also read this author's paper presented at the International No-Dig '96 conference (Gunsaulis, 1996): the torque values presented in Table 12 will appear lower than the torque values presented in the International No-Dig '96 paper. The paper presented at the conference cited the *uncorrected* torque values for the given test. The values presented in this report have had the "no-load" torque readings subtracted to obtain the values presented here. }

This difference in torque values for the two reamers is the result of three main differences between the reamers. The first of these is the outer cutting diameter. The outer cutting diameter of the winged reamer was 8.5 in (21.6 cm) compared to 7.0 in (17.8 cm) for the fluted reamer. The second major factor which should have contributed to this difference is the number and placement of the fluid orifices on the two reamers.

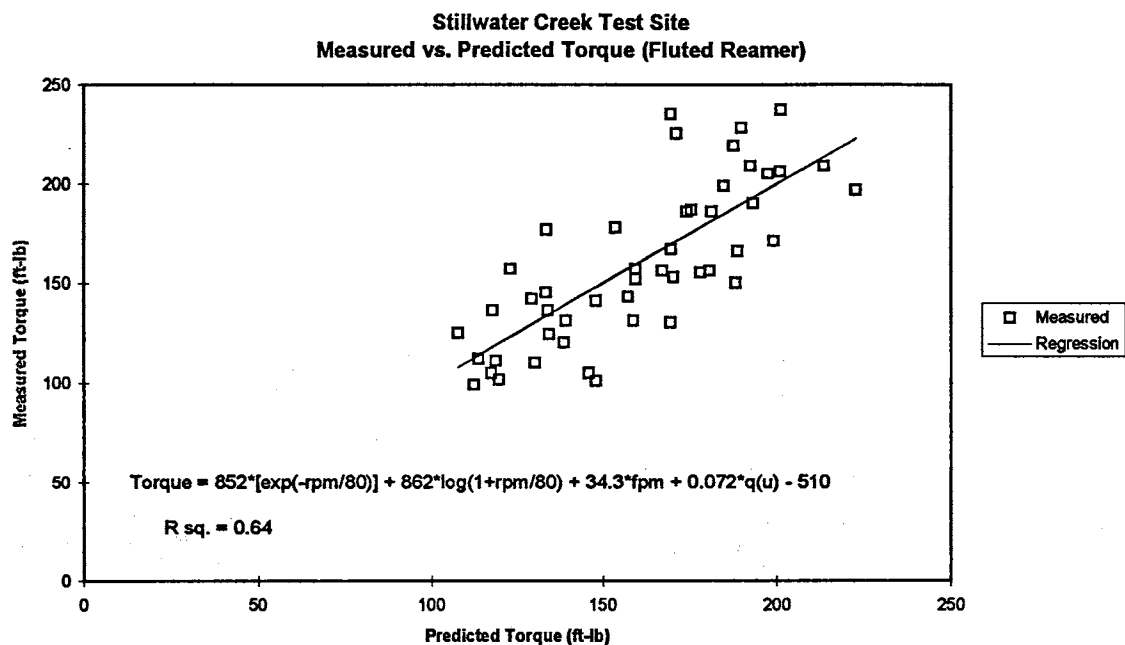


**Figure 49:** Measured vs. predicted torque for the fluted reamer at the Stillwater Creek test site as a function of controlled and covariate variables.

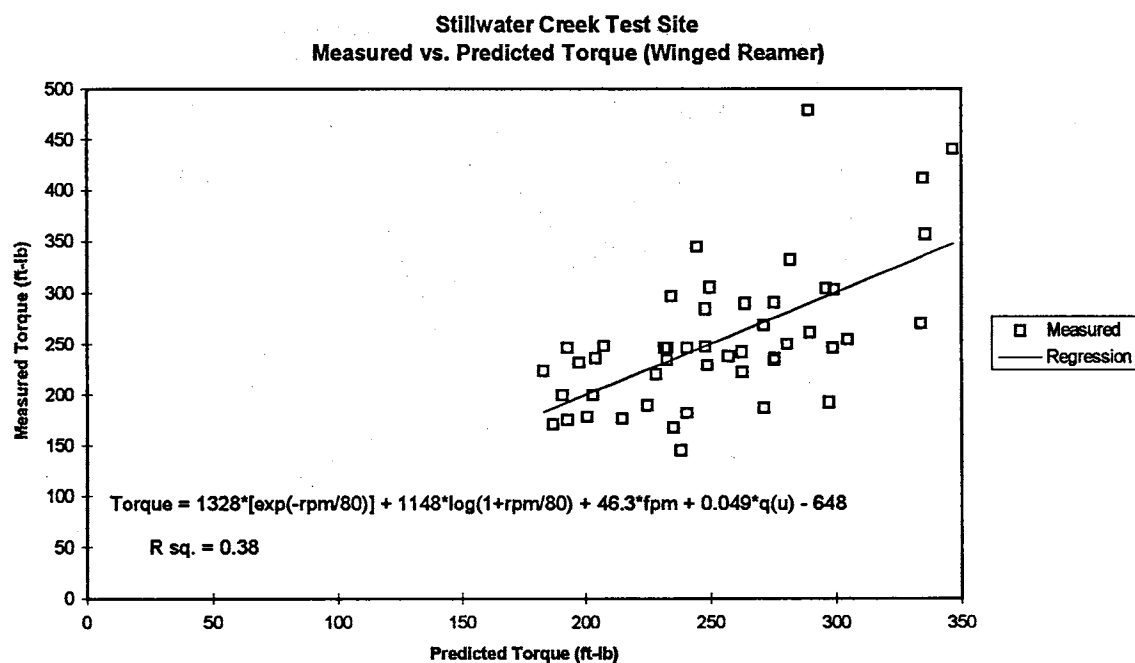


**Figure 50:** Measured vs. predicted torque for the winged reamer at the Stillwater Creek test site as a function of controlled and covariate variables.

The winged reamer had two fluid orifices located on the reamer shaft just in front of the first set of cutting “wings”, and two fluid orifices located behind the compaction cone. The fluted reamer had 6 fluid orifices located at the root of the fluted passages along the reamer body. Even though the total flow rate was equivalent for both reamers, the fluted reamer placed more drilling fluid at a closer proximity to where the reamer contacted the soil during the cutting process. A third possible contributing factor is the physical layout of the reamers. There may be some advantage to placing the cutting teeth on a sloping cone as in the case of the fluted reamer as compared to thin wings with cutting teeth as in the case of the winged reamer. Of the three explanations, the layout of the cutter would appear to account for less difference than reamer diameter or drilling fluid placement. Further testing would be required to separate out the proportions of the difference owing to these three factors.

Figure 51 on Page 154 plots the mean torque measured at the boring unit versus the rotational speed for the two reamers used in the test. The highest torque reading for both reamers was found to occur at the 96 rpm rotation speed. From that point, the rotational torque decreased to a minimum value and then began to increase again. The minimum measured torque readings for the reamers occurred at the 128 and 160 rpm settings for the fluted and winged reamers, respectively. The form of the equation relating torque to rotation speed was selected as the one most closely matching the shape of the curve for both reamers and most closely matching the concept of what occurs during the cutting process.



**Stillwater Creek Test Site  
Torque vs. Rotation Speed**

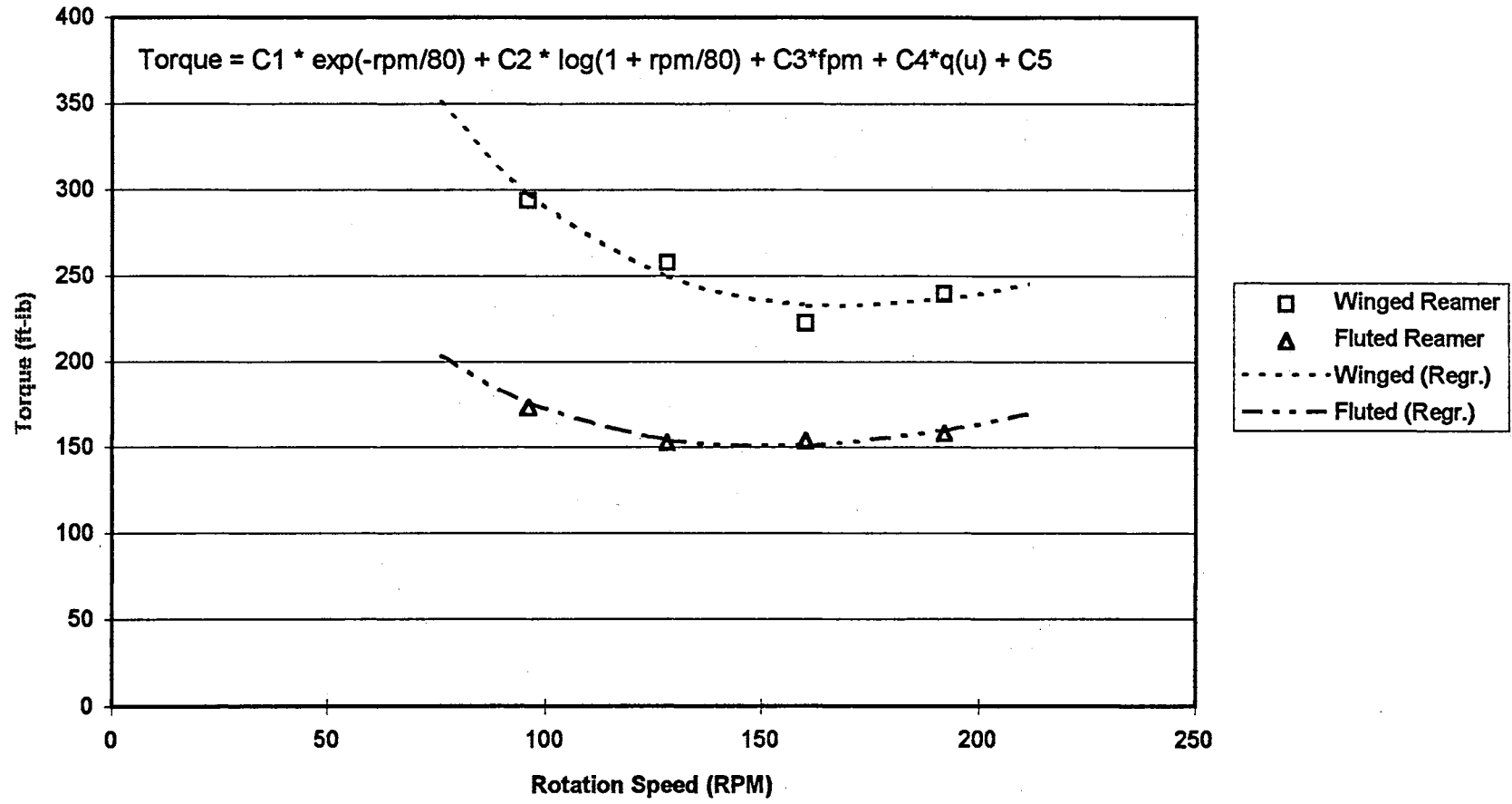


**Figure 51:** Mean torque vs. reamer rotation speed for the winged and fluted reamers at the Stillwater Creek test site.

Refer to the results from the Coyle test site. The relationship between the torque and rotation speed was found to be a decaying exponential in form for the non-cohesive soil. It was also demonstrated that moments due to frictional and soil-to-tool adhesional forces acting on the reamer ( $M_{RFA}$  and  $M_{CF}$  in Figure 31) appeared to more strongly influence the torque value than moments due to the shearing of the soil ( $M_{RS}$ ). Thus, it appears that the torque benefit gained from increasing rotational speed is related not only to a reduced “cutting depth” for the teeth, but also in the ability of the reamer teeth to more effectively break up the soil profile in front of the reamer. In the non-cohesive soil at the Coyle test site, increases in rotation speed resulted in decreases in pulling force required by the boring unit, and by extension, reductions in frictional forces acting on the reamer.

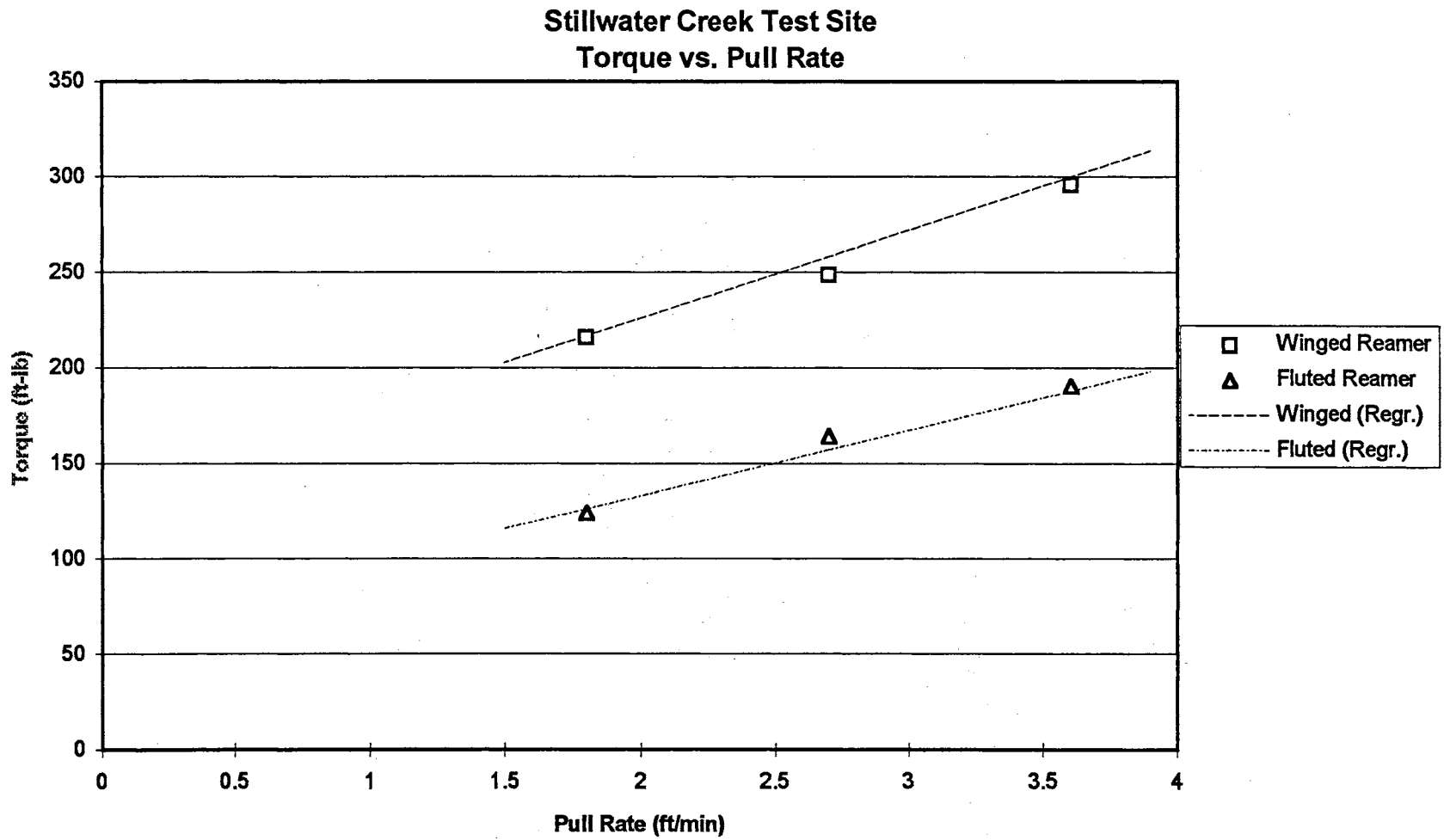
For the winged reamer at the Stillwater Creek test site, the shape of the torque curve still closely matches that of the boring unit pull force curve (see Figure 58). As will be discussed later, rotational torque for the winged reamer does seem to be heavily dependent upon frictional and soil-to-tool adhesive forces. For the fluted reamer, frictional forces seem to play a less significant role in overall torque. The boring unit pulling force means shown in Figure 58 do not match the torque curve for the fluted reamer. As discussed in the soil cutting discussion in Chapter 1, soils with substantial clay percentage show a sizable increase in shearing strength with increases in rate of shear. Wismer and Luth (1972) reported the increase in shearing strength to be directly proportional to the log of the rate of shear for tests involving a clay soil cut as a blade passing<sup>ed</sup> through the profile. This increase in shear strength of the soil with the increase in

shear rate as the reamer rotates more rapidly may contribute to the increase in torque exhibited by the fluted reamer, and possibly to the increases shown by winged reamer as well. Inertial forces involved in accelerating the severed soil material, and increases in viscous stresses from the soil/drilling fluid slurry as the reamer rotates faster, may also contribute to the torque increase seen with the fluted reamer as rotational speed increases.

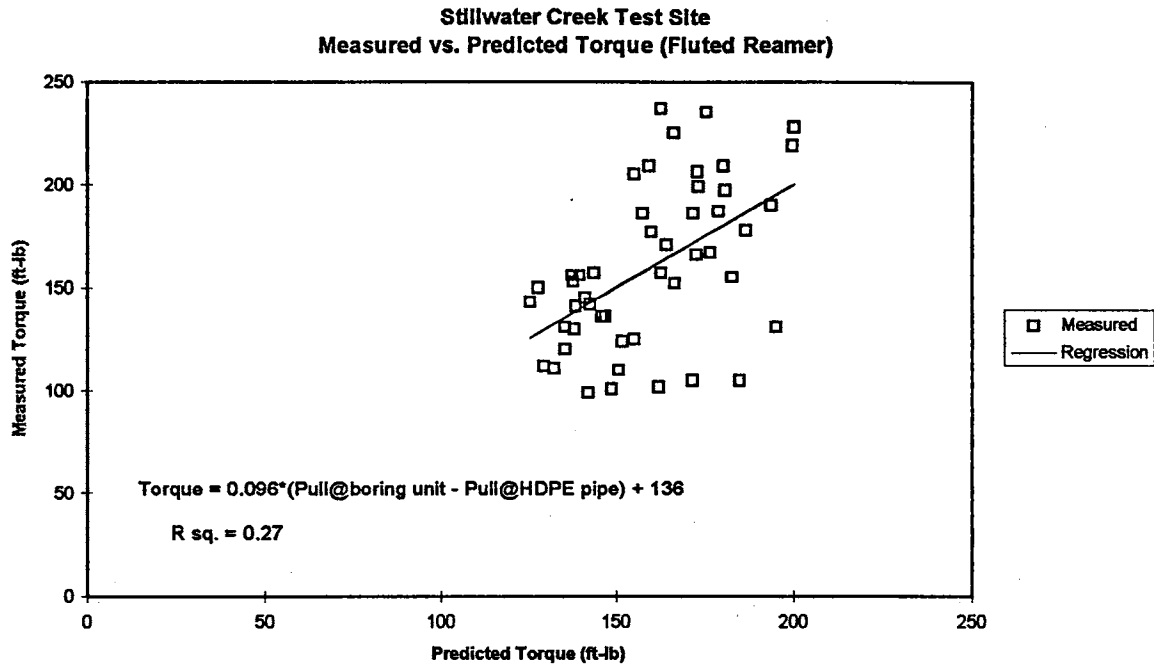
The regression model used fit to the data incorporated a sum of the decaying exponential relationship between rotational speed and torque (as developed from the Coyle test site data) and a logarithmic function of the rotation rate. This form of equation matches the torque curves for both reamers well and agrees with the rationale for the torque increases with increasing rotation speed with the fluted reamer.

Figure 52 on Page 157 shows a plot of torque versus pull rate for both reamers at the Stillwater Creek test site. While reamer/pull rate interactions were not found to be statistically significant (See Table 11), the lines plotted from the best fit regressions do show the winged reamer to have a slightly steeper slope to the torque vs. pull rate line. Regression lines in the figure were plotted using the mean penetrometer reading at the Stillwater Creek test site (573 psi), a rotational speed value of 120 rpm in Equations 24 and 25. The mean rotational speed (144 rpm) was not used because the predicted torque values are near their minimum near this value as shown in Figure 51.

Figures 53 and 54 illustrate regression analyses between the pulling force differential (the pulling force measured at the boring unit *minus* at the HDPE pipe pulling force) and the torque measured at the boring unit. The pulling force differential should be a sum of all axial forces illustrated in Figure 31 less the axial force along the installed



**Figure 52:** Mean torque vs. reamer pull rate for the winged and fluted reamers at the Stillwater Creek test site.



**Figure 53:** Measured vs. predicted torque for the fluted reamer as a function of the force differential between the boring unit and polyethylene pipe.

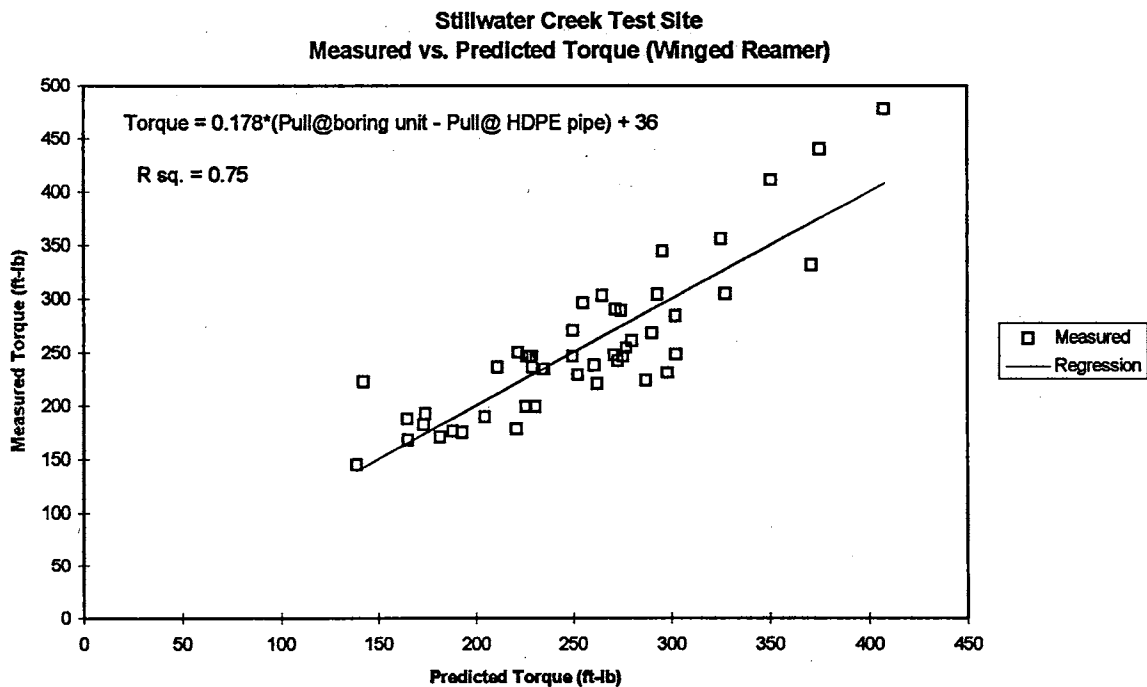


**Figure 54:** Measured vs. predicted torque for the winged reamer as a function of force differential between the boring unit and polyethylene pipe.

utility ( $F_{UA}$ ). This force value should be closely related to the moments related to frictional forces due to axial loads on the reamer and compactor ( $M_{RFA}$  and  $M_{CF}$ ). The relationship is very weak for the fluted reamer, with an  $r^2$  of 0.27. For the winged reamer, the correlation between pulling force differential and rotational torque ( $r^2 = 0.75$ ) was much higher than the model of controlled and covariate factors as given in Equation 25. The implication of a strong correlation (Figure 54) based on pull force differential for the winged reamer, and a relatively weak correlation based on pull rate and rotation speed (Figure 50) is that frictional and soil-to-tool adhesional forces must account for most of the torque measured when utilizing this reamer in this soil.

Figure 55 on Page 160 shows the plots of the mean power usage curves at the Stillwater Creek test site. The plots included are the sum of power usage due to spindle rotation and to carriage pulling force as given in Equations 1 and 2. The “Measured” values are the mean of all data points at a given pull rate and reamer combination. The regression values were developed using Equations 24 and 26 for the fluted reamer, and Equations 25 and 27 for the winged reamer. Mean values for pull rate (2.7 ft/min), penetrometer reading (573 psi), and distance (115 ft) were used as required in Equations 24 - 27. Equations 26 and 27 are the regression equations developed for pull force at the boring unit and are discussed further in the next section of this chapter.

In contrast to the power curves in the non-cohesive soil at the Coyle test site, the mean power curves increase at an increasing rate as the rotational speed changes from 96 to 192 rpm. In the non-cohesive soil, operation at rotation speeds up to 192 rpm was shown to have few deleterious effects, if any, on boring unit performance (rotational

### Stillwater Creek Test Site Mean Power Curves

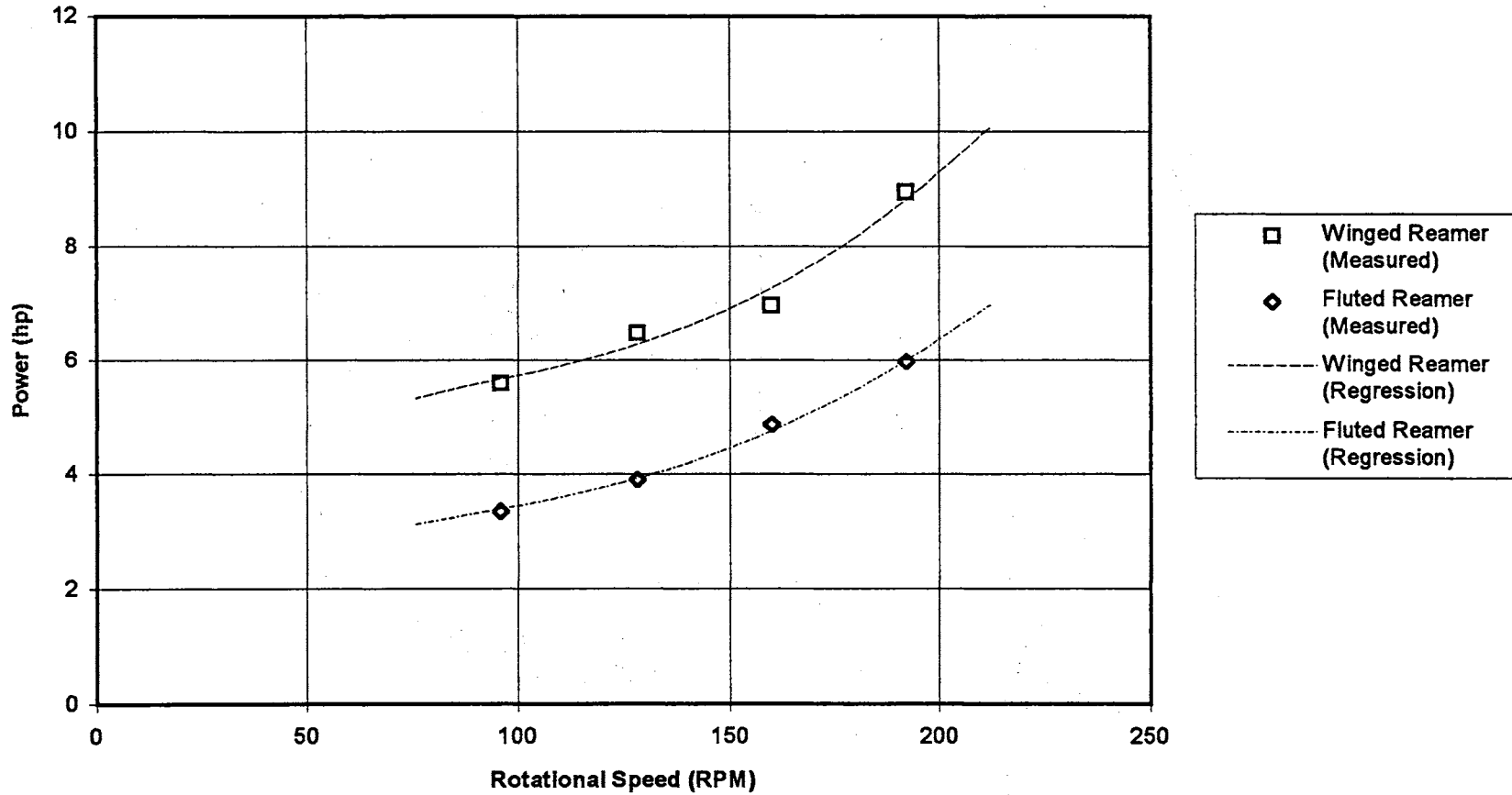


**Figure 55:** Mean power usage at boring unit as a function of rotation speed at the Stillwater Creek test site for both winged and fluted reamers.

torque, pulling force, power usage). In the cohesive soil at the Stillwater Creek test site, torque was found to reach a minimum value in the 128-160 rpm range, and then begin to increase again. The rate of increase in power was found to be the highest at the 192 rpm rotational speed.

#### Pulling Force at Boring Unit

The analysis of variance (ANOVA) table for the boring unit pull force at the Stillwater Creek test site is given in Table 13.

Table 13

ANOVA Table for Boring Unit Pulling Force at Stillwater Creek Test Site

Source	Degrees of Freedom	Type I Sum of Squares	F Value	P
Penetrometer	1	319525	2.99	0.0884
Distance Pulled	1	1169245	10.96	0.0015
Reamer	1	336759	3.16	0.3329
Bore(Reamer)	6	1822181		
Rotat. Speed [RPM]	3	608824	1.90	0.1382
Pull Rate [FPM]	2	773249	3.62	0.0323
RPM x FPM	6	68023	0.11	0.9954
Reamer x RPM	3	511416	1.60	0.1987
Reamer x FPM	2	91439	0.43	0.6534
Reamer x RPM x FPM	6	442489	0.69	0.6576
Error ( $\delta$ )	64	6830360		
Total	95	12973510		

As seen in Table 13, the only controlled parameter term reaching statistical significance at the 95% confidence level was Pull Rate. The distance pulled, a covariate term, was also statistically significant at the 95% confidence level. Note that no



statistically significant difference in the pulling force at the boring unit was found between the two reamers used at the test site.

Regression analysis was conducted on the data from both reamers. The best fit expression for pulling force at the boring unit using the fluted reamer had a coefficient of determination ( $r^2$ ) of 0.41 and is presented as Equation 26.

$$Pull_{Unit}(fluted) = 0.140 \times Dist.^{1.7} + 191 \times fpm + 1263 \quad \text{Eq. (26)}$$

Where:  $Pull_{unit}(fluted)$  = the pulling force measured at the boring unit when using the fluted reamer corrected for the “no-load” readings (lb)

dist. = the length of HDPE pipe pulled into the hole at the end of a given

10 ft test section (ft)

fpm = the pull rate of the reamer into the soil profile (ft/min)

The best fit equation for the winged reamer had an  $r^2$  value of 0.20 and is presented as Equation 27. Note that distance is not significant in determining the boring unit pulling force when using the winged reamer.

$$Pull_{unit}(winged) = 22.0 \times fpm^2 + 0.095 \times rpm^2 - 29.7 \times rpm + 4362 \quad \text{Eq. (27)}$$

Where:  $Pull_{unit}(winged)$  = the pulling force measured at the boring unit when using the winged reamer corrected for the “no-load” readings (lb)

fpm = the pull rate of the reamer into the soil profile (ft/min)

rpm = the rotation rate of the reamer (rev/min)

Plots of the measured boring unit pull force values versus those predicted by Equations 26 and 27 for the fluted and winged reamers, respectively, are given in Figures 56 and 57 on Page 164. The expressions for boring unit pulling force based on the variables controlled in this test do not provide strong correlations with the actual measured values for either reamer. Note that the penetrometer soil strength index was not significant in either correlation as might be expected. This may have been due to slight soil changes from one side of the test plot to the other. This is discussed further in the section on pulling force at the polyethylene pipe.

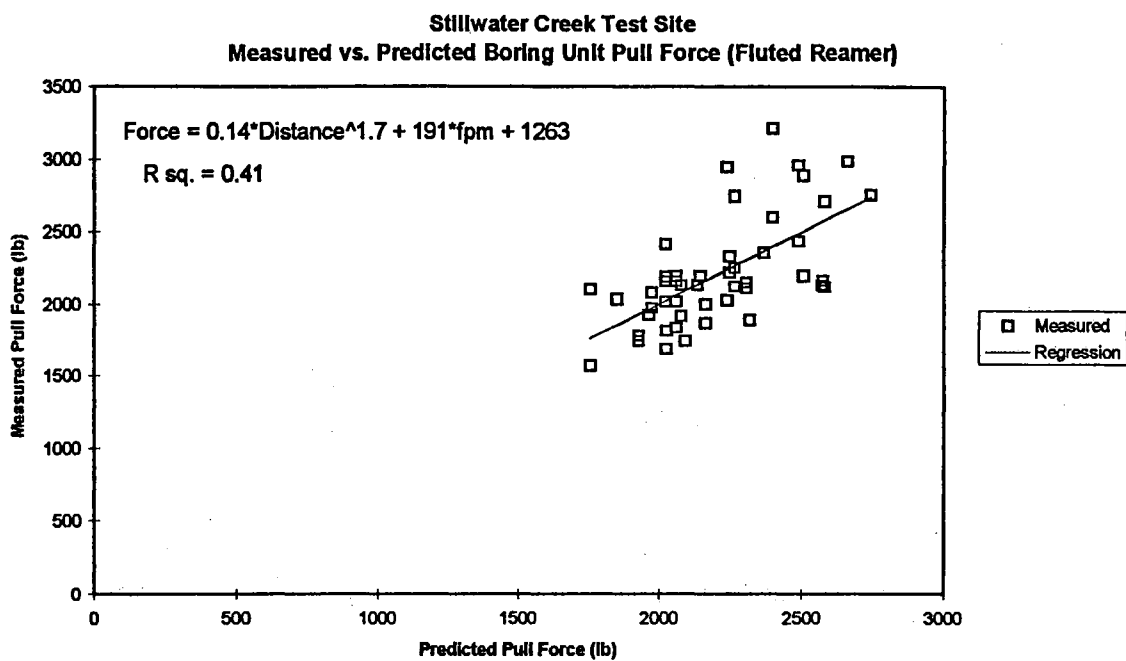
Table 14 provides a comparison of the mean pulling forces measured at the boring unit when using the two reamers tested at the Stillwater Creek test site corrected for their no-load readings. The mean pulling force using the winged reamer is slightly (6.6%) higher than that of the fluted reamer. As mentioned previously, this difference is not significant at the 95% confidence level.

Table 14

Stillwater Creek Boring Unit Pulling Force Means for Fluted and Winged Reamers

Reamer	Corrected Mean Boring Unit Pulling Force (lb)
Fluted	2206
Winged	2352

Figure 58 on Page 165 is a plot of the mean boring unit pull force versus the reamer rotation speed for both reamers tested at the Stillwater Creek test site. Recall that the analysis of variance found no significant reamer/rotation speed interaction. Of importance in Figure 58 is that the plot of the boring unit pull force means for the winged reamer closely match the shape of the curve generated for torque. The fact that the boring



**Figure 56:** Measured vs. predicted boring unit pull force for the fluted reamer as a function of controlled and covariate variables.

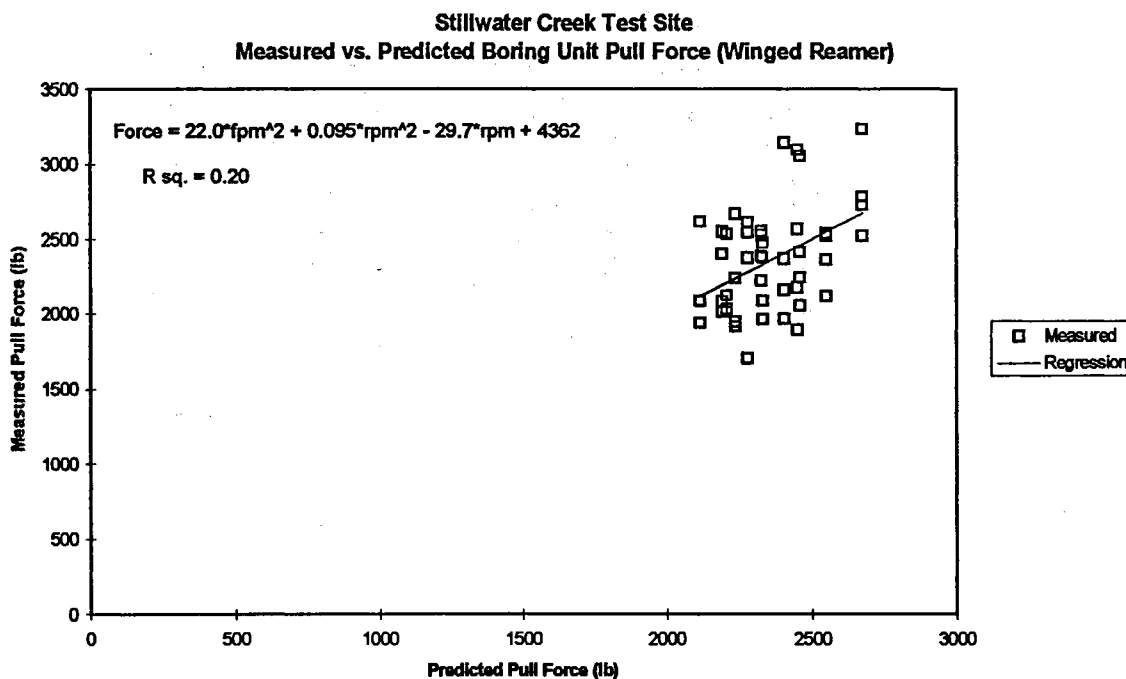


**Figure 57:** Measured vs. predicted boring unit pull force for the winged reamer as a function of controlled and covariate variables.

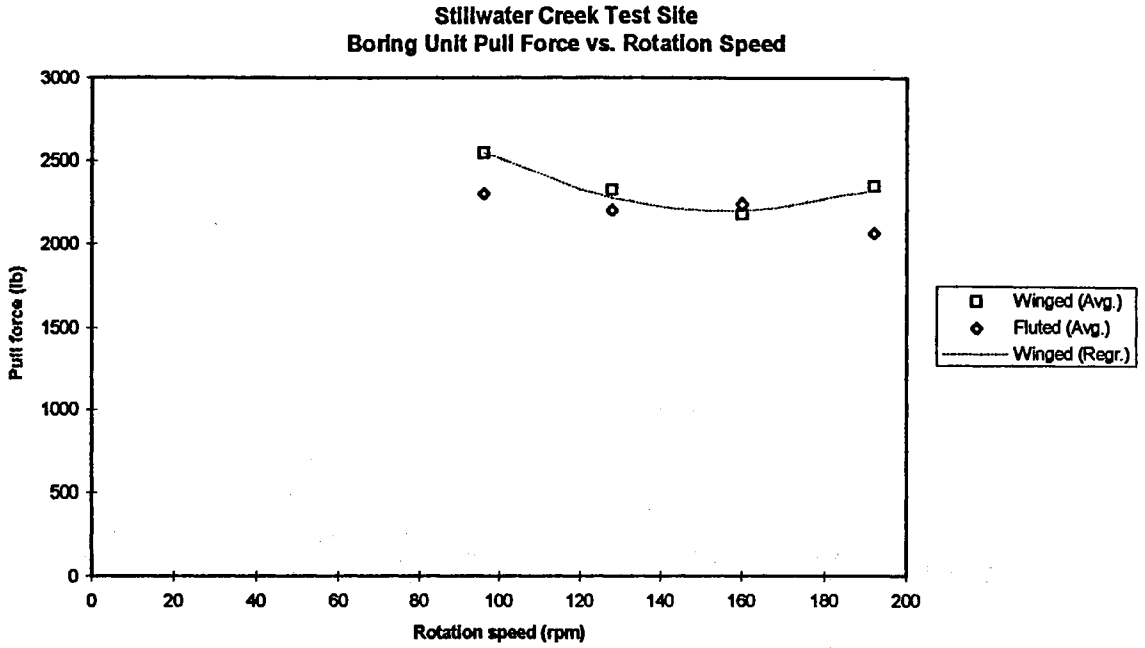


**Figure 58:** Mean boring unit pull force vs. reamer rotation speed at the Stillwater Creek test site.

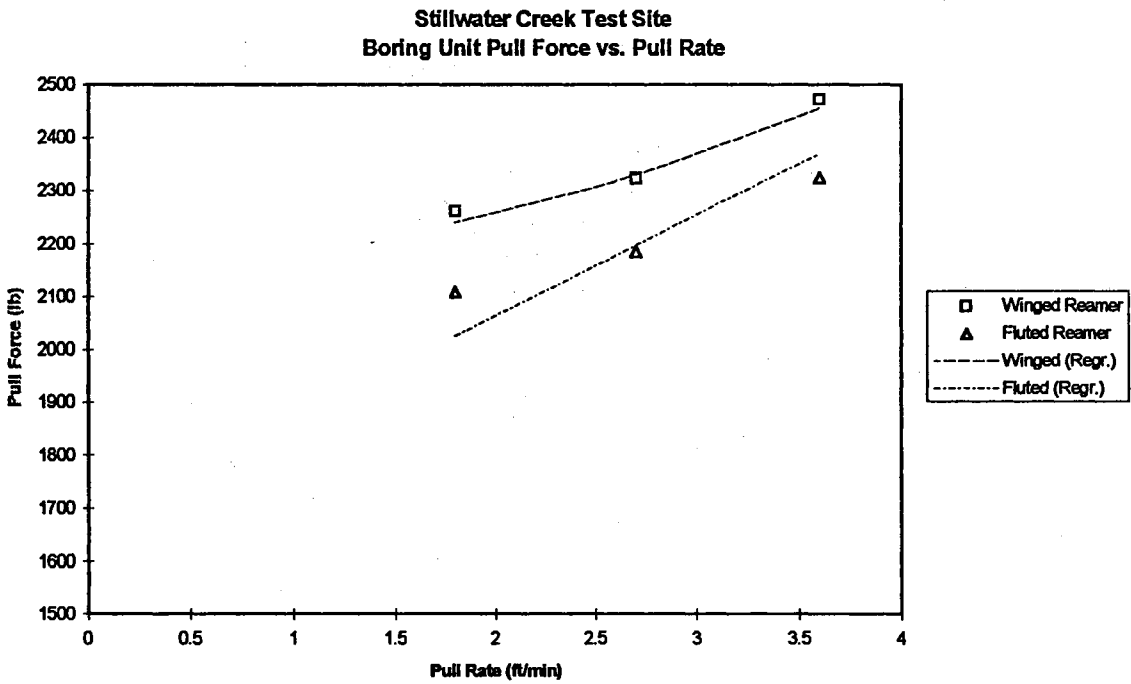
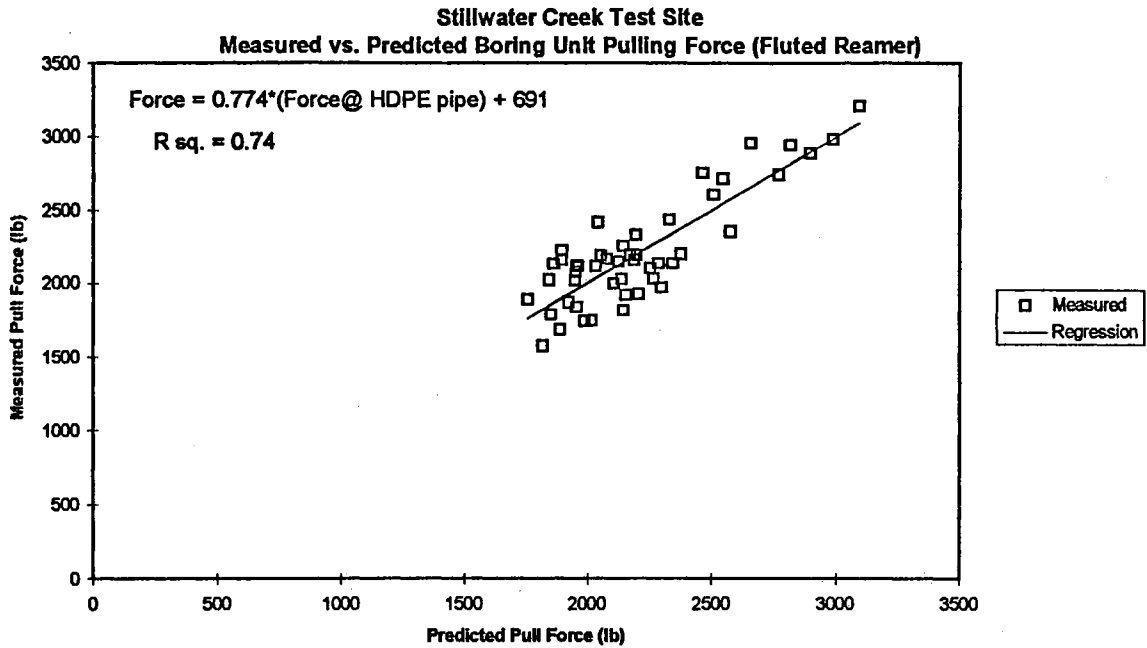


**Figure 59:** Mean boring unit pull force vs. reamer pull rate at the Stillwater Creek test site.

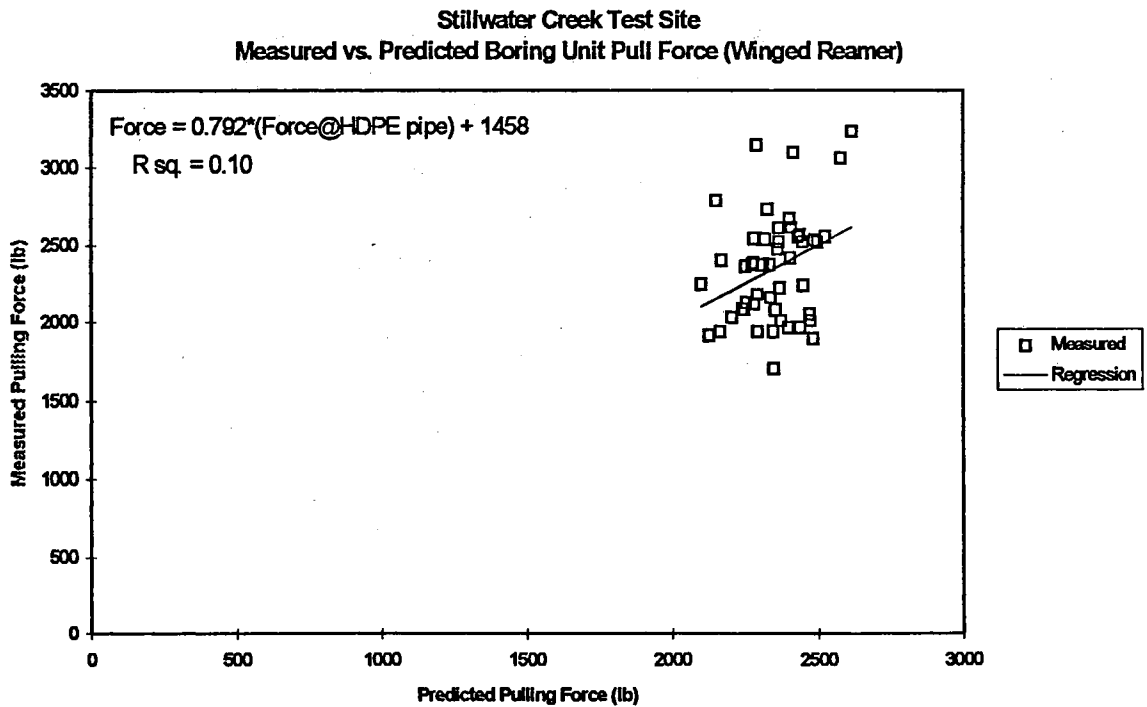
unit pulling force curve closely matches the torque curve for the winged reamer is not surprising since it was demonstrated in Figure 54 that the torque value of the winged reamer appears to be primarily due to frictional and soil-to-tool adhesive forces. However, an increase in pull force accompanying an increase in rotation speed was not expected for either reamer. The trend shown in Figure 58 for the winged reamer is consistent across all three pull rates, but the reason for an increase in boring unit pull force between the 160 and 192 rpm rotation speeds is unknown.

Figure 59 on Page 165 provides a plot of mean boring unit pulling force versus pull rate for the two reamers. The mean pull force for both reamers increased more rapidly as the pulling rate changed from 2.7 to 3.6 ft/min than as it changed from 1.8 to 2.7 ft/min. The best fit regression for the winged reamer found boring unit pull force to be a function of the square of the pull rate. This matches the trend seen in Figure 59. The correlations for the fluted reamer were stronger expressing boring unit pull force as a linear function of pull rate. The fluted reamer regression line in Figure 59 does not match the plot of the pull force means as closely as the winged reamer regression. This indicates some non-normality in the scatter of the data readings for the fluted reamer. The regression lines were plotted using values of 120 rpm for rotational speed and 110 ft for distance in Equations 26 and 27.

Figures 60 and 61 on Page 167 show the results of regression analyses relating the pulling force measured at the boring unit to the pulling force measured at the polyethylene pipe for the two reamers used at the Stillwater Creek test site. Figure 60 shows that the pulling force at the polyethylene pipe is a strong predictor ( $r^2 = 0.74$ ) of the pulling force at the boring unit for the fluted reamer. As shown in Figure 61, there is little correlation



**Figure 60:** Measured vs. predicted boring unit pull force as a function of the pull force at the polyethylene pipe for the fluted reamer.



**Figure 61:** Measured vs. predicted boring unit pull force as a function of the pull force at the polyethylene pipe for the winged reamer.

( $r^2 = 0.10$ ) between pulling force at the polyethylene pipe and pulling force at the boring unit for the winged reamer with the compaction cone pulled behind. As discussed in the next section on pulling forces at the HDPE pipe, the compaction cone with the drilling fluid released behind it is effective at reducing the pull load seen by the polyethylene pipe.

#### Pulling Force at the HDPE Pipe

The analysis of variance (ANOVA) table for the polyethylene pipe pulling force measured at the Stillwater Creek test location is given in Table 15.

Table 15

ANOVA Table for Polyethylene Pipe Pulling Force at Stillwater Creek Test Site

Source	Degrees of Freedom	Type I Sum of Squares	F Value	P
Penetrometer	1	715769	20.43	0.0001
Distance Pulled	1	73843	2.11	0.1515
Reamer	1	17433940	497.57	0.0031
Bore(Reamer)	6	4590489		
Rotat. Speed [RPM]	3	66068	0.63	0.5992
Pull Rate [FPM]	2	98832	1.41	0.2515
RPM x FPM	6	41375	0.20	0.9766
Reamer x RPM	3	117192	1.11	0.3497
Reamer x FPM	2	140577	2.01	0.1429
Reamer x RPM x FPM	6	184744	0.88	0.5156
Error ( $\delta$ )	64	2242461		
Total	95	25705291		

Of the effects controlled in this study (pull rate, rotation rate, reamer), Table 15 shows only reamer design to be statistically significant at the 95% confidence level. No two-way or three-way factor interactions were shown to be significant.

Regression analyses were performed on the HDPE pipe pull data for both reamers. The best fit regression equation for the polyethylene pipe pulling force using the fluted reamer had an  $r^2$  value of 0.30 and is given in Equation 28.

$$HDPE\ Pipe\ Pull_{fluted} = 127.1 \times fpm + 4.49 \times Dist. - 0.635 \times q(u) + 1501 \quad \text{Eq. (28)}$$

Where: HDPE Pipe Pull<sub>fluted</sub> = the pulling force on the polyethylene pipe when using the fluted reamer.

fpm = the carriage pull rate in ft/min

dist. = the length of HDPE pipe pulled into the hole at the end of a given 10 ft test section (ft)

q(u) = the penetrometer cone tip pressure corresponding to the location of interest (lb/in<sup>2</sup>)

Equation 29 presents the regression equation for polyethylene pipe pulling force with the winged reamer. The coefficient of determination for the equation is 0.19.

$$HDPE\ Pipe\ Pull_{winged} = -0.389 \times q(u) + 1344 \quad \text{Eq. (29)}$$

Where: HDPE Pipe Pull<sub>fluted</sub> = the pulling force on the polyethylene pipe when using the winged reamer.

q(u) = the penetrometer cone tip pressure corresponding to the location of interest (lb/in<sup>2</sup>)

Correlations for both the fluted and winged reamers for HDPE pipe pulling force are weak. Plots of the measured pipe pulling force values versus the values predicted from Equations 28 and 29 are given in Figures 62 and 63. Of special interest in Equations 28 and 29 is inclusion of the penetrometer cone tip pressure ( $q_u$ ) in both of the regression



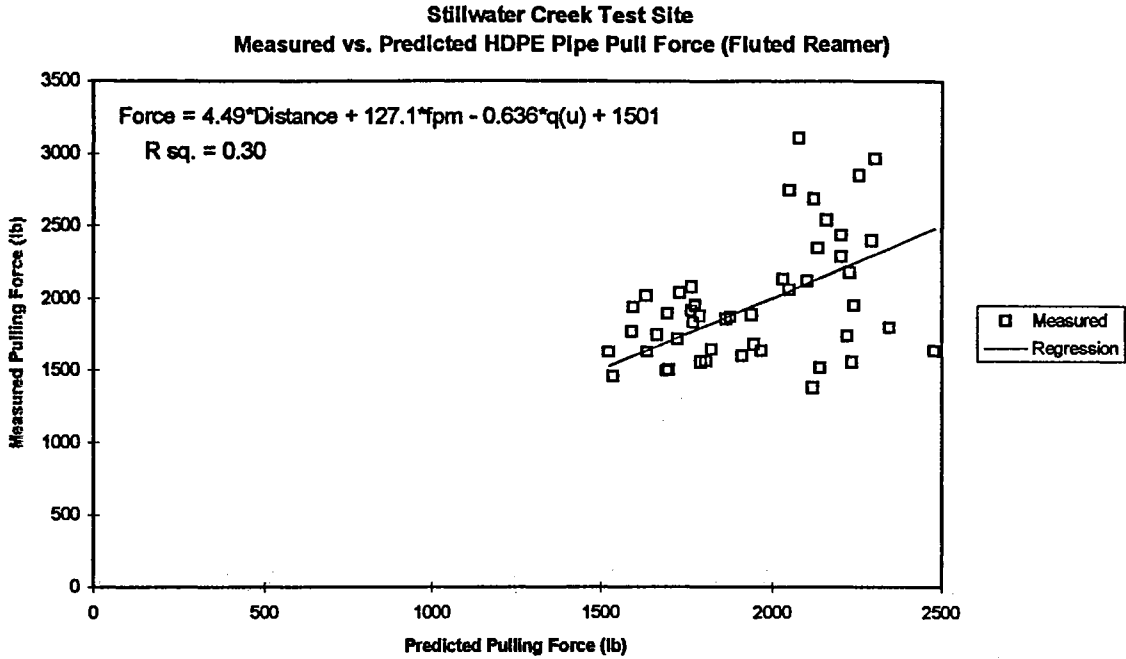


**Figure 62:** Measured vs. predicted polyethylene pipe pull force for the fluted reamer as a function of controlled and covariate variables.

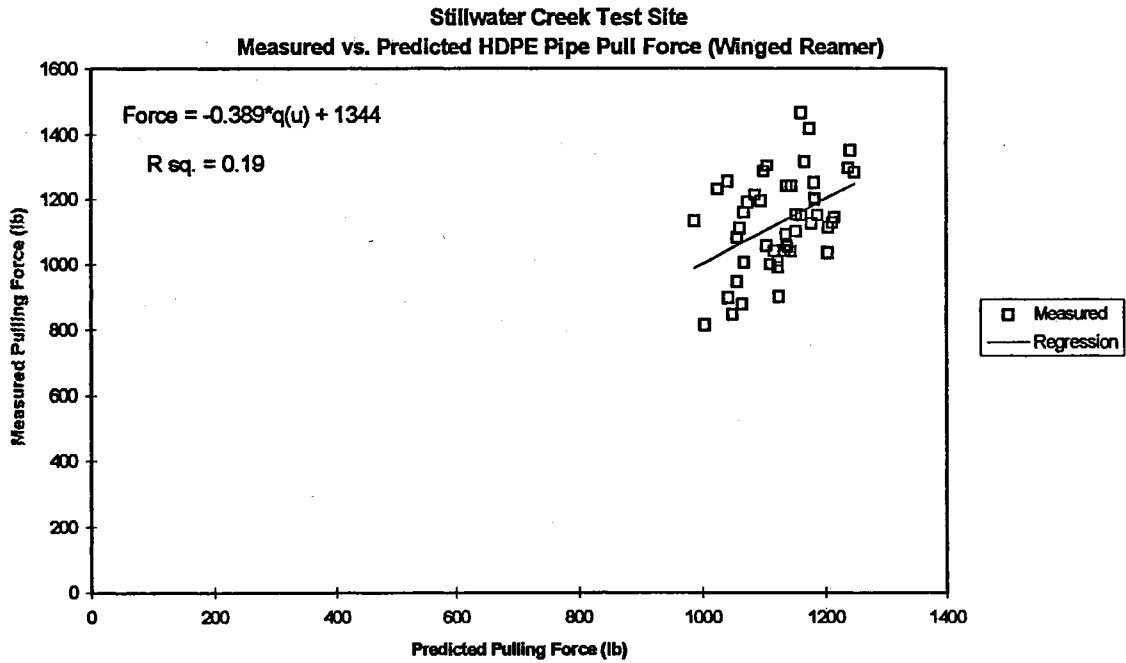


**Figure 63:** Measured vs. predicted polyethylene pipe pull force for the winged reamer as a function of controlled and covariate variables.

equations. An index of soil strength would be expected to make a difference in the rotational torque at the boring unit, and possibly in the boring unit pull force. But, it was not anticipated to see any influence of  $q_u$  on the pull at the product pipe. If an influence did occur, it would have been expected to have had a positive correlation with pulling force instead of the negative relationship noted in Equations 28 and 29.

An analysis was conducted to see if changes in soil across the test site could have influenced the weak correlations noted in Figures 62 and 63. Table 3 shows that the soil samples taken from the last three bores at the Stillwater Creek test site had a slightly higher moisture content and void ratio than the samples from the first bores. Close examination of the particle size analysis graphs in Section E of the appendix show that the soil samples from the last three bores had a slightly higher clay percentage than the samples taken in conjunction with the other bores.

Figure 64 shows the result of a regression analysis for the pulling force at the polyethylene pipe using the fluted reamer which included the moisture content of the soil samples taken along with the bore. The figure shows a substantial improvement in coefficient of determination ( $r^2 = 0.73$ ) over the value obtained with the relation in Equation 28. The relation expressed in Figure 63 should not be used to implicate an effect of soil moisture content on HDPE pipe pulling force. Rather, the moisture content variable should be viewed here as an indicator of a slight change in soil constitution at the depth of the bore in Bores 6 and 7. A similar effort at including a moisture content term in the regression analysis for the winged reamer showed no improvement.

Table 16 gives the mean values for pulling force at the polyethylene pipe for both reamers used in the analysis.

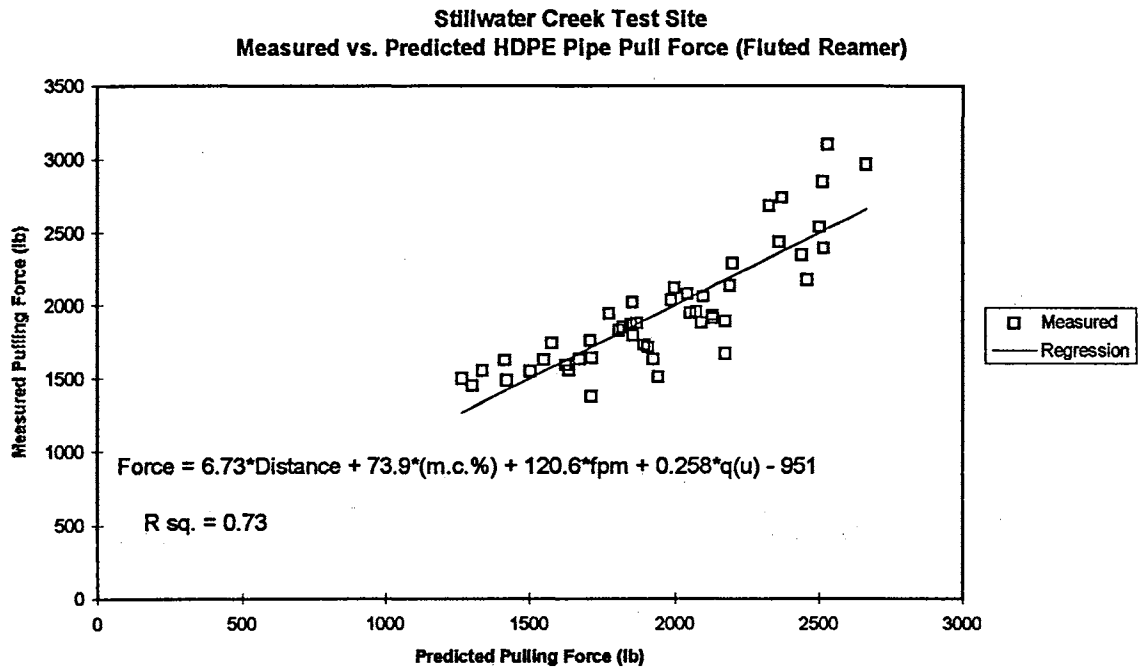


**Figure 64:** Measured vs. predicted polyethylene pipe pull force for the fluted reamer as a function of controlled, covariate, and soil sample moisture content variables.

Table 16

## Stillwater Creek HDPE Pipe Pull Means for Fluted and Winged Reamers

Reamer	Polyethylene Pipe Pull Force (lb)
Fluted	1958
Winged	1128

Means comparison via a single contrast showed the difference between the means for the two reamers to be statistically significant at the 95% confidence level. The fluted reamer is shown to have a mean pull force 74% higher than the winged reamer. {Once again, the reader familiar with the paper presented by this author at the International No-Dig '96 Conference (Gunsaulis, 1996) will note a slight discrepancy in the mean values presented here versus those presented in the No-Dig paper. The means calculated in the No-Dig paper were the average of all pipe pull readings in excess of 600 lb for the entire length of the bore. The means presented in Table 16 are the mean values of pull force readings taken during the 12 official test segments in each bore. }

The difference between the HDPE pipe pulling force for the fluted and winged reamers is attributable to three main causes. First, the winged reamer as shown in Figure 17 has a solid compaction cone behind it which helps in the formation of a more well defined hole for the pipe to pass through. Second, the winged reamer provides two fluid orifices behind the compaction cone to provide additional fluid for the lubrication of the hole formed by the compaction cone. And third, the winged reamer cuts an 8.5 in hole in the soil profile versus a 7.0 in hole for the fluted reamer. Further testing would be required to evaluate the importance of each of these differences in reamers.

It is interesting to note that while no statistically significant difference existed in mean pulling force measured at the boring unit for both reamers, a sharp difference in pulling force at the polyethylene pipe was shown to exist. This result suggests that the axial forces acting on the compaction cone ( $F_{CA}$ ) must be significant when compared with the pulling force at the boring unit. This result also indicates that pulling force at the boring unit is not a good predictor of the actual loading placed upon the installed service pipe when a solid compaction cone is in place.

## Chapter 7

### Summary and Conclusions

#### *Boring Unit/Data Collection System*

The modified Jet Trac Model 4/40 A boring unit used in this study worked well. The electronic feedback control system proved capable of maintaining set points of rotation speed and pull rate within the desired precision using a simple proportional/integral (PI) control loop. The compact “package” of the laptop computer with the IOTech Daqbook 100 data acquisition system was well suited for rapidly switching the computer from the penetrometer unit to the boring unit. Once proper sealing was achieved with the measurement system for pull load on the polyethylene pipe, the use of the hydraulic cylinder inside the pipe worked acceptably.

The following recommendations are given to enhance the functionality and reliability of the system described in Chapter 3. First, the use of electronic proportional control valves to control oil flow to the thrust and rotation functions works adequately, but is an inefficient use of available hydraulic power. Because of the inherent inefficiency when trying to meter low flow rates to a motor with a high torque requirement, a limit is placed on the range of speeds which may be tested. The use of a hydrostatic system with adjustment of thrust and rotation rates through the use of variable displacement hydraulic pumps and motors would allow the experimenter to test a wider range of rates, particularly in respect to rotation speed. Such a system would be better suited to a boring unit which did not rely on an umbilical hydraulic supply, but had the power supply engine

and hydraulic pumps integrated into the boring unit itself. An example of such a machine would be a Jet Trac 2320 boring unit.

Second, if pulling force and spindle torque at the boring unit are going to be measured indirectly using the hydraulic pressure drop across the thrust and rotation motors, the use of a single differential pressure transducer on each of the motors would cut the number of transducers which must be maintained and calibrated in half. The transducers on a piece of field equipment must be tolerant to temperature fluctuations, vibrations, and dirt. Reducing the number of components needed should improve reliability of the system.

An improved carriage velocity transducer is recommended. As discussed in Chapter 4, vibrations associated with the operation of the boring unit caused the output signal from the internal tachometer in the Unimeasure VP-150A to be sinusoidal. While the problem was compensated for using a slow response setting in the feedback control algorithm, it would be desirable not to have to make such an adjustment. The use of a similar type of transducer which utilized an optical encoder or similar device to indicate rate of cable travel would be recommended.

Third, the additional expense for obtaining a pressure transducer rated for submerged use to use inside the polyethylene pipe for measurement of pulling force would be a good investment. Even if the measures taken to seal the pipe from water failed, the integrity of the data would not be compromised.

## *Tests in Non-cohesive Soil at the Coyle Test Site*

### Coyle Test Site: Spindle Torque

**For the reamer and non-cohesive soil used in this test:**

- **Significant interactions related to spindle torque exist between drilling fluid flow rate and reamer rotation speed, and between drilling fluid flow rate and reamer pull rate.**
- **Spindle torque decreases with increasing drilling fluid flow rate, increasing rotation speed (up to 192 rpm), and decreasing reamer pull rate.**
- **Frictional and soil-to-tool adhesive forces account for most of the spindle torque.**

At the Coyle test site in the non-cohesive silty/sandy soil, significant drilling fluid flow rate/pull rate and drilling fluid flow rate/reamer rotation rate interactions were noted with respect to the torque required at the boring unit. As drilling fluid flow rate decreased, rotational torque increased more rapidly with increases in pulling rate or with decreases in reamer rotational speed. A regression equation relating drilling fluid flow rate, carriage pull rate, reamer rotational speed, and penetrometer cone tip pressure ( $q_u$ ) to the rotational torque measured at the boring unit was found with a coefficient of determination ( $r^2$ ) of 0.81. Torque was found to be a nearly linear function of pull rate, but a decaying exponential function of both drilling fluid flow rate and rotational speed. Frictional and soil-to-reamer adhesive forces were shown to be the primary contributors to rotational torque in this soil.



### Coyle Test Site: Boring Unit Pull Force

**For the reamer and non-cohesive soil used in this test:**

- **A significant interaction related to the pull force measured at the boring unit exists between drilling fluid flow rate and reamer rotation speed.**
- **Pull force at the boring unit decreases with increasing drilling fluid flow rate, increasing rotation speed (up to 192 rpm), and decreasing reamer pull rate.**
- **Pull force at the boring unit increases more rapidly with the distance of pull as the drilling fluid flow rate decreases.**

A slight drilling fluid flow rate/reamer rotation speed interaction was noted relating to the pulling force required by the boring unit. As drilling fluid flow rate decreased, pulling force at the boring unit was found to increase slightly faster with decreases in rotational speed. Pulling force at the boring unit was found to be best described by a positive linear relationship with the pulling rate of the reamer. A regression equation was developed relating drilling fluid flow rate, carriage pull rate, spindle rotation speed, penetrometer cone tip pressure ( $q_u$ ), and distance pulled to pulling force at the boring unit. The coefficient of determination ( $r^2$ ) for the regression was 0.77. The regression equation development found an interaction between drilling fluid flow rate and distance pulled. Pulling force was shown to increase more rapidly with distance as the drilling fluid flow rate decreases.

### Coyle Test Site: Polyethylene Pipe Pull Force

**For the reamer and non-cohesive soil used in this test:**

- **The pulling force at the polyethylene pipe accounts for the majority of the pulling force measured at the boring unit.**

Lost polyethylene pipe pulling force data prevented extensive analysis on relationships relating to that dependent variable. A regression expression was developed relating the distance pulled and the drilling fluid flow rate to the HDPE pipe pulling force for the four bores from which the data was saved. The equation was shown to have an  $r^2$  value of 0.77. The expression reinforced the interaction shown to exist between distance and drilling fluid flow rate found from the boring unit pulling force data. For the fluted reamer used at the Coyle test site (see Figure 16), the pulling force at the polyethylene pipe was shown to account for most of the pulling force at the boring unit.

#### Coyle Test Site: Total Power Usage

**For the reamer and non-cohesive soil used in this test:**

- **Total power (rotational power plus power used in pulling) usage increases at a decreasing rate as rotational speed increases (up to 192 rpm).**

Power usage at the boring unit was found to increase at a diminishing rate as rotational speed increased, particularly for the 7.4 gal/min drilling fluid flow rate. Increases in drilling fluid flow rate were found to substantially reduce the power required at the boring unit. Power usage for the boring unit, based on torque and pulling forces corrected for their respective no-load values, was found to have mean values between 1 and 2 hp (0.75 to 1.49 kW) for each of the tested rotational speeds at the 15.5 gal/min drilling fluid flow rate. Mean power usage based on the same criteria ranged from just below 6 hp (4.47 kW) to over 7.5 hp (5.59 kW) for the 7.4 gal/min drilling fluid flow rate.

## ***Tests in Cohesive Soil at the Stillwater Creek Test Site***

### Stillwater Creek Test Site: Spindle Torque

**For the reamers and cohesive soil used in this test:**

- **Rotational torque reaches a minimum value in the 128 to 160 rpm rotational speed range.**
- **Spindle torque increases linearly with increasing reamer pull rate.**
- **The winged reamer (Figure 17) requires more torque than the fluted reamer (Figure 16) [By an average of 59% in this study].**

The soil in which the boring tests were conducted at the Stillwater Creek test site was a cohesive soil designated as a silty clay loam by the USDA soil classification system, or as a lean clay by the Unified Soil Classification System (USCS). No statistically significant two-way or three-way interactions were found to exist between the variables controlled in this test (rotational speed, carriage pull rate, reamer design) and rotational torque. Individually, rotational speed, pull rate, and reamer design were all found to be statistically significant in the determination of spindle torque.

Regression equations for torque were developed for both of the reamers used in the test. The best expression for rotational torque with the fluted reamer (see Figure 16) had a coefficient of determination ( $r^2$ ) of 0.64. The best expression for torque with the winged reamer (Figure 17) had an  $r^2$  of 0.38.

For both reamers, mean torque as a function of rotational rate had the highest value at the 96 rpm rotation speed. The mean torque hit a minimum value at 128 rpm for the fluted reamer and 160 rpm for the winged reamer. The torque value then increased to the 192 rpm reading. For the winged reamer, the increasing torque requirement as

rotational speed increased past the minimum value was attributed to a similar response seen in the boring unit pull force curve, and its corresponding influence on frictional and soil-to-tool adhesion forces. For the fluted reamer the increase in torque as rotation speed went past 128 rpm was hypothesized as due to a combination of: increasing shearing strength known to exist in cohesive soils as shearing rate increases; increased viscous shearing forces as the reamers rotated more rapidly in the soil/drilling fluid slurry; and inertial forces involved in accelerating the severed soil particles.

Torque was found to be best represented as a positive linear function of pull rate. Torque increased more rapidly with pull rate for the winged reamer than for the fluted reamer.

On average, the winged reamer required 59% more torque than the fluted reamer. Primary factors postulated to account for this difference were the larger outer cutting diameter of winged reamer, and placement of more drilling fluid closer to the point of soil cutting by the fluted reamer.

The difference in pulling forces measured at the boring unit and at the polyethylene pipe was found to be a good predictor ( $r^2 = 0.75$ ) of the torque required for winged reamer. This provides indication that torque for the winged reamer is dominated by frictional and soil-to-reamer adhesive forces acting on the face of the reamer. A similar comparison with the fluted reamer produced a much weaker correlation ( $r^2 = 0.27$ ).

#### Stillwater Creek Test Site: Boring Unit Pull Force

**For the reamers and cohesive soil used in this test:**

- **Pull force at the boring unit increases with increasing pull rate.**

- **No statistically significant difference in pulling force at the boring unit was found between the winged (Figure 17) and fluted (Figure 16) reamers.**

No two-way or three-way interactions between controlled variables were found to be significant in determining the pulling force at the boring unit. Among individual variables only the pull rate and the pulling distance covariate were found to be statistically significant at the 95% confidence level. The mean pulling force at the boring unit for the winged reamer was found to be slightly higher than the mean for the fluted reamer, but the difference was not shown to be statistically significant. Pulling force at the boring unit was found to be a function of the square of the pulling rate for winged reamer. A linear relationship between pulling rate and pulling force at the boring unit produced the best correlations with the fluted reamer.

Regression equations were developed for both reamers relating the pulling force measured at the boring unit to the controlled and covariate variables used in the test. The best equation for the for the fluted reamer was found to have an  $r^2$  of 0.41 and was a function of pulling rate and distance pulled only. The best fit equation for the winged reamer had an  $r^2$  of 0.20 and was a function of pulling rate and rotational speed.

Regression analyses were also performed for both reamers relating the pulling force at the boring unit to the pulling force measured at the polyethylene pipe. For the fluted reamer, the pulling force at the polyethylene pipe was found to be the primary component, and highly predictive, of the pulling force measured at the boring unit. The coefficient of determination for the fluted reamer was 0.74. For the winged reamer, the correlation between pulling force at the polyethylene pipe and at the boring unit was very weak ( $r^2 = 0.10$ ).

### Stillwater Creek Test Site: Polyethylene Pipe Pull Force

#### **For the reamers and cohesive soil used in this test:**

- **The use of the fluted reamer (Figure 16) results in a higher tensile loading on the installed polyethylene pipe than does the winged reamer (Figure 17) [By an average of 74% in this study].**

For the experimental model evaluated in the analysis of variance for pulling force at the polyethylene pipe at the Stillwater Creek test site, reamer design was the only controlled variable statistically significant at the 95% confidence level. The mean pulling force at the HDPE pipe for the fluted reamer was found to be 74% higher than for the winged reamer. The following factors are postulated to account for the HDPE pipe pull force difference between the reamers: the winged reamer (Figure 17) had a solid compaction cone to create a more well defined hole for the pipe to pass through; the winged reamer had two fluid orifices located behind the compaction cone to provide better lubrication on the surface of the HDPE pipe; the winged reamer cut a larger outer diameter hole (8.5 in vs. 7.0 in for the fluted reamer). Pulling rate and distance pulled were found to significant in correlations for polyethylene pipe pulling force with the fluted reamer, but not for the winged reamer.

### Stillwater Creek Test Site: Total Power Usage

#### **For the reamers and cohesive soil used in this test:**

- **Total power (rotational power plus power used in pulling) usage at the boring unit increases at an increasing rate as rotational speed increases (up to 192 rpm).**

Power usage at the boring unit was found to increase at an increasing rate as rotational speed was incremented from 96 to 192 rpm. The shape of the power curves was similar for both reamers as shown in Figure 55.

### ***General Comparisons Between Soil Types***

In the non-cohesive material at the Coyle test site there appeared to be few detrimental effects to operating the boring unit at a rotational speed of 192 rpm, or possibly higher. Rotational torque requirements were reduced, pulling force at the boring unit was reduced, and power increases at the higher rotational speeds were only slight. However, in the cohesive soil at the Stillwater Creek test site, there appeared to be a definite advantage to operating the boring unit in the 128 to 160 rpm range. This was the range at which torque for both reamers was found to be the lowest.

In the non-cohesive material at the Coyle test site, it was possible to develop regression equations which strongly correlated the controlled and covariate variables to the pulling force at the boring unit and at the product pipe. Correlations at the Stillwater Creek test site were much weaker for pulling force at the boring unit and at the product pipe. This was due in part to the whole plot term at the Stillwater Creek test site (reamer design) being non-numeric, and thus unable to be included in a regression equation.

### ***Limitations of Test Method***

An important concept needs to be grasped when reading the results of this study. While this study reveals important trends of the effect of rotation speed and pull rate on rotational torque; and to a lesser extent, pulling force measured at the boring unit; the way the experiment was designed for making efficient use of each bore reduced the ability to discern possible effects on the pulling force of the polyethylene pipe. The polyethylene

pipe pulling force tends to be based on the cumulative effects of everything which occurs during the bore. In this light, this study was well suited for testing the whole plot variables (fluid flow rate at the Coyle test site, and reamer design at the Stillwater Creek test site) for their effects on polyethylene pipe pulling force. However, to get a true understanding of the cumulative effects of one rotation speed or on pull rate versus another on the tensile loading placed on an installed service line, it would be necessary to run a series of tests where these variables were held constant during an entire bore.

### ***Recommendations for Future Research***

For future work in this area it is recommended that studies be conducted to develop quantitative relationships between reaming diameter and torque, boring unit pulling force, and polyethylene pipe pulling force. An understanding of this relationship coupled with the relationships determined in this study would give a better overview of the expected torque in any given situation.

Ideally, this type of study should be conducted over an expanded group of soil types. Soils which may yield important information from a similar study would be more coarse grained, poorly graded sands like the "sugar sands" of the gulf coast, and sticky, swelling clays like the Alligator or Sharkey clays of the Mississippi delta region.

The third area where future study could be beneficial in the testing of other mixes of drilling fluid. From this study, the importance of frictional and adhesive forces in determining overall torque is clear. More documented studies into which fluids might reduce torque and installed utility tensile loading would help the industry.



## REFERENCES

- 1) ASAE Standards 1993. ASAE D497.1 Agricultural machinery management data. American Society of Agricultural Engineers, St. Joseph, MI. Pp. 328-334.
- 2) ASTM 1994. ASTM D421-85 Standard practice for dry preparation of soil samples for particle-size analysis and determination of soil constants. Annual Book of ASTM Standards, Sec. 4, Vol 04.08, Soil and Rock. American Society for Testing and Materials, Philadelphia, PA. Pp. 8-9.
- 3) ASTM 1994. ASTM D422-63 Standard test method for particle-size analysis of soils. Annual Book of ASTM Standards, Sec. 4, Vol. 04.08, Soil and Rock. American Society for Testing and Materials, Philadelphia, PA. Pp. 10-16.
- 4) ASTM 1994. ASTM D1586-84 Standard test method for penetration test and split-barrel sampling of soils. Annual Book of ASTM Standards, Sec. 4, Vol. 04.08, Soil and Rock. American Society for Testing and Materials, Philadelphia, PA. Pp. 129-133.
- 5) ASTM 1994. ASTM D3441-86 Standard test method for deep, quasi-static, cone and friction-cone penetration tests of soil. Annual Book of ASTM Standards, Sec. 4, Vol. 04.08, Soil and Rock; Building Stones. American Society for Testing and Materials, Philadelphia, PA. Pp. 338-343.
- 6) Baroid Drilling Fluids, Inc. 1992. Quik-Gel and EZ-Mud product bulletins (IDP-009 and IDP-008). Baroid Drilling Fluids, Denver, CO.
- 7) Bennett, D., Khan, S., and D.T. Iseley 1994. Mini-horizontal directional drilling: Field evaluation at WES. Technical Report #102, Construction Productivity Advancement Research (CPAR) program. Trenchless Technology Center, Louisiana Tech University, Ruston, LA. pp. 7 - 36
- 8) Bennett, D., Guice, L.K., Khan, S., and K. Staheli 1995. Guidelines for trenchless technology: Cured in place pipe (CIPP), fold and formed pipe (FFP), Mini-horizontal directional drilling (mini-HDD), microtunneling. Technical Report #400, Construction Productivity Advancement Research (CPAR) program. Trenchless Technology Center, Louisiana Tech University, Ruston, LA. pp. 3.1 - 3.30
- 9) Cary, D. 1993. Test results of fluid assisted mini-directional horizontal boring. Proceedings: North American No-Dig '93 Conference. North American Society of Trenchless Technology, Chicago, IL. P1:2 - P1.5.
- 10) Chilingarian, G.V. and P. Vorabutr 1981. Drilling and Drilling Fluids. Developments in Petroleum Science, V. 11. Elsevier Science Publishers. Amsterdam, the Netherlands. pp. 50 - 51, 121 - 127, 271 - 293, 726

- 11) Cochran, W.G., and G.M. Cox 1957. Experimental Designs, 2nd. Edn., John Wiley & Sons, Inc. New York, NY. Pp. 293-315.
- 12) Fredericksen, T.M. 1984. Intuitive IC Op Amps. Printed by R.R. Donnelley & Sons. Pp. 212-214.
- 13) Gray, F., and E. Nance 1978. Lake Carl Blackwell Experimental Range Area. Oklahoma State University Agricultural Experiment Station Research Report P-763. OSU, Stillwater, OK.
- 14) Gunsaulis, F.R. 1996. A system for comparison of boring parameters of mini-HDD machines. Proceedings: International No-Dig '96 Conference. North American Society of Trenchless Technology, Chicago, IL. pp. 61 - 77
- 15) Huey, D.P., Hair, J.D., and K.B. McLeod 1996. Installation loading and stress analysis involved with pipelines installed by horizontal directional drilling. Proceedings: International No-Dig '96 Conference. North American Society of Trenchless Technology, Chicago, IL. pp. 37-59
- 16) Institute for Electrical and Electronics Engineers (IEEE) 1994. IEEE Standard 1333-1994 Guide for installation of cable using the guided boring method. IEEE, New York, N.Y.
- 17) IOtech, Inc. 1993. DaqBook User's Manual. IOtech, Inc. Cleveland, OH
- 18) Jonnes, N. 1995. Easy directional drilling in sand. Proceedings: North American No-Dig '95 Conference. North American Society of Trenchless Technology, Chicago, IL. Section 3C pp. 2:2 - 2:8
- 19) Kepner, R.A., Bainer, R., and E.L. Barger 1982. Principles of Farm Machinery, 3rd. Edn. AVI Publishing Company, Westport, CT. Pp. 112-134.
- 20) Khan, A.S. 1995. Soil/Drilling Interaction Investigation and Guideline Development For Mini-Horizontal Directional Drilling Installations. Unpublished M.S. thesis. Louisiana Tech University, Ruston, LA. pp. 42-73
- 21) Khan, S., Bennett, D., McCrary, S., and D.T. Iseley 1994. Mini-Horizontal Directional Drilling: State of the Art Review. Technical Report #101, Construction Productivity Advancement Research (CPAR) program. Trenchless Technology Center, Louisiana Tech University, Ruston, LA pp. 3 - 45
- 22) Kirby, M.J., Kramer, S.R., Pittard, G.T., and M. Mamoun 1996. Design guidelines and procedures for guided horizontal drilling. Proceedings: International No-Dig '96

- 23) McKyes, E. 1985. Soil Cutting and Tillage. Developments in Agricultural Engineering, V. 7. Elsevier Science Publishing, Amsterdam, the Netherlands.
- 24) Nichols, M.L. 1931. The dynamic properties of soil: II. Soil and metal friction. Agricultural Engineering. Vol. 12, No. 8. pp. 321-324
- 25) Payton, M. 1996. Assistant Professor, Department of Statistics. Oklahoma State University, Stillwater, OK. Personal contact.
- 26) Peck, R.B., Hanson, W.E., and T.H. Thornburn 1974. Foundation Engineering, 2nd Edn. John Wiley & Sons, New York, NY.
- 27) Reece, A.R. 1965. The fundamental equation of earthmoving mechanics. Symposium on Earthmoving Machinery, Institute of Mechanical Engineers, 179, Part 3F, London.
- 28) Snethen, D.R. 1996. Professor, Department of Civil Engineering. Oklahoma State University, Stillwater, OK. Personal contact.
- 29) Stangl, G.A. 1991. Horizontal boring methods. Pipeline and Gas Journal. February edn., pp. 35- 38
- 30) Stone, M.L. 1995. Associate Professor, Department of Biosystems and Agricultural Engineering. Oklahoma State University, Stillwater, OK. Personal contact.
- 31) Tanwani, R. and D.T. Iseley 1994. Tracking and steering systems in trenchless construction. Journal of Construction Engineering and Management. v. 120, No. 1, pp. 65 - 76.
- 32) Terzaghi, K. 1943. Theoretical Soil Mechanics. Wiley and Sons, New York. pp. 118-127.
- 33) USDA Soil Conservation Service 1987. Soil Survey of Payne County, Oklahoma. United States Department of Agriculture.
- 34) Wilcox, R. 1990. Horizontal directional drilling: Application of drilling fluids for friction reduction and hole stabilization. Baroid Drilling Fluids, Houston, TX. pp. 2-8
- 35) Wismer, R.D. and H.J. Luth 1972. Performance of plane soil cutting blades in a clay. ASAE Transactions. Vol. 15, No. 2. Pp. 211-216.
- 36) Wray, W.K. 1986. Measuring Engineering Properties of Soil. Prentice-Hall, Inc. Englewood Cliffs, NJ.

# Appendix

## Section A

### Glossary of Terms

**Back Reamer:** Cutter head attached to leading end of drill string to enlarge the initial pilot hole during a pullback operation, facilitating the subsequent placement of product pipe.

**Carriage:** The rigid housing for the spindle and associated drive motor which traverses along the boring unit during the drilling or reaming process. Thrust and pulling forces are transmitted to the drilling pipe by the movement of the carriage.

**Cutter head/Drill Bit:** Tool attached to front of drill string that cuts through soil, using fluid jet cutting and/or mechanical cutting.

**Drilling Fluid:** Combination of water and (usually) bentonite or polymer continuously pumped to the cutting head to facilitate removal of cuttings, stabilize the borehole, cool the cutter head, and lubricate the product pipe to reduce friction during pullback.

**Drill String:** Total length of individual drill rods/stems in ground used to form the borehole. Typically each rod or segment is 5 to 30 feet (1.52 to 9.15 m) long and up to 5 inches (12.7 cm) in diameter with tensile strengths approaching 135,000 psi (931 MPa). Mini-HDD machines, intended primarily for placing service lines/laterals, are typically designed for use with shorter rods.

**Entry Angle/Exit Angle:** Vertical angle to the local ground surface at which the drill string enters and exits the ground, respectively, during the drilling of the pilot hole. Entry angles are typically 5° to 20°, and exit angles  $\leq 10^\circ$ .

**Fluid Pump:** Pumping unit, typically of piston-type, which pumps drilling fluid to the cutter head under pressure.

**Locator:** Equipment and instruments to ascertain drill head position providing basis for guidance correction.

**Mini-Horizontal Directional Drilling (mini-HDD):** Surface launched method for installing product pipes or utility lines of diameter up to 10 inches (25 cm), in lengths up to 600 feet (183 m) or more, at depths typically less than 15 feet (4.6 m). Maximum thrust/pullback capability is approximately 20,000 lb (89 kN).

**Pilot Hole:** Hole formed by the initial, guided pass of drill string.

**Product Pipe:** Pipe (e.g., plastic, steel, etc.) or utility line or cable to be permanently placed in final bored hole.

**Pullback:** In this process the drill string, attached with a reaming assembly at the far end from the drill rig, is pulled back from the drill rig through the pilot hole. The product pipe which is attached to the reaming assembly is also pulled back along with the drill string.

**Reaming (Back reaming):** A process by which a pilot hole is made large enough to accommodate the product pipe. A cutter-head is used to drill the soil from the opposite direction of pilot hole drilling.

**Spindle:** The rotating drive located on the boring unit which mates with the drilling pipe. Torque is transferred to the drilling pipe. In fluid-assisted systems, drilling fluid will pass through the spindle into the drilling pipe.

**Trenchless Technology:** Family of techniques for utility line installation, replacement, or renovation with no minimum excavation from the ground surface.

## Appendix Section B

### Omnidata Polycorder Program

```

FMT
FLOYD.F
9999
/N6/MODA//
/N5/HRMN//
/N5.1/VOLTS//
/N8.1/PRESS1//
&
DAT
PRESS1.D
FLOYD.F
&
PGM
TIME
TIM
POP
XAB
STO 23
POP
STO 24
END
&
PGM
PRESS1
ACD 21,5V,0
SCN Z,21
RCL 0
STO 31
CON .8648
SUB
CON 910.75
MLT
STO 32
END
&
PGM
RECORD
RCL 23
STF
ICP
RCL 24
STF
ICP
RCL 31
STF
ICP

```

(Sets format for data storage: Month and Day, Hour and Minute, Volts measured across shunt resistor, and Calculated pressure)

(Time call subroutine)

(Subroutine to measure voltage across shunt resistor and calculate pressure)

(Subroutine to store time, voltage, and pressure values in data file)



```

RCL 32
STF
ICP
END
&
PGM                               (Subroutine to display current pressure reading on viewer screen)
UPDATE
DCM 1
WID 7
CDS 8,0
RCL 32
VUA
END
&
PGM                               (Subroutine to print "PRESSURE:" on viewer screen when updating
DISPLAY                           numerical value)
CDS 0,64
WID 10
VUM "PRESSURE: "
END
&
PGM                               (Autolog subroutine. Primary subroutine to orchestrate automated collection of
AUTOLOG                           data. Calls Time, Shunt voltage reading/voltage calculation, Screen update,
AON                                and data storage subroutines)
OPN PRESS1.D
DLY 5
GSB TIME
SNG 10,20
SNG 30,40
GSB PRESS1
GSB DISPLAY
GSB UPDATE
DLY 10
GSB RECORD
DLY 10
AFF
ZZZ
END
&
PGM
MAIN                               (Program Main section. Calls formatting program for data collection, and then
OPN PRESS1.D                       dumps program into Autolog subroutine)
CON 1
PSH
PSH
SLC
GSB AUTOLOG
END
#□

```

## Section B: Polycorder Program

## Section C

### Boring Unit Data Acquisition and Control Program

\*\*\*\*\*

Draft IV of control program for horizontal boring data acquisition.

Includes two low-pressure loop transducers.

Floyd R. Gunsaulis, M.S.Ag.E., P.E.

7/26/95

\*\*\*\*\*/

```
#include <stdlib.h>
#include <conio.h>
#include "daqbook.h"
#include <stdio.h>
#include <dos.h>
#include <math.h>
#include <alloc.h>
#include <graphics.h>
#include <string.h>
#include <time.h>
#include <stdarg.h>

#define TimerResolution 1193181.667
/* #define GATETM 70 */ /* establish measuring period (in ms) for frequency */
#define CTRTEETH 120 /* establish number of teeth on cutting gear */
#define TORQCALV 958.4 /* value in psi/v */
#define FORCCALV 967.7 /* value in psi/v */
#define POSCALV .00664 /* value in V/V/in */
#define TEMPCALV 107 /* value in V/DegF */
#define DELTAT 90.0 /* loop time in milliseconds */
#define KC1 .50 /* Rotary proportional control constant */
#define KC2 5.0 /* Pull proportional control constant */
#define TauI1 0.10 /* Rotary integration control divisor */
#define TauI2 0.25 /* Pull integration control divisor */
#define TLOCAL 768.9
```

Section C: C++ Data Acquisition and Control Program

```

#define PLOCAL 757.1

void gripe(void);
void _far _pascal myhandler(int error_code);
void datascan(void);
double cardinal (long);
double elapsedtime(long, long);
long readtimer(void);
void initializetimer(void);
void restoretimer(void);
void controloop(float,float,float,float,float,float);
void screenupdate(void);
void startloop(float,float);
void stoploop(void);
void initscreen(void);

FILE *boredata; /* Data File Designation */

int gdriver, gmode, test, test0, test2, test3, test4, test5, adder, tempflag;
int flag0, flag1, flag2, controlflag, startflag, stopflag, runctr, errorcode;
char filename[12], answ, answ2, stopans;
float rotspeed, pullrate, measrotspd, measpullrt, pullerr, rotterr, AA, BB;
float torque, force, position, oiltemp, rotterr_1,pullerr_1,rotsig_1,pullsig_1;
float rotvelerr, pullrtterr,q, rotvoltdif, pullvoltdif, An_Val[10], p_1;
float torqlo, forclo, torqhi, forchi;
unsigned int sample, chans[10], x, y;
unsigned int rotoutsig, pulloutsig, z;
unsigned char gains[10],*config, bitVal;
unsigned int _far ptr1, A_Dchans[100];

long A_Davgs[10], start, stop, diftime;

time_t now;
char *timest;

main()
{gdriver = VGA;
gmode = VGAHI;
diftime = 90;

readtimer();
clrscr();
printf("\n          Horizontal Boring System Control Program");
printf("\n\n Enter the data file name --> ");

```

```

scanf("%s",&filename);
printf("\n\n Enter the target rotational speed (in rpm) --> ");
scanf("%f",&rotspeed);
printf("\n\n Enter the target pull back rate (ft/min) --> ");
scanf("%f",&pullrate);

do{
  clrscr();
  printf("\n\n Filename = %s\n\n Rotational speed = %5.1f rpm \
\n\n Pull back rate = %6.2f ft/min",filename,rotspeed,pullrate);
  printf("\n\n\n Are these values acceptable? (Y/N) ");
  do{ answ = getch();
  if(strchr("NnYy\xd",answ)==0)
  {gripe();
  test = 1;}
  else test = 0;} while(test);

  if(answ == 'N' || answ == 'n')
  {printf("\n\n Which value do you wish to change:\
\n\n File name --> Type 'F'\
\n\n Rotational speed --> Type 'R'\
\n\n Pull back rate --> Type 'P'\n\n ");
  do{ scanf("%s",&answ2);

  if(strchr("FfRrPp\xd",answ2) == 0)
  {gripe();
  test2 = 1;}

  if(answ2 == 'F' || answ2 == 'f')
  {printf("\n Enter new file name --> ");
  scanf("%s",&filename);
  test2 = 0;}
  else if(answ2 == 'R' || answ2 == 'r')
  {printf("\n Enter new value for rotational speed (rpm) --> ");
  scanf("%f",&rotspeed);
  test2 = 0;}
  else if(answ2 == 'P' || answ2 == 'p')
  {printf("\n Enter new value for pull back rate (ft/min) --> ");
  scanf("%f",&pullrate);
  test2 = 0;} test3 = 1;} while(test2);}

  else {test3 = 0;} }while(test3);

```

```

/***** Initializations *****/

```

### Section C: C++ Data Acquisition and Control Program

```

daqSetErrHandler(myhandler); /* establish error handler function */

daqInit(LPT1,7); /* initialize Daqbook 100 */

daqDigGetConf(1,0,0,0,config); /* Configure the mode of port A on P2 of the daqbook /
    for input */

daqDigConf(DdcLocal,*config); /* Set the configuration */

initializetimer();

controlflag = 1; /* One for pot control, Zero for program control */
flag0 = 0;
runctr = 1;
startflag = 1;
stopflag = 0;
test5 = 1;

do{
    daqDigRdBit(DdpLocalA, 0, &bitVal); /* read digital I/O channel 0 to see if unit is in/
        manual control or auto-bore mode */

        if(bitVal == 0)
        {
            if(!flag0)
            {clrscr();
                printf(" Drill unit is in manual operation mode. Set switch to 'Automatic'\n\
                    to start control loop. ");
                flag0 = 1;
                test0 = 1;}
            else {test0 = 1;}}

        else {test0 = 0;}} while(test0);

if ((boredata = fopen(filename,"w")) == NULL)
    {printf("\n Unable to open %s. \n", filename);
    daqClose();
    exit(1);
    }

/***** Prepare A/D Functions for Daqbook readings *****/

/* Setting of gains of all A/D channels */

```

```

gains[0] = DgainX1;
chans[0] = 0;
for(x=1;x<=9;x++)
  { chans[x] = x;
    gains[x] = DgainX2; }
gains[3] = DgainX1;
gains[5] = DgainX8;

daqAdcSetScan(chans, gains, 10); /* Load scan sequencer with channels and gains */

daqAdcSetTag(0); /* Disable channel tagging */

daqAdcSetClk(10,20); /* Set sampling rate at 5,000 Hz */

daqCtrSetCtrMode(1,DgcNoGating,1,DcsSrc1,0,0,0,0,1,0);

/***** Initialize the output screen *****/

initscreen();

time(&now);
timest = ctime(&now);

/***** Send out header info to file *****/

fprintf(boredata, "%s\n",timest);
fprintf(boredata, "%s%5.1f%s%5.2f\n", "Rot. set point = ",rotspeed," Pull rate set point
= ",pullrate);
fprintf(boredata, "%s\n\n", " Rot. Rate Pull Rate Torque HiTorqPres \
Force HiForcPres Position Oil Temp.");

/***** Primary Loop Starts Here *****/

do{

start = readtimer(); /* read start time */

daqCtrMultCtrl(DmccArm,1,0,0,0,0); /* start counting on P3 port */

datascan();

rotvelerr = rotspeed - measrotspd;

```

### Section C: C++ Data Acquisition and Control Program

```

pullrterr = pullrate - measpullrt;

if(startflag)
    startloop(rotvelerr,pullrterr);

if(stopflag)
    stoploop();

if(controlflag)
{
    /* Set potentiometer voltage to go directly to PWM driver board */
    /* x=A_Davgs[6];
    y=A_Davgs[7];

    printf("%10d%10d",x, y); */

    rotoutsig = (int)A_Davgs[6];
    pulloutsig = (int)A_Davgs[7]; }

else { controlloop(rotvelerr,pullrterr,roterr_1,pullerr_1,rotsig_1,pullsig_1);}

if(rotoutsig > 4095) rotoutsig = 4095; /* limit output value to 5 V */

if(pulloutsig > 4095) pulloutsig = 4095;

daqDacWtBoth(rotoutsig, pulloutsig); /* Write to PWM driver board */

roterr_1 = rotvelerr;
pullerr_1 = pullrterr;
rotsig_1 = rotoutsig;
pullsig_1 = pulloutsig;

if(runctr > 9)

{ /* Update screen */
    screenupdate();
    runctr = 0;}

runctr++;

if(kbhit())
{ stopans = getch();
  if(stopans == 'x' || stopans == 'X')
    test5 = 0;}

```

```

do { stop = readtimer(); /* 10 Hz loop speed */

    diftime = elapsedtime (start, stop);

    if(diftime <= DELTAT) test4 = 1;

    else test4 = 0;} while(test4);

daqCtrMultCtrl(DmccDisarm,1,0,0,0,0); /*Stop counting RPM pulses on P3 port */

daqCtrMultCtrl(DmccSave,1,0,0,0,0);

daqCtrGetHold(1,&ptr1);

daqCtrSetLoad(1,0);

daqCtrMultCtrl(DmccLoad,1,0,0,0,0);

daqDigRdBit(DdpLocalA, 0, &bitVal); /* Check for manual or automatic operation
mode */

if(bitVal == 0) /* If manual mode is activated, then stop control shifts back to pots */
{ stopflag = 1;
  controlflag = 1;}

} while(test5);

fclose(boredata);

daqInit(LPT1,7); /*set outputs to zero*/

daqClose();

closegraph();

system("cls");

}

/***** Primary data acquisition sub-routine *****/

void datascan(void)

```



```

{ int k,l;

daqAdcSetTrig(DtsSoftware,0,0,0,0); /* Set A/D triggering for Software trigger */
daqAdcSoftTrig(); /* Trigger the data acquisition */

daqAdcRdNFore(A_Dchans, 10); /* Read 10 samples from the 10 A/D channels */

for(x=0;x<10;x++)
    A_Davgs[x] = 0; /* Zero out A/D values */

for(k=0;k<10;k++) /*** 10 point average of scanned values *****/
{ for(l=0;l<10;l++)
  { adder = (k*10) + l;
    A_Davgs[l] += (A_Dchans[adder])/10.0; }
  }

/* Convert Digital readings to analog values */

for(x=0; x<10; x++)

{ An_Val[x] = (10.0/pow(2,(int)gains[x]))*(((float)A_Davgs[x])/4096);

/* Calculate rotational rate in rpm */

measrotspd = 0.6 * (ptr1/((float)diftime/1000.0))*(30/(float)CTRTEETH);

/* Calculate pull back rate in ft/min */

measpullrt = (An_Val[5] * (100/.297)/12.0); /* Calculate pullback rate in ft/min */

/* Calculate torque value in ft-lb */

torqhi = TORQCALV * An_Val[1] - 50.3; /* hi-side loop pressure */

torqlo = TLOCAL * (An_Val[8] - 1.0163); /* lo-side loop pressure */

torque = 19.0 * (torqhi - torqlo) * .022104; /* .022104 = 25/15 * 1/(24 * pi) */

/* Calculate force value in lb */

forchi = FORCCALV * An_Val[2] + 44.1; /* hi-side loop pressure */

```

### Section C: C++ Data Acquisition and Control Program

```

forclo = PLOCAL * (An_Val[9] - 0.993);    /* lo-side loop pressure */
force = 11.9 * (forchi - forclo) * 0.32283;    /* 0.32283 = (2*4.5)/(2 * pi * 4.437) */
/* Calculate hydraulic oil temperature in Degrees F */
oiltemp = TEMPCALV * (An_Val[4]) - 2.0;
if(An_Val[0] > 0.5)
{
/* Calculate linear position in ft */
    position = (An_Val[3] - .016) / (POSCALV * (2*An_Val[0]) * (12.0)); }
else { position = 20;}    /* Give dummy value to prevent division by 0 */
if(oiltemp > 200) tempflag = 1;
else tempflag = 0;
}

/***** PI control loop using difference equation in velocity form *****/
void controlloop(float errA, float errB, float errA_1, float errB_1, float sigA_1, float
sigB_1)
{ AA = sigA_1 + (KC1 + (KC1 *(DELTA T/1000.0)/TauI1))*errA - KC1*errA_1;
  BB = sigB_1 + (KC2 + (KC2 *(DELTA T/1000.0)/TauI2))*errB - KC2*errB_1;
  rotoutsig = (int) AA; pulloutsig = (int) BB;
  rotvoltdif = rotoutsig - A_Davgs[6];
  pullvoltdif = pulloutsig - A_Davgs[7];
  if(rotvoltdif < 200 && rotvoltdif > -200) flag1 = 1;
  else flag1 = 0;
  if(pullvoltdif < 200 && pullvoltdif > -200) flag2 = 1;
  else flag2 = 0;}

```

```

void startloop(float err1, float err2)

{ /* Is the current rotation rate within 10% of the desired rate? */

rotterr = (err1)/rotspeed;
if(abs(rotterr *100) < 10)
  { flag1 = 1;}
  else {flag1 = 0; }

/* Is the current pull rate within 10% of the desired rate? */

pullerr = (err2)/pullrate;
if(abs(pullerr * 100) < 10)
  flag2 = 1;
else flag2 = 0;

if(flag1 && flag2 )
  { controlflag = 0;
  startflag = 0; }

else controlflag = 1;

}

void stoploop(void)
{ /* Stop execution when thrust and rotation are approx. zero */
  if(measrotspd < 5 && measpullrt < 0.25)
    test5 = 0;
  }

/* Millisecond timer routine ( via Gordon Couger) */
/* Calculates elapsed time between start and stop in milliseconds */

double elapsedtime(long start, long stop)
{ double r;
  r = cardinal(stop-start);
  return (double) (1000 * r)/TimerResolution;
}

double cardinal(long l)
{ return (double) ((l<0)? 4294967296.0 + (long)l : (long)l );
}

void initializetimer(void)

```

```

{

    outportb(0x043,0x034);
    asm jmp short NullJump1

NullJump1::

    outportb(0x040,0x000);
    asm jmp short NullJump2

NullJump2::

    outportb(0x040,0x000);

}

void restoretimer(void)
{
    outportb(0x043,0x036);
    asm jmp short NullJump1

NullJump1::

    outportb(0x040,0x000);
    asm jmp short NullJump2

NullJump2::

    outportb(0x040,0x000);

}

#pragma warn - rvl
long readtimer(void)
{
    asm cli          /* Disable interrupts */
    asm mov dx,020h /* Address PIC ocw3 */
    asm mov al,00Ah /* Ask to read irr */
    asm out dx,al
    asm mov al,00h /* Latch timer 0 */
    asm out 043h,al
    asm in al,dx /* Read irr */
    asm mov di,ax /* Save it in DI */
    asm in al,040h /* Counter --> bx*/

```

```

asm mov bl,al /* LSB in BL */
asm in al,040h
asm mov bh,al /* MSB in BH */
asm not bx /* Need ascending counter */
asm in al,021h /* Read PIC imr */
asm mov si,ax /* Save it in SI */
asm mov al,00FFh /* Mask all interrupts */
asm out 021h,al
asm mov ax,040h /* read low word of time */
asm mov es,ax /* from BIOS data area */
asm mov dx,es:[06Ch]
asm mov ax,si /* Restore imr from SI */
asm out 021h,al
asm sti /* Enable interrupts */
asm mov ax,di /* Retrieve old irr */
asm test al,001h /* Counter hit 0? */
asm jz done /* Jump if not */
asm cmp bx,0FFh /* Counter > 0x0FF? */
asm ja done /* Done if so */
asm inc dx /* Else count int req. */
done:;
asm mov ax,bx /* set function result */
}
#pragma warn + rvl

void gripe(void) /* Beeps when error occurs */
{
    sound(500);
    delay(100);
    nosound(); }

void _far _pascal myhandler(int error_code)
{
    printf("\nError! Program aborted\nDaqbook Error: 0x%x\n", error_code);
    exit(1); }

void initscreen(void)
{

    initgraph(&gdriver, &gmode, " ");
    errorcode = graphresult();
    if(errorcode != grOk)
        {printf("Graphics error: %s\n", grapherrormsg(errorcode));

```

```

printf("Press any key to halt: ");
getch();
exit(1);
}

cleardevice();

setfillstyle(SOLID_FILL, BLACK);
bar(1,1,640,480);

setcolor(GREEN);
settextstyle(DEFAULT_FONT, HORIZ_DIR,2);
settextjustify(LEFT_TEXT, CENTER_TEXT);
outtextxy(190,50,"BACKREAM STATUS");

settextstyle(TRIPLEX_FONT, HORIZ_DIR,1);
outtextxy(50, 90, "ROTATION");
outtextxy(50,240,"PULL RATE");
outtextxy(480, 90, "POTS");
outtextxy(427, 165, "ROTATION");
outtextxy(425, 250, "PULL RATE");
outtextxy(430, 355, "TEMP. STATUS");
outtextxy(540, 165, "5%");
outtextxy(540, 250, "5%");

setcolor(LIGHTGREEN);
outtextxy(50, 130, "SET POINT: ");
outtextxy(50, 165, "RATE: ");
outtextxy(50, 200, "TORQUE: ");
outtextxy(50, 280, "SET POINT: ");
outtextxy(50, 315, "RATE: ");
outtextxy(50, 350, "FORCE: ");
outtextxy(50, 390, "POSITION: ");
outtextxy(50, 430, "OIL TEMP: ");
outtextxy(280, 130, "RPM ");
outtextxy(280, 165, "RPM ");
outtextxy(280, 200, "FT-LB ");
outtextxy(280, 280, "FT/MIN ");
outtextxy(280, 315, "FT/MIN ");
outtextxy(280, 350, "LB ");
outtextxy(280, 390, "FT ");
outtextxy(280, 430, "°F ");

setlinestyle(SOLID_LINE,0,NORM_WIDTH);

```

```
setcolor(WHITE);
rectangle(400,115,590,300);
```

```
setcolor(YELLOW);
circle(520,165,15);
circle(520,250,15);
circle(470,400,20);
}
```

```
void screenupdate(void)
```

```
{ /* Updates screen and saves data to data file */
```

```
int gprintf(int, int, char *, ...);
```

```
extern float measrotspd, measpullrt, torque, force, position, oiltemp;
extern float rotspeed, pullrate, torqhi, forchi;
extern int flag1, flag2, tempflag;
```

```
fprintf(boredata, "%5.1f%s%5.3f%s%5.1f%s%5.1f%s%5.1f%s%5.2f%s%5.1f\n"
```

```
measrotspd, "", measpullrt, "", torque, "", torqhi, "", force, "", forchi, "", position, "", oiltemp);
```

```
setcolor(BLACK);
setfillstyle(SOLID_FILL, BLACK);
bar(190,100,279,440);
```

```
setcolor(YELLOW);
settextstyle(TRIPLEX_FONT, HORIZ_DIR, 1);
settextjustify(LEFT_TEXT, CENTER_TEXT);
```

```
/* print the values */
```

```
gprintf(201,130, "%5.1f", rotspeed);
gprintf(201,165, "%5.1f", measrotspd);
gprintf(201,200, "%5.1f", torque);
gprintf(201,280, "%5.1f", pullrate);
gprintf(201,315, "%5.1f", measpullrt);
gprintf(201,350, "%5.1f", force);
gprintf(201,390, "%5.1f", position);
gprintf(201,430, "%5.1f", oiltemp);
```

```

if(flag1)
{ setfillstyle(SOLID_FILL, GREEN);
  sector(520,165,0,360,15,15);
  setfillstyle(SOLID_FILL, BLACK); }

else sector(520,165,0,360,15,15);

if(flag2)
{ setfillstyle(SOLID_FILL, GREEN);
  sector(520,250,0,360,15,15);
  setfillstyle(SOLID_FILL, BLACK); }

else sector(520,250,0,360,15,15);

if(tempflag)
{ setfillstyle(SOLID_FILL, RED);
  sector(470,400,0,360,20,20);
  setfillstyle(SOLID_FILL, BLACK); }

else sector(470,400,0,360,20,20);
}

int gprintf( int xloc, int yloc, char *fmt, ...)
{
  va_list argptr;
  char str[50];
  int cnt;

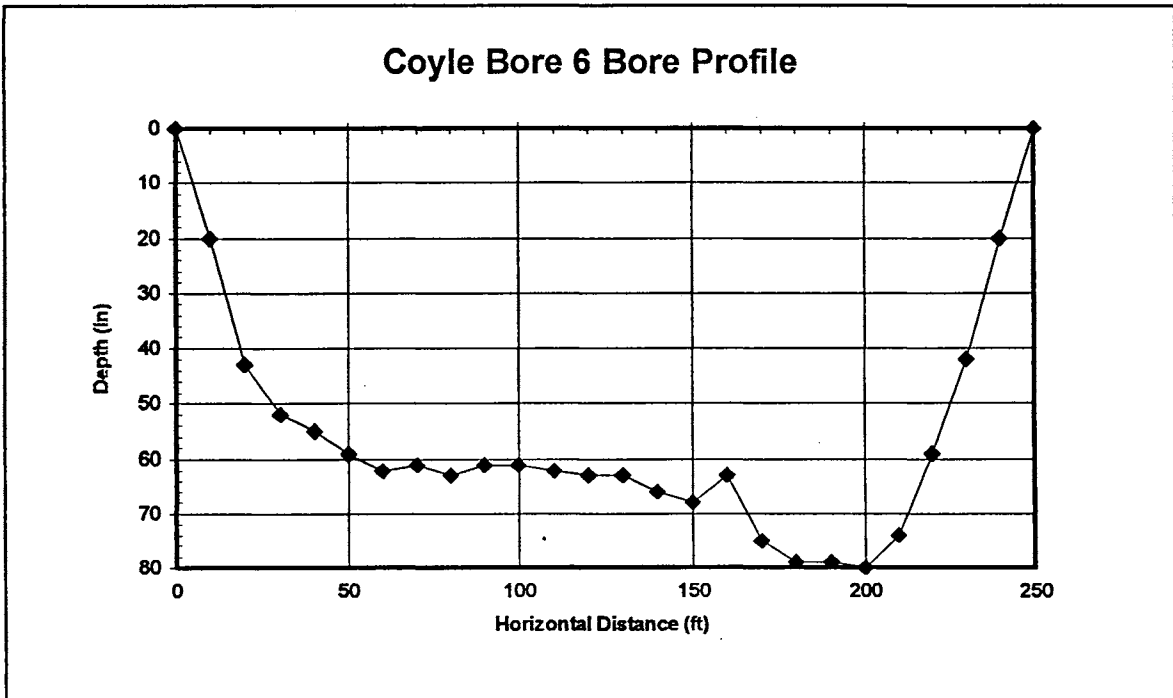
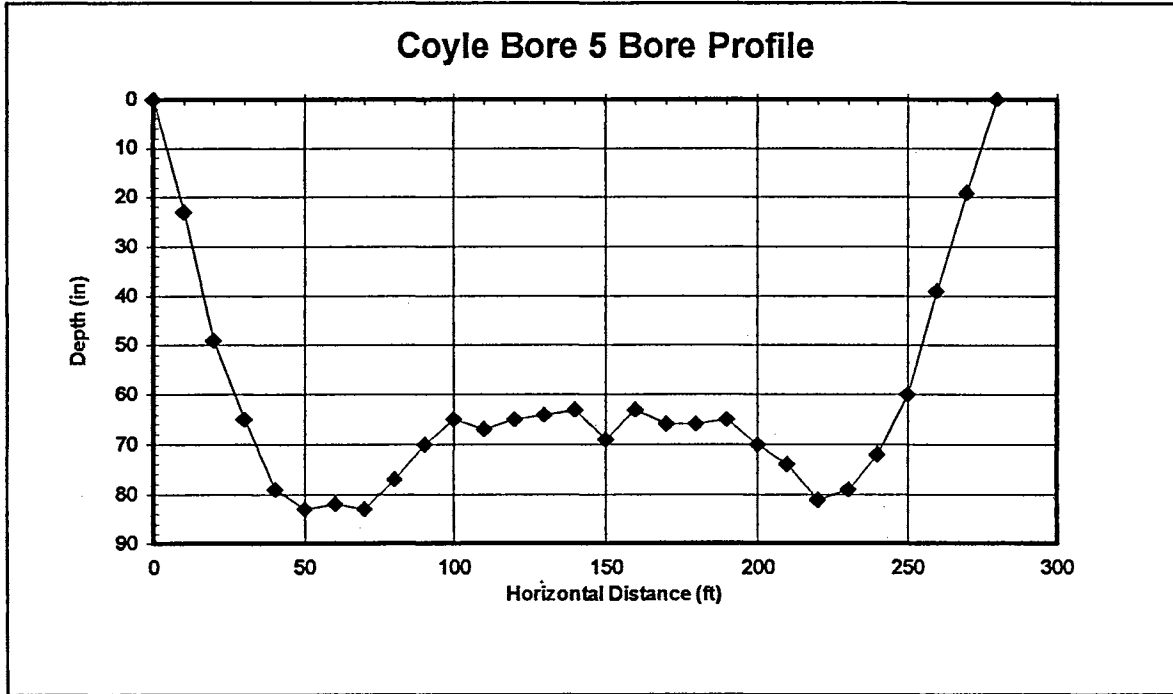
  va_start(argptr, fmt);
  cnt = vsprintf(str, fmt, argptr);
  cnt = 0;
  outtextxy( xloc, yloc, str);
  va_end(argptr);
  return(cnt);
}

```

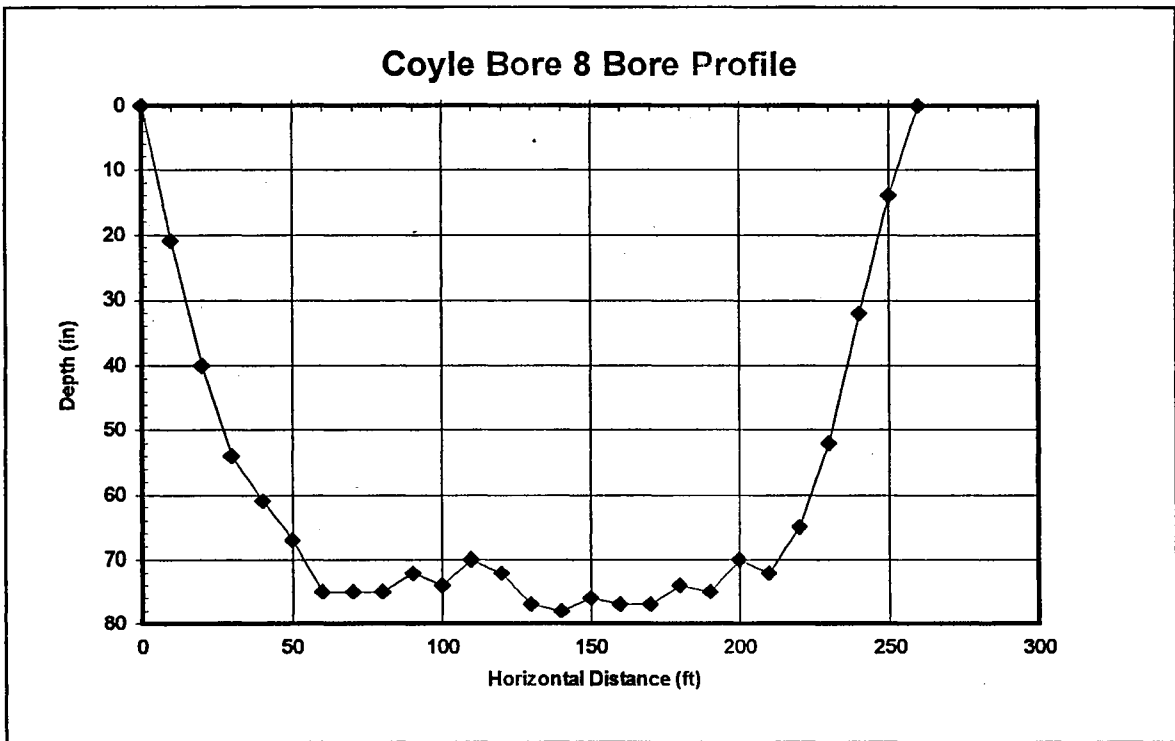
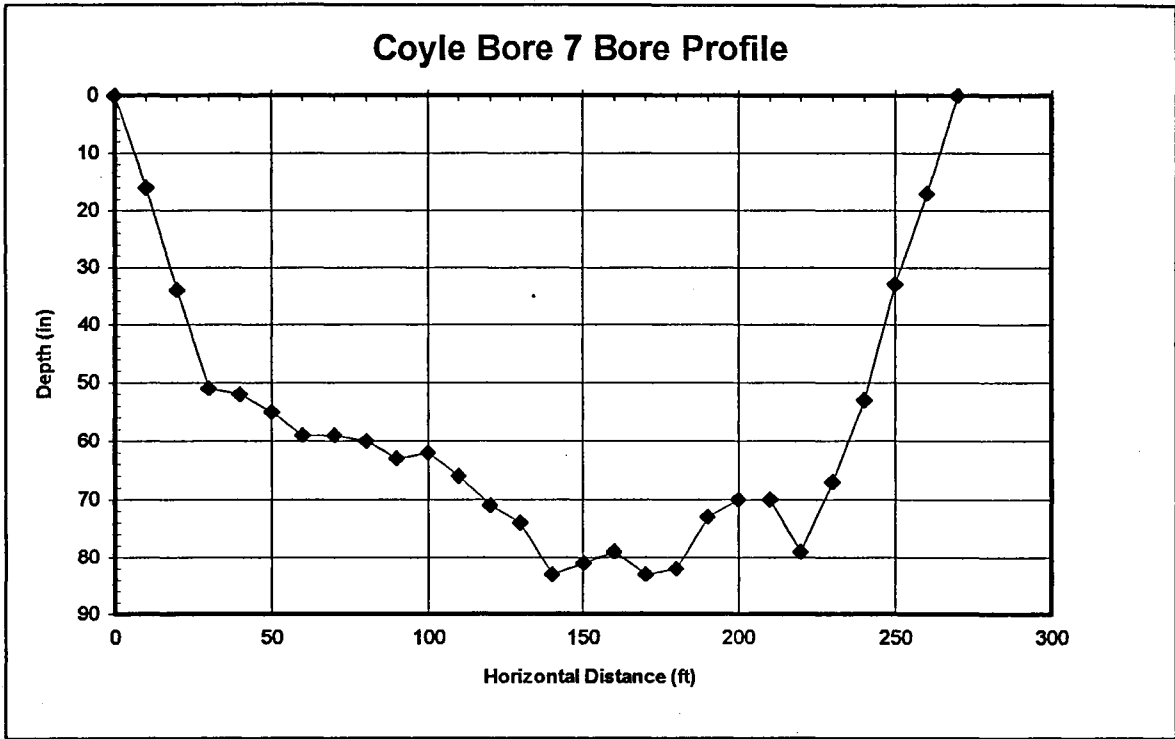


Section D

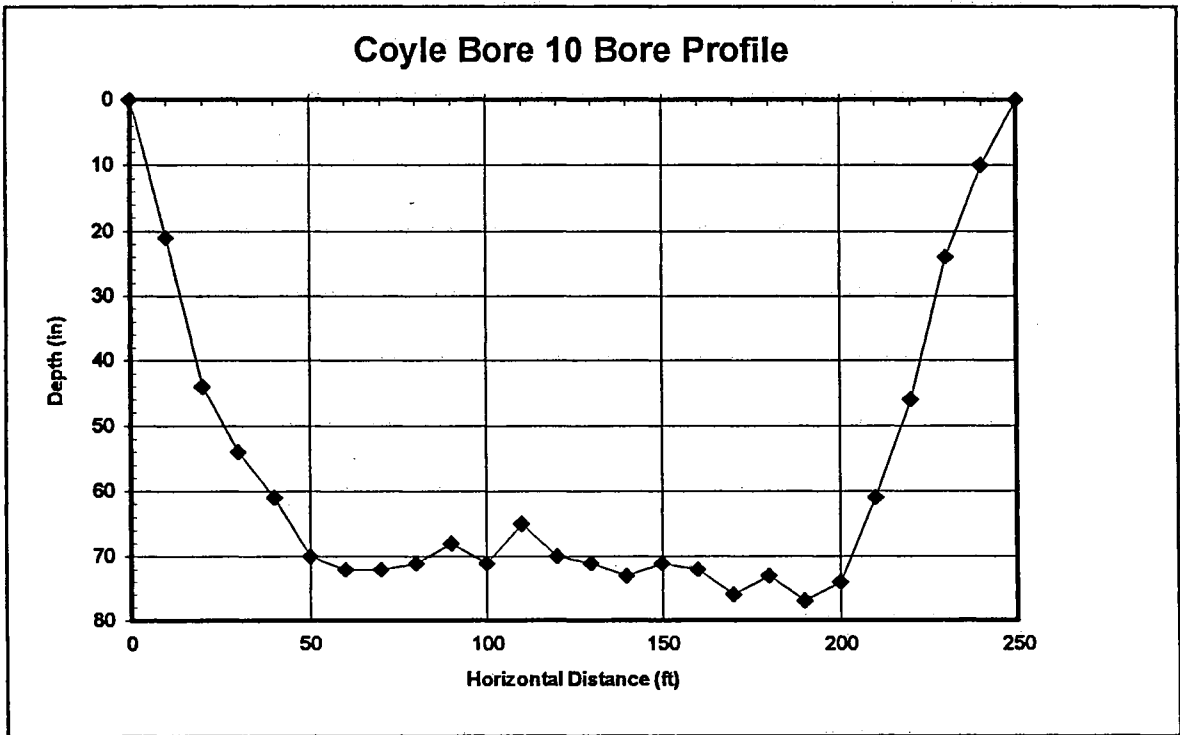
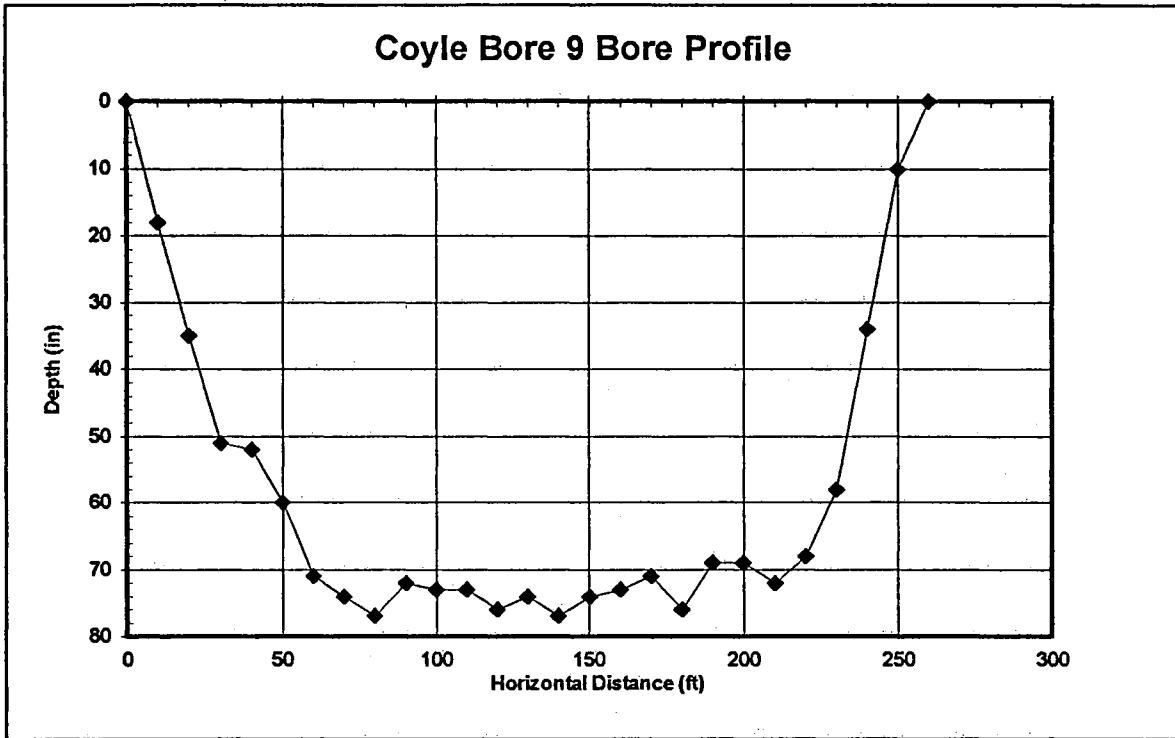
Bore Profiles



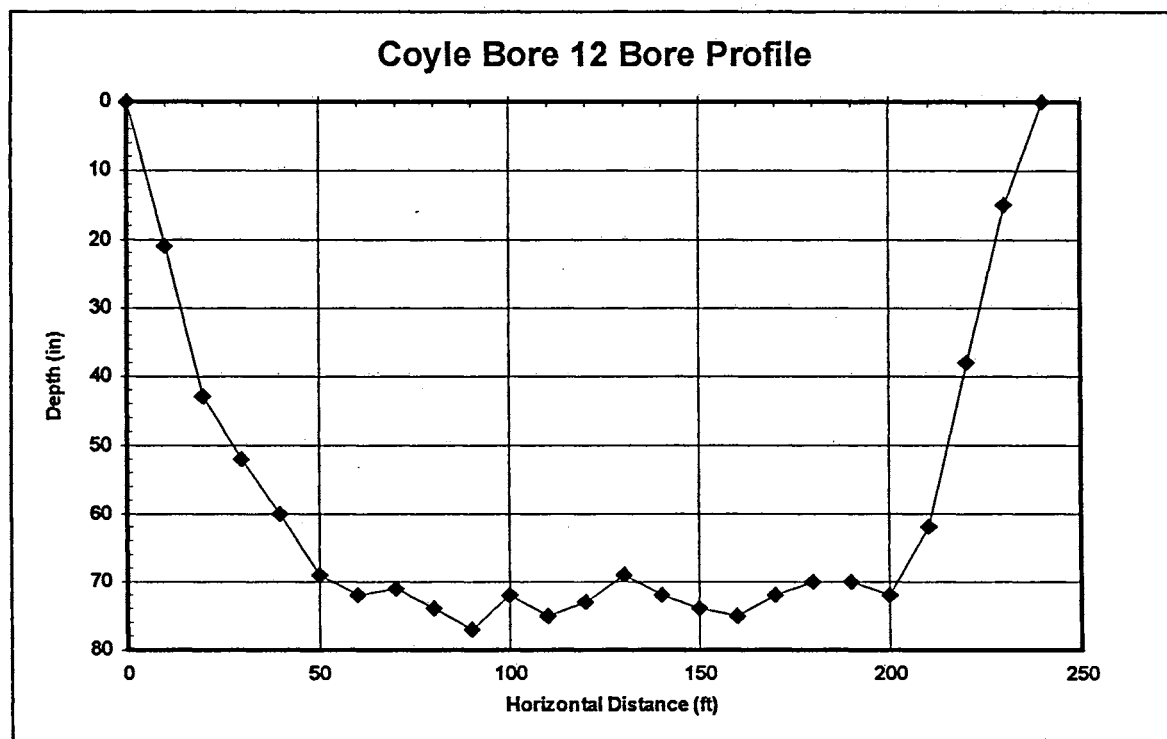
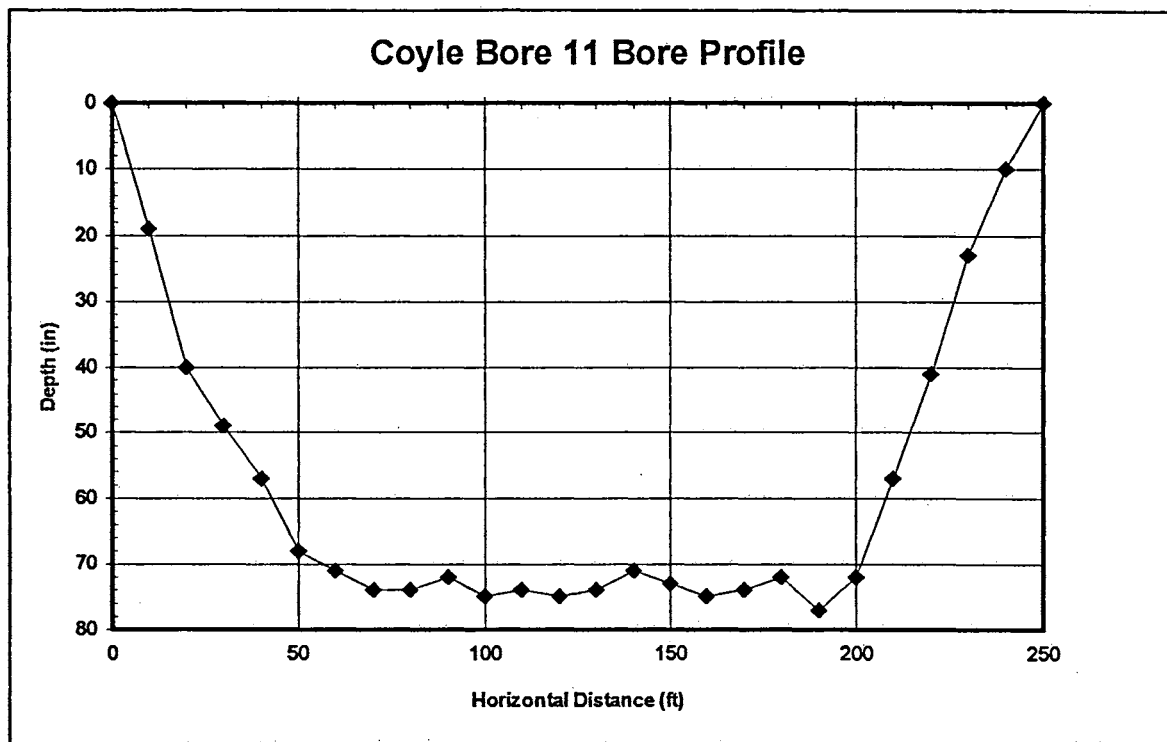
Section D: Bore Profiles



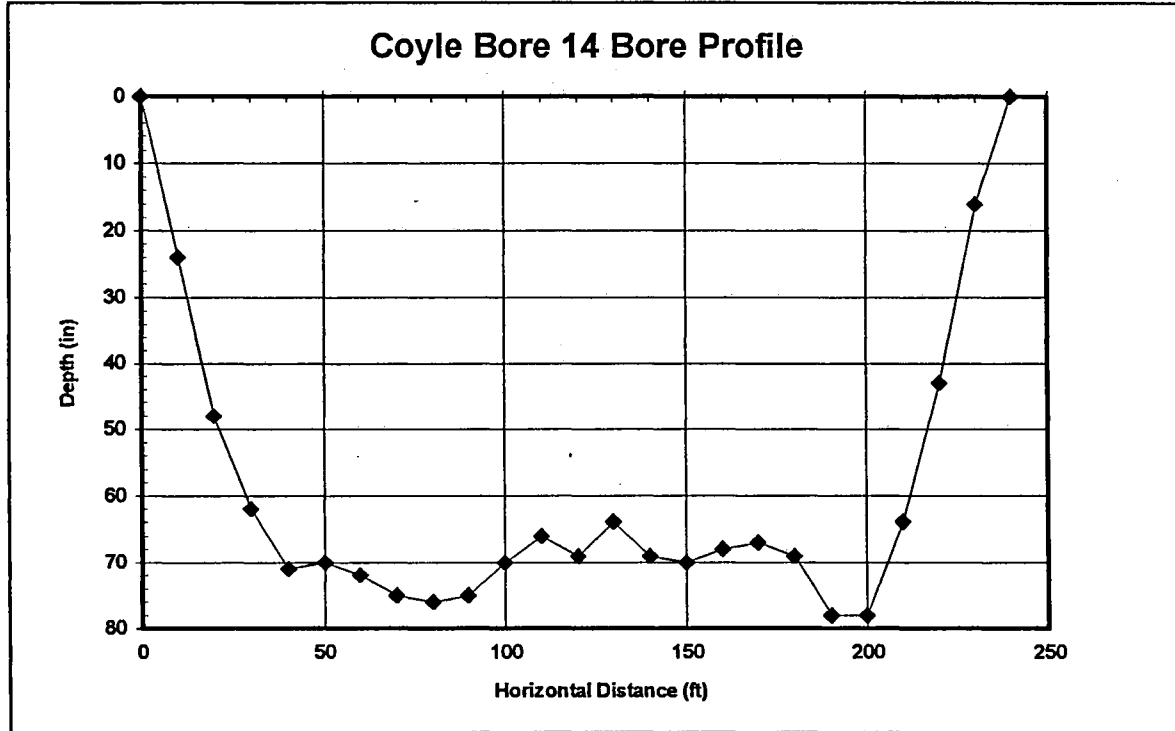
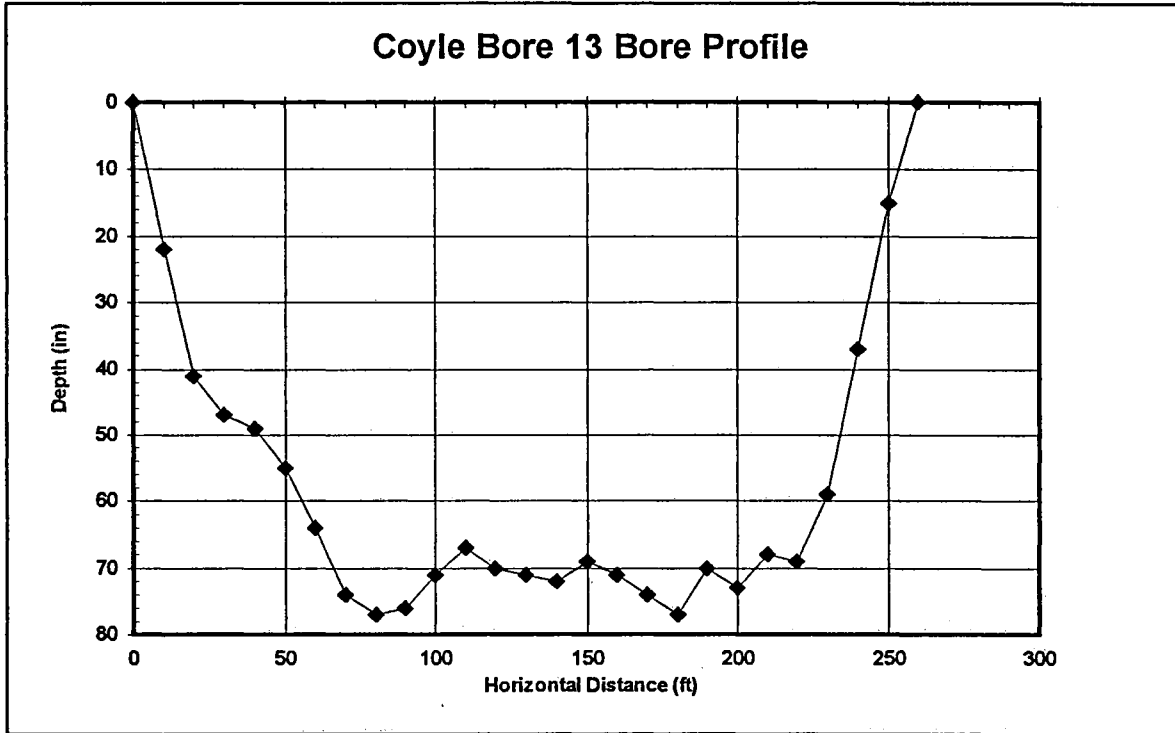
Section D: Bore Profiles



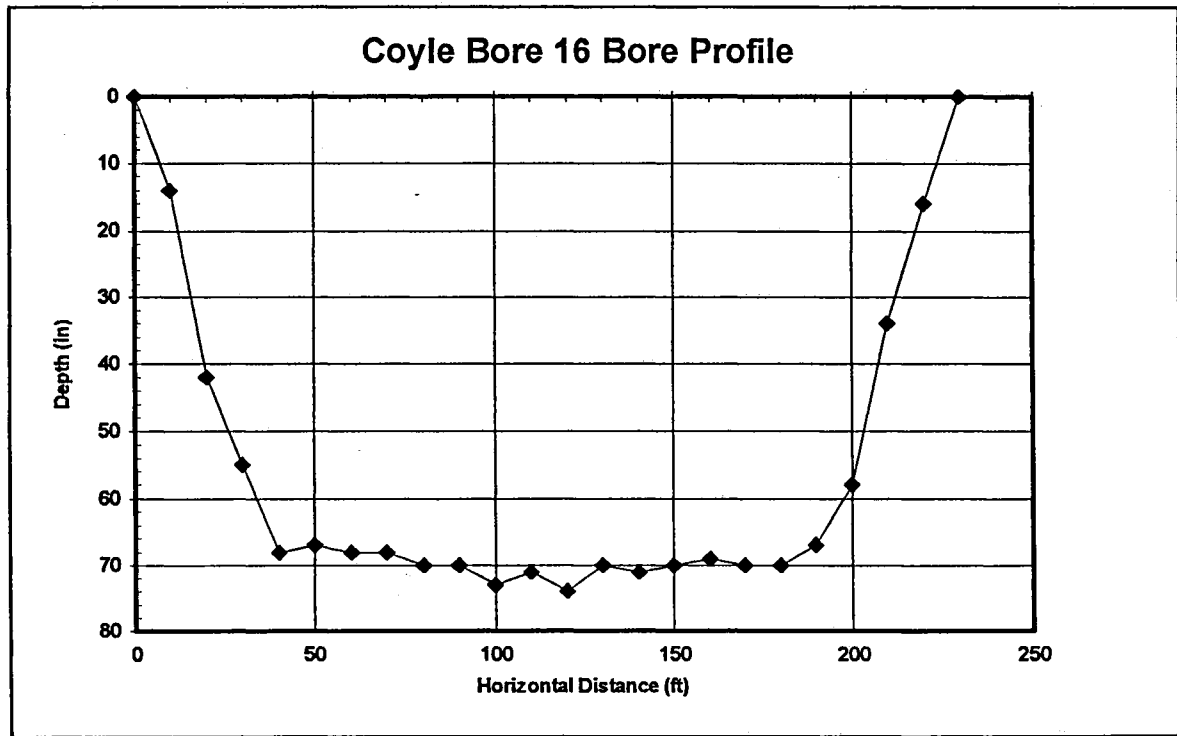
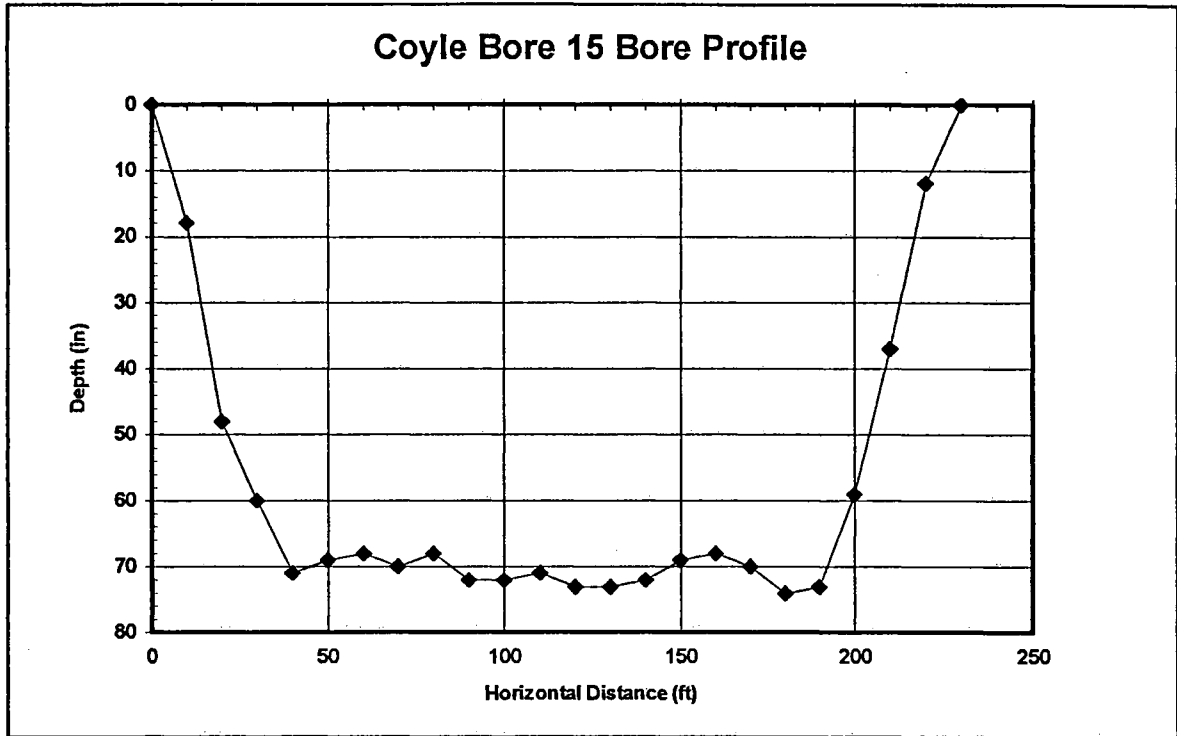
Section D: Bore Profiles



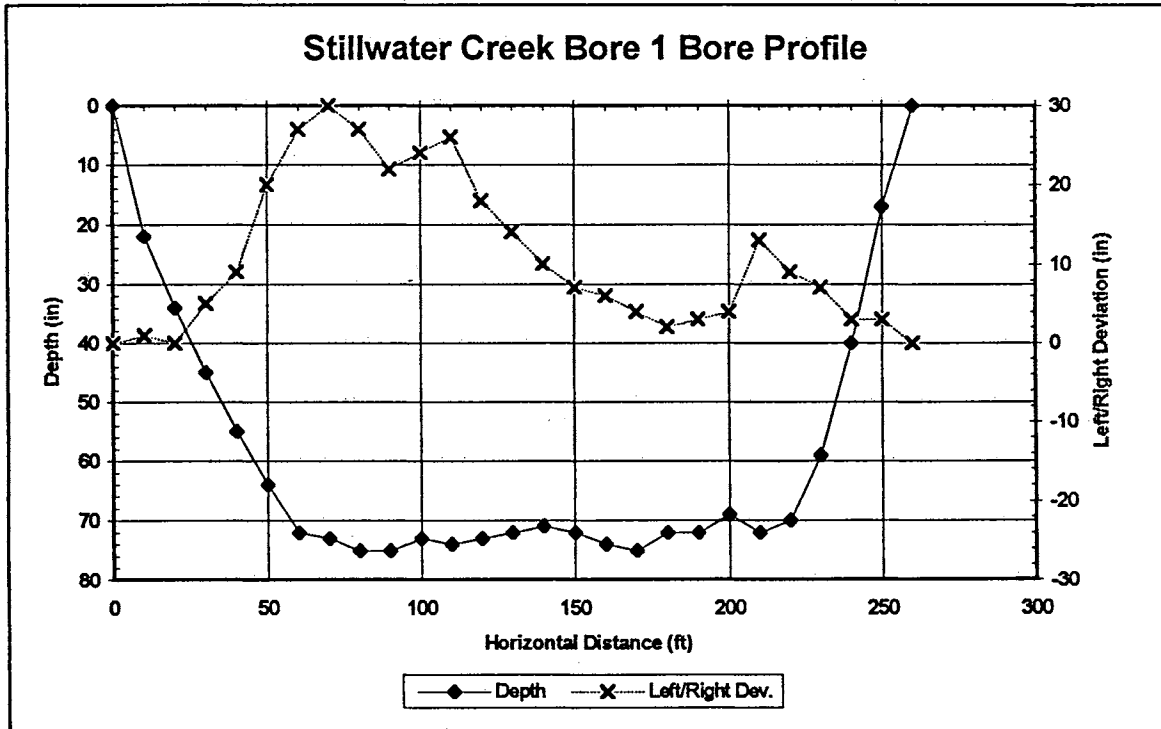
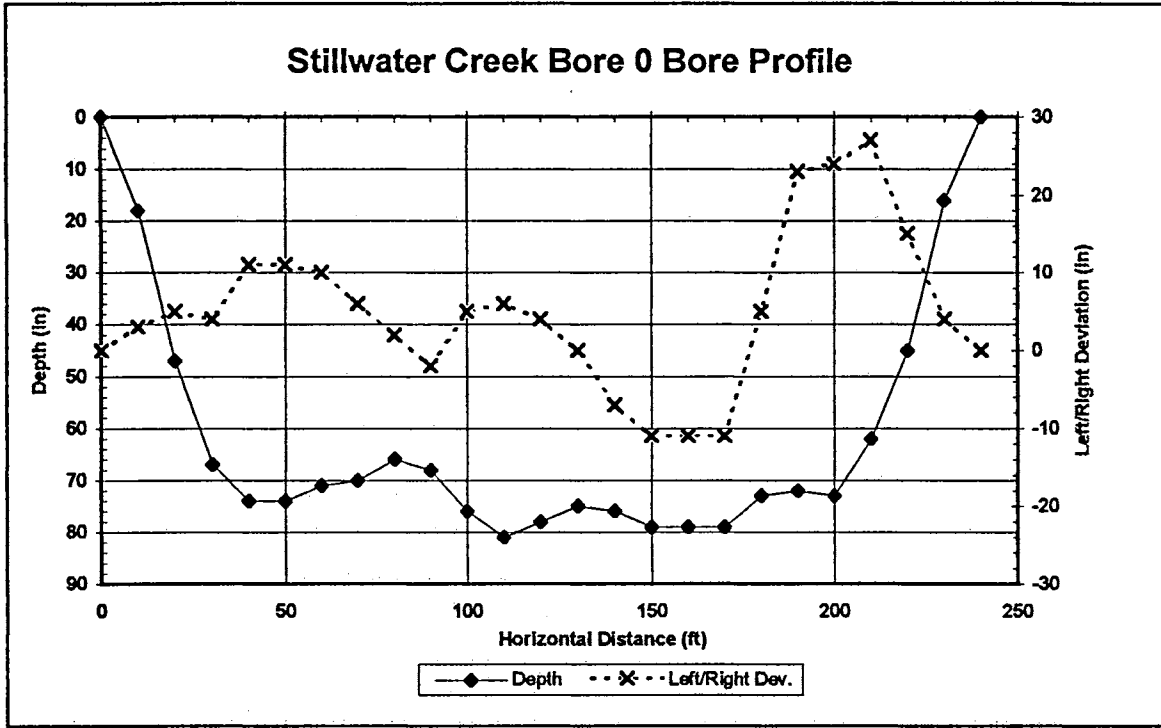
#### Section D: Bore Profiles



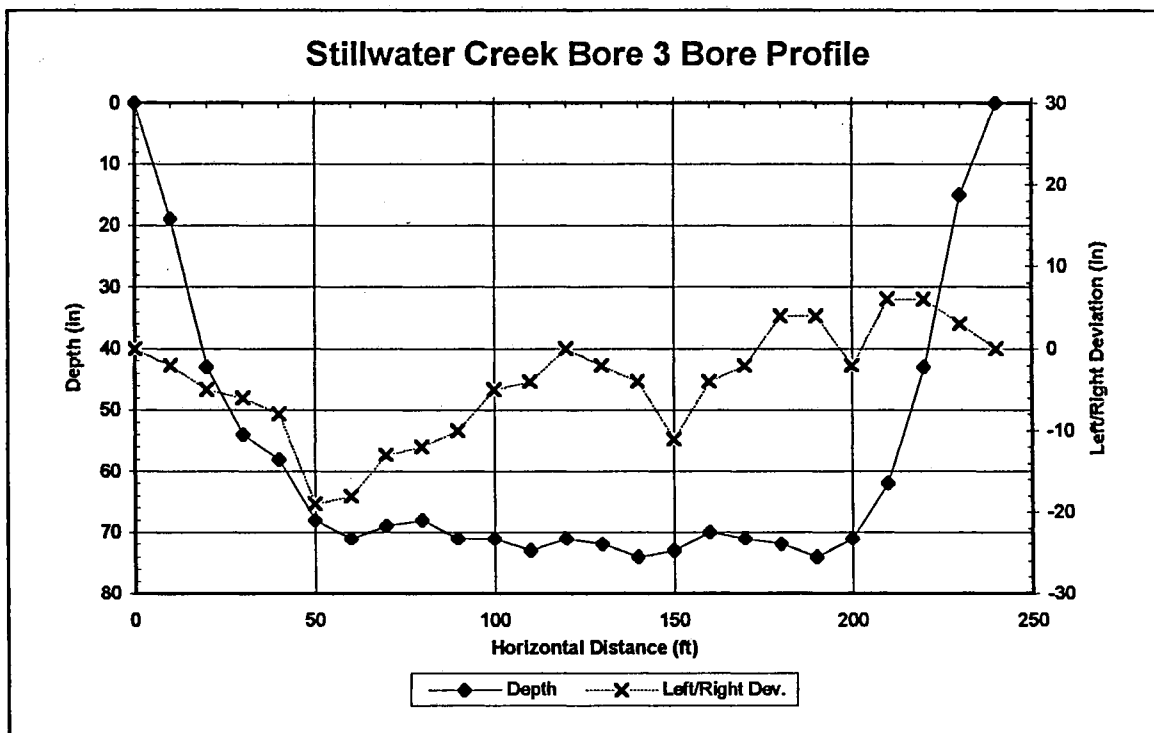
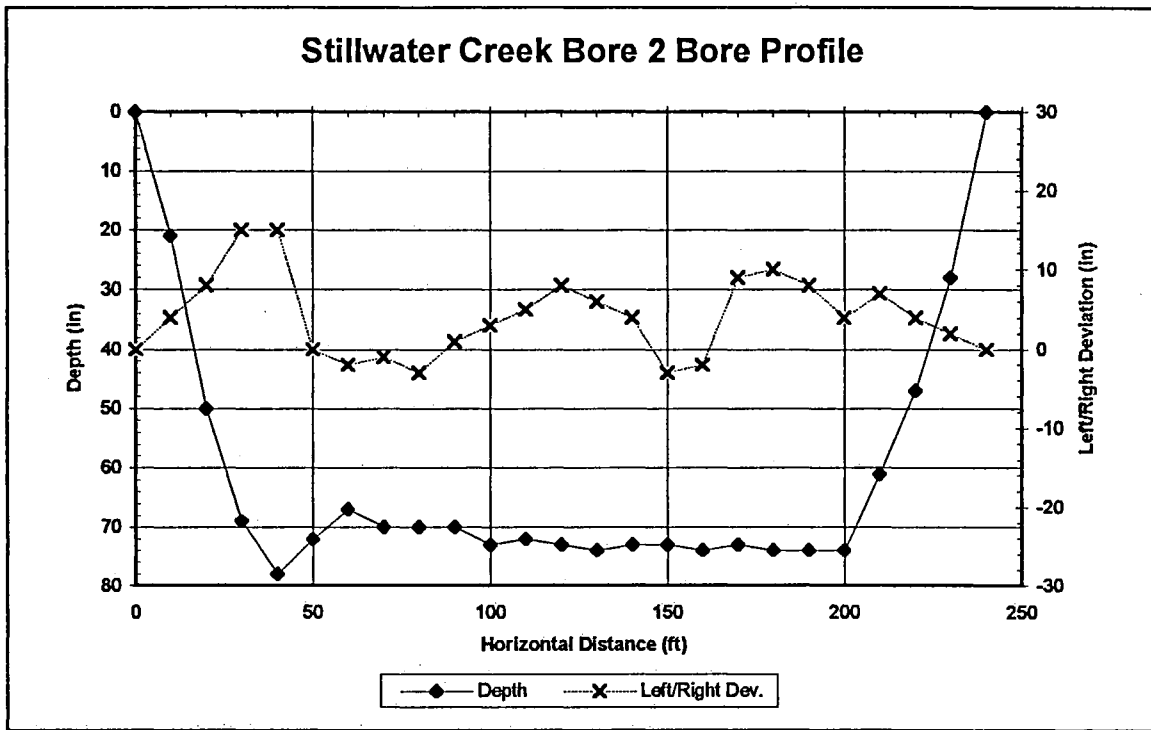
Section D: Bore Profiles



Section D: Bore Profiles

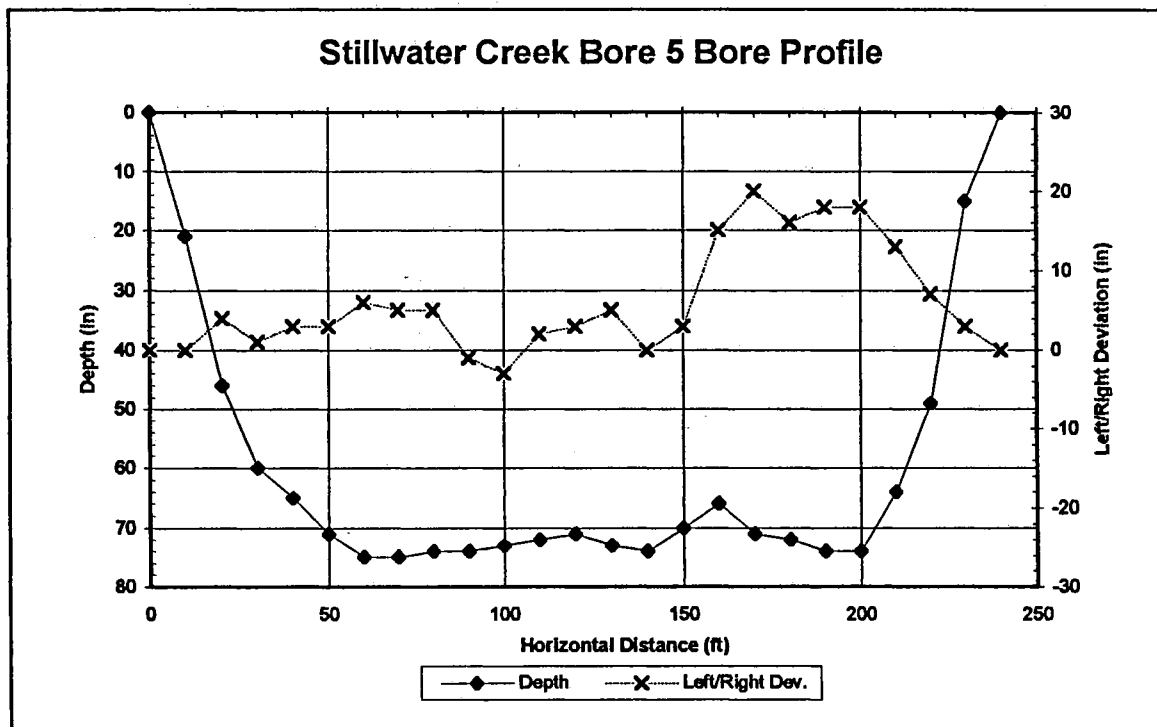
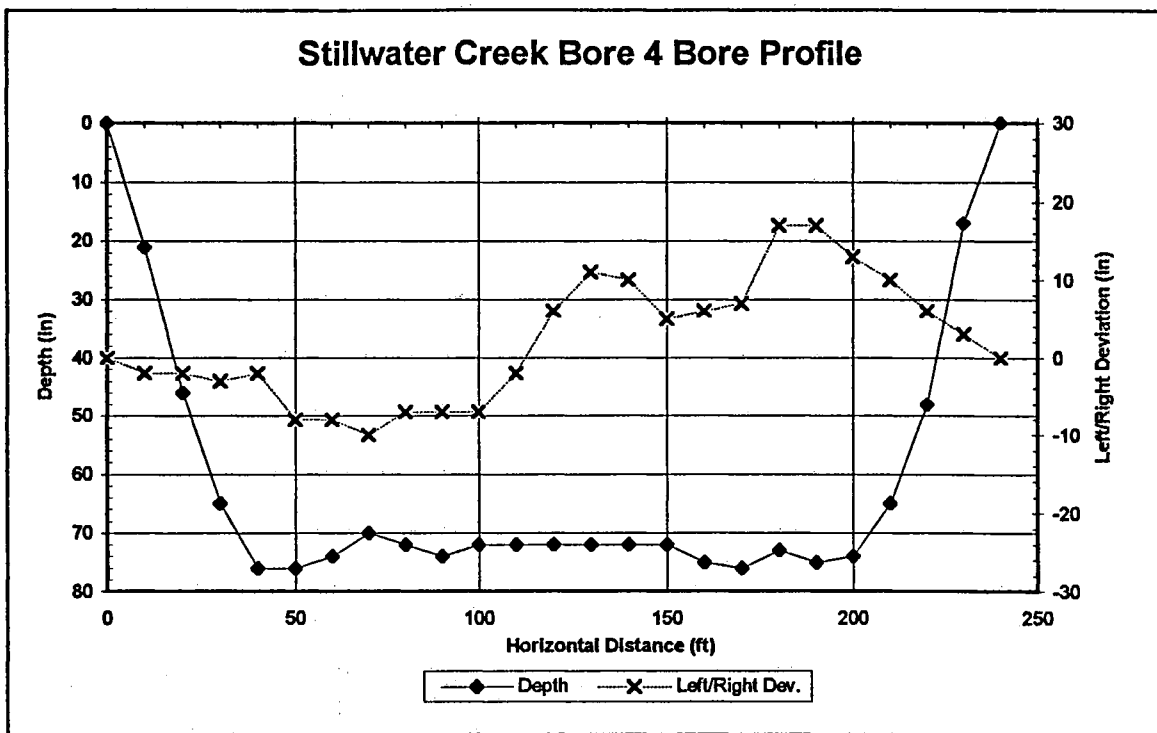


Section D: Bore Profiles

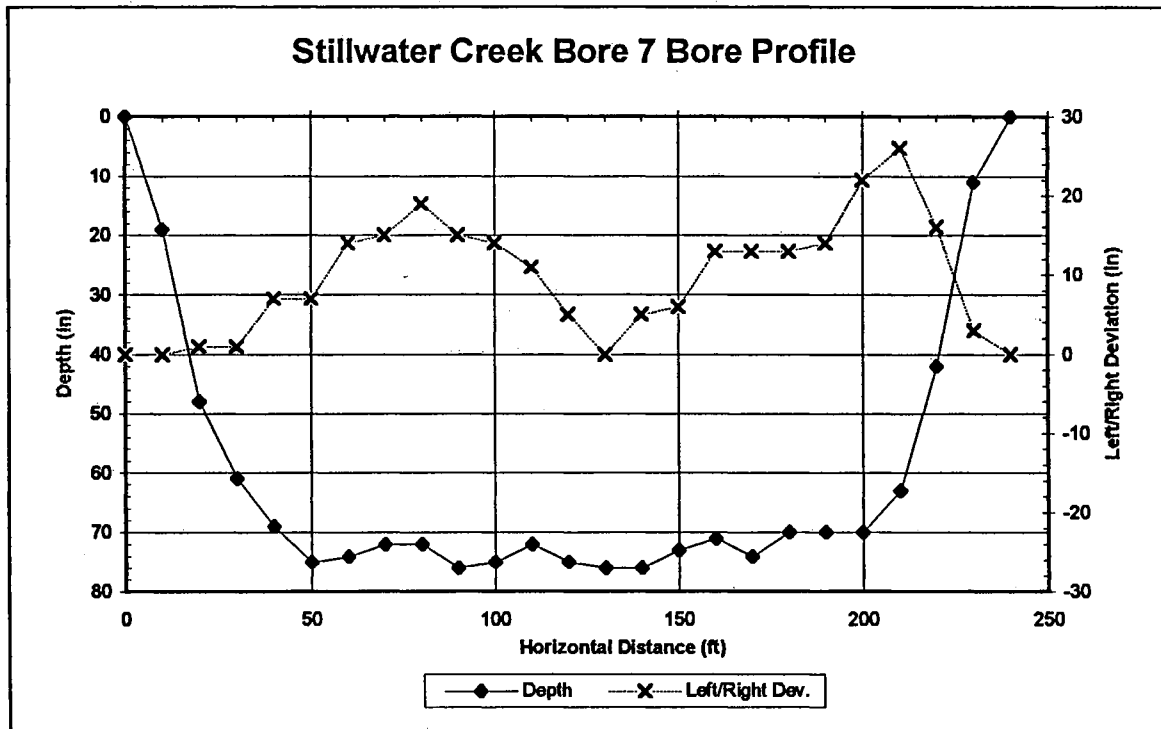
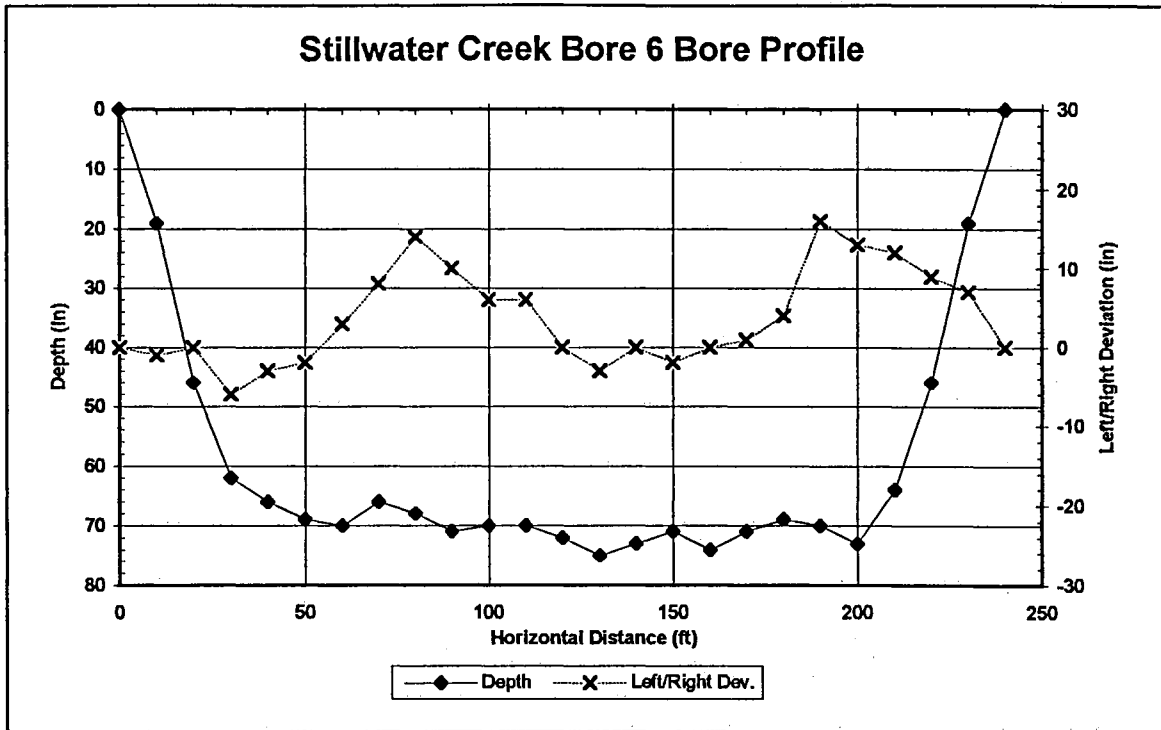


Section D: Bore Profiles





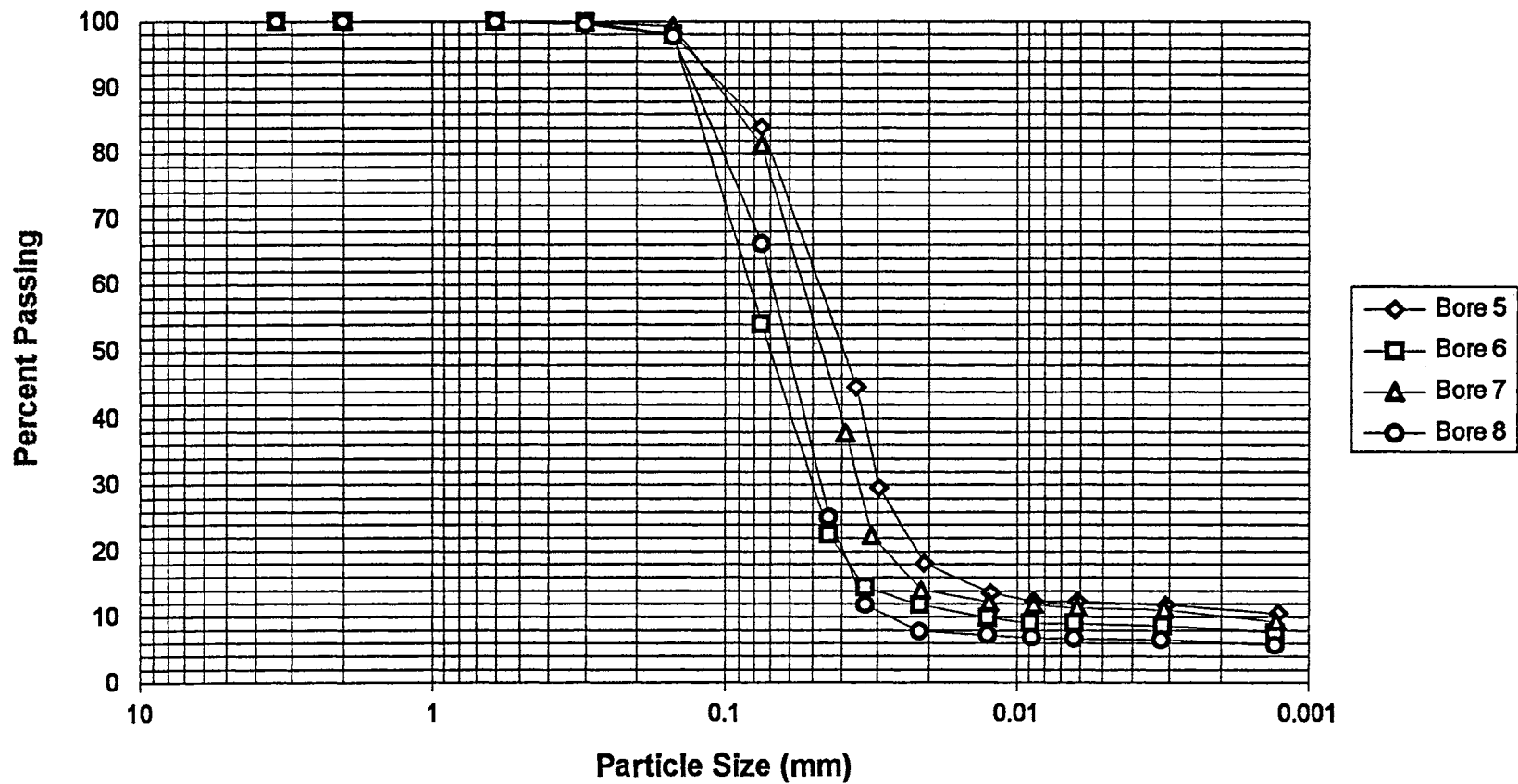
Section D: Bore Profiles



Section D: Bore Profiles

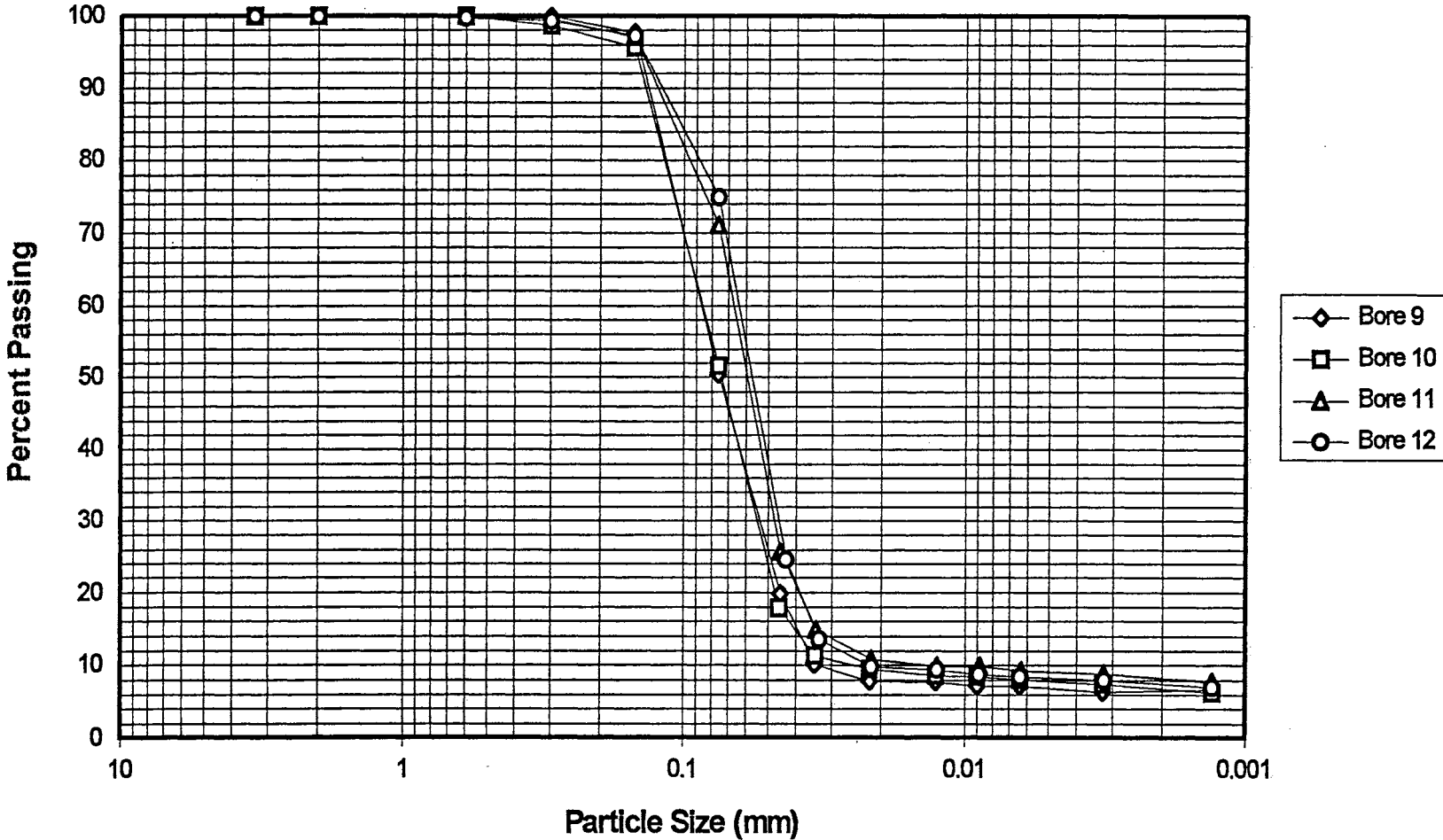
Section E: Soil Particle Size Analysis

**Coyle Particle Size Analysis**



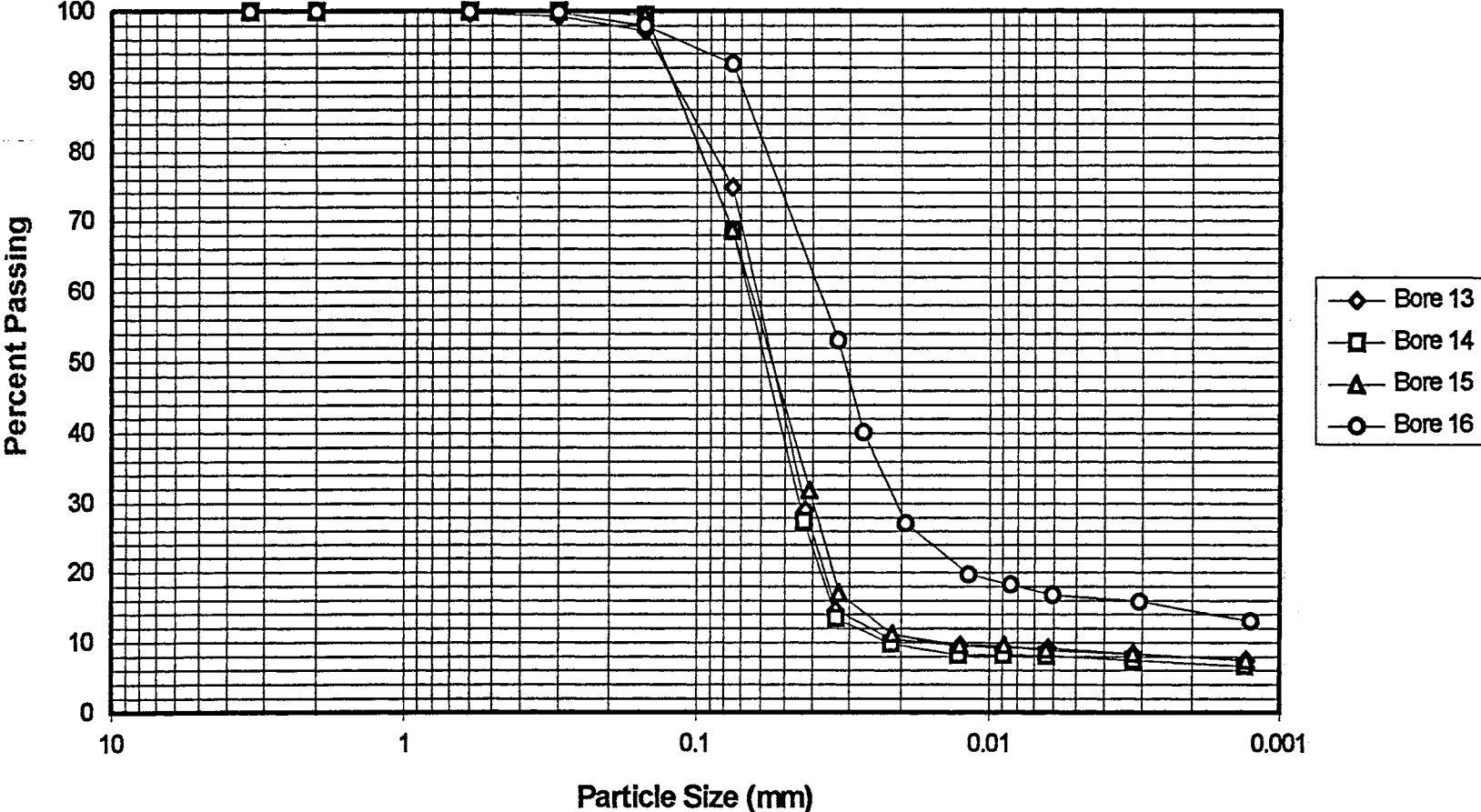
Section E: Soil Particle Size Analyses

# Coyle Particle Size Analysis



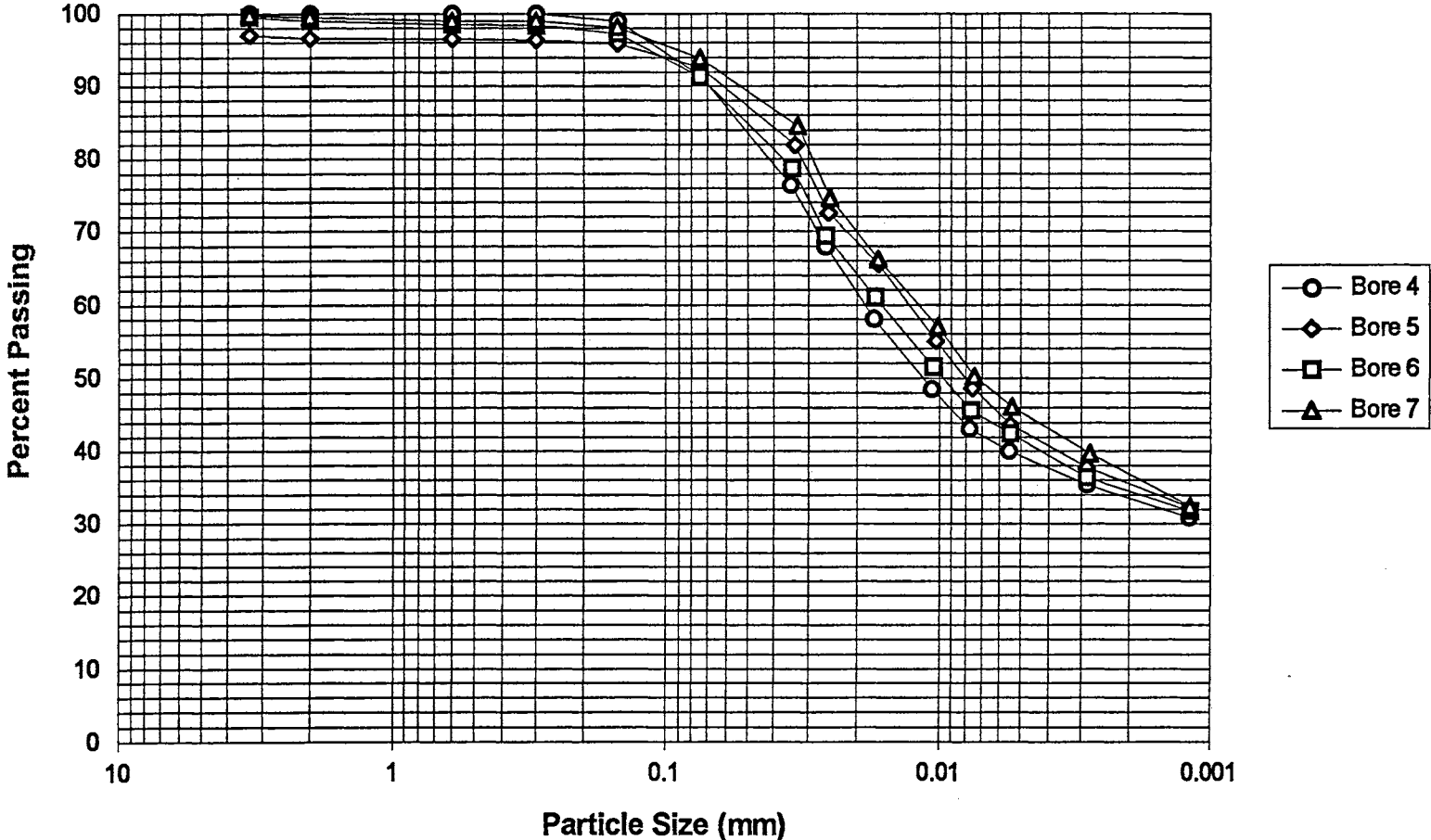
Section E: Soil Particle Size Analyses

# Coyle Particle Size Analysis



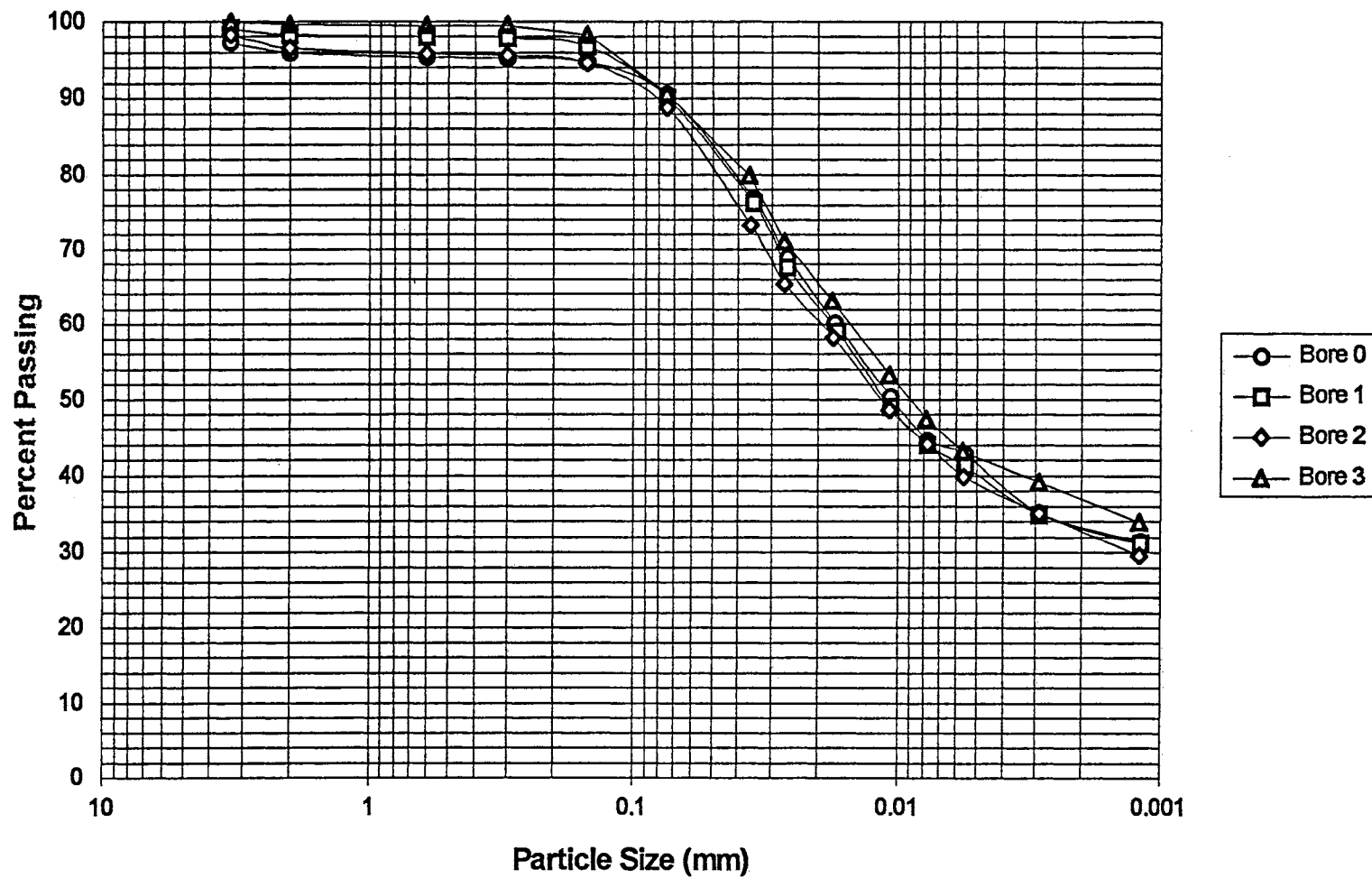
Section E: Soil Particle Size Analyses

# Stillwater Creek Particle Size Analysis



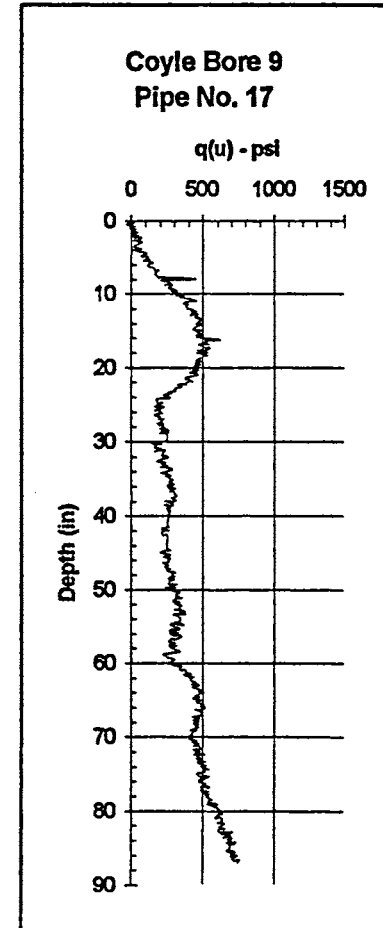
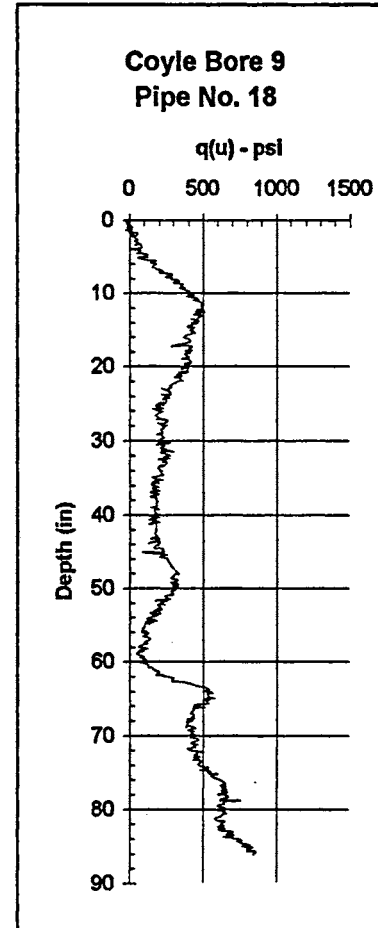
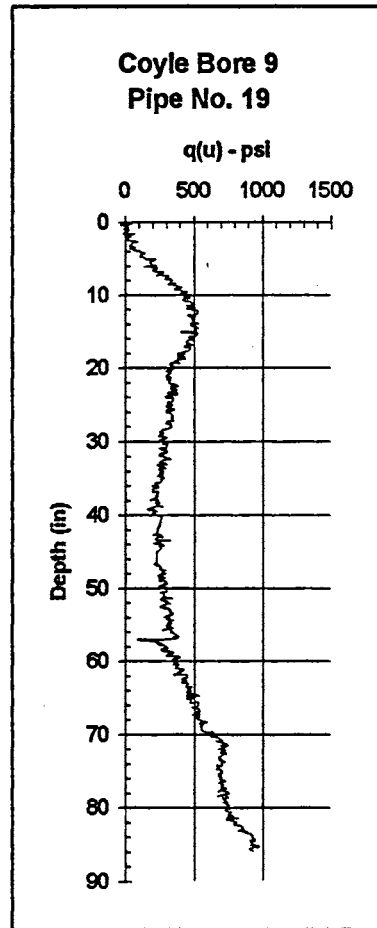
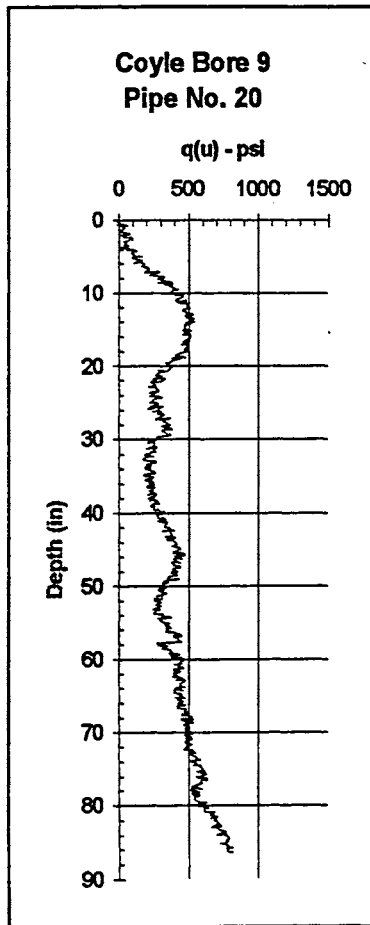
Section E: Soil Particle Size Analyses

# Stillwater Creek Particle Size Analysis



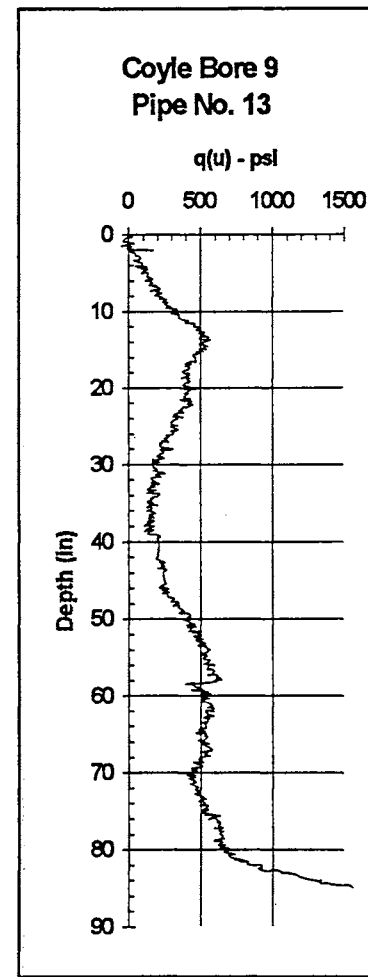
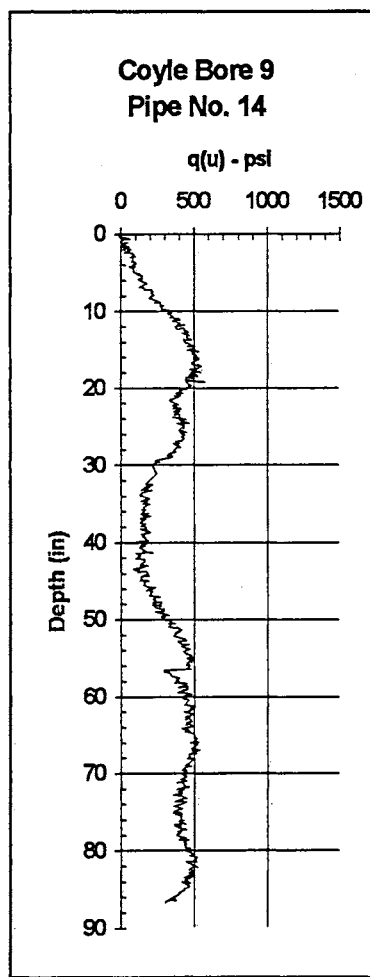
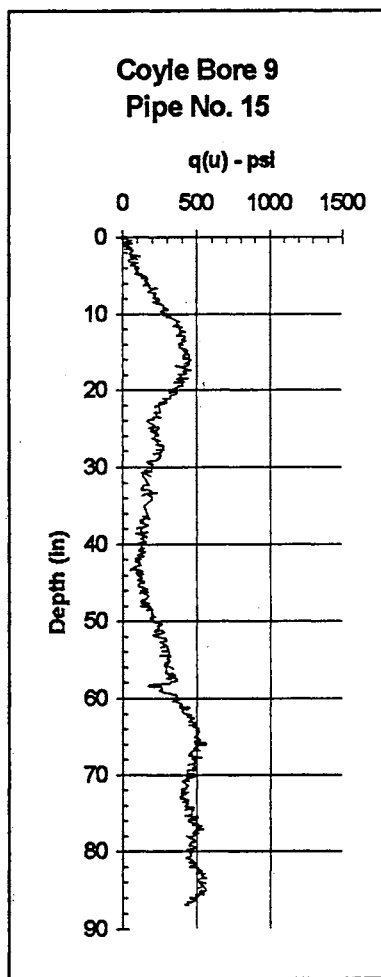
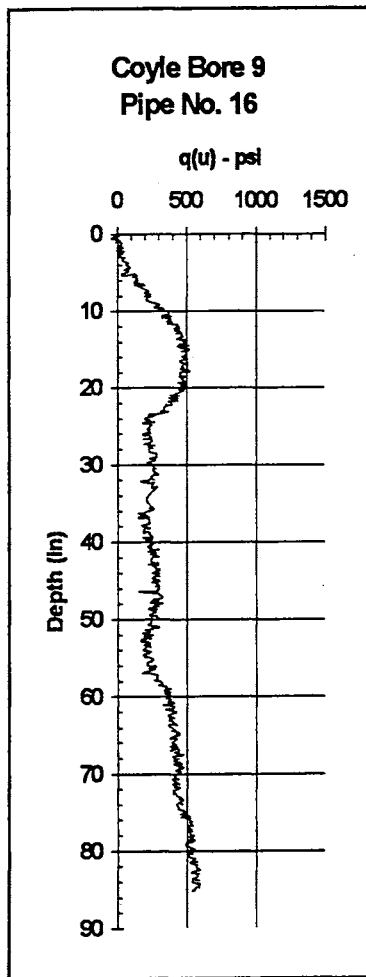
Section E: Soil Particle Size Analyses

## Section F: Penetrometer Readings

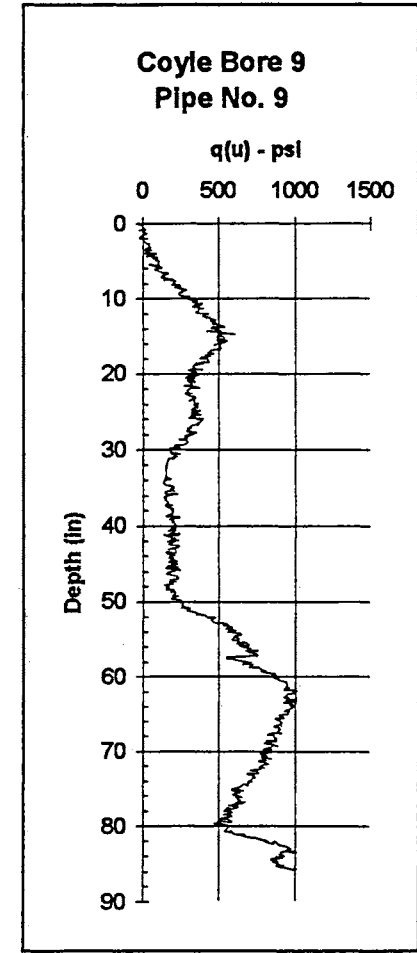
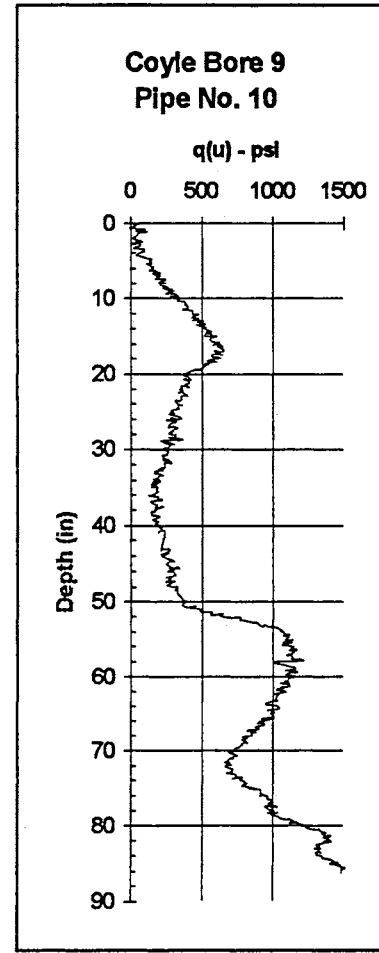
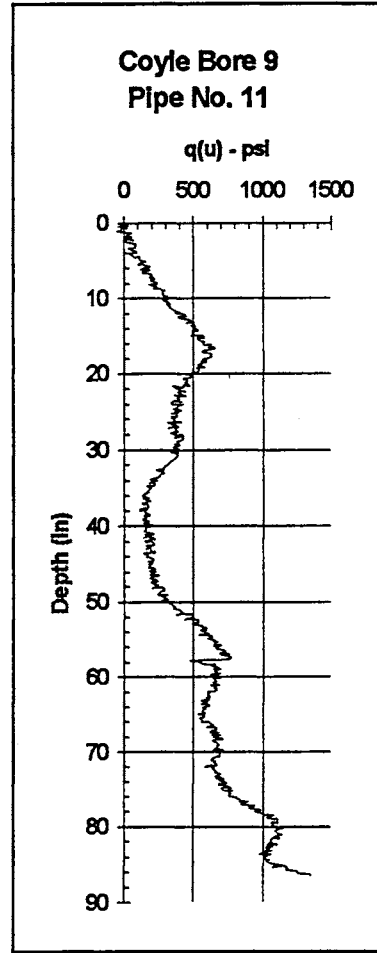
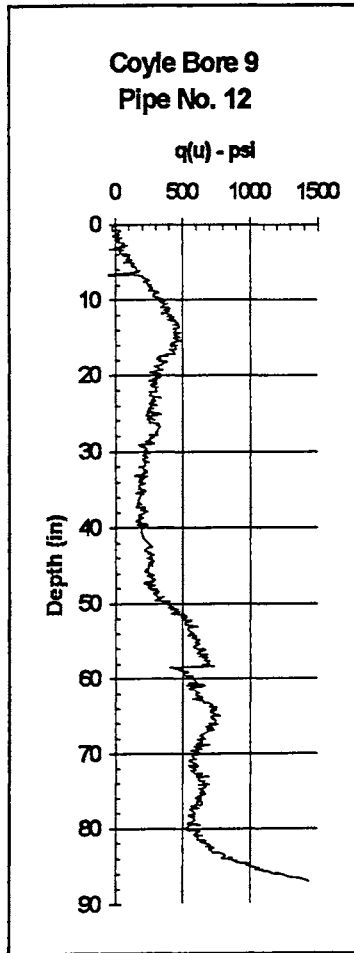


## Section F: Penetrometer Readings

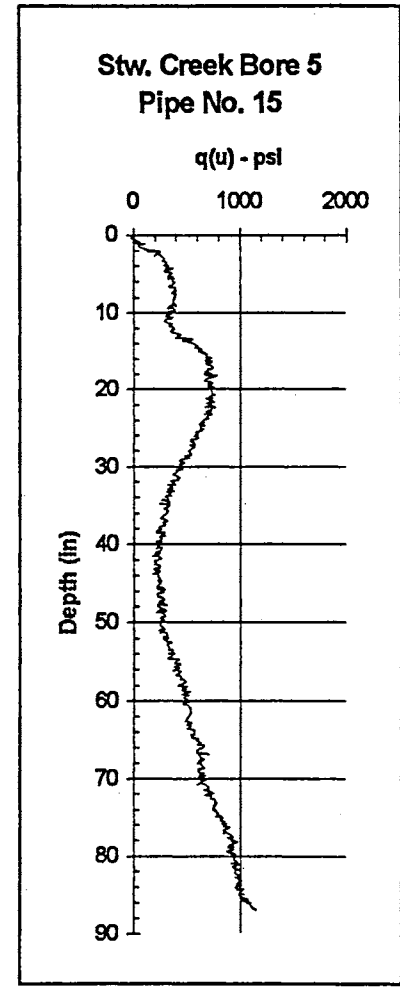
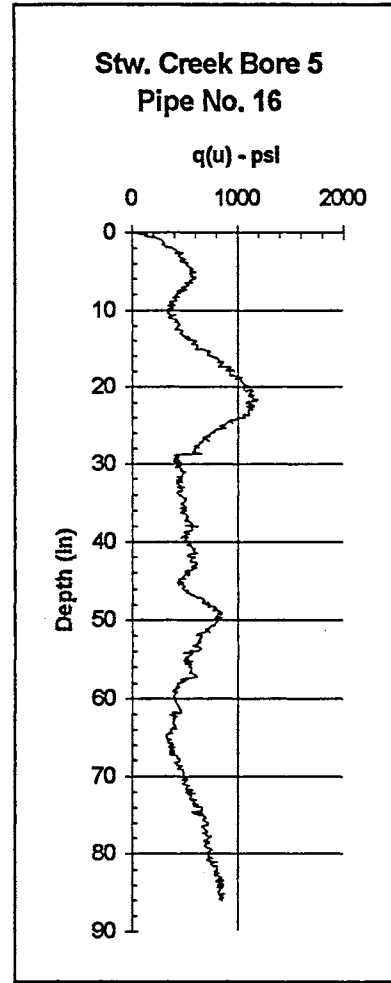
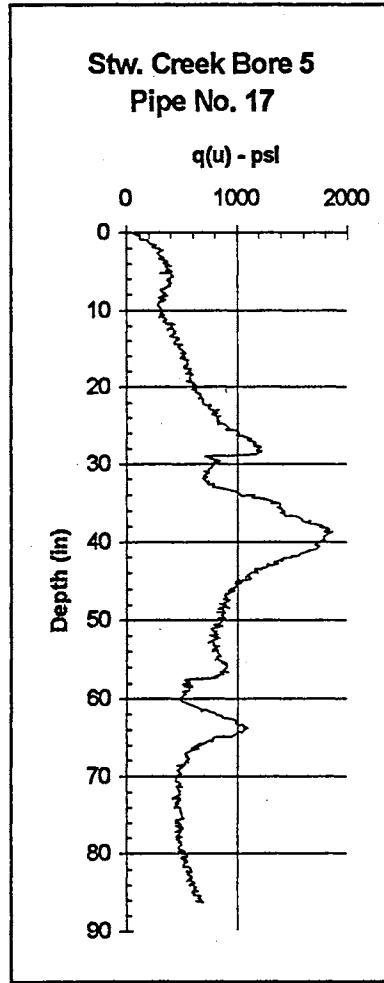
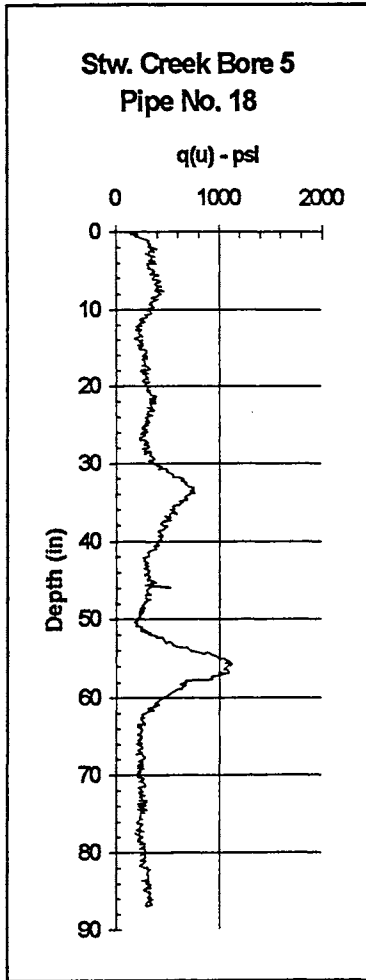




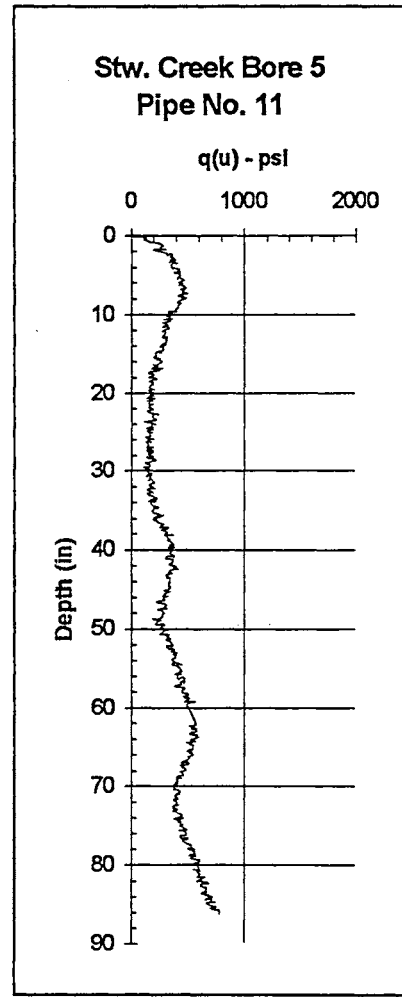
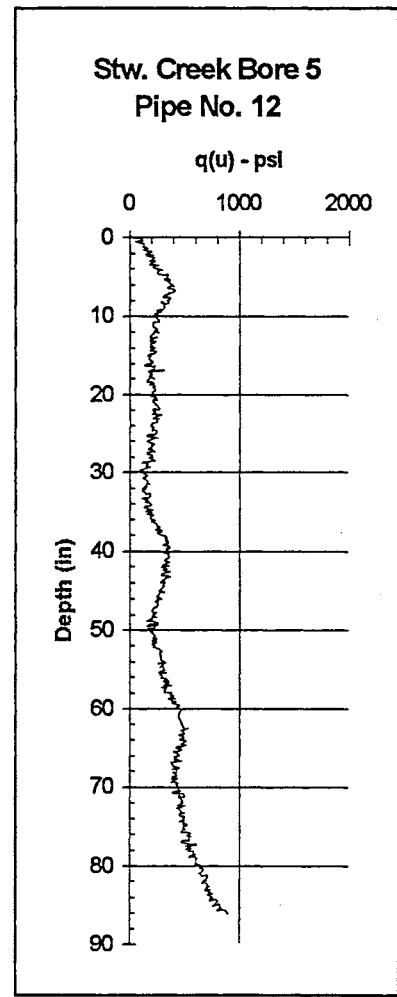
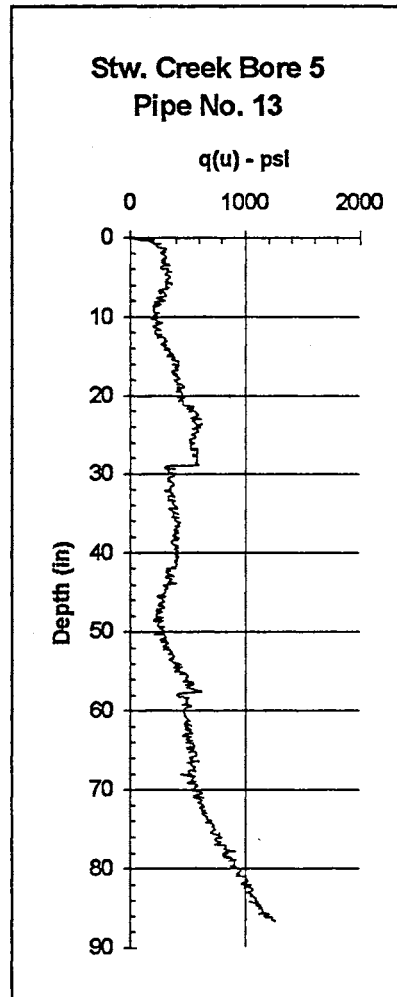
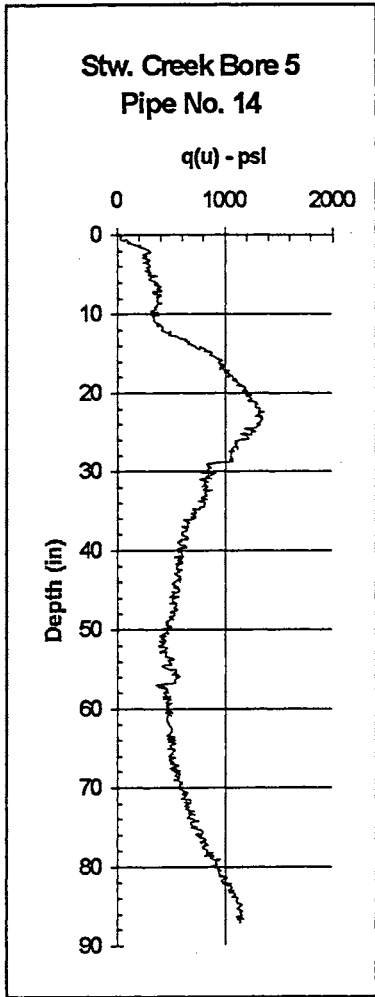
Section F: Penetrometer Readings



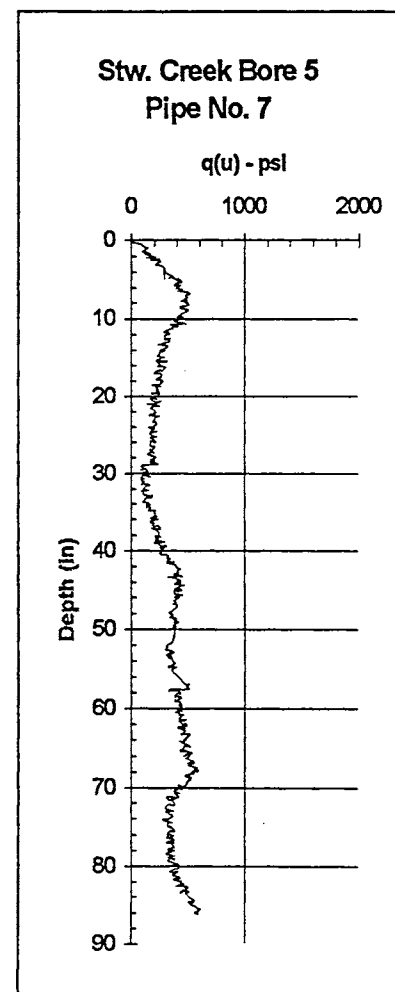
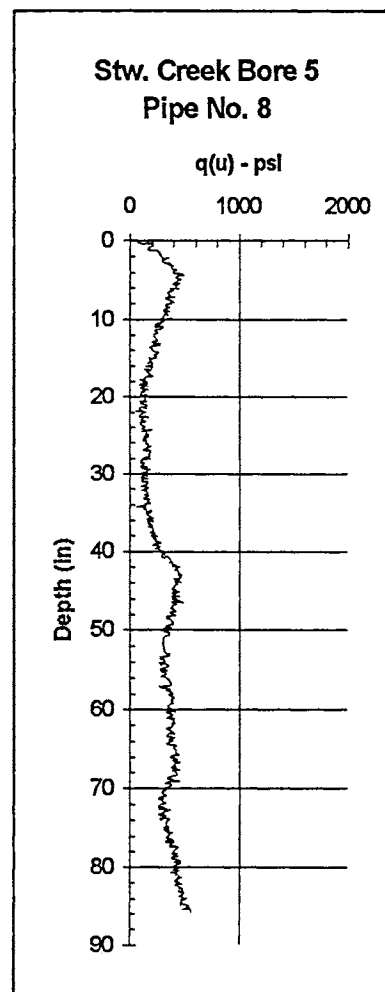
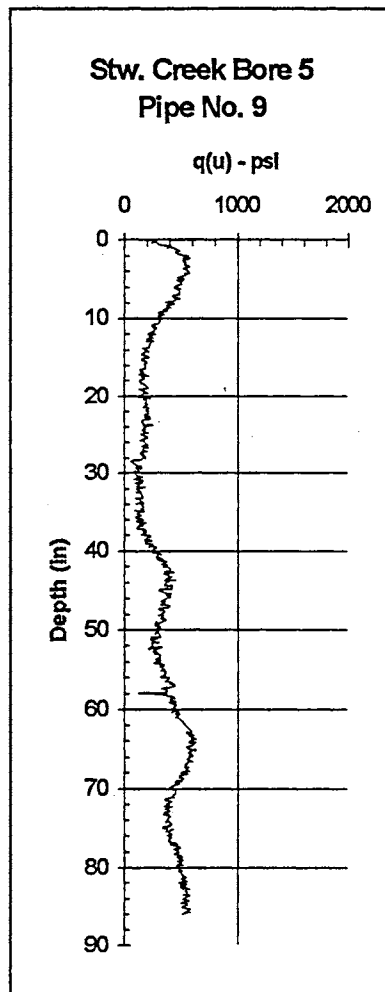
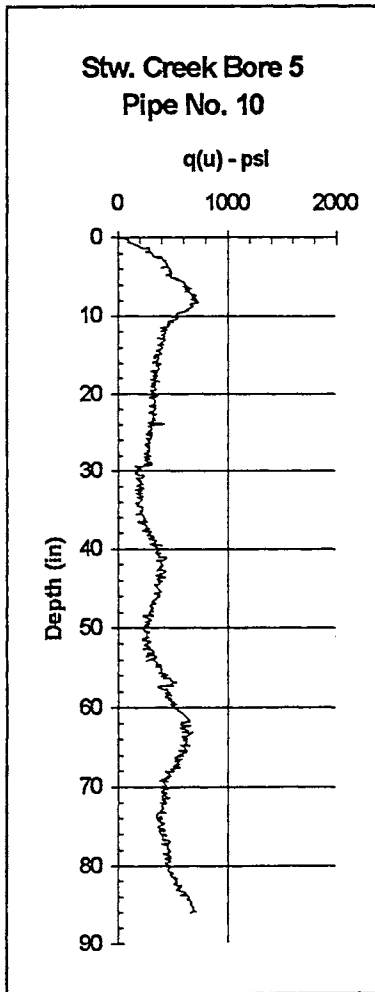
Section F: Penetrometer Readings



Section F: Penetrometer Readings



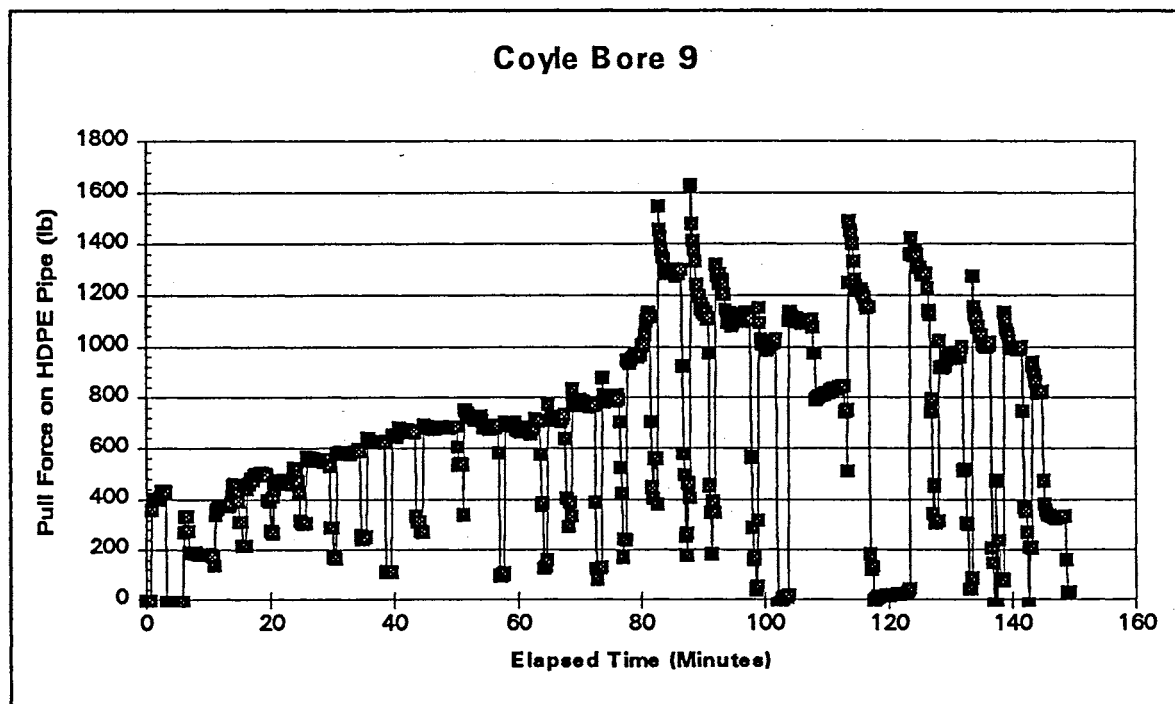
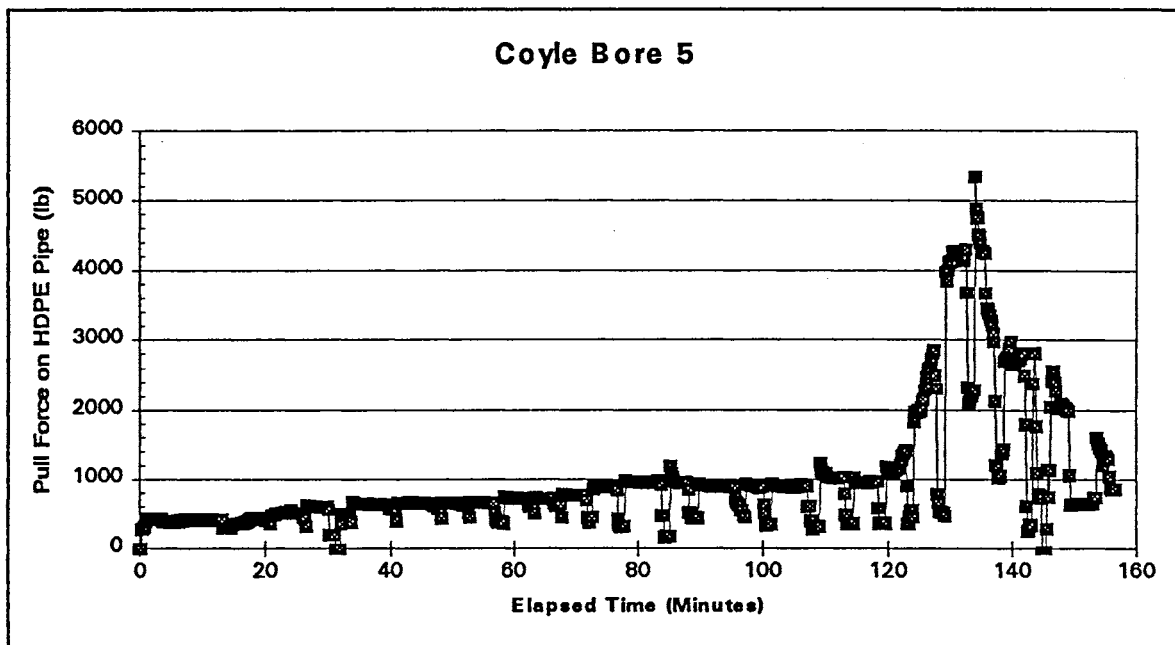
Section F: Penetrometer Readings



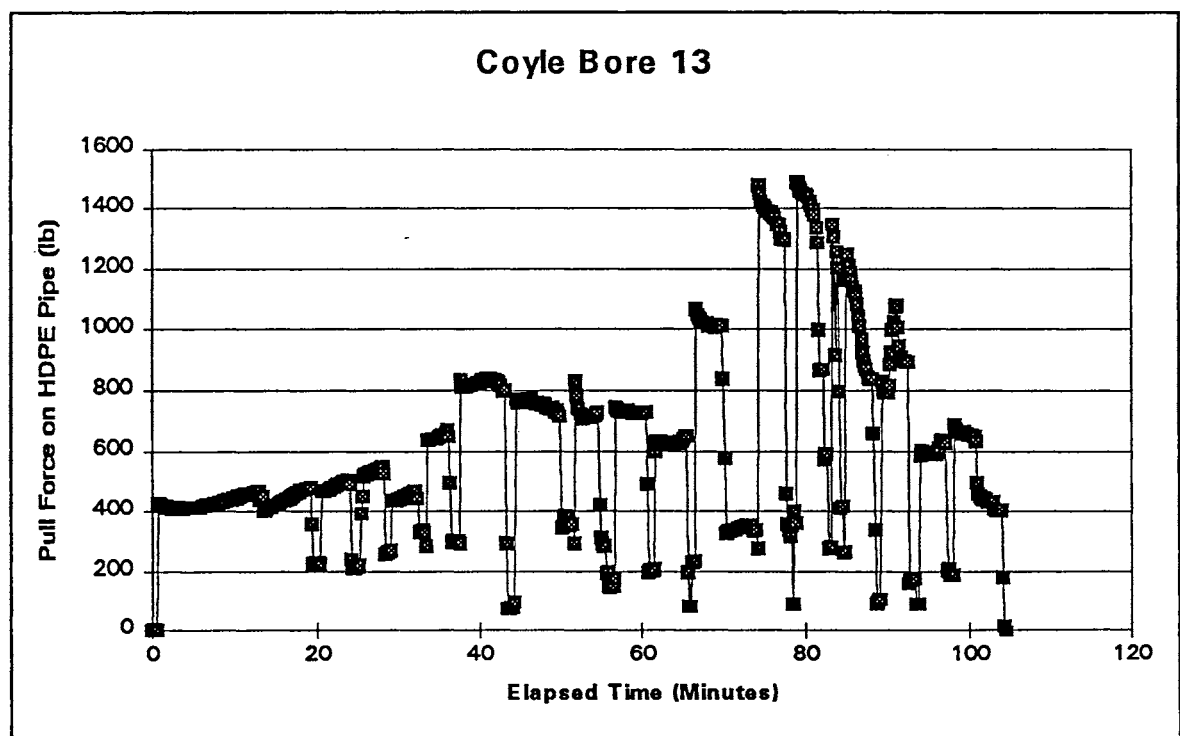
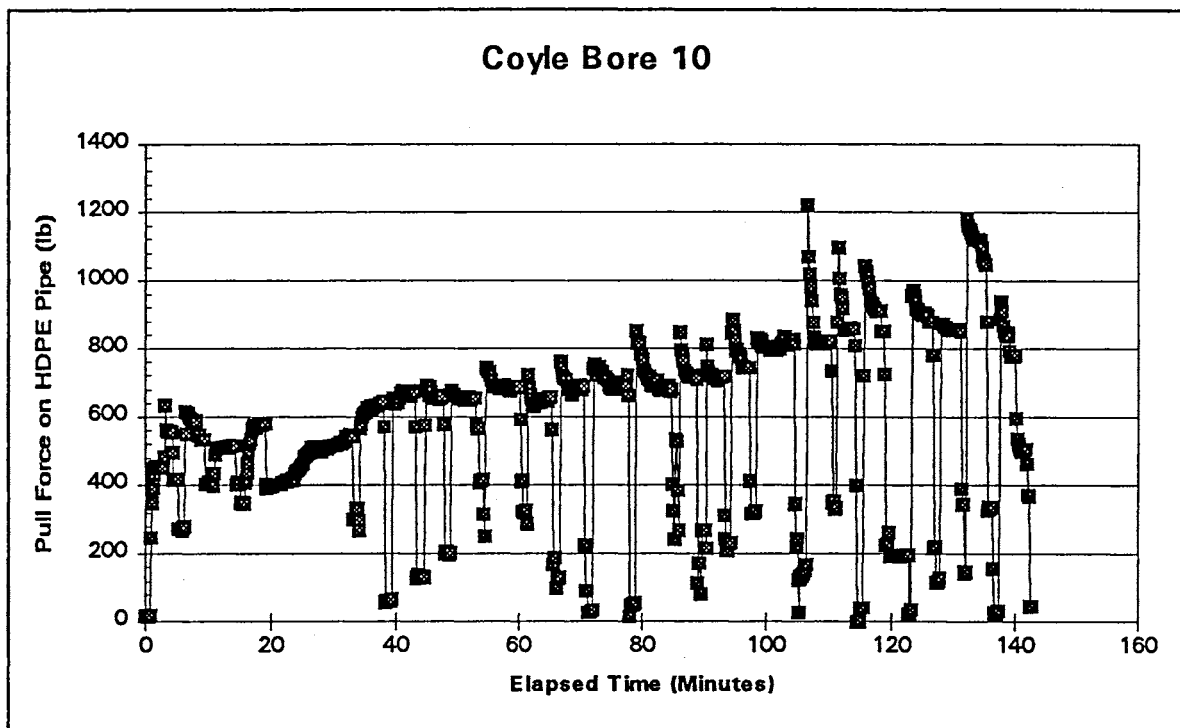
Section F: Penetrometer Readings

## Section G

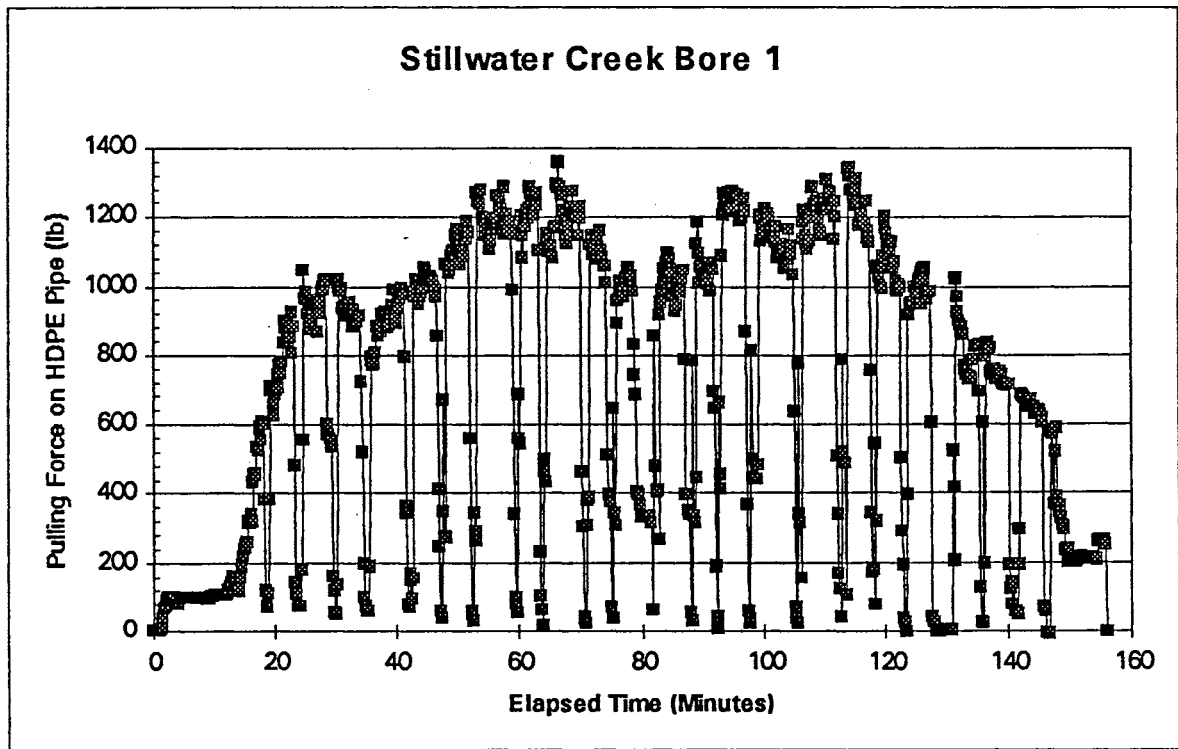
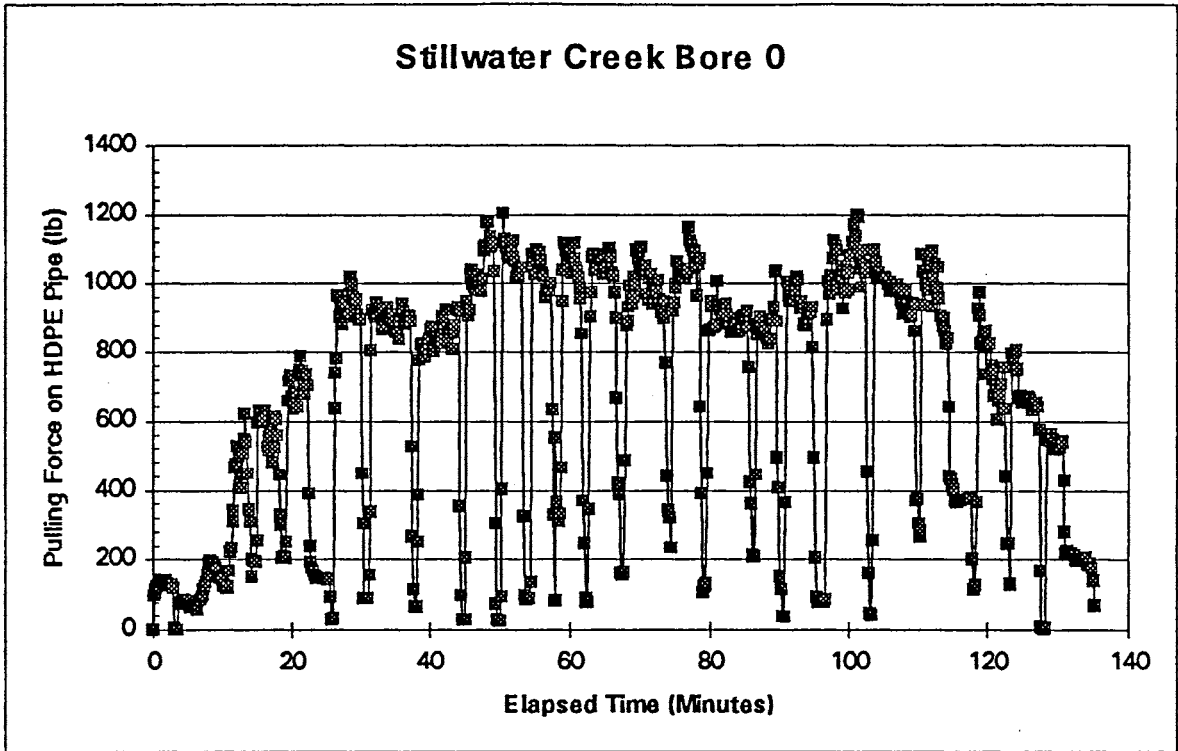
### Pull Force Readings on HDPE Pipe



### Section G: Pull Force Readings on HDPE Pipe

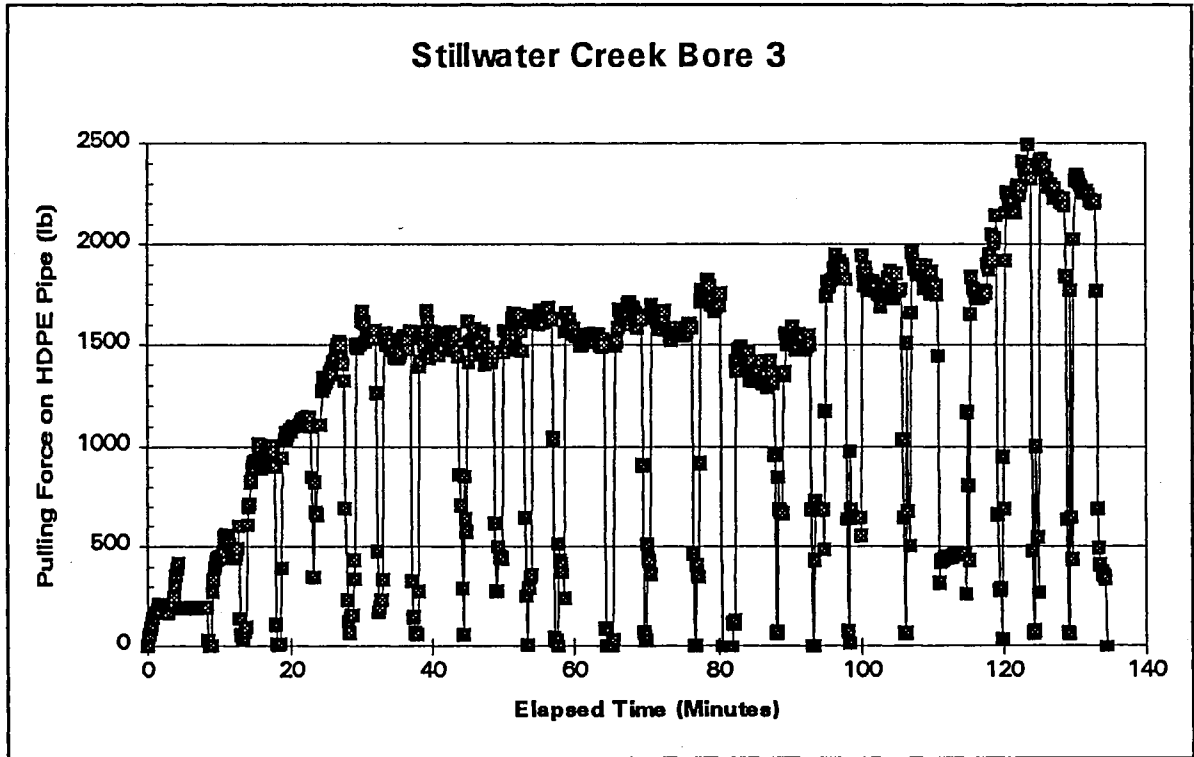
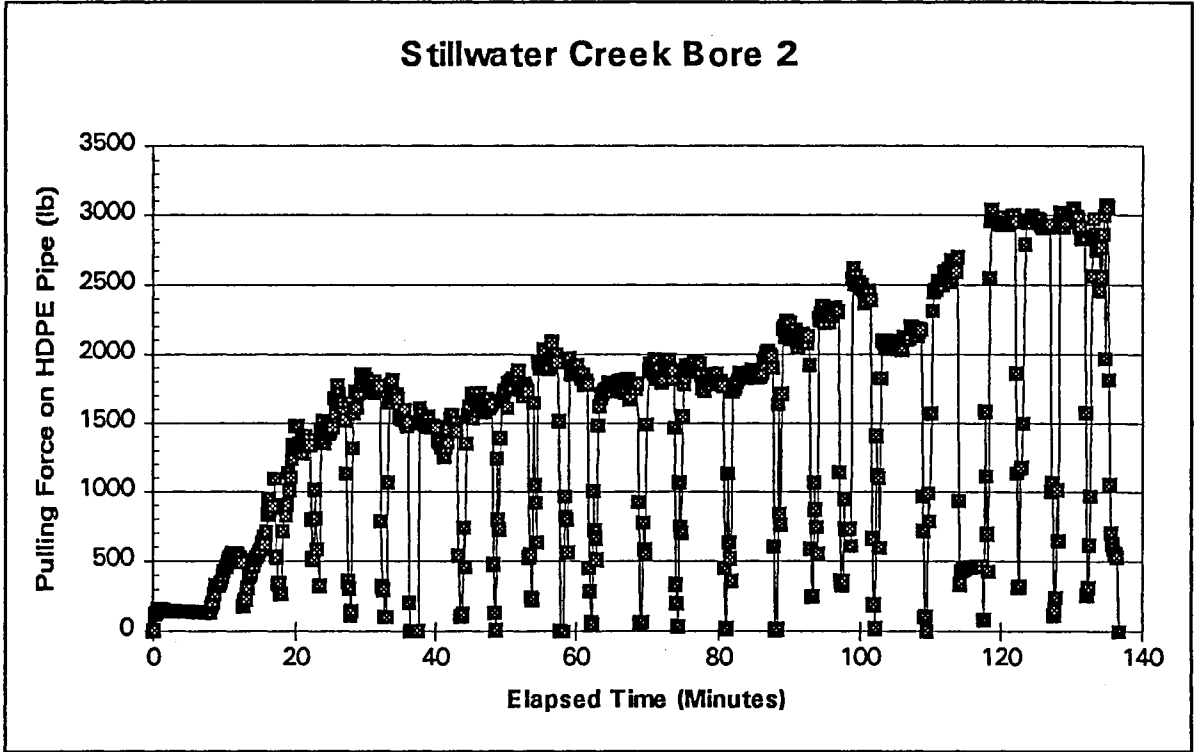


Section G: Pull Force Readings on HDPE Pipe

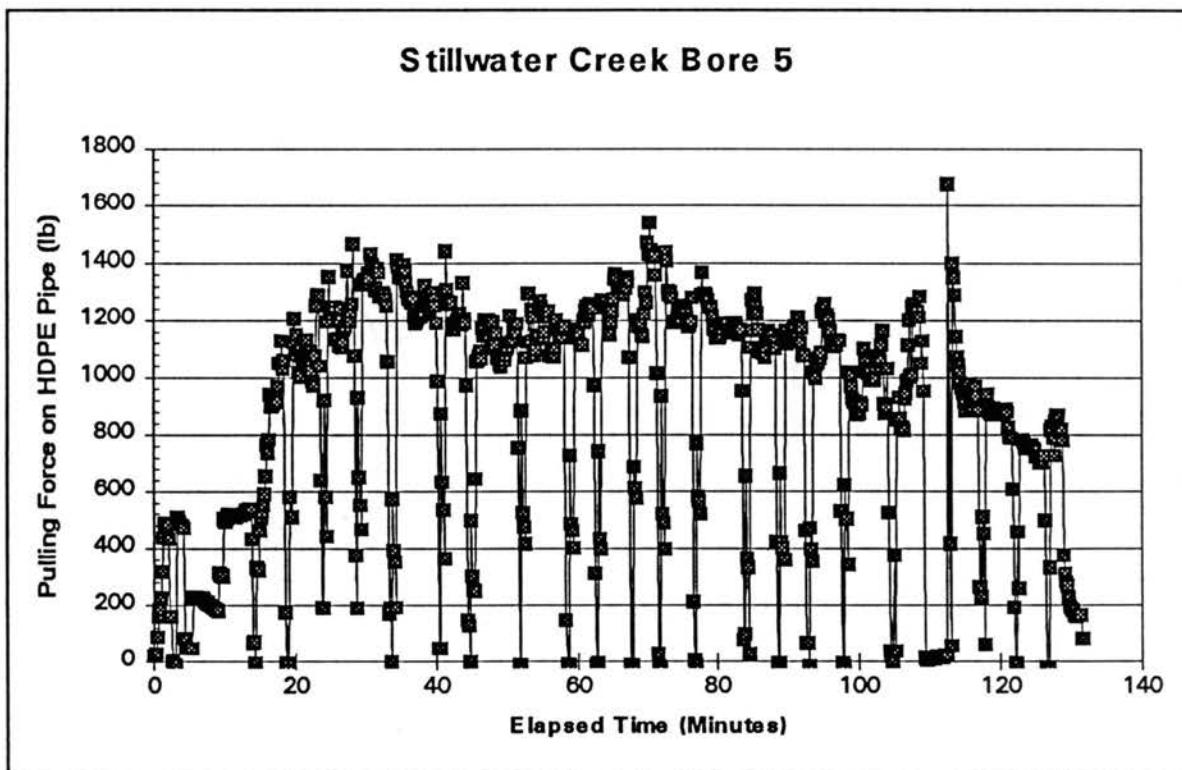
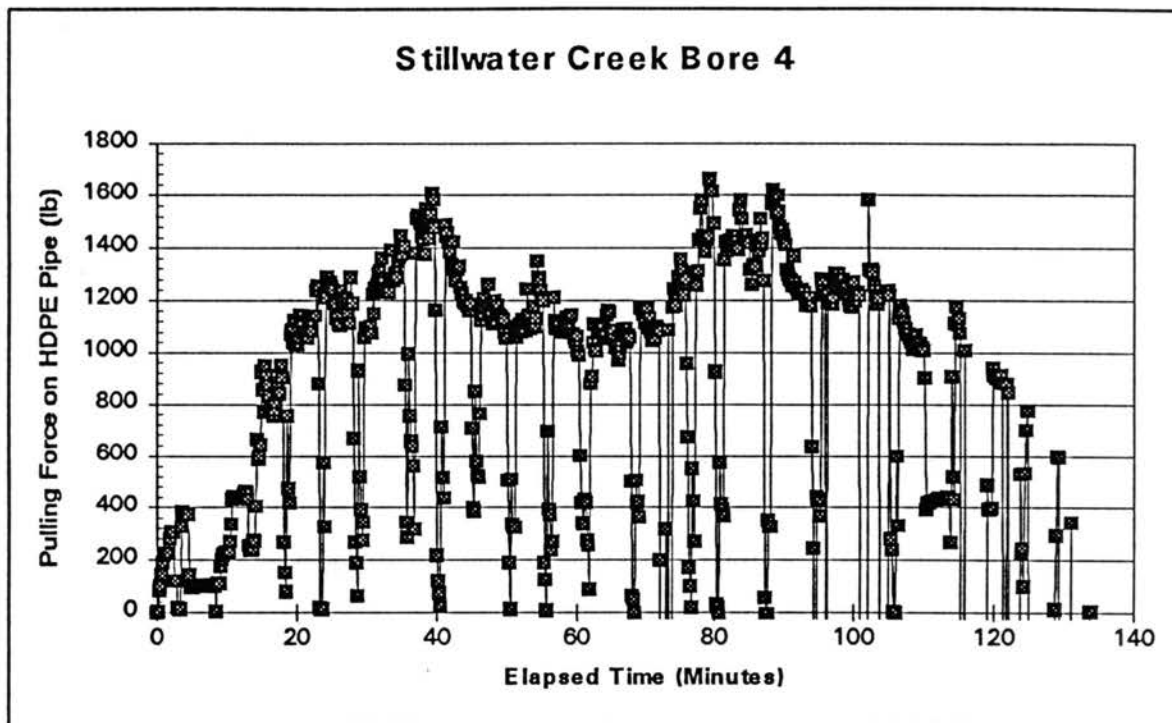


Section G: Pull Force Readings on HDPE Pipe

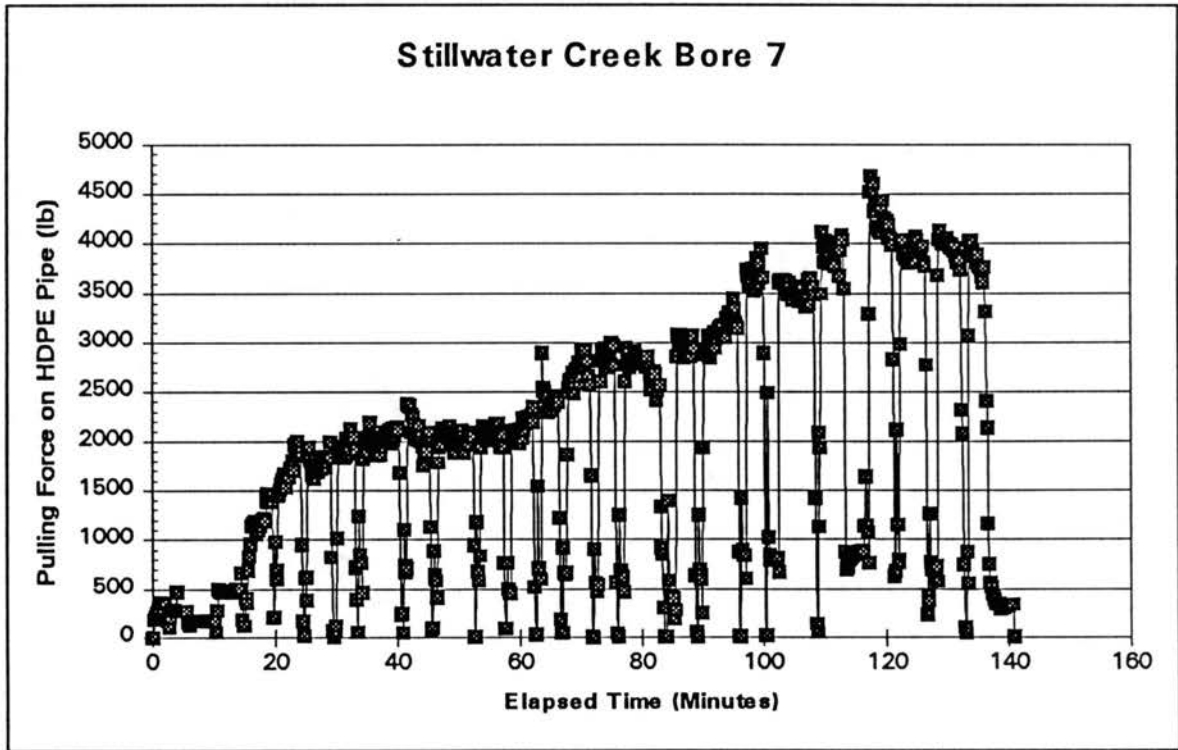
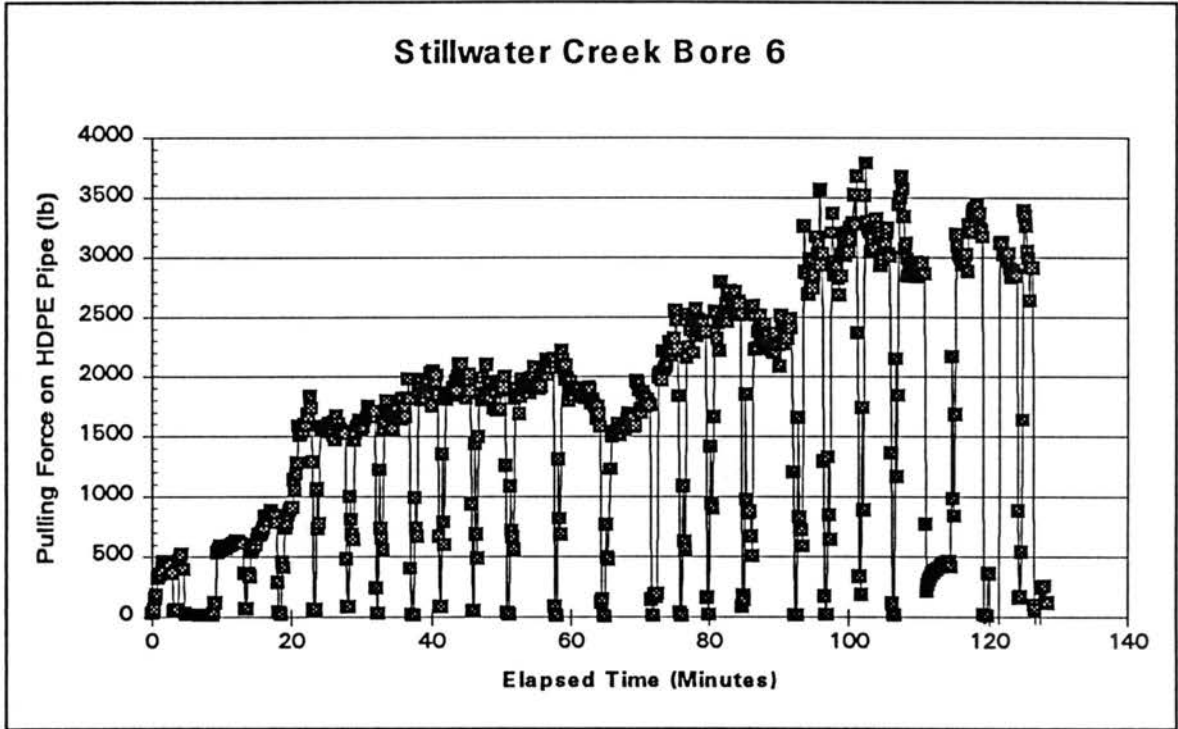




Section G: Pull Force Readings on HDPE Pipe



Section G: Pull Force Readings on HDPE Pipe



Section G: Pull Force Readings on HDPE Pipe

## Section H

### Data from Boring Tests

#### COYLE TEST SITE

##### Bore 5

Pipe No.	Depth (in)	Penetr. $q_u$ (psi)	Dist. from exit (ft)	Flow rate (gpm)	Pull rate (fpm)	Rot. rate (rpm)	Corr. Torque (ft-lb)	Cor. Pull (lb)	HDPE Pipe Pull (lb)
10	67.5	447	190	10.6	1.8	128	65	939	895
11	66	422	180	10.6	3.6	96	182	1114	890
12	66	652	170	10.6	1.8	96	87	985	893
13	64.5	507	160	10.6	3.6	160	51	822	970
14	63.5	723	150	10.6	1.8	160	25	985	947
15	66	748	140	10.6	2.7	192	30	878	881
16	66	836	130	10.6	2.7	96	30	768	760
17	64.5	584	120	10.6	3.6	128	90	813	707
18	66	554	110	10.6	2.7	128	77	790	714
19	65.5	717	100	10.6	2.7	160	103	791	653
20	67.5	187	90	10.6	3.6	192	90	765	646
21	72	466	80	10.6	1.8	192	108	815	645

##### Bore 6

Pipe No.	Depth (in)	Penetr. $q_u$ (psi)	Dist. from exit (ft)	Flow rate (gpm)	Pull rate (fpm)	Rot. rate (rpm)	Corr. Torque (ft-lb)	Cor. Pull (lb)	HDPE Pipe Pull (lb)
9	62	504	160	10.6	2.7	128	130	836	---
10	61	307	150	10.6	2.7	96	170	913	---
11	61.5	416	140	10.6	1.8	192	71	782	---
12	62.5	701	130	10.6	1.8	96	125	824	---
13	63	887	120	10.6	2.7	160	106	744	---
14	64.5	448	110	10.6	1.8	128	97	775	---
15	67	961	100	10.6	1.8	160	109	822	---
16	65.5	589	90	10.6	3.6	192	164	954	---
17	69	409	80	10.6	3.6	128	175	858	---
18	77	385	70	10.6	3.6	160	173	838	---
19	79	694	60	10.6	2.7	192	127	841	---
20	79.5	238	50	10.6	3.6	96	230	968	---

## COYLE TEST SITE

## Bore 7

Pipe No.	Depth (in)	Penetr. $q_u$ (psi)	Dist. from exit (ft)	Flow rate (gpm)	Pull rate (fpm)	Rot. rate (rpm)	Corr. Torque (ft-lb)	Cor. Pull (lb)	HDPE Pipe Pull (lb)
11	64	773	160	7.4	1.8	128	187	1003	---
12	68.5	889	150	7.4	1.8	160	165	944	---
13	72.5	776	140	7.4	3.6	192	237	987	---
14	78.5	838	130	7.4	2.7	160	201	886	---
15	82	466	120	7.4	1.8	192	143	838	---
16	80	263	110	7.4	3.6	128	288	959	---
17	81	577	100	7.4	2.7	128	242	826	---
18	82.5	433	90	7.4	2.7	192	181	784	---
19	77.5	253	80	7.4	1.8	96	177	748	---
20	71.5	173	70	7.4	3.6	160	225	727	---
21	70	553	60	7.4	3.6	96	328	965	---
22	74.5	555	50	7.4	2.7	96	354	1048	---

## Bore 8

Pipe No.	Depth (in)	Penetr. $q_u$ (psi)	Dist. from exit (ft)	Flow rate (gpm)	Pull rate (fpm)	Rot. rate (rpm)	Corr. Torque (ft-lb)	Cor. Pull (lb)	HDPE Pipe Pull (lb)
8	75	538	180	7.4	2.7	192	213	1373	---
9	73.5	1061	170	7.4	3.6	96	493	1569	---
10	73	554	160	7.4	1.8	128	190	1416	---
11	72	674	150	7.4	2.7	128	265	1578	---
12	71	865	140	7.4	2.7	160	265	1580	---
13	74.5	867	130	7.4	2.7	96	345	1579	---
14	77.5	811	120	7.4	1.8	192	180	1311	---
16	76.5	425	100	7.4	3.6	160	319	984	---
17	77	616	90	7.4	3.6	128	396	1219	---
18	75.5	456	80	7.4	1.8	160	240	1008	---
19	74.5	471	70	7.4	3.6	192	272	929	---
20	72.5	629	60	7.4	1.8	96	271	931	---

## Section H: Data from Boring Tests

## COYLE TEST SITE

## Bore 9

Pipe No.	Depth (in)	Penetr. $q_u$ (psi)	Dist. from exit (ft)	Flow rate (gpm)	Pull rate (fpm)	Rot. rate (rpm)	Corr. Torque (ft-lb)	Cor. Pull (lb)	HDPE Pipe Pull (lb)
9	74.5	679	170	7.4	1.8	160	262	1243	1116
10	72.5	751	160	7.4	3.6	128	354	1470	1255
11	73	694	150	7.4	2.7	128	337	1534	1334
12	74.5	616	140	7.4	2.7	160	308	1205	1003
13	75	552	130	7.4	3.6	160	355	1140	809
14	75.5	402	120	7.4	2.7	192	165	921	787
15	75.5	458	110	7.4	3.6	192	203	936	729
16	73.5	454	100	7.4	1.8	192	137	773	694
17	72	468	90	7.4	1.8	128	150	802	715
18	73.5	504	80	7.4	1.8	96	232	981	691
19	72.5	679	70	7.4	2.7	96	222	957	671
20	69	482	60	7.4	3.6	96	260	980	635

## Bore 10

Pipe No.	Depth (in)	Penetr. $q_u$ (psi)	Dist. from exit (ft)	Flow rate (gpm)	Pull rate (fpm)	Rot. rate (rpm)	Corr. Torque (ft-lb)	Cor. Pull (lb)	HDPE Pipe Pull (lb)
8	71.5	476	170	10.6	1.8	192	32	825	809
9	69.5	644	160	10.6	3.6	96	192	1024	780
10	69.5	322	150	10.6	3.6	128	127	874	723
11	68	276	140	10.6	3.6	160	96	765	738
12	67.5	460	130	10.6	1.8	96	43	671	716
13	70.5	602	120	10.6	1.8	160	42	702	708
14	72	418	110	10.6	2.7	96	104	843	692
15	72	485	100	10.6	2.7	192	117	713	651
16	71.5	368	90	10.6	1.8	128	118	785	695
17	74	533	80	10.6	2.7	128	269	1238	655
18	74.5	537	70	10.6	3.6	192	122	805	661
19	75	469	60	10.6	2.7	160	125	841	659

## Section H: Data from Boring Tests

## COYLE TEST SITE

## Bore 11

Pipe No.	Depth (in)	Penetr. $q_u$ (psi)	Dist. from exit (ft)	Flow rate (gpm)	Pull rate (fpm)	Rot. rate (rpm)	Corr. Torque (ft-lb)	Cor. Pull (lb)	HDPE Pipe Pull (lb)
8	73	762	170	7.4	1.8	192	108	1120	---
9	73.5	620	160	7.4	3.6	96	430	1577	---
10	74.5	624	150	7.4	2.7	96	512	1650	---
11	74.5	469	140	7.4	2.7	160	161	971	---
12	74.5	449	130	7.4	1.8	160	127	930	---
13	72.5	394	120	7.4	1.8	128	207	1150	---
14	72	467	110	7.4	2.7	192	136	946	---
15	74	432	100	7.4	3.6	160	308	1178	---
16	74.5	414	90	7.4	1.8	96	234	1040	---
17	73	529	80	7.4	3.6	128	401	1377	---
18	74.5	379	70	7.4	2.7	128	185	874	---
19	74.5	208	60	7.4	3.6	192	164	766	---

## Bore 12

Pipe No.	Depth (in)	Penetr. $q_u$ (psi)	Dist. from exit (ft)	Flow rate (gpm)	Pull rate (fpm)	Rot. rate (rpm)	Corr. Torque (ft-lb)	Cor. Pull (lb)	HDPE Pipe Pull (lb)
8	72.5	609	160	10.6	3.6	128	203	1069	---
9	75.5	477	150	10.6	1.8	192	23	890	---
10	74.5	501	140	10.6	3.6	160	91	915	---
11	73.5	411	130	10.6	2.7	160	89	889	---
12	74	456	120	10.6	1.8	160	62	846	---
13	71	391	110	10.6	2.7	96	119	816	---
14	70.5	338	100	10.6	1.8	96	68	780	---
15	73	413	90	10.6	2.7	128	39	644	---
16	74.5	529	80	10.6	2.7	192	50	654	---
17	73.5	199	70	10.6	3.6	192	65	623	---
18	71	56	60	10.6	1.8	128	50	677	---
19	70	447	50	10.6	3.6	96	181	904	---

## Section H: Data from Boring Tests

## COYLE TEST SITE

## Bore 13

Pipe No.	Depth (in)	Penetr. $q_u$ (psi)	Dist. from exit (ft)	Flow rate (gpm)	Pull rate (fpm)	Rot. rate (rpm)	Corr. Torque (ft-lb)	Cor. Pull (lb)	HDPE Pipe Pull (lb)
8	75	465	180	15.5	2.7	96	20	772	629
9	76.5	460	170	15.5	2.7	160	10	728	729
10	73.5	436	160	15.5	3.6	128	8	598	728
11	69	485	150	15.5	1.8	128	1	670	753
12	68.5	227	140	15.5	1.8	192	15	754	822
13	70.5	435	130	15.5	3.6	96	26	689	647
14	71.5	475	120	15.5	3.6	192	33	640	448
15	70.5	458	110	15.5	3.6	160	32	592	533
16	70	583	100	15.5	2.7	128	19	504	485
17	72.5	542	90	15.5	1.8	96	9	496	445
18	75.5	419	80	15.5	1.8	160	11	446	445
19	73.5	433	70	15.5	2.7	192	35	508	413

## Bore 14

Pipe No.	Depth (in)	Penetr. $q_u$ (psi)	Dist. from exit (ft)	Flow rate (gpm)	Pull rate (fpm)	Rot. rate (rpm)	Corr. Torque (ft-lb)	Cor. Pull (lb)	HDPE Pipe Pull (lb)
7	73.5	481	170	15.5	2.7	192	25	659	---
8	75.5	391	160	15.5	3.6	160	57	644	---
9	75.5	393	150	15.5	3.6	96	73	645	---
10	72.5	477	140	15.5	1.8	192	35	434	---
11	68	645	130	15.5	2.7	128	77	620	---
12	67.5	693	120	15.5	1.8	160	47	546	---
13	66.5	717	110	15.5	2.7	160	61	635	---
14	66.5	490	100	15.5	3.6	128	86	670	---
15	69.5	465	90	15.5	3.6	192	102	690	---
16	69	455	80	15.5	1.8	128	57	562	---
17	67.5	403	70	15.5	1.8	96	58	558	---
18	68	409	60	15.5	2.7	96	86	599	---

## Section H: Data from Boring Tests



## COYLE TEST SITE

## Bore 15

Pipe No.	Depth (in)	Penetr. $q_u$ (psi)	Dist. from exit (ft)	Flow rate (gpm)	Pull rate (fpm)	Rot. rate (rpm)	Corr. Torque (ft-lb)	Cor. Pull (lb)	HDPE Pipe Pull (lb)
7	69	350	160	15.5	2.7	192	22	700	---
8	69	243	150	15.5	2.7	128	26	619	---
9	70	331	140	15.5	2.7	96	62	655	---
10	72	490	130	15.5	1.8	160	55	718	---
11	71.5	442	120	15.5	3.6	128	142	818	---
12	72	72	110	15.5	3.6	160	77	611	---
13	73	293	100	15.5	1.8	96	38	580	---
14	72.5	506	90	15.5	1.8	128	47	591	---
15	70.5	210	80	15.5	1.8	192	58	571	---
16	68.5	467	70	15.5	3.6	192	128	754	---
17	69	364	60	15.5	3.6	96	137	761	---
18	72	407	50	15.5	2.7	160	130	732	---

## Bore 16

Pipe No.	Depth (in)	Penetr. $q_u$ (psi)	Dist. from exit (ft)	Flow rate (gpm)	Pull rate (fpm)	Rot. rate (rpm)	Corr. Torque (ft-lb)	Cor. Pull (lb)	HDPE Pipe Pull (lb)
7	68	363	160	15.5	2.7	128	86	810	---
8	69	480	150	15.5	3.6	192	45	674	---
9	70	484	140	15.5	3.6	96	72	721	---
10	71.5	497	130	15.5	3.6	160	36	576	---
11	72	846	120	15.5	1.8	96	30	529	---
12	72.5	689	110	15.5	3.6	128	77	654	---
13	72	291	100	15.5	2.7	192	43	534	---
14	70.5	369	90	15.5	1.8	160	28	553	---
15	70.5	314	80	15.5	2.7	160	41	509	---
16	69.5	403	70	15.5	1.8	192	38	519	---
17	69.5	379	60	15.5	2.7	96	61	536	---
18	70	378	50	15.5	1.8	128	52	565	---

## Section H: Data from Boring Tests

## STILLWATER CREEK TEST SITE

## Bore 0

Pipe No.	Depth (in)	Penetr. $q_u$ (psi)	Dist. from exit (ft)	Reamer Design	Pull rate (fpm)	Rot. rate (rpm)	Corr. Torque (ft-lb)	Cor. Pull (lb)	HDPE Pipe Pull (lb)
7	70.5	738	170	winged	2.7	160	246	2033	945
8	68	718	160	winged	3.6	96	440	2787	876
9	67	564	150	winged	1.8	128	248	2401	900
10	72	585	140	winged	2.7	96	246	2119	1040
11	78.5	568	130	winged	1.8	160	199	2087	991
12	79.5	513	120	winged	2.7	192	246	2387	1039
13	76.5	531	110	winged	3.6	192	234	2179	1056
14	75.5	358	100	winged	3.6	160	289	2377	1034
15	77.5	737	90	winged	3.6	128	303	2371	1081
16	79	539	80	winged	2.7	128	284	2542	1042
17	79	758	70	winged	1.8	192	199	1915	845
18	76	874	60	winged	1.8	96	268	2245	813

## Bore 1

Pipe No.	Depth (in)	Penetr. $q_u$ (psi)	Dist. from exit (ft)	Reamer Design	Pull rate (fpm)	Rot. rate (rpm)	Corr. Torque (ft-lb)	Cor. Pull (lb)	HDPE Pipe Pull (lb)
9	75	916	170	winged	1.8	128	189	2083	1133
10	74	821	160	winged	2.7	192	247	2554	1230
11	73.5	526	150	winged	3.6	128	478	3145	1052
12	73.5	570	140	winged	2.7	160	234	2126	1009
13	72.5	599	130	winged	3.6	160	236	2086	999
14	71.5	491	120	winged	3.6	96	356	2729	1100
15	71.5	414	110	winged	1.8	96	229	2416	1197
16	73	664	100	winged	3.6	192	332	3098	1211
17	74.5	639	90	winged	1.8	192	231	2671	1194
18	73.5	726	80	winged	2.7	128	238	2374	1108
19	72	708	70	winged	2.7	96	254	2363	1004
20	70.5	775	60	winged	1.8	160	178	1937	896

## Section H: Data from Boring Tests

## STILLWATER CREEK TEST SITE

## Bore 2

Pipe No.	Depth (in)	Penetr. $q_u$ (psi)	Dist. from exit (ft)	Reamer Design	Pull rate (fpm)	Rot. rate (rpm)	Corr. Torque (ft-lb)	Cor. Pull (lb)	HDPE Pipe Pull (lb)
8	70	677	160	fluted	3.6	96	209	2752	2288
9	70	582	150	fluted	2.7	192	152	2436	2115
10	71.5	685	140	fluted	1.8	128	110	2025	1868
11	72.5	786	130	fluted	1.8	160	124	1995	1827
12	72.5	865	120	fluted	2.7	128	186	2251	1875
13	73.5	926	110	fluted	1.8	96	167	2187	1760
14	73.5	784	100	fluted	3.6	128	171	2148	1851
15	73	855	90	fluted	3.6	160	206	2330	1942
16	73.5	777	80	fluted	2.7	96	228	2415	1742
17	73.5	928	70	fluted	2.7	160	187	2076	1626
18	73.5	658	60	fluted	1.8	192	136	1570	1454
19	74	507	50	fluted	3.6	192	199	2015	1623

## Bore 3

Pipe No.	Depth (in)	Penetr. $q_u$ (psi)	Dist. from exit (ft)	Reamer Design	Pull rate (fpm)	Rot. rate (rpm)	Corr. Torque (ft-lb)	Cor. Pull (lb)	HDPE Pipe Pull (lb)
6	69.5	162	180	fluted	1.8	96	105	2164	1791
8	68.5	597	160	fluted	2.7	128	131	2130	1511
9	69.5	382	150	fluted	1.8	128	105	1888	1376
10	71	509	140	fluted	3.6	192	166	2116	1731
11	72	561	130	fluted	1.8	160	102	1865	1591
12	72	583	120	fluted	2.7	96	155	2122	1631
13	71.5	612	110	fluted	1.8	192	101	1682	1547
14	73	852	100	fluted	3.6	96	197	2110	1640
15	73.5	805	90	fluted	3.6	160	219	2221	1553
16	71.5	666	80	fluted	2.7	160	178	2018	1487
18	71.5	584	60	fluted	2.7	192	157	1780	1499
19	73	702	50	fluted	3.6	128	190	2157	1552

## Section H: Data from Boring Tests

## STILLWATER CREEK TEST SITE

## Bore 4

Pipe No.	Depth (in)	Penetr. $q_u$ (psi)	Dist. from exit (ft)	Reamer Design	Pull rate (fpm)	Rot. rate (rpm)	Corr. Torque (ft-lb)	Cor. Pull (lb)	HDPE Pipe Pull (lb)
6	75	271	180	winged	3.6	192	222	1893	1295
8	71	264	160	winged	1.8	128	246	2552	1348
9	73	436	150	winged	1.8	96	305	3058	1416
10	73	471	140	winged	3.6	96	411	3235	1464
11	72	511	130	winged	3.6	160	187	1964	1239
12	72	356	120	winged	3.6	128	250	2160	1113
13	72	613	110	winged	1.8	160	175	1939	1055
14	72	534	100	winged	2.7	96	304	2538	1091
15	72	491	90	winged	2.7	192	246	2223	1152
16	73.5	470	80	winged	2.7	128	344	2612	1149
17	75.5	612	70	winged	2.7	160	296	2536	1302
19	74	778	50	winged	1.8	192	236	2240	1254

## Bore 5

Pipe No.	Depth (in)	Penetr. $q_u$ (psi)	Dist. from exit (ft)	Reamer Design	Pull rate (fpm)	Rot. rate (rpm)	Corr. Torque (ft-lb)	Cor. Pull (lb)	HDPE Pipe Pull (lb)
7	75	340	170	winged	2.7	128	145	1704	1126
8	74.5	331	160	winged	3.6	160	242	2477	1143
9	74	401	150	winged	2.7	96	261	2523	1149
10	73.5	412	140	winged	1.8	160	223	2616	1202
11	72.5	417	130	winged	2.7	192	220	2524	1250
12	71.5	456	120	winged	3.6	96	270	2521	1315
13	72	627	110	winged	2.7	160	167	2012	1285
14	73.5	693	100	winged	3.6	128	192	1965	1188
15	72	711	90	winged	1.8	128	176	2013	1157
16	68	427	80	winged	1.8	192	170	1944	1124
17	68.5	531	70	winged	3.6	192	290	2567	1239
18	71.5	246	60	winged	1.8	96	182	2053	1281

## Section H: Data from Boring Tests

## STILLWATER CREEK TEST SITE

## Bore 6

Pipe No.	Depth (in)	Penetr. $q_u$ (psi)	Dist. from exit (ft)	Reamer Design	Pull rate (fpm)	Rot. rate (rpm)	Corr. Torque (ft-lb)	Cor. Pull (lb)	HDPE Pipe Pull (lb)
8	67	426	160	fluted	1.8	96	177	2601	2348
9	69.5	495	150	fluted	2.7	96	235	2956	2540
10	70.5	395	140	fluted	3.6	128	225	2712	2394
11	70	427	130	fluted	3.6	160	153	2196	2175
12	71	439	120	fluted	1.8	128	99	1738	1673
13	73.5	377	110	fluted	1.8	192	112	1814	1879
14	74	569	100	fluted	1.8	160	111	1922	1957
15	72	800	90	fluted	2.7	128	130	1914	1890
16	72.5	887	80	fluted	2.7	192	186	2156	1930
17	72.5	734	70	fluted	3.6	192	237	2192	1911
18	70	547	60	fluted	2.7	160	141	1741	1713
19	69.5	454	50	fluted	3.6	96	205	1834	1633

## Bore 7

Pipe No.	Depth (in)	Penetr. $q_u$ (psi)	Dist. from exit (ft)	Reamer Design	Pull rate (fpm)	Rot. rate (rpm)	Corr. Torque (ft-lb)	Cor. Pull (lb)	HDPE Pipe Pull (lb)
8	72	513	160	fluted	1.8	128	136	3209	3104
9	74	449	150	fluted	3.6	192	156	2985	2967
10	75.5	417	140	fluted	1.8	160	125	2946	2745
11	73.5	382	130	fluted	3.6	160	156	2888	2849
12	73.5	343	120	fluted	2.7	160	145	2741	2686
13	75.5	325	110	fluted	3.6	96	150	2353	2437
14	76	345	100	fluted	2.7	96	131	2131	2135
15	74.5	243	90	fluted	2.7	128	142	2131	2059
16	72	496	80	fluted	1.8	96	120	2031	2034
17	72.5	553	70	fluted	2.7	192	143	1969	2076
18	72	506	60	fluted	1.8	192	157	2100	2017
19	70	691	50	fluted	3.6	128	209	2191	1945

2  
VITA

Floyd Ray Gunsaulis

Candidate for the Degree of

Doctor of Philosophy

**Dissertation: OPTIMAL PARAMETER SELECTION FOR BACKREAMING OPERATIONS WITH FLUID ASSISTED, MINI-HORIZONTAL DIRECTIONAL DRILLING MACHINES**

**Field of Study: Biosystems Engineering**

**Biographical:**

**Personal: Born on July 25, 1966 in Fayetteville, Arkansas to Len and Retha Gunsaulis. Married to Cindy (Kinsman) Gunsaulis.**

**Education:**

- 1984 Honor Graduate from Siloam Springs High School in Siloam Springs Arkansas
- Bachelor of Science in Agricultural Engineering in May, 1988. University of Arkansas, Fayetteville, Arkansas.
- Master of Science in Agricultural Engineering in May 1990. University of Arkansas, Fayetteville, Arkansas.
- Completed the Requirements for the Doctor of Philosophy degree at Oklahoma State University in December 1996.

**Experience: February 1990 - July 1993, Test Engineer with the Charles Machine Works in Perry, Oklahoma.**

**Professional Registration: Registered Professional Engineer, State of Arkansas**

**Professional Memberships: ASAE, Society of Automotive Engineers (SAE), North American Society for Trenchless Technology (NASTT)**